PI ZERO PHOTOPRODUCTION FROM HYDROGEN BETWEEN 574 AND 1211 MEV

Thesis by

Franklin Bruce Wolverton

In Partial Fulfillment of the Requirements

For the Degree of

Doctor of Philosophy

California Institute of Technology

Pasadena, California

1968

(Submitted May 9, 1968)

ACKNOWLEDGMENTS

I would like to thank Professor R. L. Walker for suggesting and supervising this experiment. The wisdom of his counsel in times of difficulty was demonstrated frequently in the progress of this research.

Doctors S. D. Ecklund, M. G. Hauser, and H. A. Thiessen, who were experienced with much of the equipment used in this experiment, contributed most helpfully their assistance, advice, and computer programs. I would particularly like to thank Dr. Thiessen for considerable assistance with the electronics and for enduring the inconvenience of having the preliminary measurements for this experiment proceed in parallel with the data accumulation for his thesis.

Mr. E. Emery and Mr. R. Wileman kept the liquid hydrogen target operating dependably. Mr. Emery's assistance with the equipment construction and checkout and data accumulation was very much appreciated.

Mr. R. Ault, Mr. J. Downum, Mr. D. Erlich, Mr. T. Humphreys, Mr. P. Scheffler, Mr. K. Jacobs, Mr. C. Maxwell, and Mr. W. Metcalf aided, at various stages of the experiment, with the construction of equipment, collection of data, and writing of computer programs. Their very able assistance was crucial in enabling the data analysis to keep fairly close pace with the data collection.

I would like to express my appreciation to Mr. D. Sell and his assistants for their cooperation and their ingenuity in the apparatus design and construction. Mr. L. Nesleny and his staff were of great assistance in the electronics fabrication and repair.

Mr. A. Neubieser and his staff of beam tuners, the crew, headed originally by Mr. Lawrence Loucks and more recently by Mr. Paul Van Ligten, and Mr. Sell struggled long and hard to keep the synchrotron operating dependably.

I would like to thank Mrs. A. B. Hall, Mrs. D. W. Bianchi, and Miss J. Bruce for ably performing many secretarial and clerical functions.

The patience and cooperation of other staff and students at the Synchrotron Laboratory, the computing center, and the graphic arts department, were very much appreciated.

I am indebted to the National Science Foundation, the Atomic Energy Commission, and the California Institute of Technology for their financial support.

Of course, the persons who sacrificed more than any others for this experiment were my wife, Margaret, and our sons, David and Glen. Their patient support cannot be adequately described.

ABSTRACT

Cross section angular distributions for π^o photoproduction from hydrogen were measured for 28 laboratory photon energies from 574 to 1211 MeV. At most energies, the π^o center of mass angle was varied from 60^o to 170^o in steps of 10^o. A magnetic spectrometer was used to measure the momentum and angle of the recoil proton. A scintillation counter hodoscope with lead convertors was used to detect the presence of at least one of the π^o decay gamma rays. For a majority of the measurements the π^o rates were separated from a contamination of pi pair rates using the difference in their distribution among the gamma counters. For the remainder of the measurements, charged pi pairs were eliminated using veto counters in front of the gamma counters. Internal inconsistency and comparison with other experiments indicate that the veto data are 10 to 15% low near 90^o in the region of 750 MeV. The remainder of the data show good internal consistency and fair agreement with data of other experiments. The results show a peak at 140^o near 1050 MeV which had been expected but not previously measured. Comparison of the backward angle data with that from experiments measuring cross sections very near 180^o indicates either an inconsistency between experiments or a rapid drop in the cross section near 180^o in the region around 800 MeV.

To Marg

TABLE OF CONTENTS

APPENDICES

LIST OF FIGURES

LIST OF TABLES

I. INTRODUCTION

In his thesis, written in 1963, Diebold (1) reviewed most of the data then available on π^o photoproduction near the second and third resonances. He commented at that time that the various experiments did not agree well with one another due to wide resolutions and various systematic errors. In the five years since then, the number of experiments measuring π^o cross sections has doubled. The increase in beam intensities and electronic sophistication has enabled experimenters to measure more points with greater statistical accuracy than before. But, unfortunately, the results are not much better with regard to consistency between experiments. We are certainly obtaining a better understanding of the qualitative features of the differential cross section, but the precise information necessary for model fitting is somewhat wanting. The basic problem at this point seems to be systematic rather than statistical errors.

Table 1 lists in roughly chronological order most of the experiments to date that have measured π^o cross sections in the range covered by this thesis (laboratory photon energy k = 574 MeV to 1211 MeV and $\theta_{\pi^o}^{cm} = 60^o$ to 170^o). The 180^o data are included also. Most of the information on the earlier experiments is taken from Table 1 of Diebold's thesis. The table lists the angle and energy ranges, the energy by which the synchrotron endpoint energy exceeded the incoming photon energy, the photon energy resolution, and the major characteristics of the method of detecting the reaction.

Table 1

Summary of Experiments

Experiment (First name author)	Ref.	$\theta_{\pi^o}^{cm}$	k(MeV)	E_o-k(MeV)	Δk/k	Method of detection: proton energy telescope	proton energy magnet	proton energy TOF	decay gammas 1	decay gammas 2
Vette	1	32 - 147	490 - 940	130 - 230	~ .11		X			
De Wire	1	50, 90, 125	450 - 1140		.09 - .22	X			X	
Stein	1	60, 90, 120	500 - 900	120	~ .13	X				
Worlock	1	51 - 137	600 - 800	120	.06 - .21	X				
Cortellesa	1	56, 90	600 - 800	200 - 400	.06 - .08	X			X	
Jackson	2	47, 90, 125	950 - 1150	50	.1	X*			X	
Deutsch	1	90	620 - 810		.03	X			(X)	
Talman	1	0 - 100	750 - 1160	120	.15	(X**)				X
Diebold	1	60, 90, 120	600 - 1200	50 - 100	.05 - .11		X		(X)	
Alvarez	3	60, 90	900 - 4000	E_o below 2π	.037 - .07		X		X	
DeStaebler	4	40 - 180	660 - 800	E_o below 2π			X			
Ward	5	51 - 135	600 - 1200	< 500	.04 - .12			X	X	
Belletini	6	30, 40, 60	600 - 1000	E_o below 2π			X		X	
Hatch	7	3 - 90	911 - 1390	100	~ .15					X
Bacci	8	90, 120, 135	400 - 800	< 250	.02 - .03	X			X	
Kenton	9	90	550 - 1200		.07 - .12			X	X	
Lundquist	10	(P=755,	833, 684)	< 100	.025 - .06		X			
Bloom	11	60	750 - 1075	100 - 400	.04	X				X
Buschhorn	12	180	800 - 3300	40	.05		X			
Loh	13	180	500 - 1700	30 - 90	.02		X			
This expt.		60 - 170	574 - 1211	50 - 180	.04 - .1		X		X	(X)

*k determined by synchrotron subtraction.

**k determined by gamma counters and E_o.

In the energy region under consideration, the measurement of the differential cross section for

$$\gamma + p \rightarrow p + \pi^0$$

is usually accomplished by measuring the energy and angle of the proton, which, with conservation of energy and momentum give the complete kinematics of the reaction. There seems to be no particular problem achieving sufficient angular resolution to resolve the degree of structure thus far seen in the π^0 differential cross section. On the other hand, the photon energy resolution of some of the experiments has been limited by the accuracy of the proton angle or energy measurement. Although the smearing of the cross section caused by the wide energy resolution of some of the experiments is undesirable, it is not a major obstacle to intercomparison of experiments, since a cross section measured by a higher resolution experiment with many points can always be folded with the resolution of a lower resolution experiment to provide numbers for comparison. The table indicates the primary method used by each experiment to measure the proton energy and the resultant incoming photon resolution. Only three experiments did not use the proton energy and angle: those of Talman (1) and Hatch (7), which were designed primarily for small pion angles, where the proton has too low energy to be observed, and the experiment of Jackson (2), where a synchrotron subtraction was used to find the photon energy. The major problems in detecting the proton are the nuclear scattering corrections and, to a lesser extent, the determination of apertures of the apparatus. The magnet experiments will be less susceptible to scattering corrections than the others, but will be more susceptible to errors in apertures.

The real difficulty in measuring π^o cross sections comes in trying to eliminate or correct for hydrogen associated backgrounds. A (hopefully) minor background which remains in most of the measurements comes from Compton scattering, which most of the experiments are not able to distinguish from π^o production. The cross section at 90^o is of order 2% of the π^o cross section, but little is known experimentally about the angular distribution (9). An experiment by J. Berk of UCLA is underway at the Caltech Synchrotron to measure the angular dependence. Experiments such as the one reported in this thesis, which detect both π^o and Compton photons, unfortunately enhance the Compton contamination by the reciprocal of the π^o photon geometric efficiency.

Another background, which becomes important at the smaller π^o angles, is the effect of the so-called "ghost protons" which have been discussed by Diebold (1), Lundquist (10) and others. These are protons which cannot be produced by photoproduction from hydrogen and which are apparently produced by a two-step process involving the hydrogen. Belletini (6) has shown that requiring one of the decay photons eliminates this background.

By far the most troublesome background is the production of charged and neutral pi pairs. Three methods have been employed to cope with this contamination. The simplest method, conceptually, is to measure the proton momentum with high resolution and then set the synchrotron endpoint energy low enough that no protons from pi pairs have sufficiently high momentum to be counted. The trouble with this method is that it requires using photons from very near the end of the bremsstrahlung spectrum where the spectrum is changing rapidly and difficult to know accurately. A second method is to measure the momentum spectrum of the pi pairs and fit it with some model, such as phase space. The disadvantage of this method is clearly the model dependence. A third technique used is to require one or two of the decay photons from the π^0 in addition to the proton. If veto counters are used in front of the gamma counters, this technique eliminates charged pairs. If the angular dependence of the decay gammas is used, it is possible to eliminate the neutral pairs also. The trouble with this method is that it requires a very complicated efficiency correction.

The results of the individual experiments are discussed in Part V, where they are viewed in the context of the results of the present experiment.

Table 1 shows that two thirds of the experiments measured energy distributions at one, two, or three angles. While energy distributions are more convenient to measure than angular distributions, and, while energy distributions are convenient for unfolding energy resolutions, they are not the type of data most useful for phenomenological analysis. Phenomenological fitting at present concentrates on fits of angular distributions, with the only energy dependence being the insertion of various energy dependent resonance forms and a requirement of continuity on the fitting coefficients. The inconsistency between experiments makes it very difficult to fit together data from various experiments to make angular distributions. If we look at the experiments which do give angular distributions we find that Hatch and Talman cover the forward hemisphere only. Vette, Worlock, and DeStaebler et al. cover the region below 950 MeV. The only angular distributions at higher energies are those of Ward et al., which only go back to 137°. Even the Ward data did not exist at the time the present experiment was started.

In view of this situation, the present experiment was begun with the intent to:

(1) Measure angular distributions at 10° intervals in the π^{0} c. m. angle over as wide an angular range as feasible with the spectrometer.

(2) Cover both the second and third resonances to provide comparison data at the second resonance and new data at the third.

(3) Pay particular attention to systematic errors.

Because of the many points to be measured and the low rates at the synchrotron, it was decided to use all four channels of the spectrometer. The overall width of 10% for the four channels prevented running with the endpoint low enough to eliminate all pi pairs.

An initial survey indicated a background of protons from the target materials, comparable to the rate of protons from π^{0} production, at the very backward pion angles. To reduce this background, a set of counters was installed to detect the decay gamma rays from the π^{0}. The counters were very successful in reducing the background. The background rate was reduced almost to the 3% rate expected from the hydrogen in the target materials and the hydrogen gas left in the target. The gamma counters proved to be even more important as a means of eliminating the pi pair rates, which become several percent of the π^o rates, particularly around k = 800 and $\theta_p^{lab} = 16^o$. The counters were run in two configurations. One configuration provided charged particle veto counters to eliminate charged pairs, and the other provided a measurement of the gamma angular distributions for eliminating both charged and neutral pairs.

With the gamma counters, it was possible to record rates for three methods of detection simultaneously:

(a) proton alone,

(b) proton and one gamma ray,

(c) proton and two gamma rays.

These three "signatures", as they are referred to, are designated by P, $P \cdot \gamma$, and $P \cdot 2\gamma$, respectively. The intercomparison of the results of the three signatures is valuable in assessing the systematic accuracy of the experiment. The comparisons are discussed in Parts III B and III C. The $P \cdot \gamma$ signature provided the most accurate cross sections and these are the ones quoted as our final results. The experiment provided measurements of 328 cross sections lying on a grid of photon energies from 574 to 1211 MeV and π^o c.m. angles from 60 to 170 degrees.

II. EXPERIMENTAL METHOD

Figure 1 contains a plan view of the experimental area.

The incident photons were provided by the 1.5 GeV Caltech Synchrotron. The endpoint energy, E_0, of the bremsstrahlung beam was normally set about 1.12 times the photon energy corresponding to the central momentum of the spectrometer. The target protons were contained in a 3 inch liquid hydrogen target. More detailed descriptions of the beam and the hydrogen target are contained in Appendix I.

The spectrometer in which the protons were detected could be rotated around a pivot beneath the hydrogen target to select the laboratory proton angle. This angle together with the magnet field setting determined the incoming photon energy accepted by each channel. Since the momentum spacing of the four channels was held constant by the spectrometer and since dk/dp changes with angle, it was not possible to take distributions at constant energy with all four channels at once. Instead, distributions were taken at constant central k value and the four cross sections at each setting were interpolated to give cross sections at standard k values as explained in Appendix VII. The data, taken at seven central photon energies with four standard energies each, yielded angular distributions at 28 energies from 574 to 1211 MeV.

The data were taken at constant proton laboratory angle instead of constant center of mass angle. However, the center of mass angle changes less than 2.6° from its average value for a given proton laboratory angle over the entire range of energies measured. The laboratory angles chosen, $\theta_p^{lab} = 4, 8, 12, 16,$

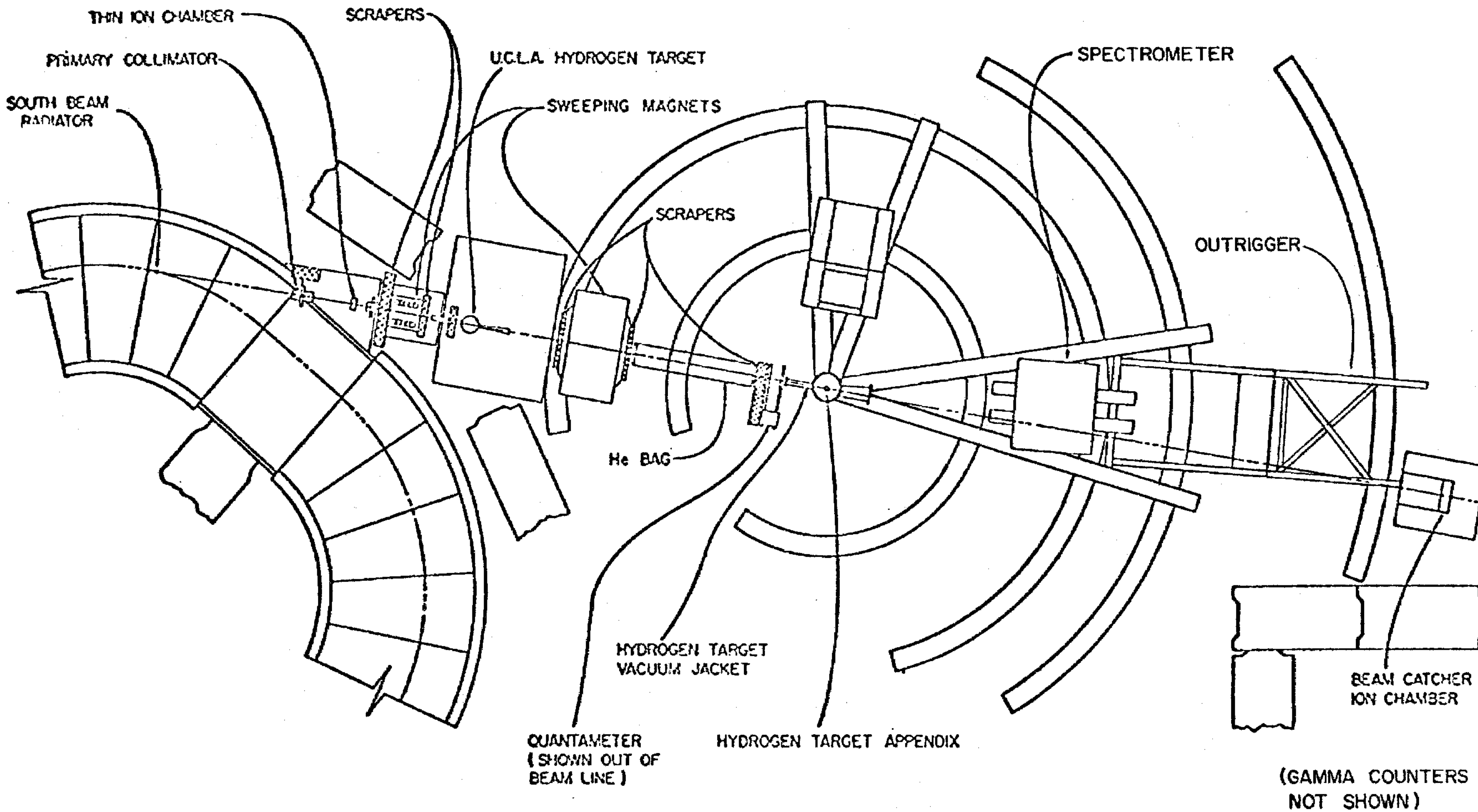

Figure 1. Plan View of the Experimental Area

20.5, 25, 29.5, 34, 39, 44, 49, and 54 degrees, correspond very nearly to π^o center of mass angles from 170^o to 60^o in steps of 10^o. An additional set of data was taken at $\theta_p^{lab} = 41.9^o$, for a smaller range of k values. At $\theta_p^{lab} = 49^o$ and 54^o, points are missing for the lowest energies because the protons had too low momenta to be detected reliably in the spectrometer as it was arranged for this experiment.

To cover the ranges of proton momenta and angles required for this experiment, it was necessary to use the spectrometer in two configurations. The first (referred to as the HEMA configuration) had a maximum momentum of 1200 MeV/c and was similar to the 1200 MeV/c configuration (the HEM configuration) used by previous experiments at Caltech (see, for example, Reference 14). The second (referred to as the OUTR configuration) had a maximum momentum of 1670 MeV/c and a maximum angle of 39.1^o. The two configurations are shown in Figures 2 and 3. The same counters were used in both configurations, only the positions of the counters were changed. A1 defined the angular aperture. The S2 hodoscope defined the four momentum channels. The Freon and Lucite Cherenkov counters vetoed electrons and pions. S1 served as a reference for fast coincidences. A2 and S3 helped eliminate counts from showers and scatters. The fans vetoed particles that scattered from the pole faces. The spectrometer configurations are discussed in more detail in Appendix II and Reference 15.

Also shown in Figures 2 and 3 is one of the set of four counters used to detect the decay photons from the π^o. Each counter consisted of simply a 1/4 inch plastic scintillator behind a 1/2 inch lead convertor. These counters were not used to

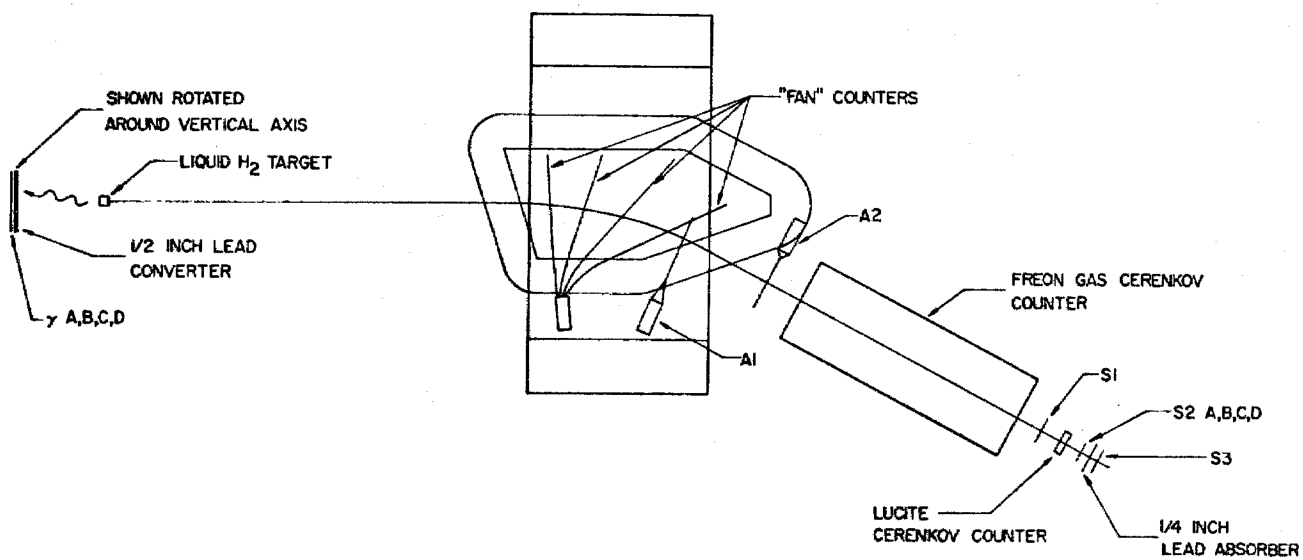

Figure 2. 1200 MeV/c Spectrometer Configuration (HEMA)

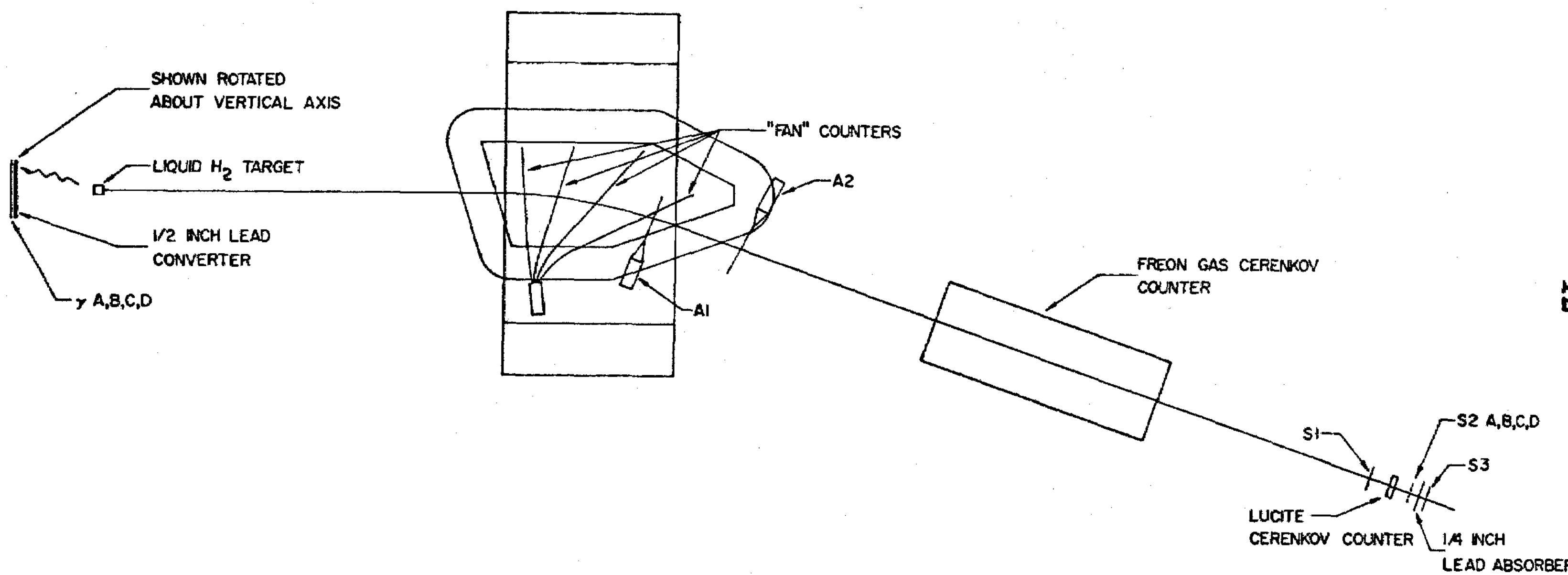

Figure 3. 1670 MeV/c Spectrometer Configuration (OUTR)

measure the energy of the gamma rays, but only to detect their presence. The rudimentary design of the gamma counters was the result partly of severe space limitations caused by the design of the hydrogen target stand (it has since been modified) and partly by a desire for counters which could be constructed in a short period of time.

Figure 4 shows a plan view of the gamma counters arranged around the target in what will be referred to as the "four counter" configuration. In this configuration the counters were placed side by side to form a four counter hodoscope. With this arrangement, the rates in the side counters could be compared with those in the central counters to find the amount of pi pair contamination. This method had the advantage that it allowed correcting for both charged and neutral pairs. It had the disadvantage that the statistical error in the result was large when the π^o rates in the center and side counters were not sufficiently different from one another.

Figure 5 shows a plan view of the counters in the veto configuration. In this configuration the convertors were removed from the side counters and the side counters were placed in front of the center ones to veto charged particles. This arrangement had the advantage that charged pi pairs were eliminated with no significant loss in statistical accuracy. It had the disadvantage that no correction was possible for neutral pi pairs. The veto arrangement had the practical problem of high singles rates in the veto counters.

Both gamma counter configurations were used with both magnet configurations. The results of the different methods are compared in Part III A.

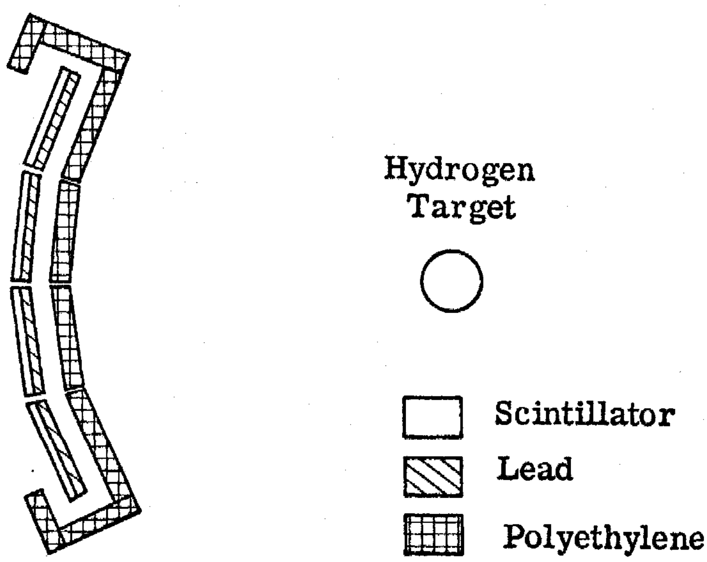

Figure 4. Four Counter Gamma Counter Configuration

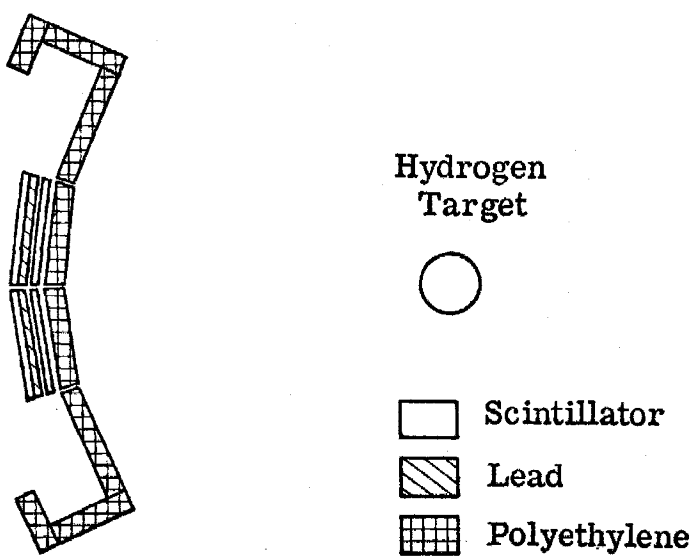

Figure 5. Veto Gamma Counter Configuration

The accuracy of this experiment depended on the accuracy with which the gamma counter efficiency was known. The efficiency of the counters for detecting gamma rays was measured as a function of energy in the external tagged photon beam of the Caltech Synchrotron. With this information, the efficiency of the counters for detecting π^o production was computed by the Monte Carlo technique. The details of the gamma counter design and efficiency analysis are given in Appendix III.

The electronics to detect the coincidences between the counter signals and count the events is described in Appendix IV.

Lucite calibration runs were used to keep a day-to-day check on the functioning of the equipment. They are described in Appendix V.

For each data point a background run was taken in which the target contained only one atmosphere of hydrogen gas instead of the normal liquid hydrogen. The background runs are discussed in more detail in Appendix VI A.

For the four counter gamma configuration, the side counter rates had to be used to extract the pi pair contaminations from the center counter rates. At $\theta_p^{lab} = 4^o$ and 8^o this correction was not feasible and a correction was made based on extrapolating rates from other angles. The pi pair corrections are discussed in Appendix VI B.

Corrections for nuclear scattering of the protons were based partly on special measurements and partly on calculations using existing scattering data. The corrections to the cross sections were typically 10 to 15 per cent. These corrections are discussed in Part VI C.

With four momentum channels and sixteen possible rates for different combinations of gamma counters for each channel, plus various diagnostic rates, there were a great many rates to record for this experiment. Some of the data was recorded by hand and punched on cards. But the bulk of the data was stored in a 1024 channel pulse height analyzer, via a scaling adaptor designed by H. A. Thiessen (16), and punched onto paper tape for direct processing by the IBM 7094 computer. The card and paper tape data were combined and stored on magnetic disk for further processing. The processing to transform rates to cross sections is described in Appendix VII. Also in Appendix VII is a discussion of errors.

Appendix VIII shows the results of an excitation curve taken by varying the endpoint energy. This serves as a check on the accuracy of the pi pair correction.

Appendix IX contains tables of the measured rates, intermediate results and measured cross sections.

III. CROSS SECTION ENERGY DISTRIBUTIONS

A. Proton plus one gamma

For purposes of assessing the systematic accuracy of the cross sections, energy distributions are more useful than angular distributions.

Figure 6 shows cross sections, before interpolating and averaging, for each of the 13 proton laboratory angles used in this experiment. The square symbols denote measurements with the 1200 MeV/c magnet configuration. The diamonds denote measurements with 1670 MeV/c magnet configuration. The symbols are open if the gamma counters were in the four counter configuration and filled in if they were in the veto configuration.

Comparing the open diamonds and open squares where they overlap indicates very good agreement between the two magnet configurations.

Comparing closed squares to the open squares indicates that the veto results may be systematically about 10% low with respect to the four counter configuration results. The difference has the wrong sign to be caused by neutral pi pair contamination. If neutral pairs were at fault, the veto configuration would count them and give cross sections that would be higher than the four counter cross sections.

In Part V, comparisons with other experiments are shown which indicate that our data are 15% low at 90° at the second resonance. Since those cross sections were measured by the veto configuration, it appears that it is the veto configuration results, rather than the four counter configuration results, which are in

Figure 6

Energy distributions before interpolating and averaging. Along with θ_p^{lab} is $\langle \theta_{\pi^o}^{cm} \rangle$, the average $\theta_{\pi^o}^{cm}$ for the points shown.

The symbol code is as follows:

	Magnet Configuration	Gamma Counter Configuration
□	1200 MeV/c	four counter
■	1200 MeV/c	veto
◇	1670 MeV/c	four counter
◆	1670 MeV/c	veto

Figure 6.1

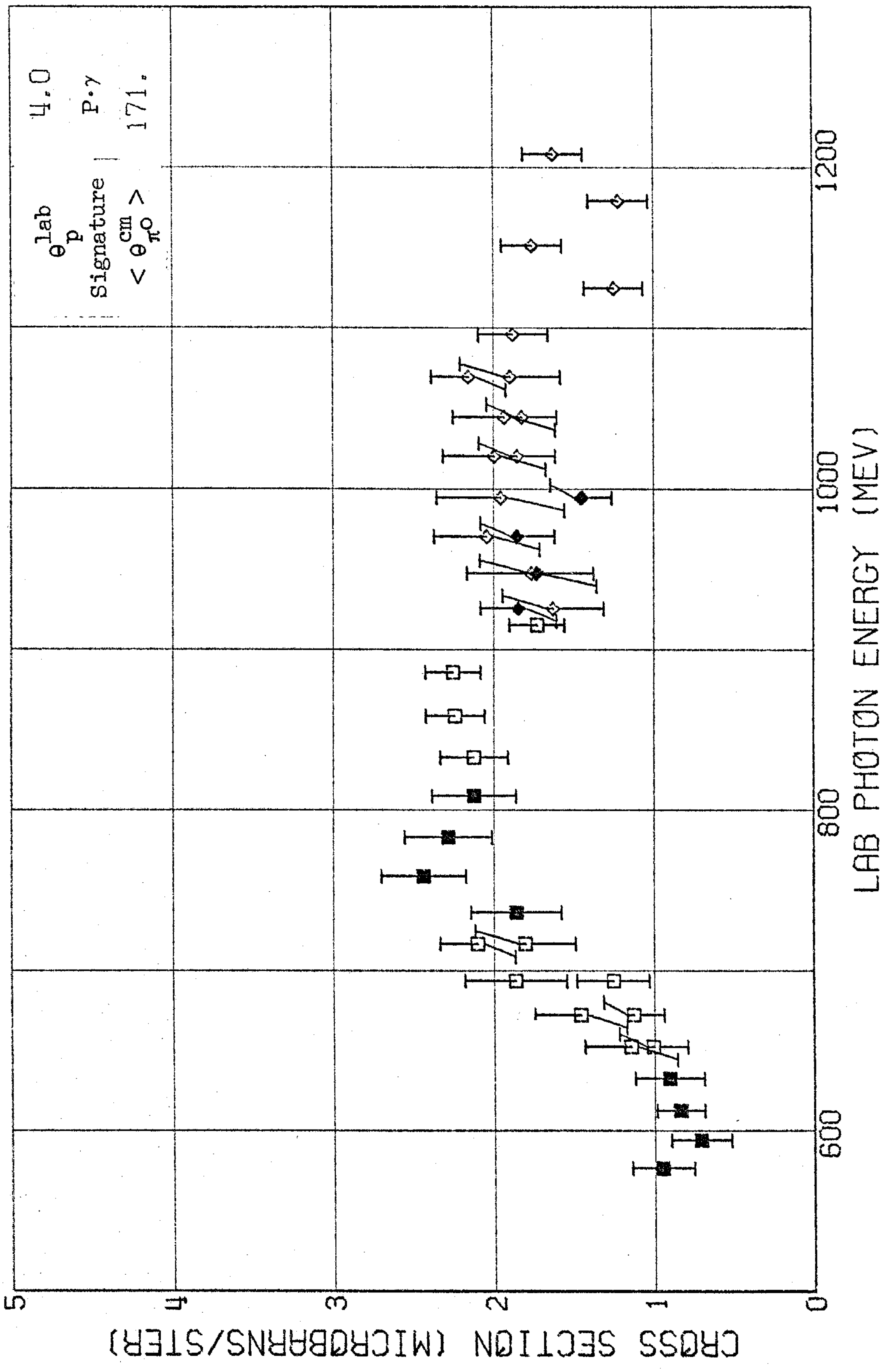

CROSS SECTION (MICROBARNS/STER)
0
1
2
3
4
5
LAB PHOTON ENERGY (MEV)
600
800
1000
1200
θ_p^{lab} 4.0
Signature P·γ
$< \theta_{\pi^o}^{cm} >$ 171.

Figure 6.2

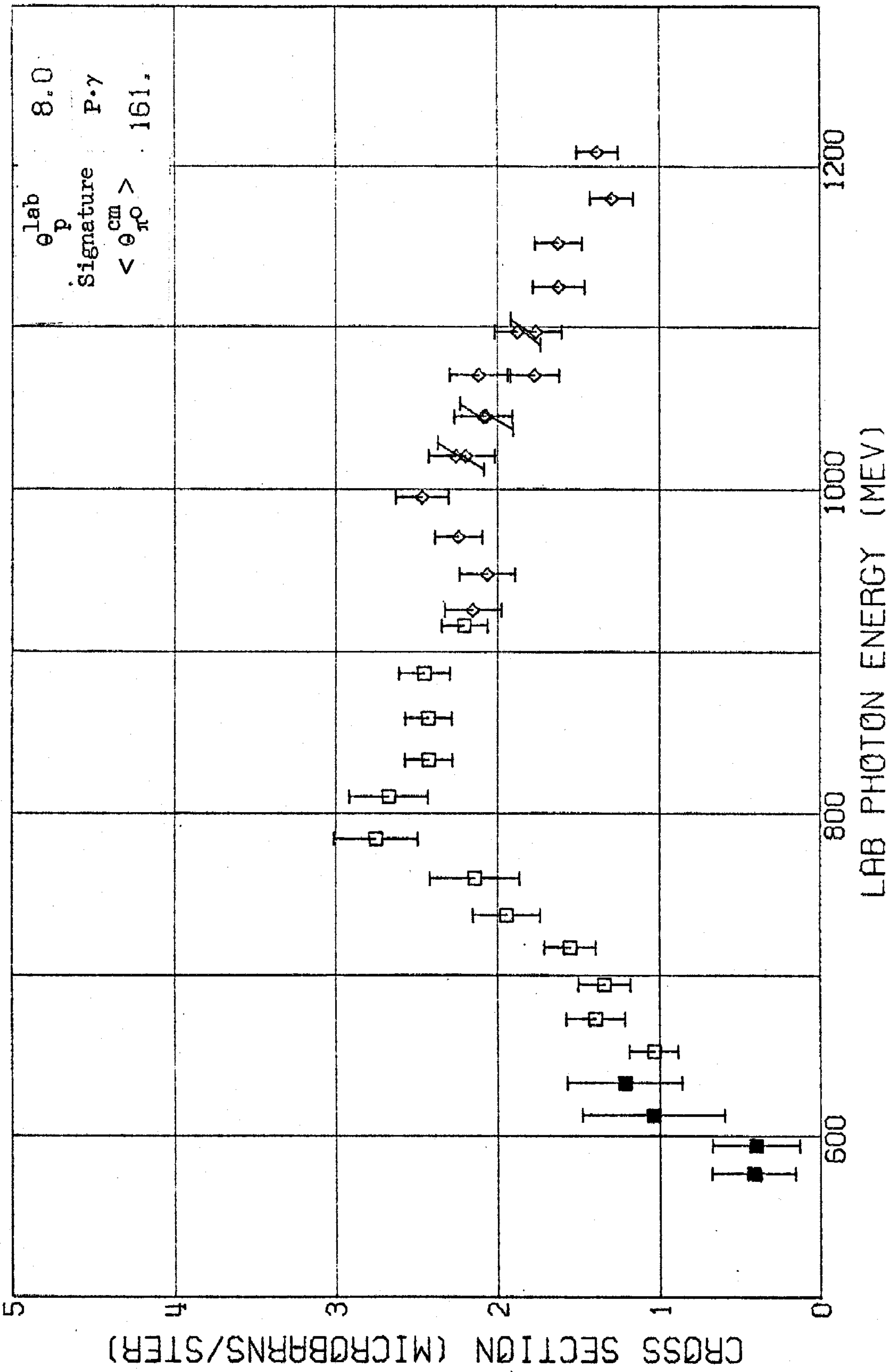

θ_p^{lab} 8.0
Signature P·γ
$< \theta_{\pi^o}^{cm} >$ 161.
LAB PHOTON ENERGY (MEV)
CROSS SECTION (MICROBARNS/STER)
600
800
1000
1200
0
1
2
3
4
5

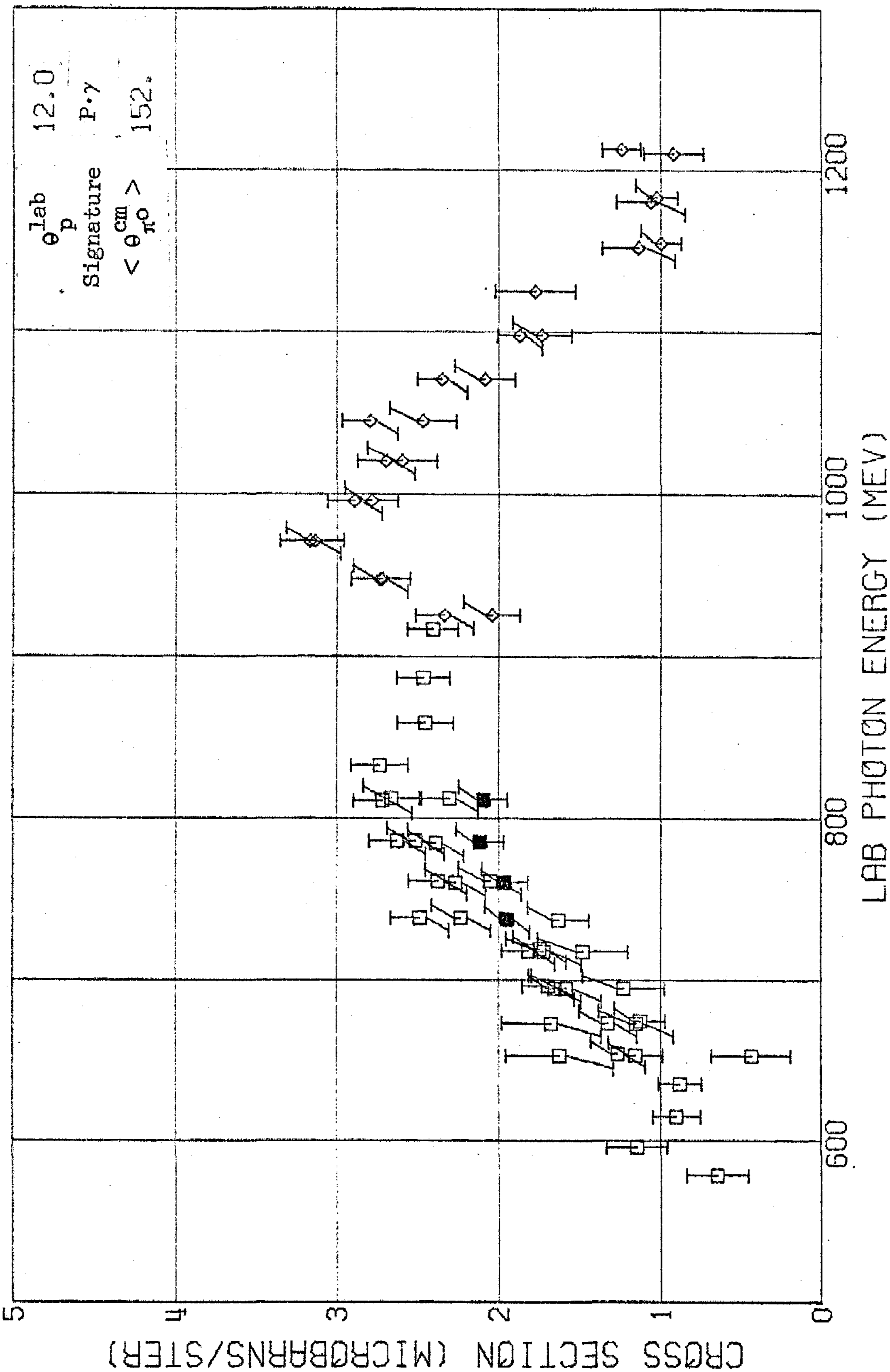
θ_p^lab 12.0
Signature P·γ
< θ_π°^cm > 152.
CROSS SECTION (MICROBARNS/STER)
0
1
2
3
4
5
LAB PHOTON ENERGY (MEV)
600
800
1000
1200

Figure 6.3

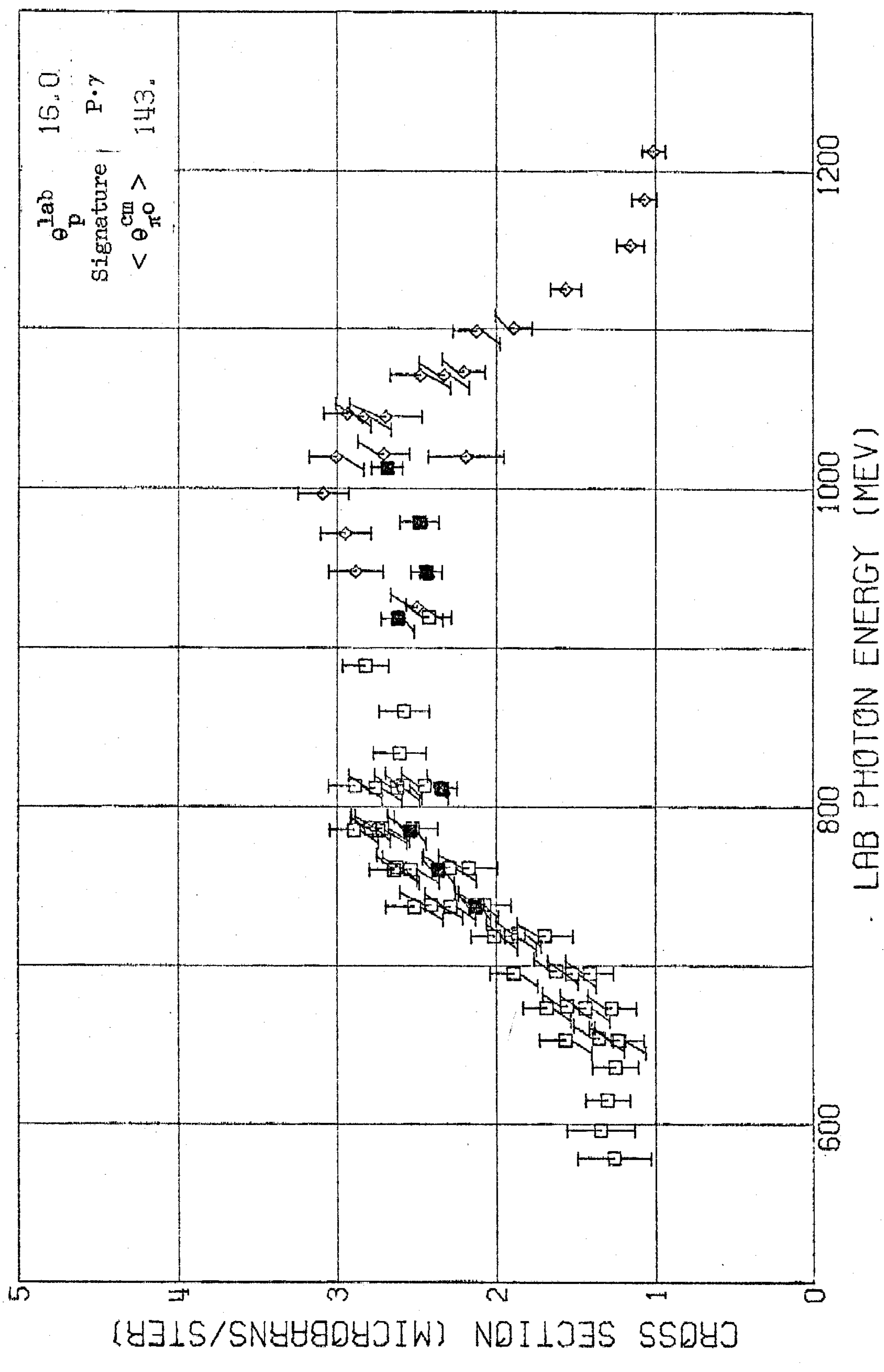

θ_p^{lab} 16.0
Signature P·γ
$< \theta_{\pi^o}^{cm} >$ 143.
CROSS SECTION (MICROBARNS/STER)
LAB PHOTON ENERGY (MEV)
0
1
2
3
4
5
600
800
1000
1200

Figure 6.4

Figure 6.5

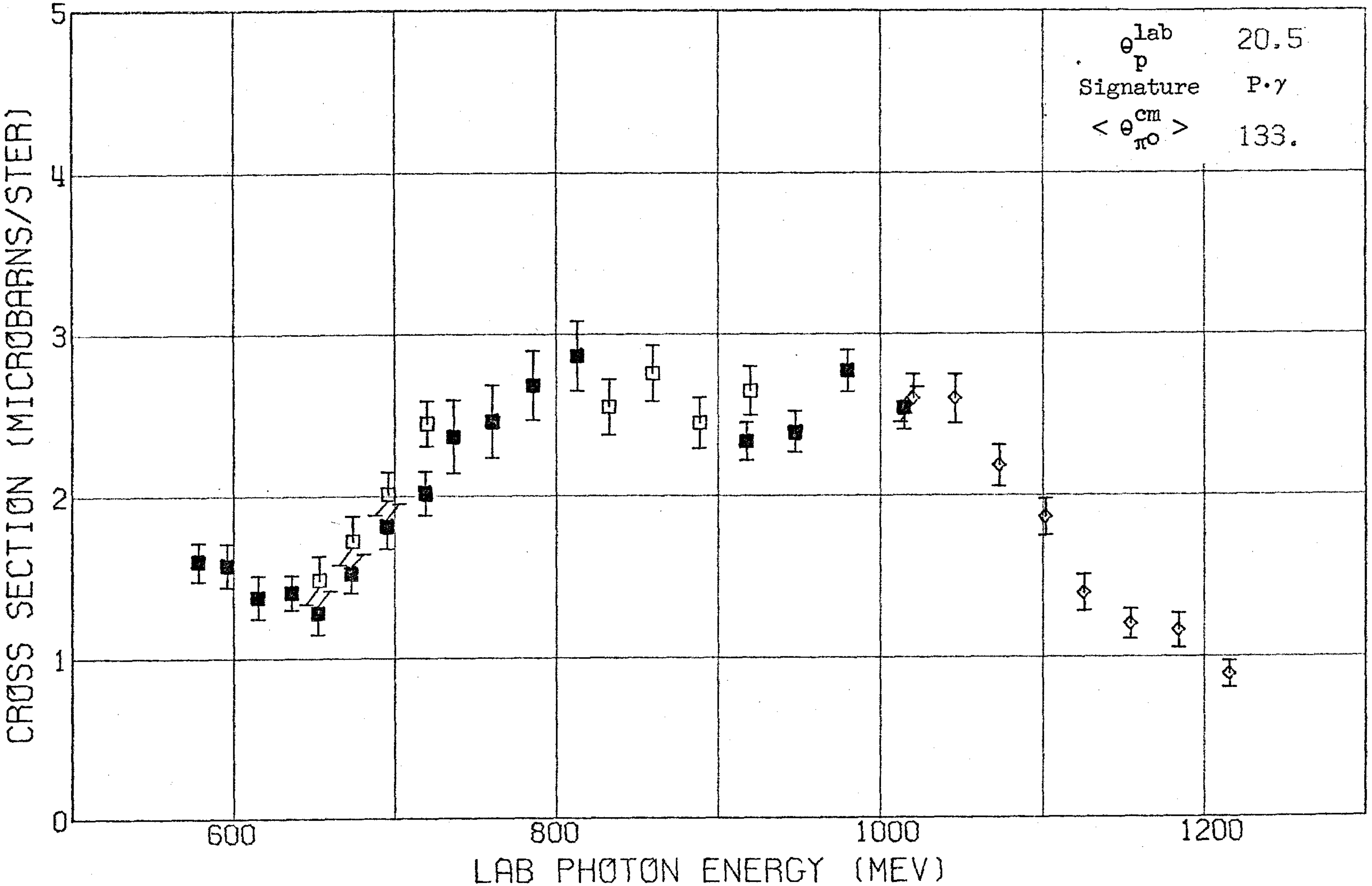
θ_p^lab 20.5
Signature P·γ
< θ_π°^cm > 133.
5
4
3
2
1
0
600
800
1000
1200
CROSS SECTION (MICROBARNS/STER)
LAB PHOTON ENERGY (MEV)

Figure 6.6

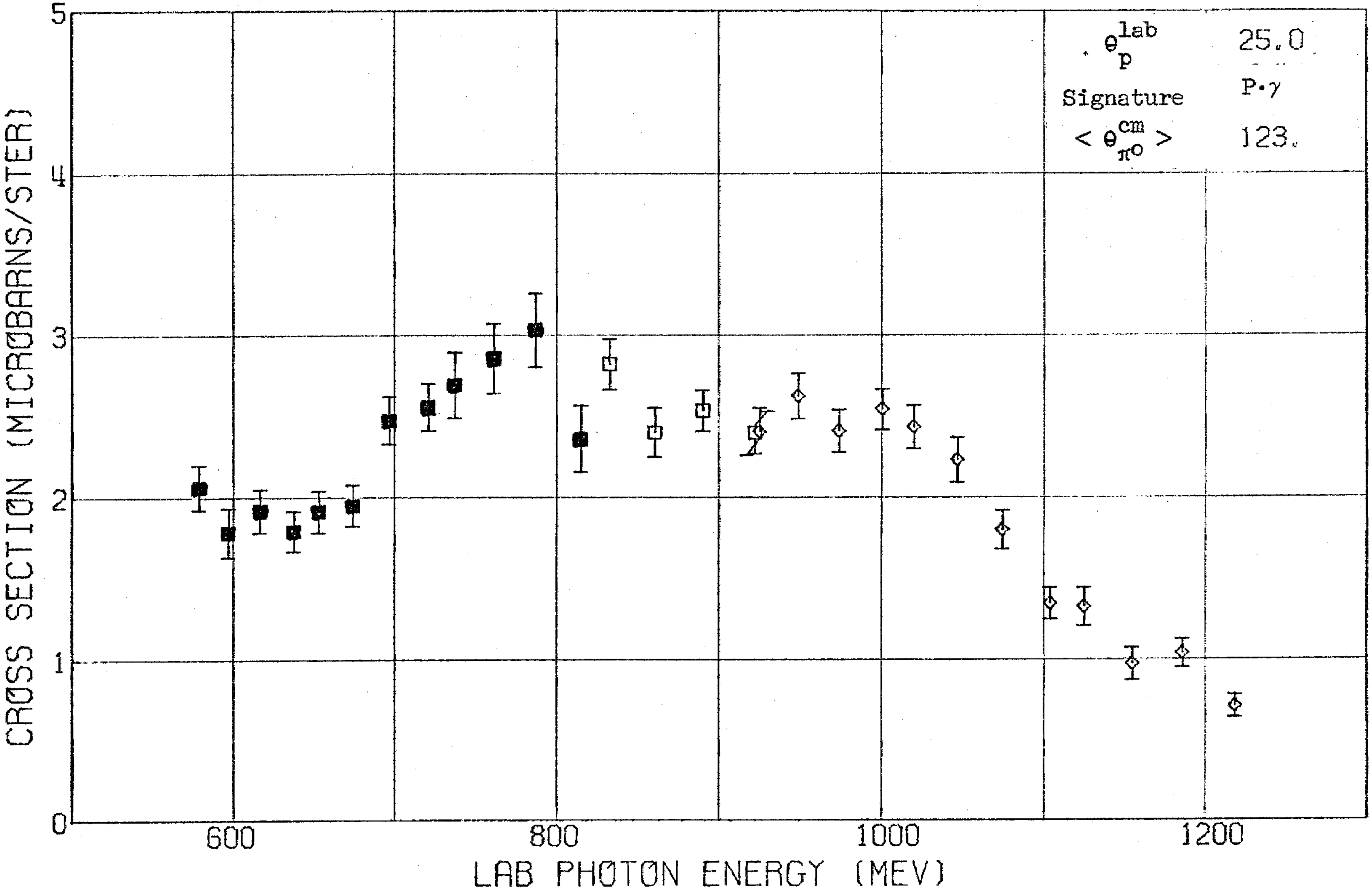
θ_p^{lab} 25.0
Signature P·γ
$< \theta_{\pi^o}^{cm} >$ 123.
CROSS SECTION (MICROBARNS/STER)
0
1
2
3
4
5
600
800
1000
1200
LAB PHOTON ENERGY (MEV)

Figure 6.7

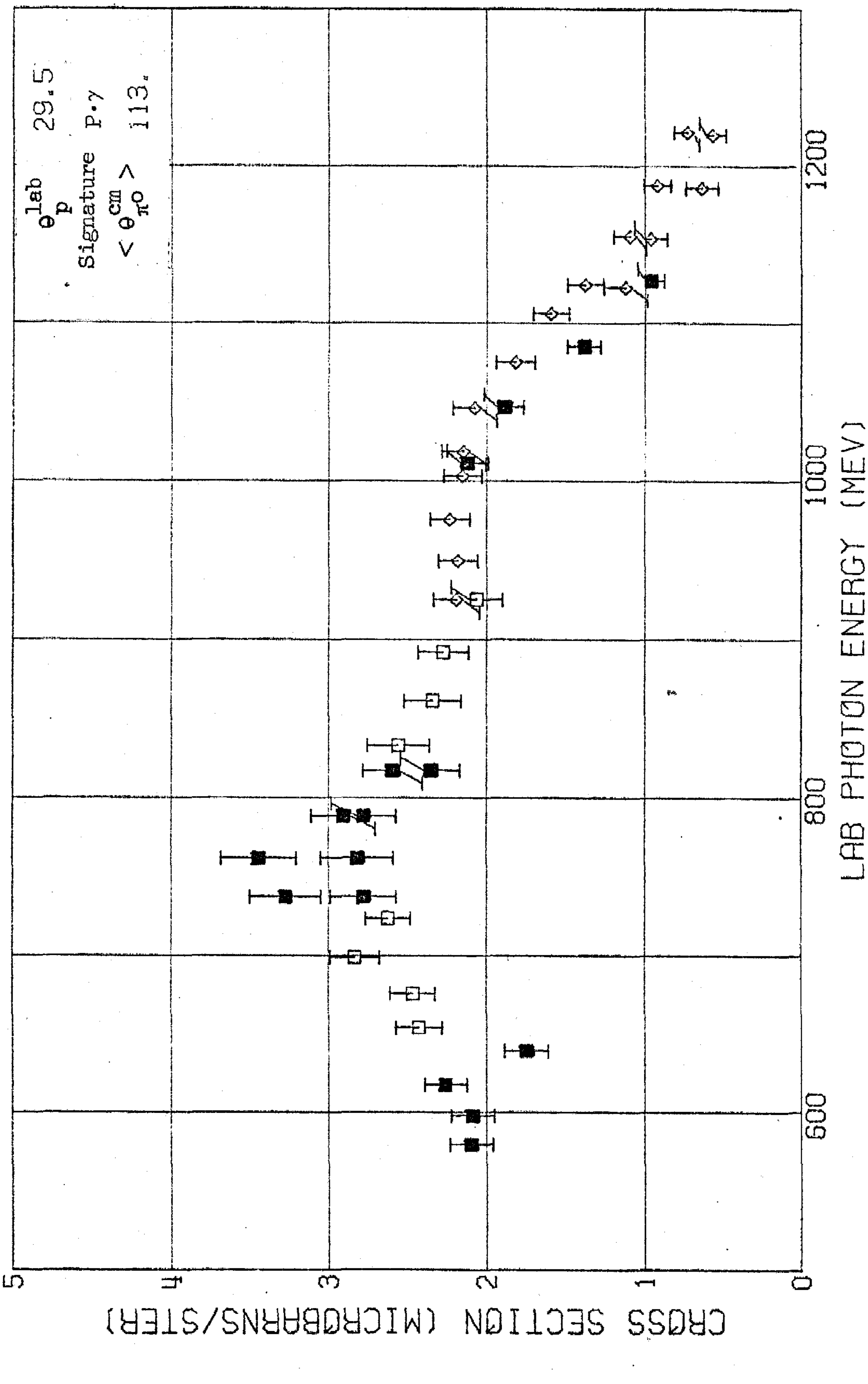
θ$_p^{lab}$ 29.5
Signature P·γ
< θ$_{\pi^0}^{cm}$ > 113.
600
800
1000
1200
LAB PHOTON ENERGY (MEV)
0
1
2
3
4
5
CROSS SECTION (MICROBARNS/STER)

Figure 6.8

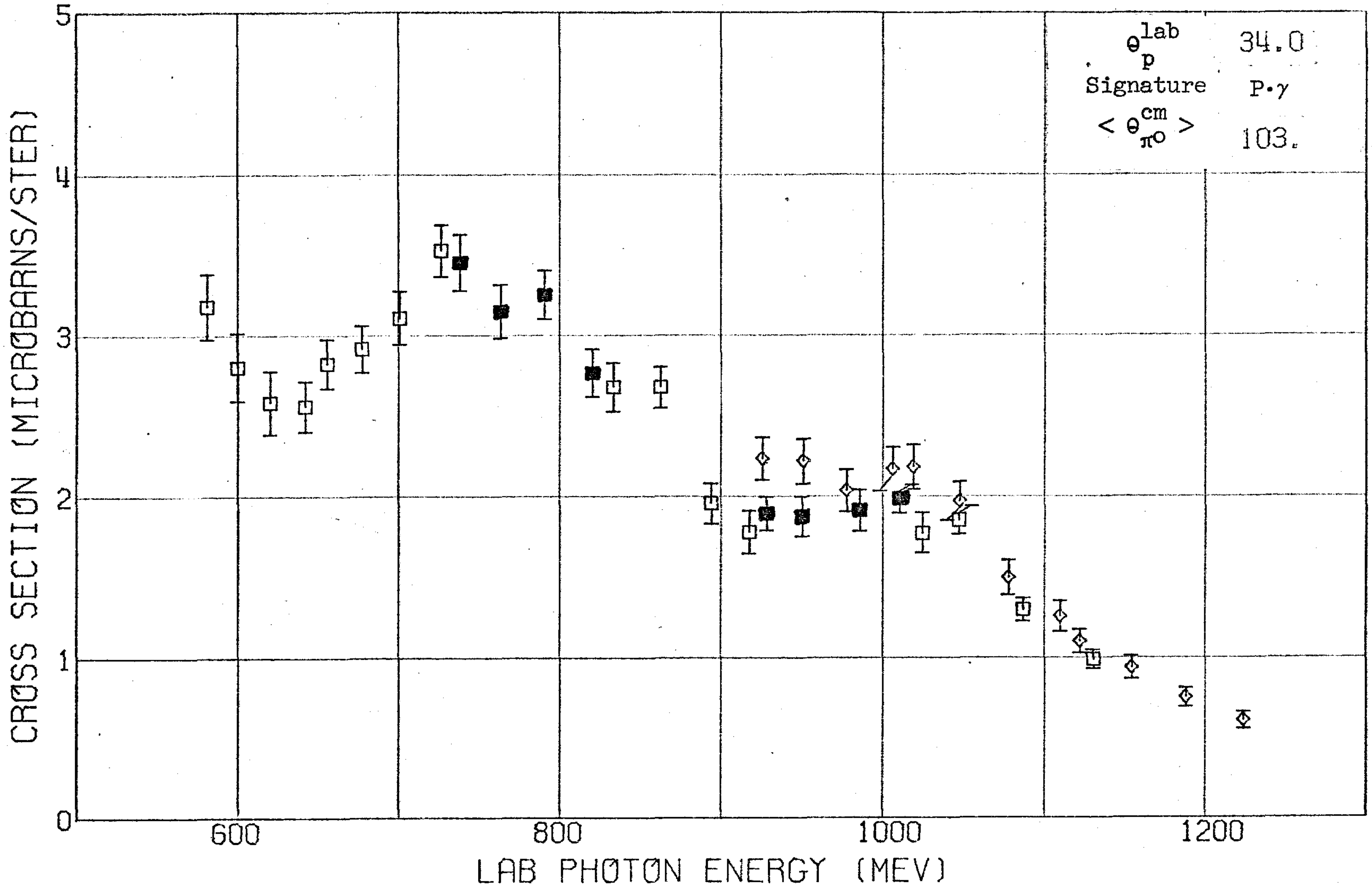

CROSS SECTION (MICROBARNS/STER)
LAB PHOTON ENERGY (MEV)
0
1
2
3
4
5
600
800
1000
1200
θ_p^lab 34.0
Signature P·γ
< θ_π0^cm > 103.

Figure 6.9

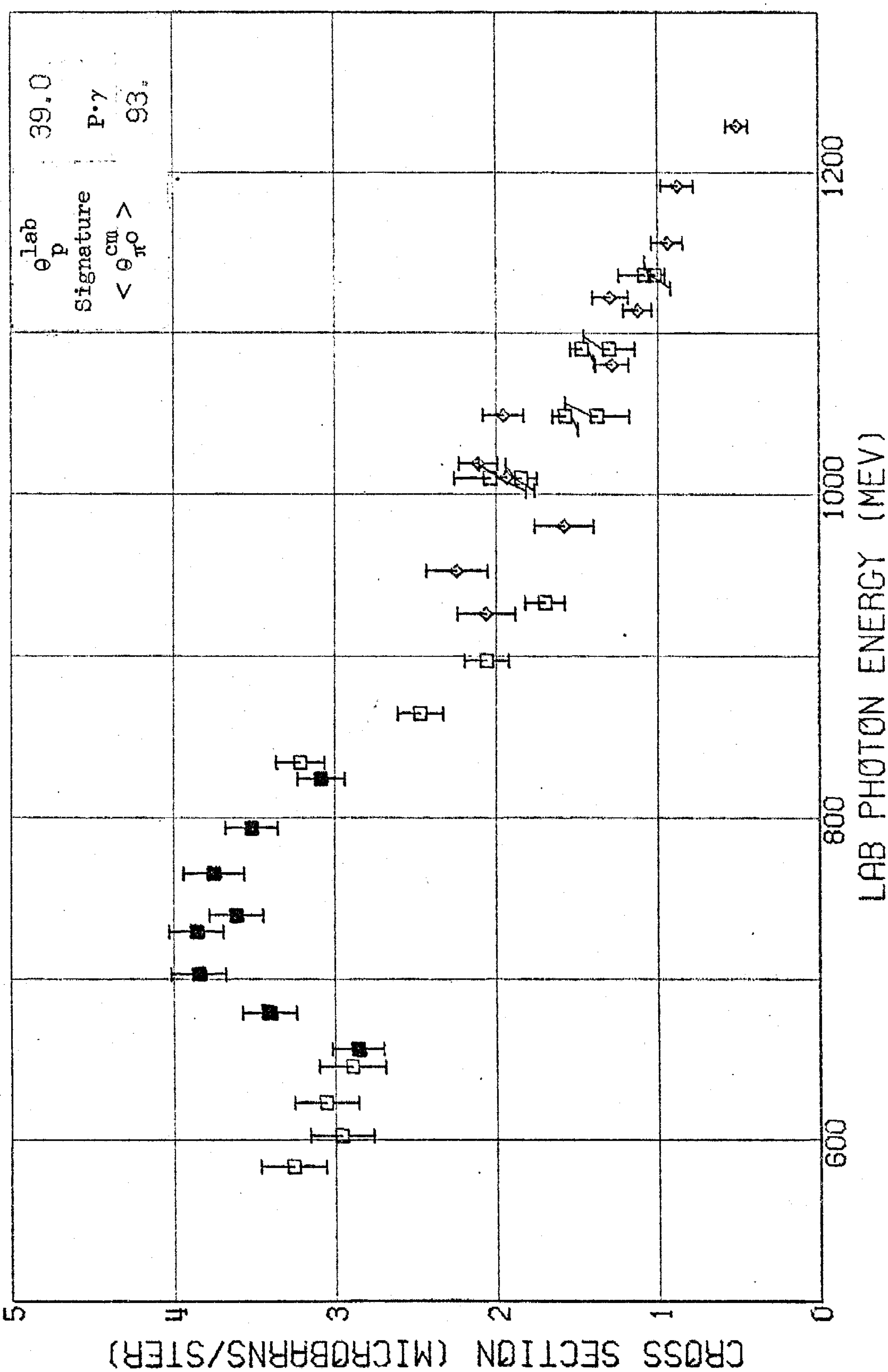

θ_p^{lab} 39.0
Signature P·γ
$< \theta_{\pi^0}^{cm} >$ 93.
CROSS SECTION (MICROBARNS/STER)
0
1
2
3
4
5
LAB PHOTON ENERGY (MEV)
600
800
1000
1200

Figure 6.10

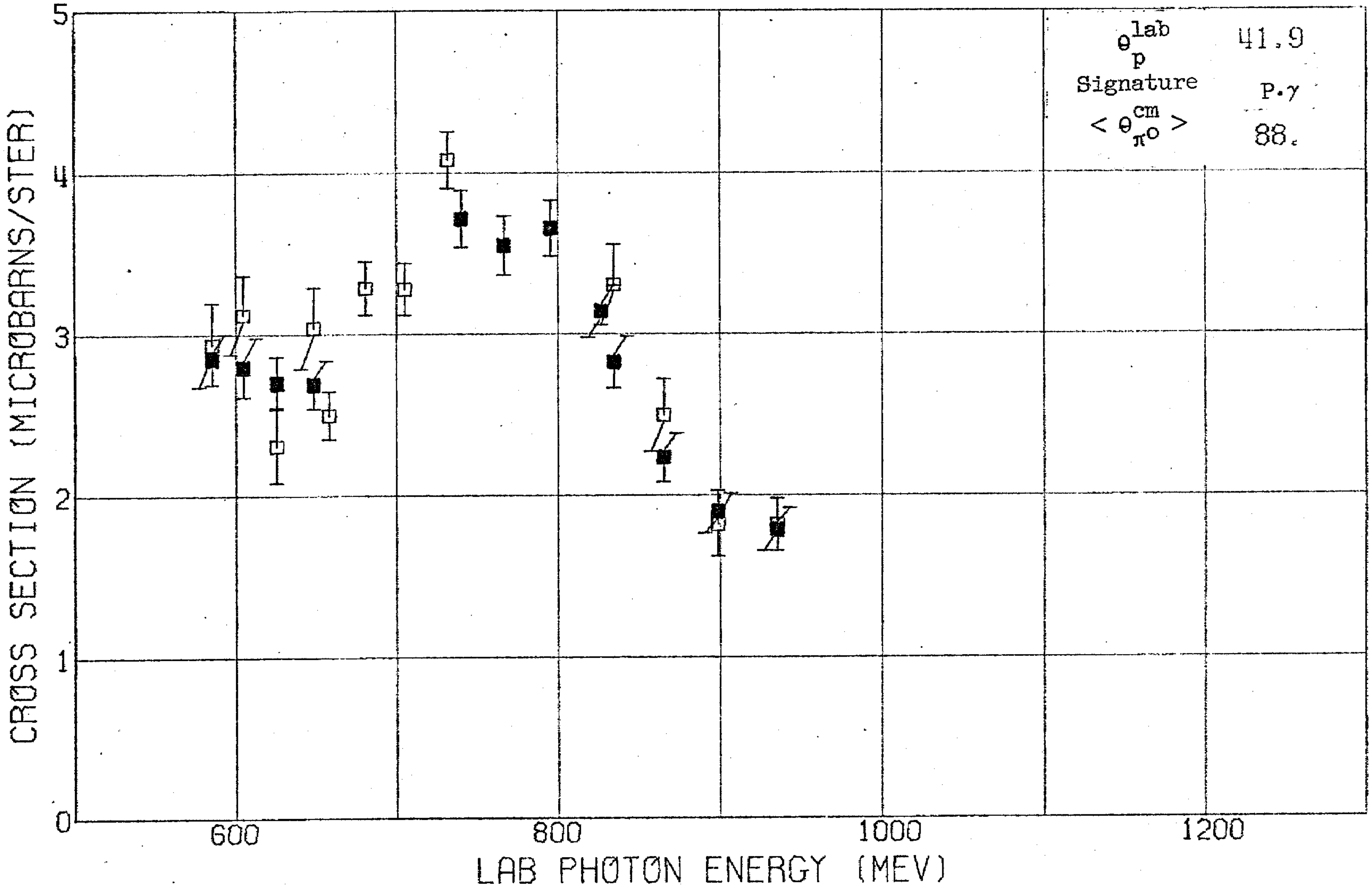

θ_p^{lab} 41.9
Signature P·γ
$< \theta_{\pi^o}^{cm} >$ 88.
5
4
3
2
1
0
600
800
1000
1200
CROSS SECTION (MICROBARNS/STER)
LAB PHOTON ENERGY (MEV)

Figure 6.11

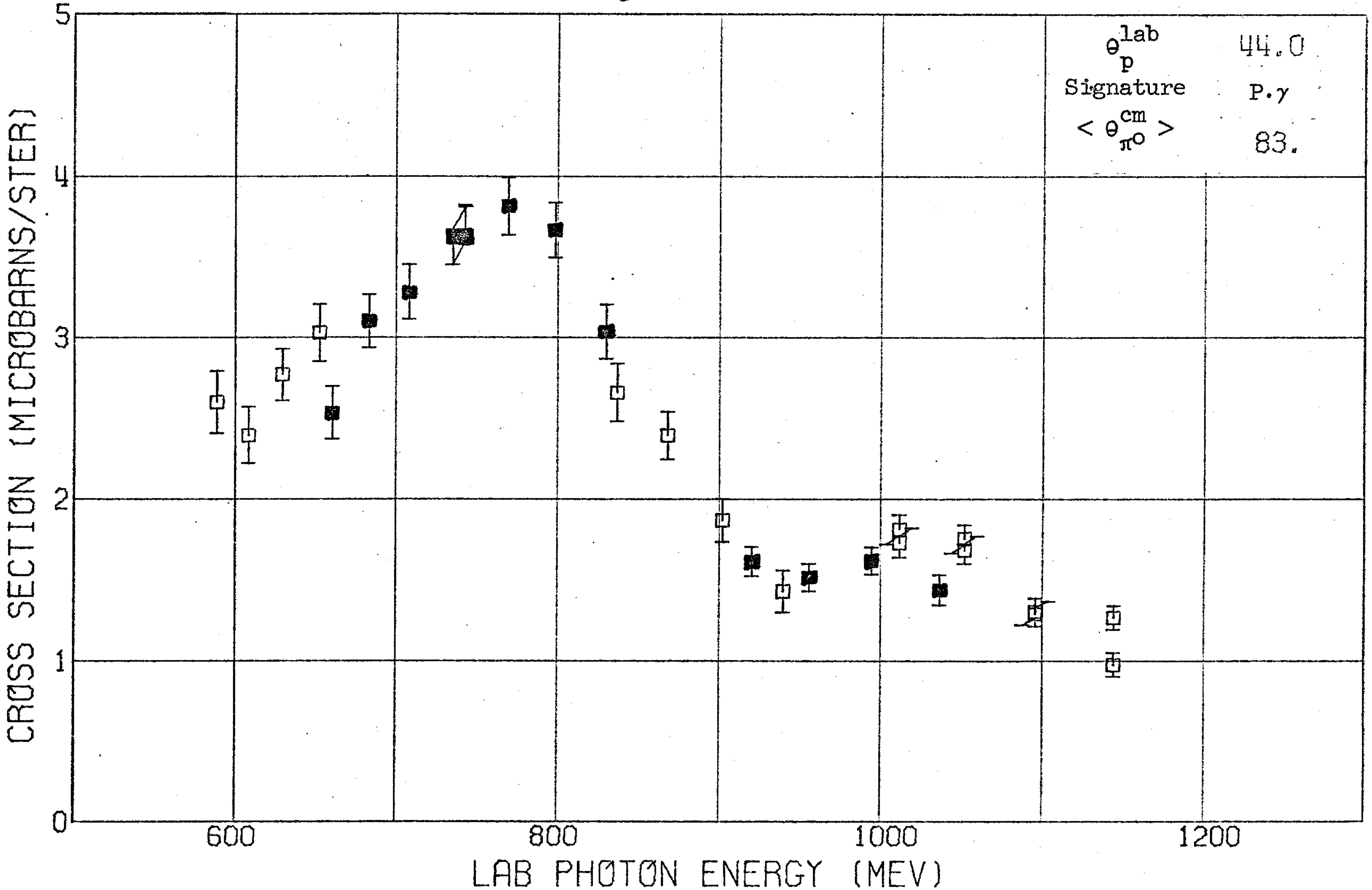

θ_p^{lab} 44.0
Signature P.γ
$< \theta_{\pi^0}^{cm} >$ 83.
CROSS SECTION (MICROBARNS/STER)
LAB PHOTON ENERGY (MEV)
0
1
2
3
4
5
600
800
1000
1200

Figure 6. 12

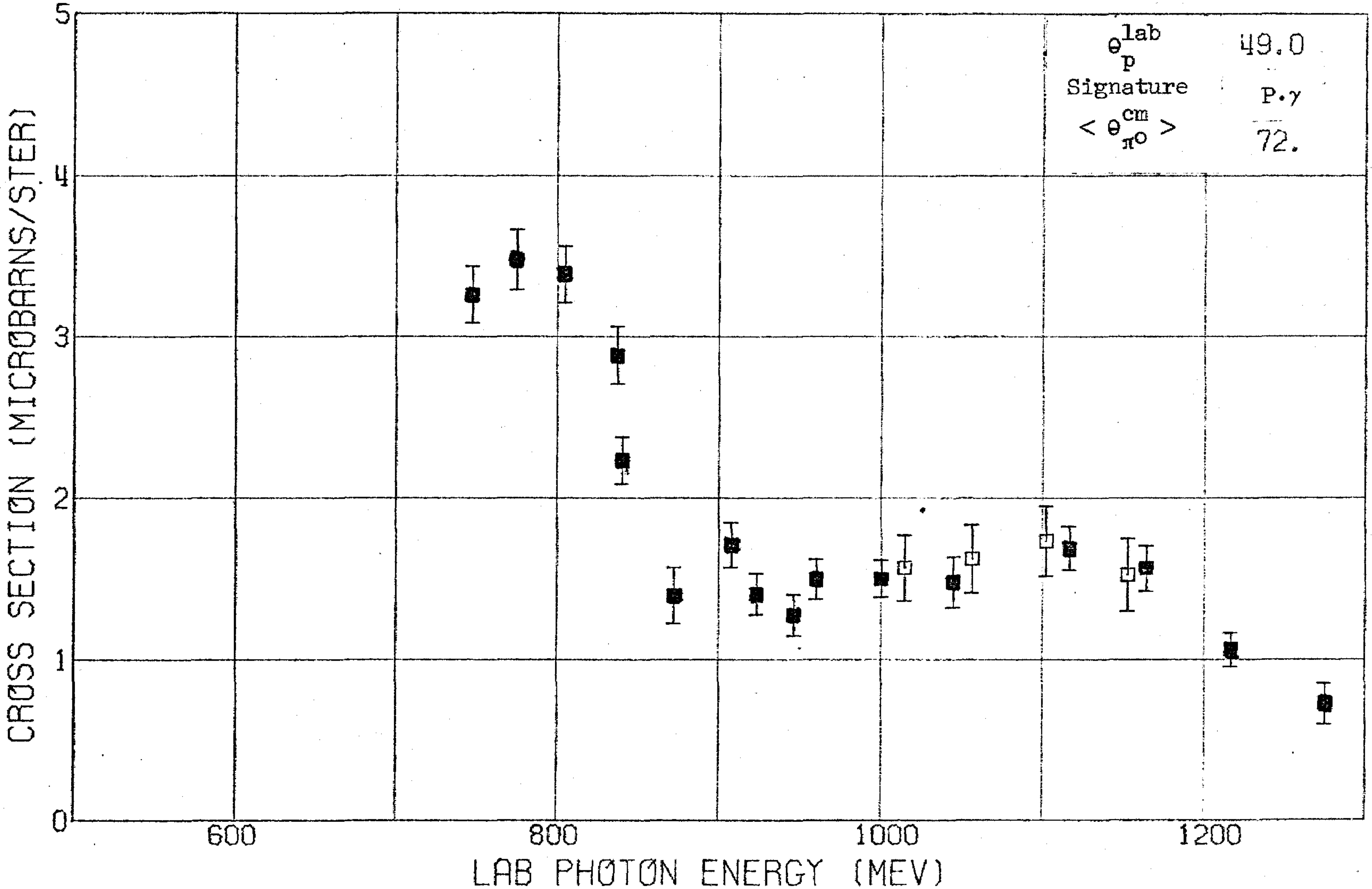
θ_p^{lab} 49.0
Signature P·γ
$< \theta_{\pi^o}^{cm} >$ 72.
CROSS SECTION (MICROBARNS/STER)
LAB PHOTON ENERGY (MEV)
0
1
2
3
4
5
600
800
1000
1200

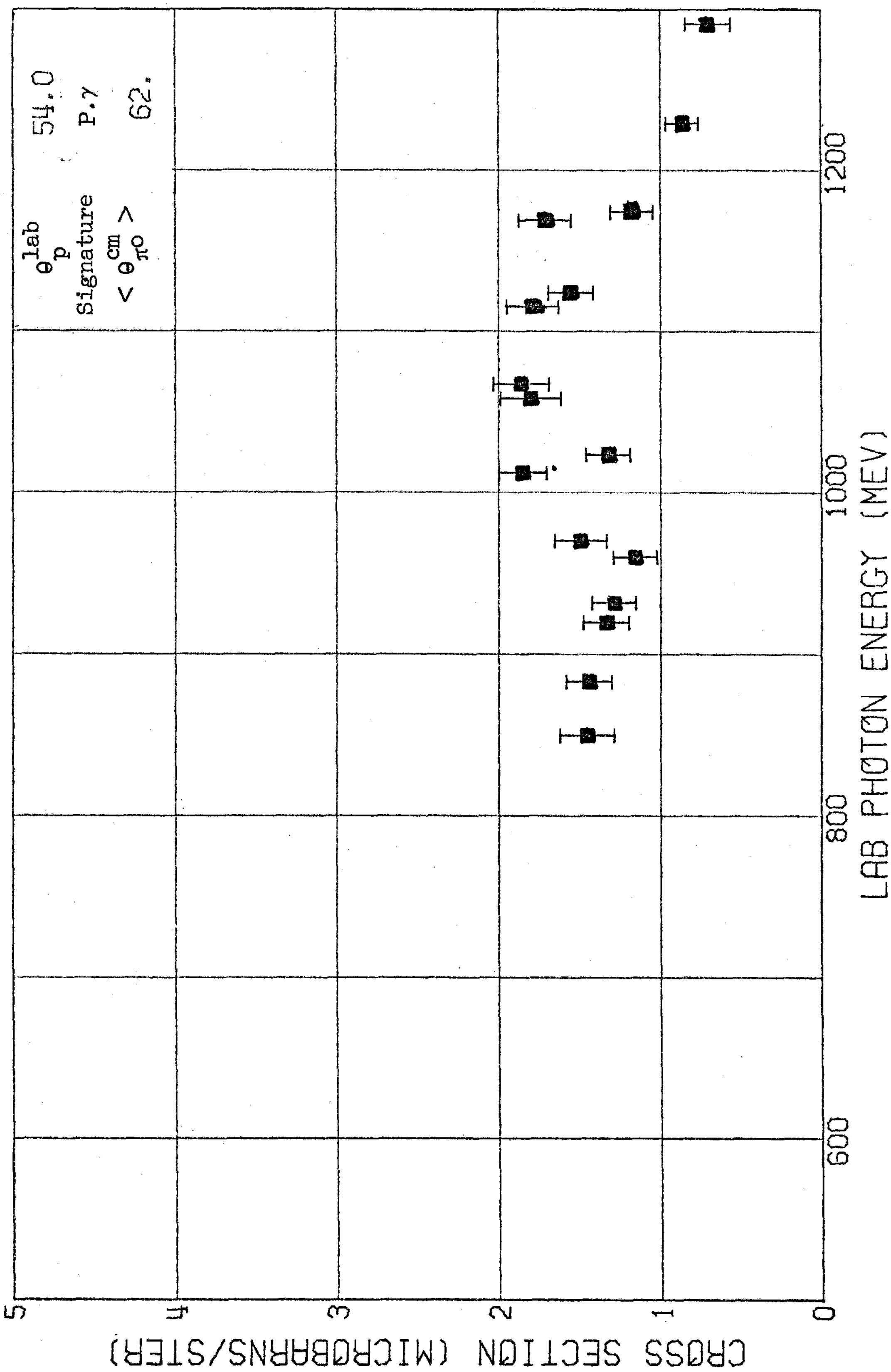
θ_p^{lab} 54.0
Signature P.γ
$< \theta_{\pi^o}^{cm} >$ 62.
LAB PHOTON ENERGY (MEV)
600
800
1000
1200
CROSS SECTION (MICROBARNS/STER)
0
1
2
3
4
5

Figure 6.13

error. Of course, the error, if it exists, may have nothing to do with the veto configuration. Something else may have been wrong during the time the veto data were being taken.

It is possible to use the energy distributions to check for pi pair contamination. If pi pairs are being counted, the contamination will normally be largest in the bottom channel of the spectrometer. Since each set of four cross sections in a distribution comes from the four channels of a given magnet setting, one can simply look for jumps in the cross section every fourth channel. The absence of jumps in the graphs of Figure 6 indicates that there is probably no pi pair contamination in the $P \cdot \gamma$ signature cross sections.

Figure 7 shows the final cross sections obtained after interpolating and averaging the data as explained in Appendix VII. At some points the values to be averaged were farther apart than would have been expected from their errors. In such cases the error on the result was increased to the error in the mean of a distribution with the observed spread. Tables of these cross sections appear in Part IV.

Even with the improved statistical accuracy of the averaged points, there is no pi pair contamination apparent.

Most of the curves show pronounced peaks at the second and third resonances.

The curves through the points were drawn freehand and are for the purpose of aiding comparisons in the next two parts.

Figure 7

Energy distributions of final cross sections.

Along with θ_p^{lab} is given $\langle \theta_{\pi^o}^{cm} \rangle$, the average of $\theta_{\pi^o}^{cm}$ for the points shown.

Figure 7.1

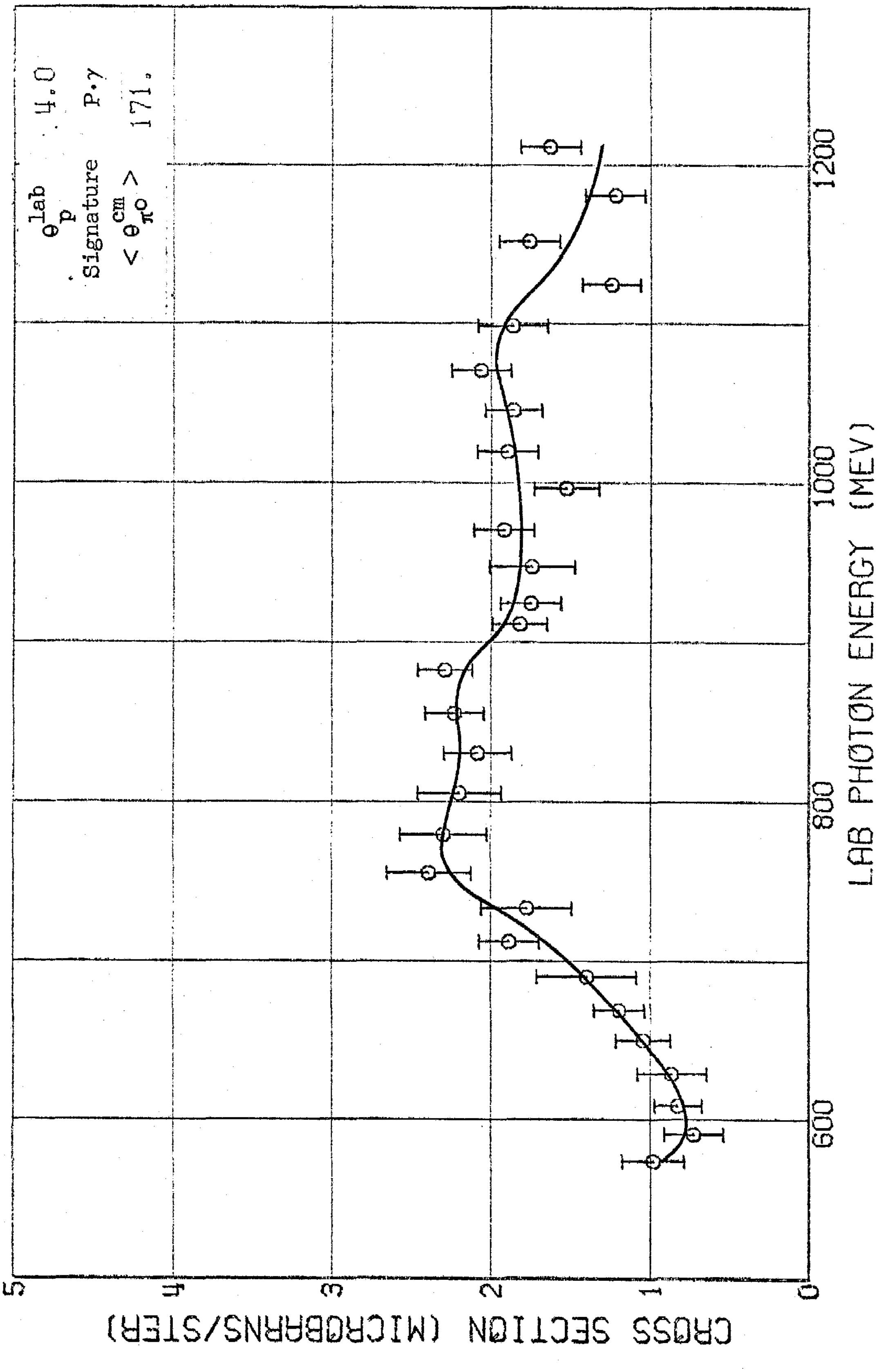
θ_p^{lab} 4.0
Signature P.γ
$< \theta_{\pi^o}^{cm} >$ 171.
LAB PHOTON ENERGY (MEV)
CROSS SECTION (MICROBARNS/STER)
600
800
1000
1200
0
1
2
3
4
5

Figure 7.2

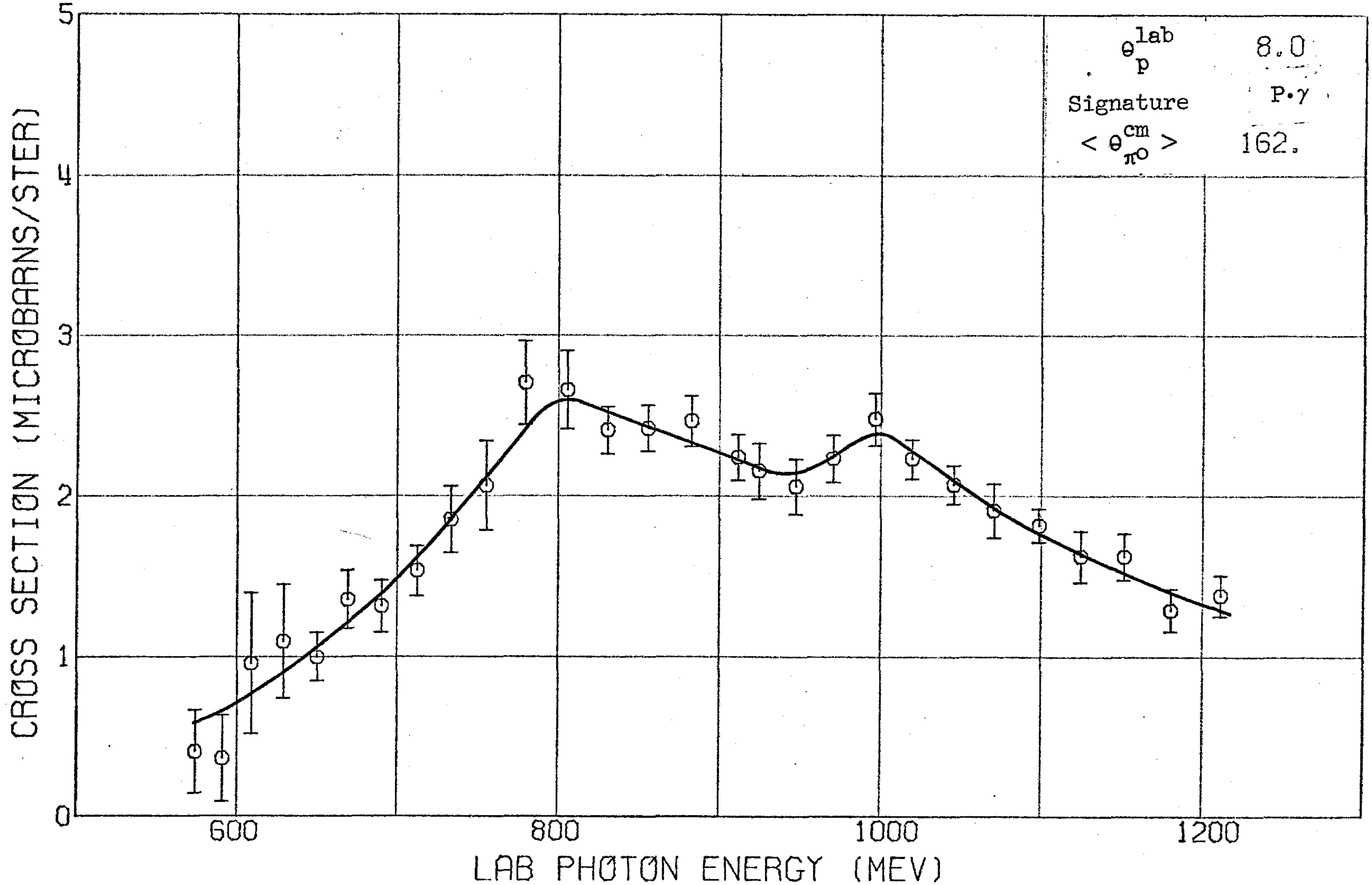

θ_p^{lab} 8.0
Signature P·γ
$< \theta_{\pi^o}^{cm} >$ 162.
CROSS SECTION (MICROBARNS/STER)
LAB PHOTON ENERGY (MEV)
0
1
2
3
4
5
600
800
1000
1200

Figure 7.3

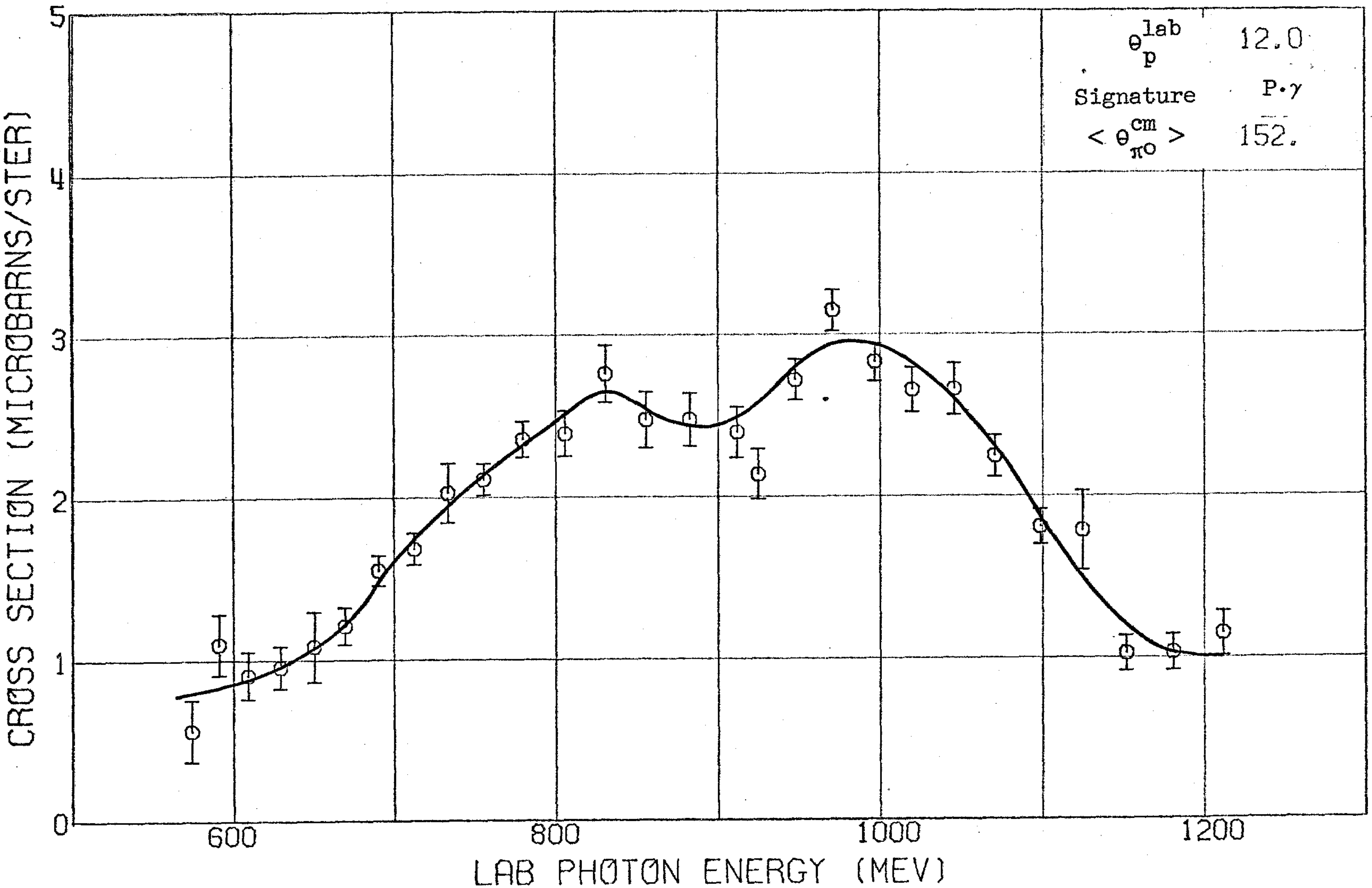
θ_p^lab 12.0
Signature P·γ
< θ_π0^cm > 152.
CRØSS SECTIØN (MICRØBARNS/STER)
0
1
2
3
4
5
600
800
1000
1200
LAB PHØTØN ENERGY (MEV)

Figure 7.4

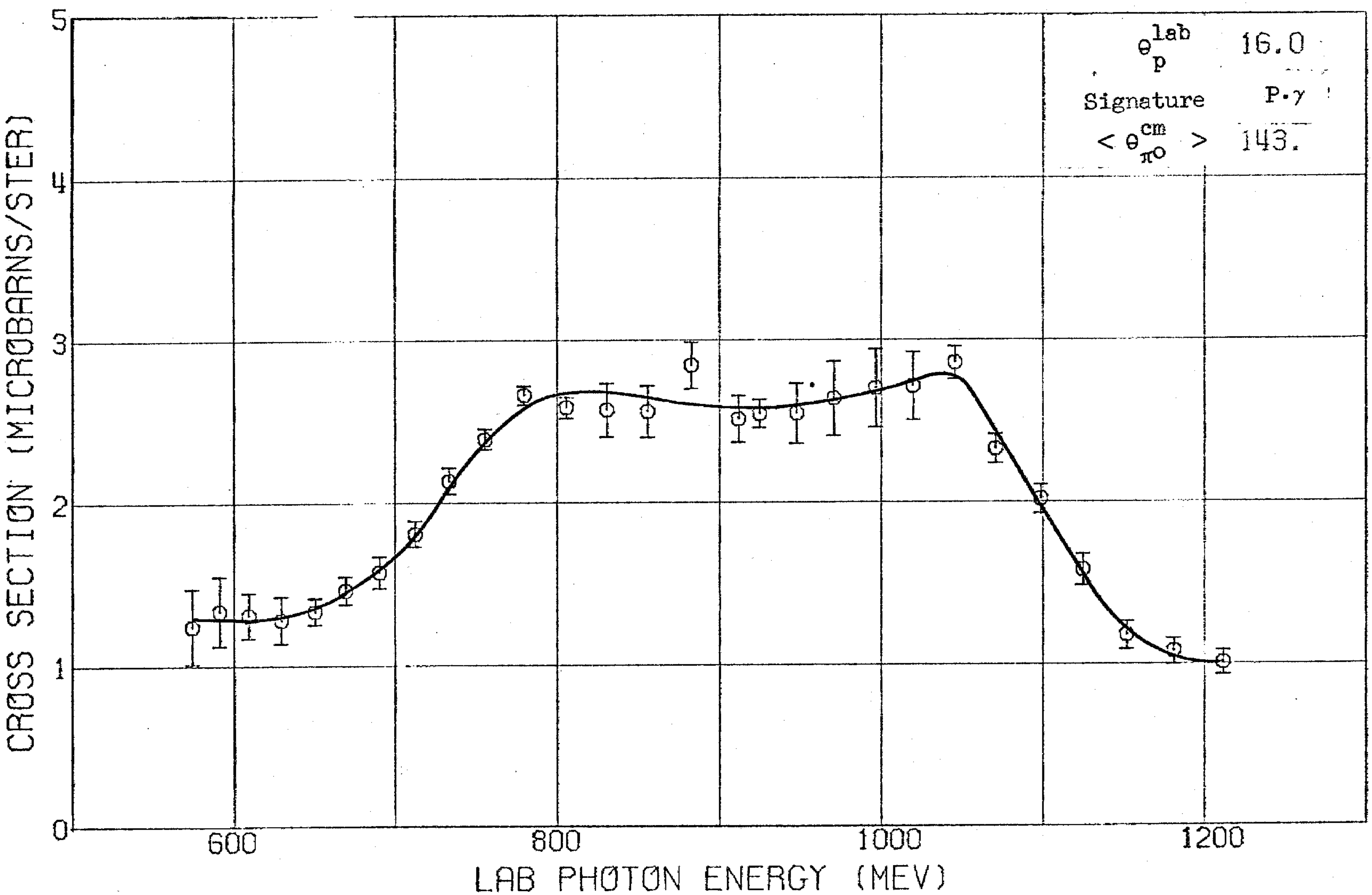

θ_p^{lab} 16.0
Signature P·γ
$< \theta_{\pi^0}^{cm} >$ 143.
CROSS SECTION (MICROBARNS/STER)
0
1
2
3
4
5
600
800
1000
1200
LAB PHOTON ENERGY (MEV)

Figure 7.5

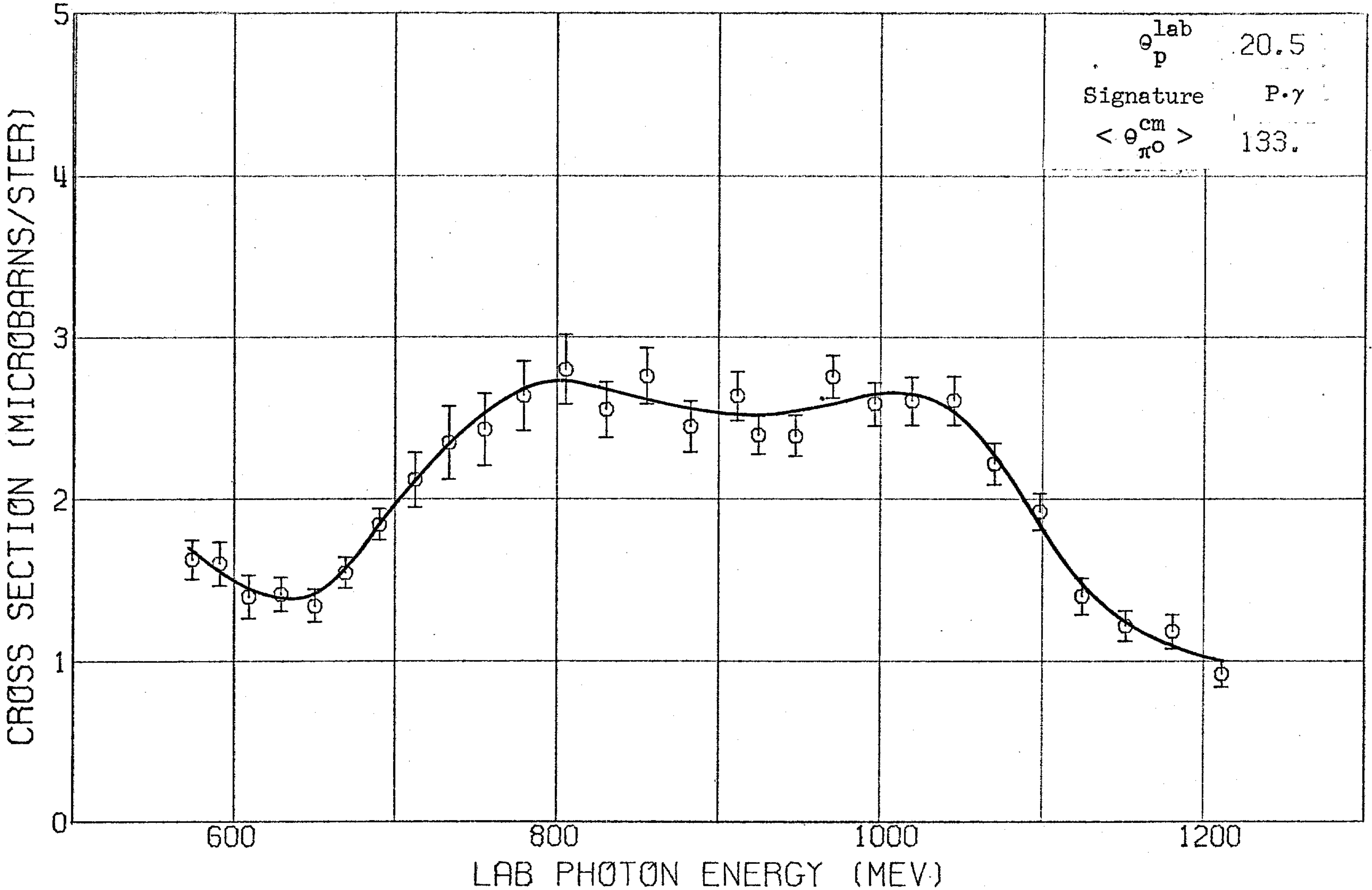
θ_p^{lab} 20.5
Signature P·γ
$< \theta_{\pi^0}^{cm} >$ 133.
CROSS SECTION (MICROBARNS/STER)
0
1
2
3
4
5
600
800
1000
1200
LAB PHOTON ENERGY (MEV)

Figure 7.6

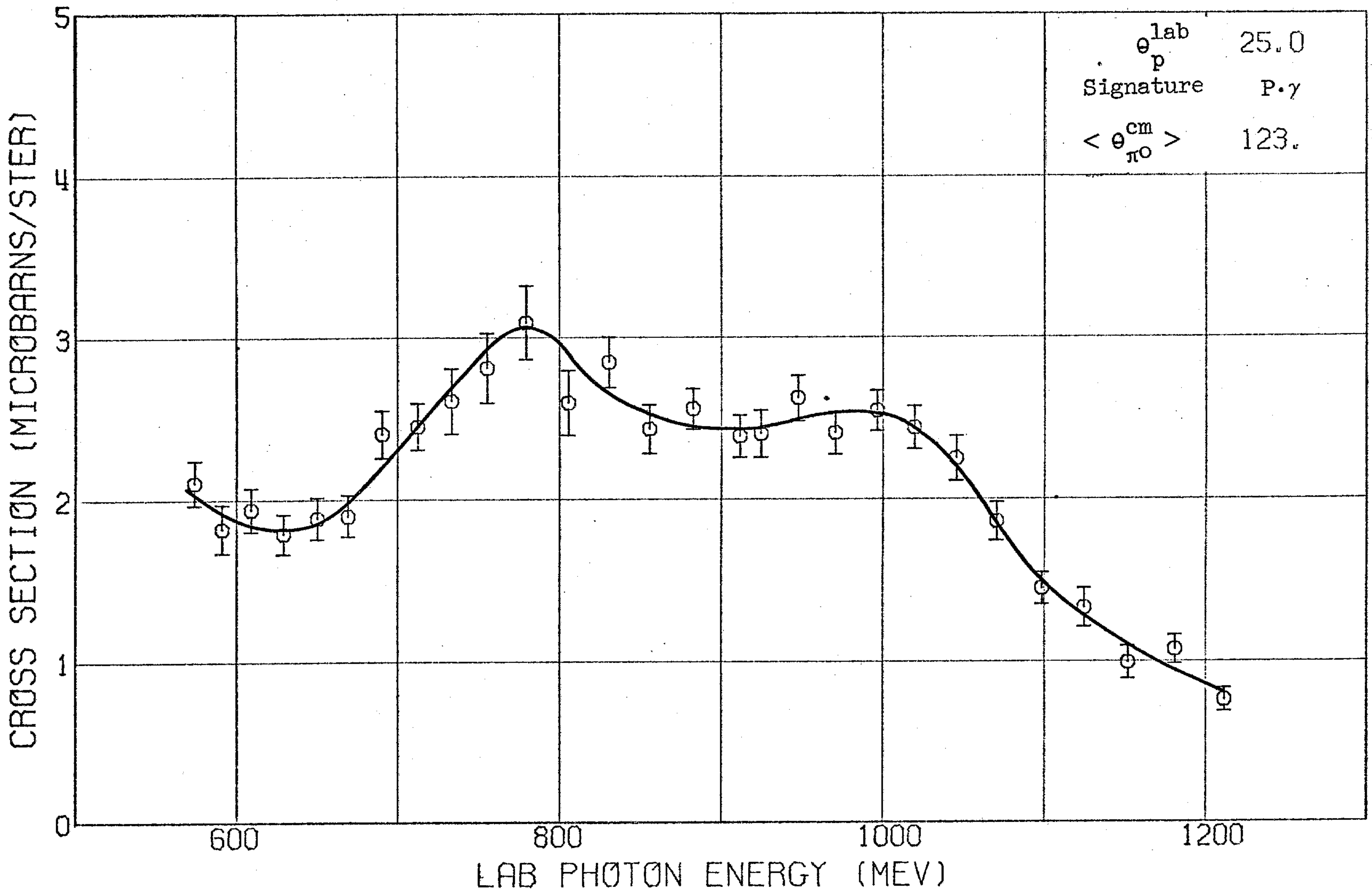

θ_p^{lab} 25.0
Signature P·γ
$< \theta_{\pi^0}^{cm} >$ 123.
CROSS SECTION (MICROBARNS/STER)
0
1
2
3
4
5
600
800
1000
1200
LAB PHOTON ENERGY (MEV)

Figure 7.7

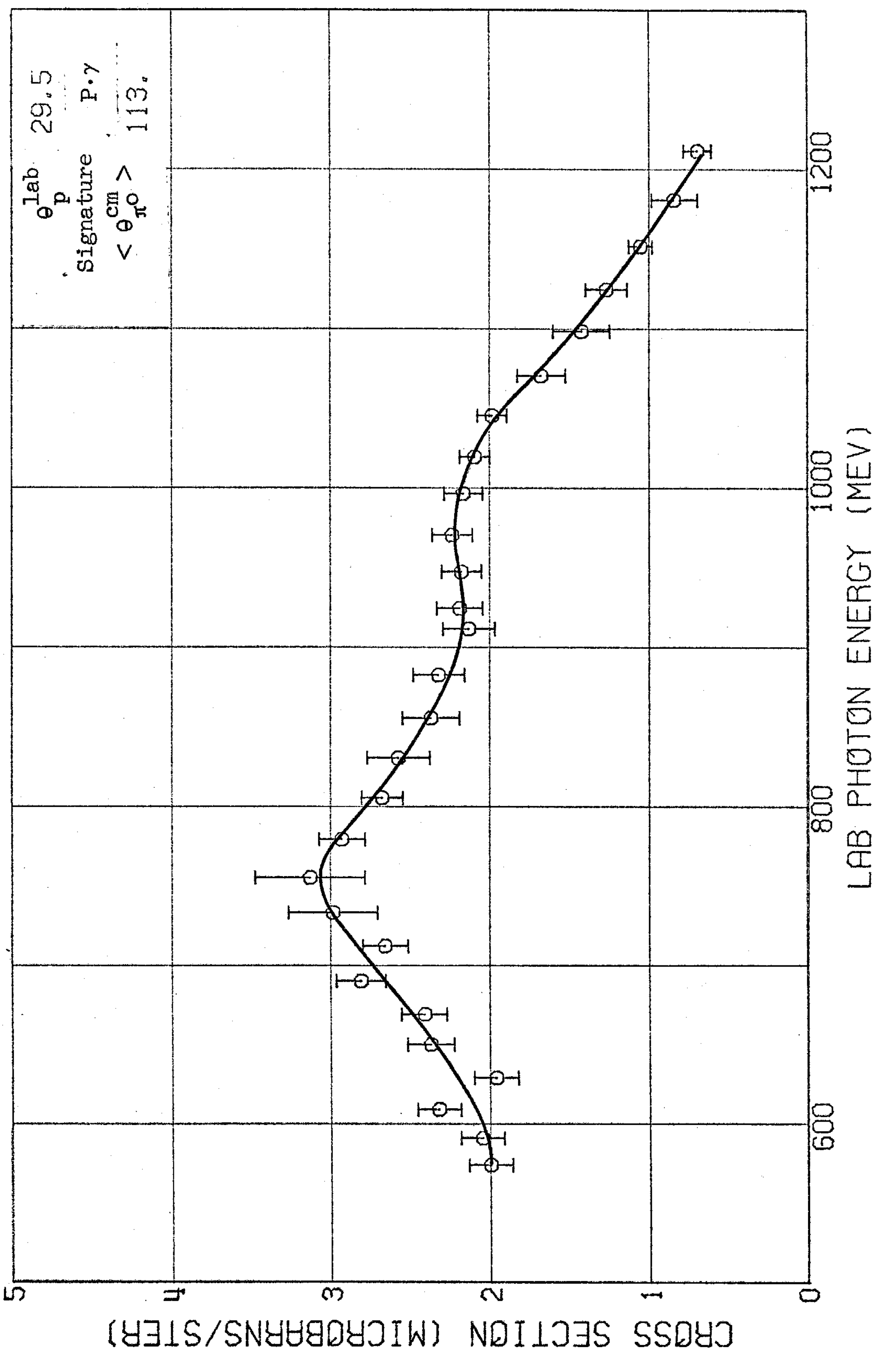

θ_p^{lab} 29.5
Signature P.γ
$< \theta_{\pi^o}^{cm} >$ 113.
600
800
1000
1200
LAB PHOTON ENERGY (MEV)
0
1
2
3
4
5
CROSS SECTION (MICROBARNS/STER)

Figure 7.8

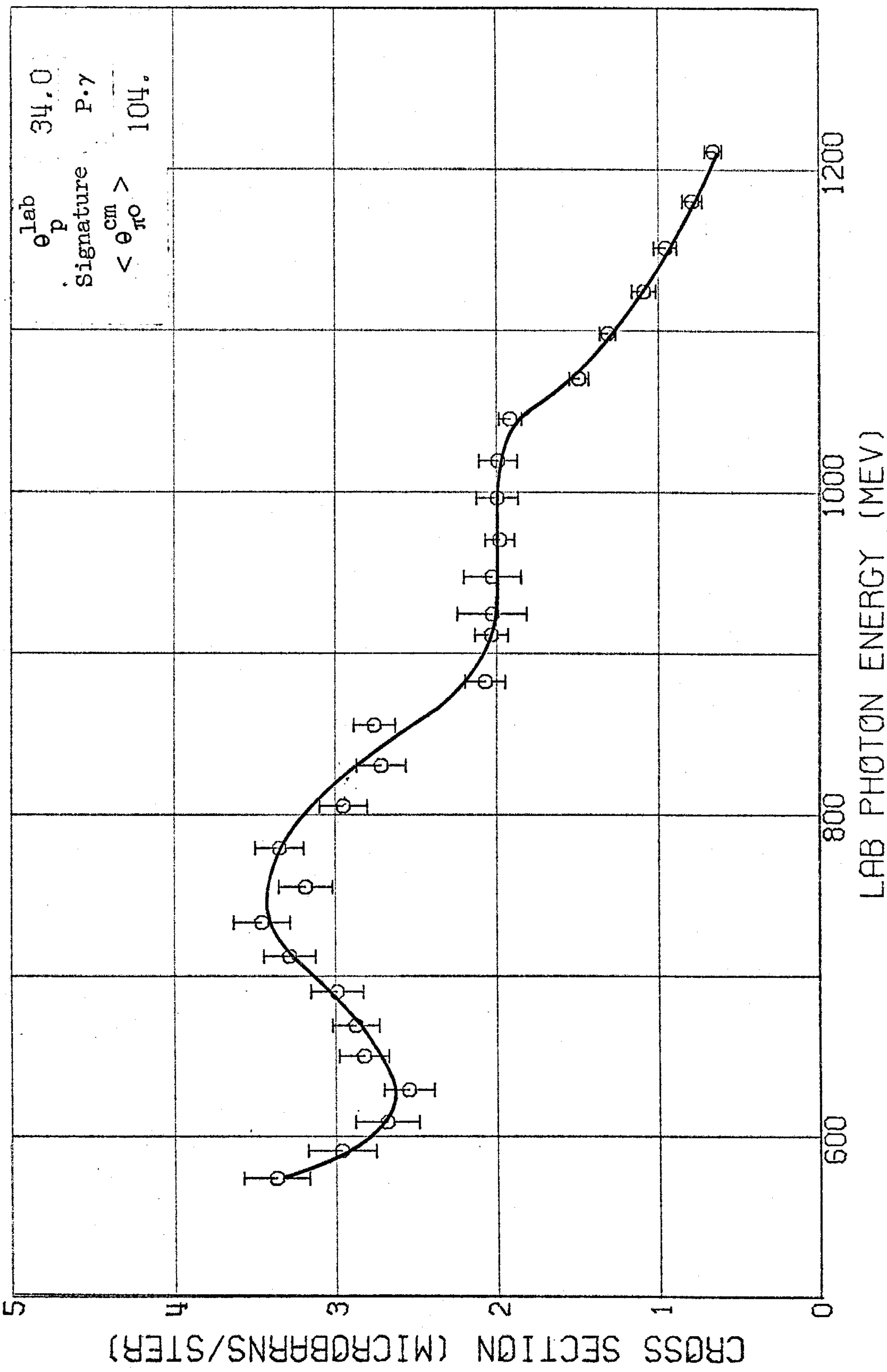

θ_p^{lab} 34.0
Signature P.γ
$< \theta_{\pi^o}^{cm} >$ 104.
0
1
2
3
4
5
CROSS SECTION (MICROBARNS/STER)
600
800
1000
1200
LAB PHOTON ENERGY (MEV)

Figure 7.9

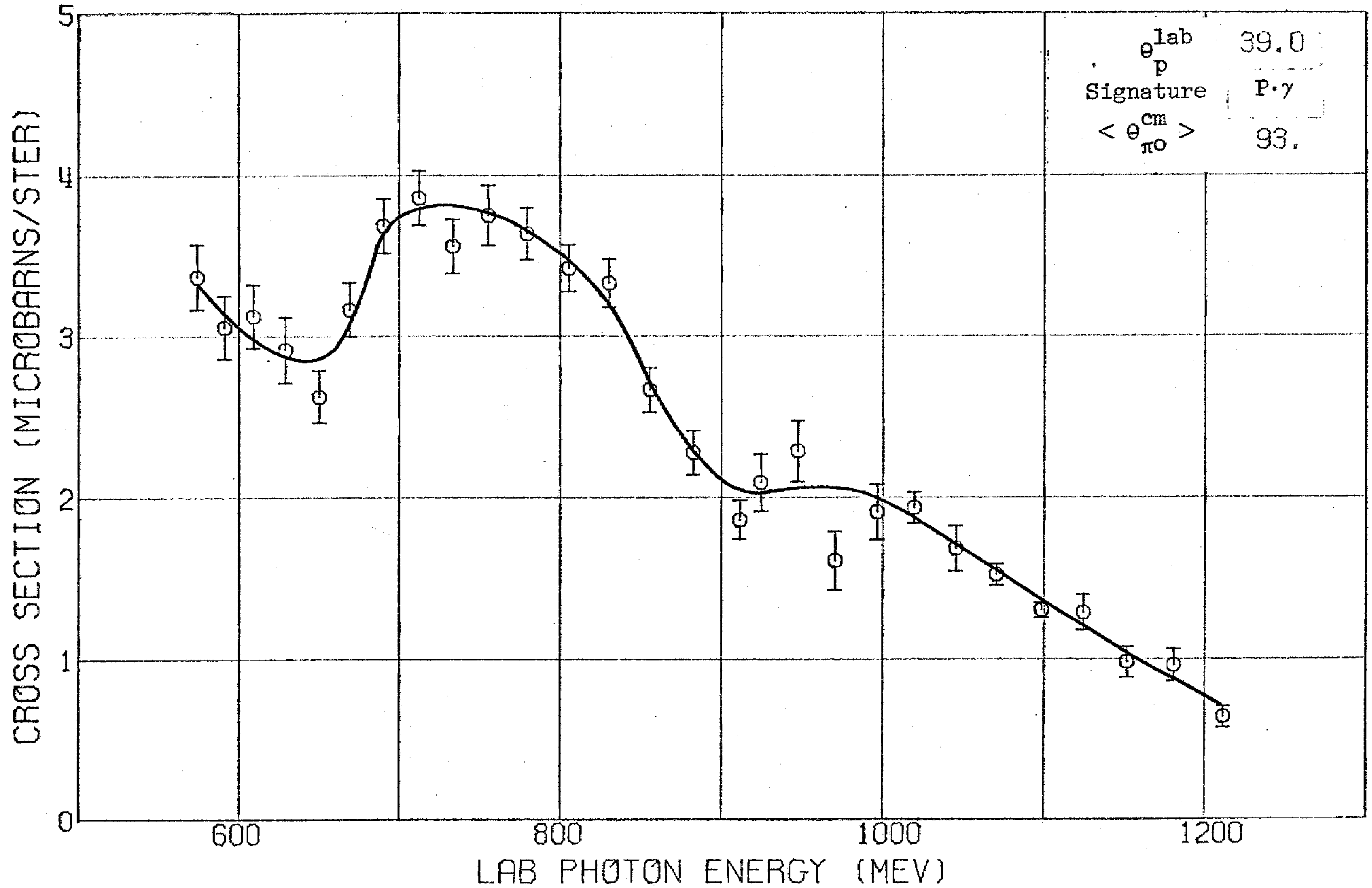

θ_p^{lab} 39.0
Signature P·γ
$< \theta_{\pi o}^{cm} >$ 93.
CROSS SECTION (MICROBARNS/STER)
0
1
2
3
4
5
600
800
1000
1200
LAB PHOTON ENERGY (MEV)

Figure 7.10

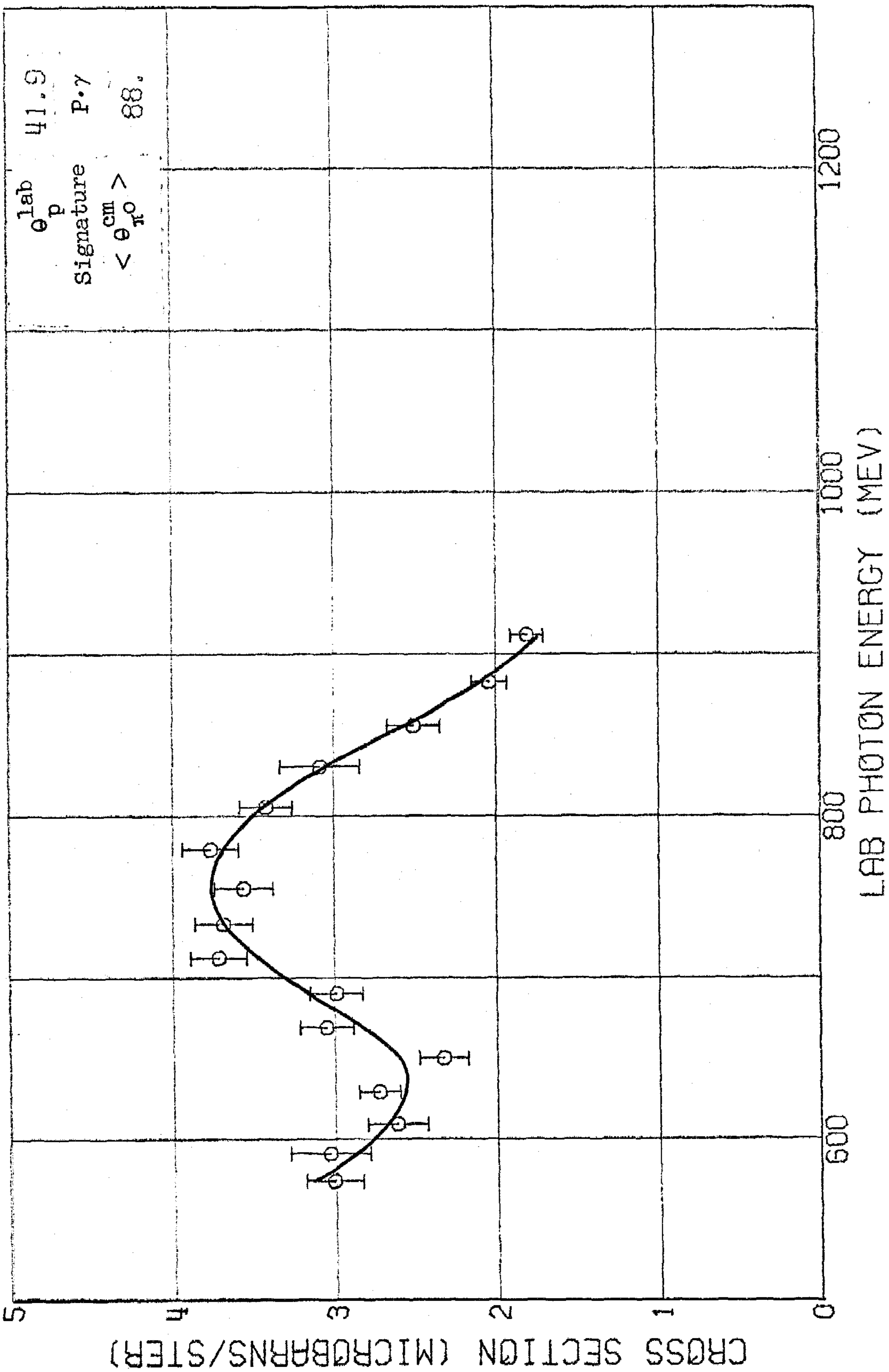

θ_p^{lab} 41.9
Signature P·γ
$< \theta_{\pi^o}^{cm} >$ 88.
CROSS SECTION (MICROBARNS/STER)
0
1
2
3
4
5
600
800
1000
1200
LAB PHOTON ENERGY (MEV)

Figure 7.11

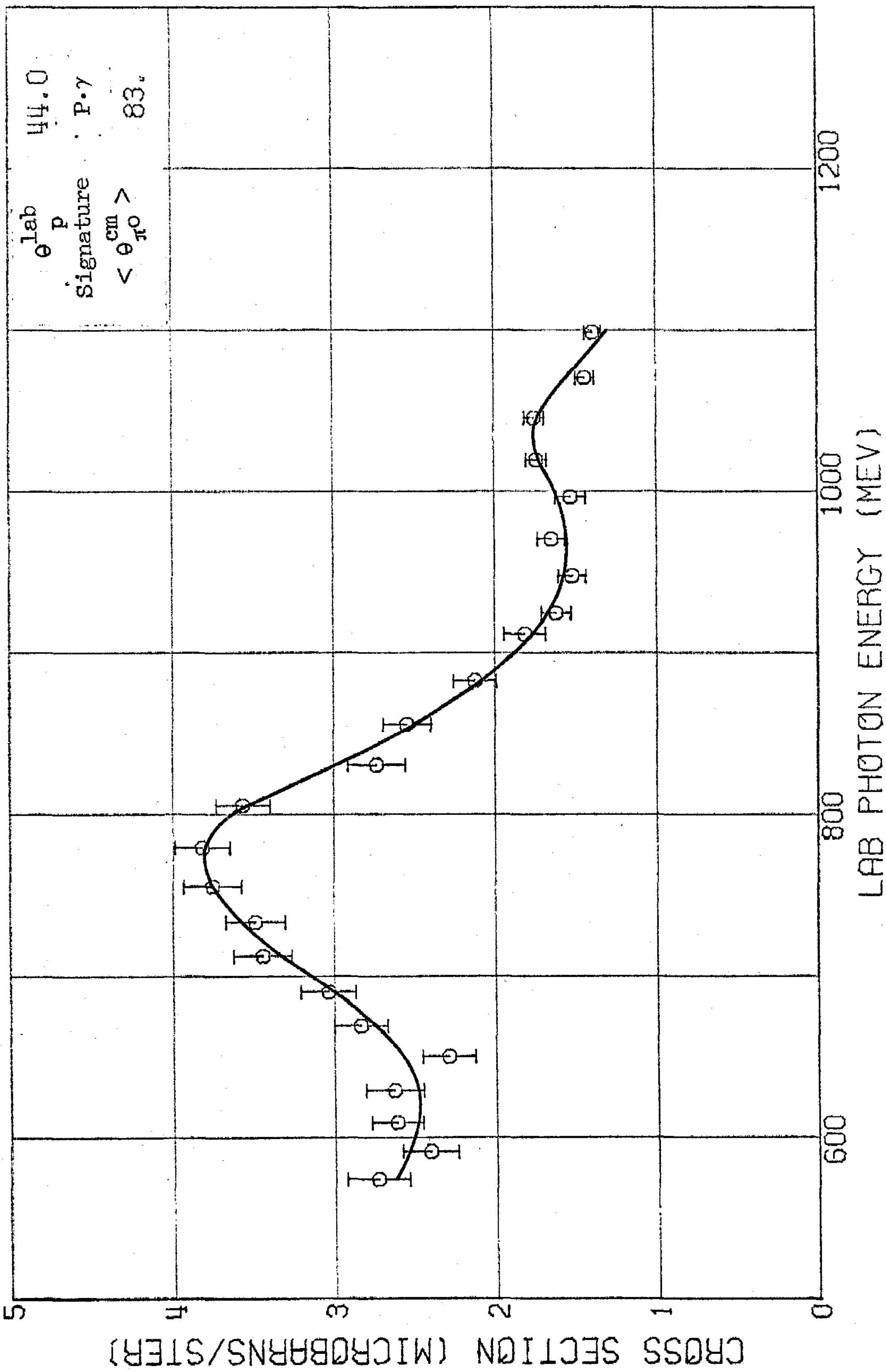
θ p lab 44.0
Signature P·γ
< θ π0 cm > 83.
CROSS SECTION (MICROBARNS/STER)
0
1
2
3
4
5
600
800
1000
1200
LAB PHOTON ENERGY (MEV)

Figure 7.12

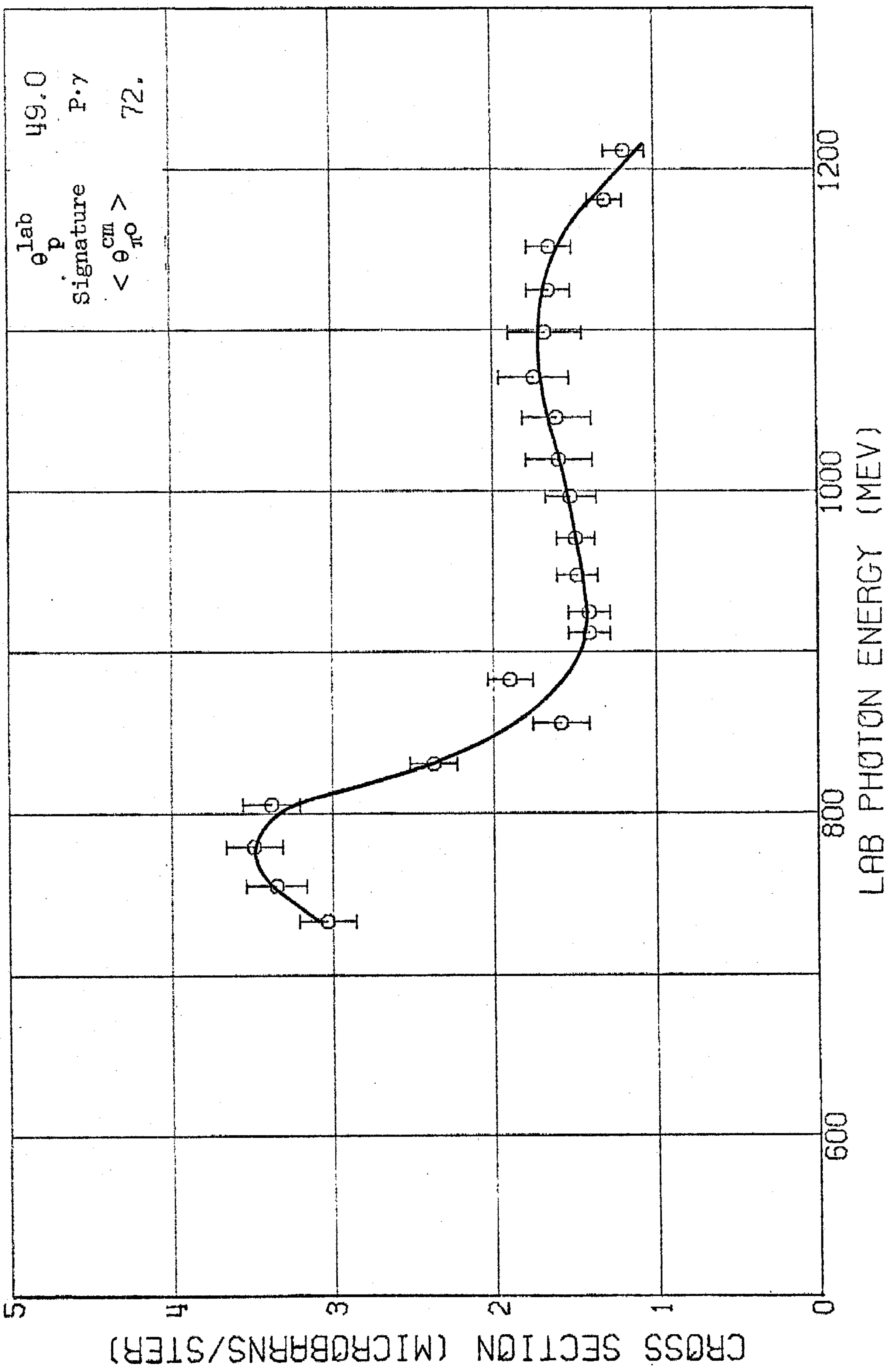

θ_p^{lab} 49.0
Signature P.γ
$< \theta_{\pi^0}^{cm} >$ 72.
600
800
1000
1200
LAB PHOTON ENERGY (MEV)
0
1
2
3
4
5
CROSS SECTION (MICROBARNS/STER)

Figure 7.13

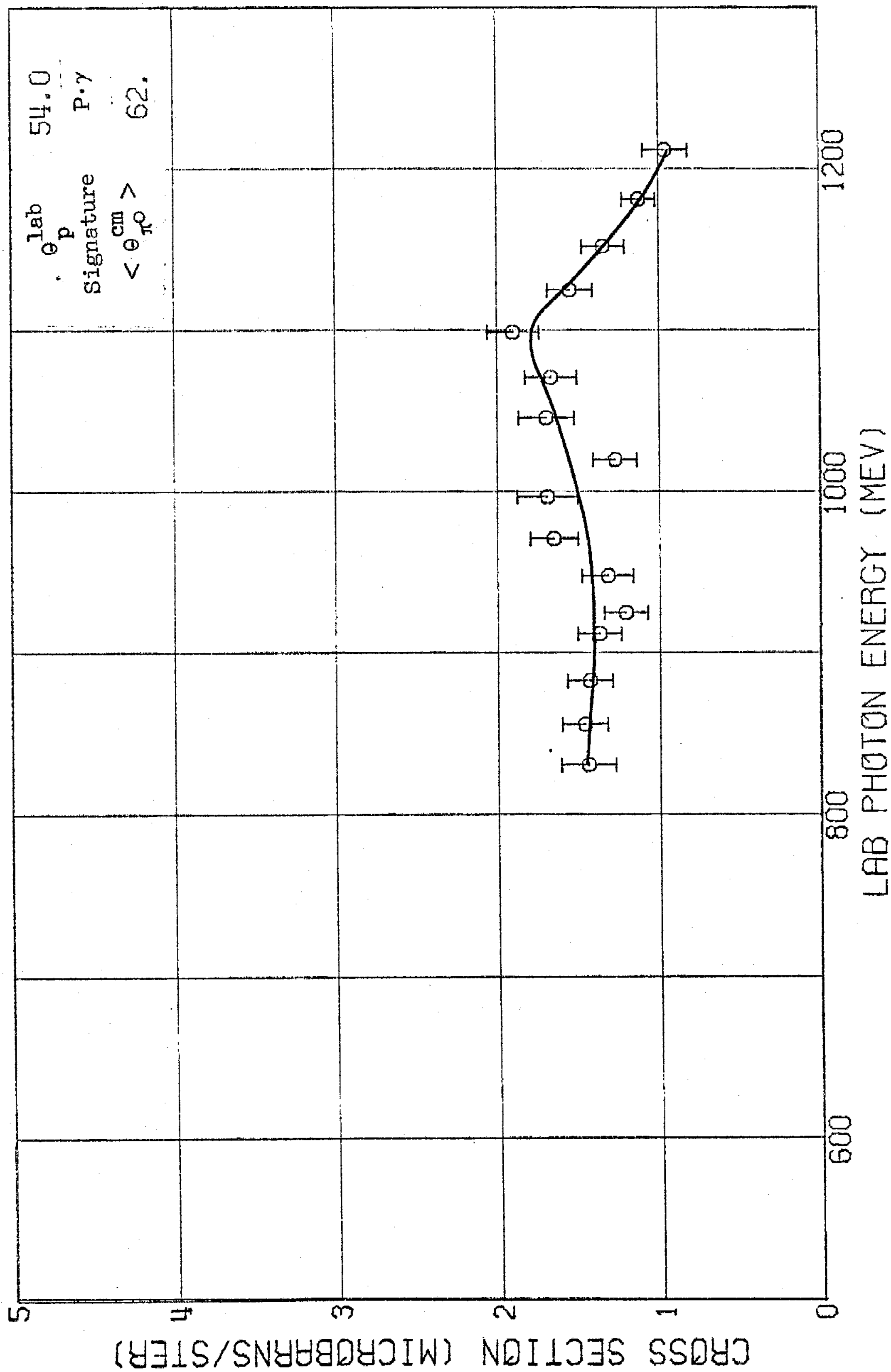

θ_p^{lab} 54.0
Signature P.γ
$< \theta_{\pi^o}^{cm} >$ 62.
CROSS SECTION (MICROBARNS/STER)
0
1
2
3
4
5
600
800
1000
1200
LAB PHOTON ENERGY (MEV)

B. Comparison with proton only

At most proton angles, the proton rates had pi pair contaminations of several per cent in the lower momentum channels. Figure 8 shows cross sections computed from these rates for $\theta_p^{lab} = 16^o$. The apparent discontinuities in the P signature cross sections every fourth point are due to bottom channel points with large pair contamination being next to top channel points with little contamination. This angle is one of the worst cases in regard to contamination.

At the more backward proton angles, the P signature cross sections show little or no pi pair contamination, as judged by the lack of discontinuities. It is interesting to compare these cross sections to the $P \cdot \gamma$ signature cross sections. Figure 9 shows cross sections at $\theta_p^{lab} = 44^o$, 49^o, and 54^o. All these data are taken with the 1200 MeV/c magnet configuration. Although the gamma counter configuration has no significance for the P signature, the veto points are filled in to aid in comparison. The curves are the freehand curves through the final cross sections from Part III A. The curves agree fairly well with the open squares indicating agreement between the P signature and the $P \cdot \gamma$ signature four counter results. However, near the second resonance, the curves drop below the P signature cross sections indicating, again, that the $P \cdot \gamma$ veto cross sections are low.

Note that the $P \cdot \gamma$ signature statistical errors are smaller than those for the P signature (cf. Figure 6). Requiring the gamma ray reduces the π^o efficiency and, therefore, the number of counts.

Figure 8

P signature cross sections at $\theta_p^{lab} = 16^o$. The jumps indicate pi pair contamination. The squares and diamonds denote the 1200 MeV/c and 1600 MeV/c magnet configurations, respectively.

Figure 8

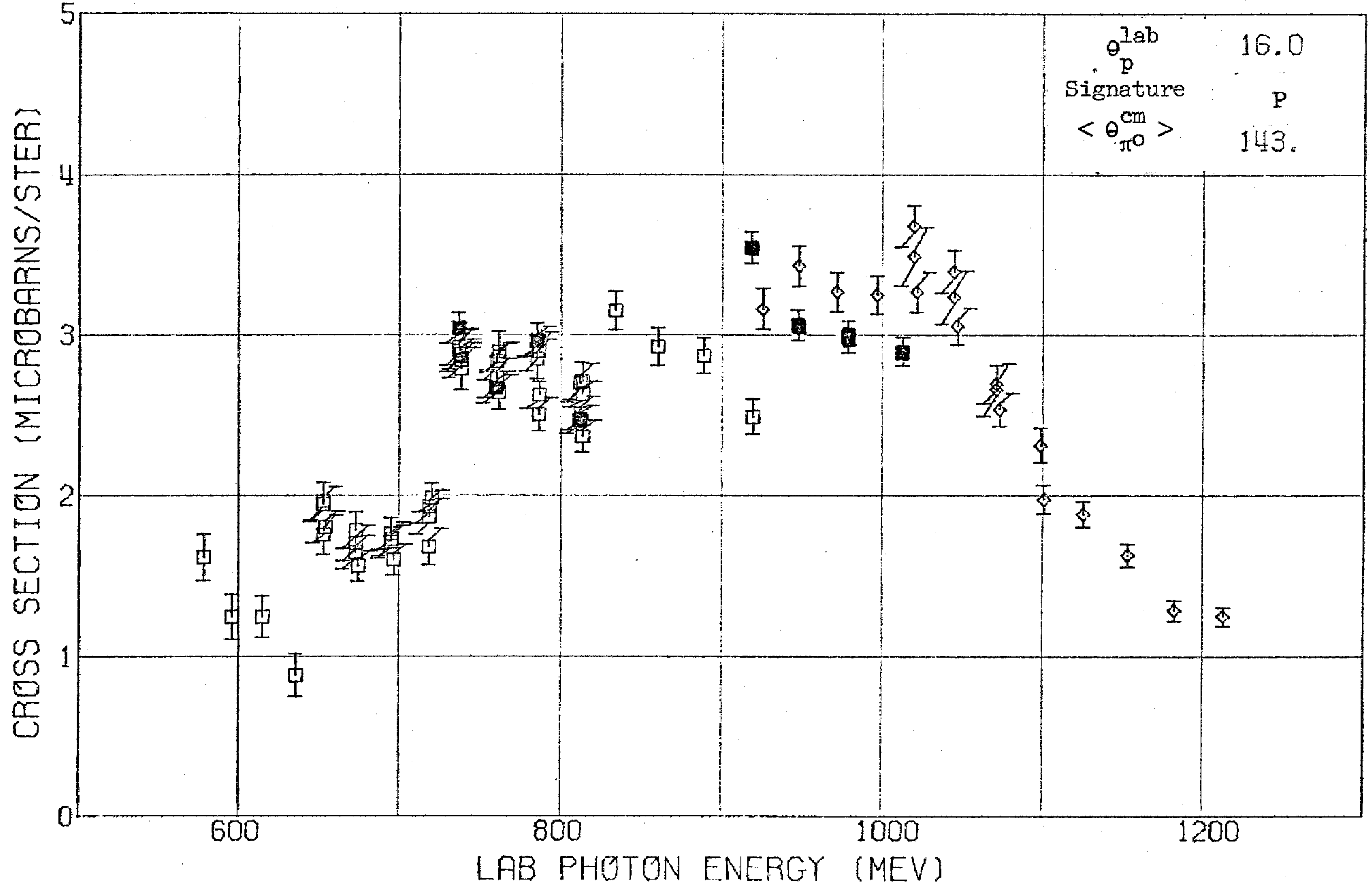

θ_p^{lab} 16.0
Signature P
$< \theta_{\pi^o}^{cm} >$ 143.
CROSS SECTION (MICROBARNS/STER)
0
1
2
3
4
5
600
800
1000
1200
LAB PHOTON ENERGY (MEV)

Figure 9

P signature cross sections at $\theta_p^{lab} = 44^o$, 49^o, and 54^o. All points measured with 1200 MeV/c magnet configuration. Open and filled in squares denote four counter and veto measurements, respectively. Curves are from Figure 7 and indicate final cross section values.

Figure 9.1

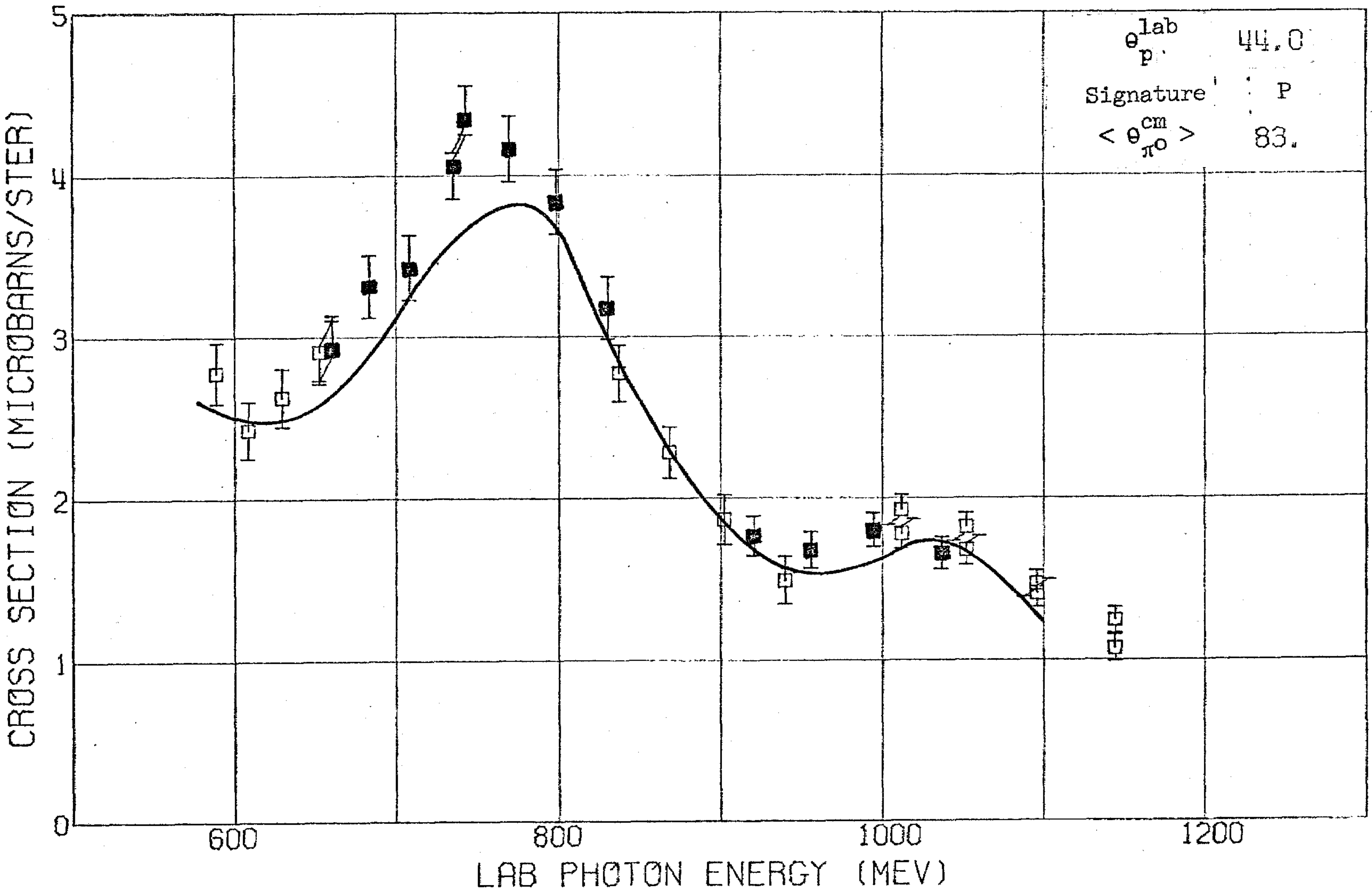

θ_p^{lab} 44.0
Signature : P
$< \theta_{\pi^o}^{cm} >$ 83.
CROSS SECTION (MICROBARNS/STER)
LAB PHOTON ENERGY (MEV)
0
1
2
3
4
5
600
800
1000
1200

Figure 9.2

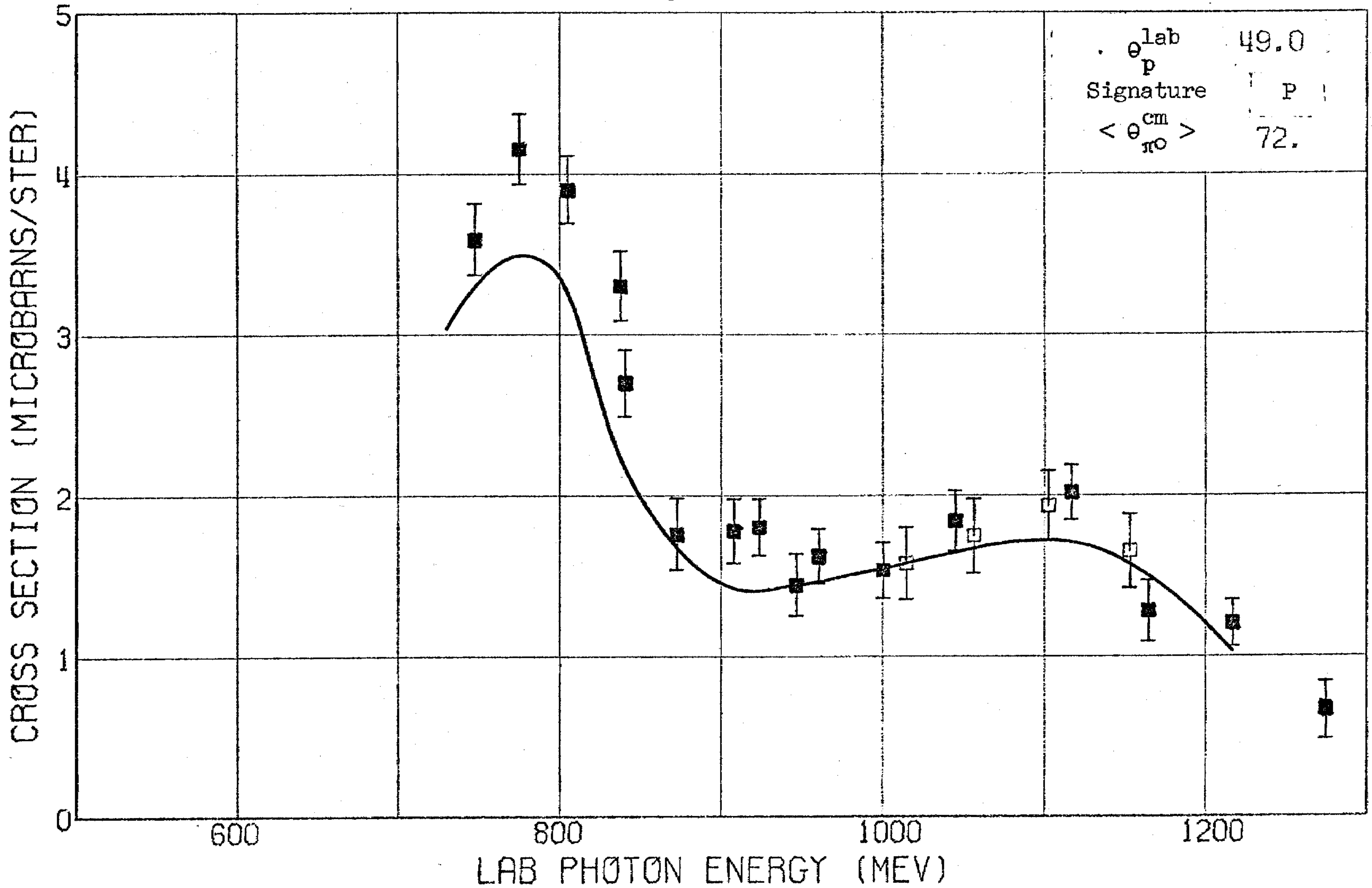
θ_p^{lab} 49.0
Signature P
$< \theta_{\pi^o}^{cm} >$ 72.
CROSS SECTION (MICROBARNS/STER)
LAB PHOTON ENERGY (MEV)
0
1
2
3
4
5
600
800
1000
1200

Figure 9.3

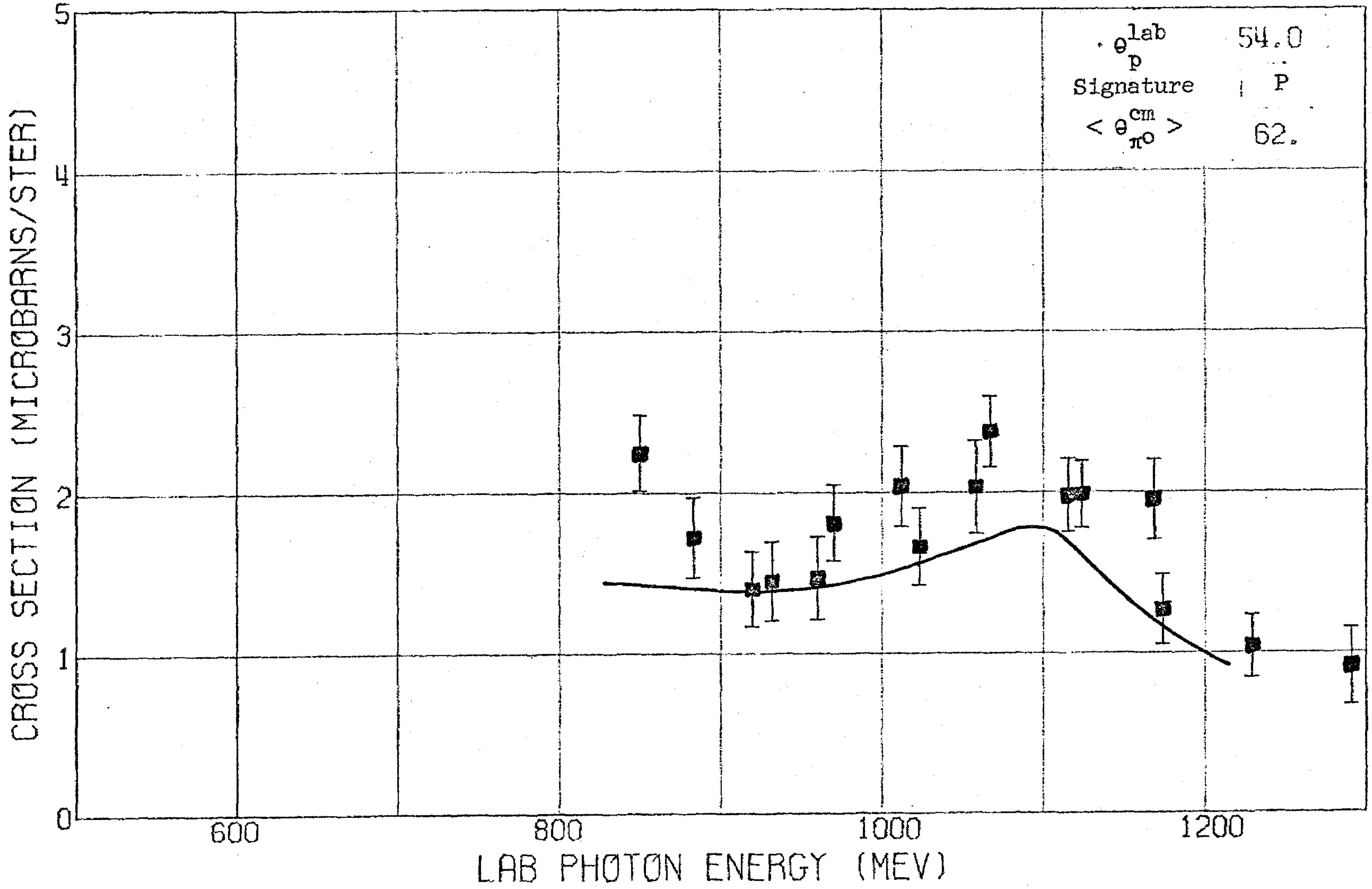

θ p lab 54.0
Signature P
< θ π0 cm > 62.
CROSS SECTION (MICROBARNS/STER)
0
1
2
3
4
5
600
800
1000
1200
LAB PHOTON ENERGY (MEV)

This would make the $P \cdot \gamma$ errors larger except that requiring the gamma ray reduces the empty target backgrounds, more than compensating for the effect of the efficiency loss.

C. Comparison with proton plus two gammas.

At 4^{o} and 8^{o}, physical obstructions around the incoming photon beam prevented placing the counters in a position with good two gamma efficiency.

At 12^{o}, 16^{o}, and 20.5^{o} the π^{o} had low energy so that its decay cone was large. However, the gamma counters were placed next to one another to optimize the $P \cdot \gamma$ rates. In this situation the $P \cdot 2\gamma$ efficiency was low and very susceptible to small errors. Figure 10 shows the interpolated and averaged $P \cdot 2\gamma$ cross sections at $\theta_p^{lab} = 16^{o}$. The interpolated and averaged events were used in order to get as good statistical accuracy as possible. The data still have large errors and are systematically high.

For $\theta_p^{lab} = 25^{o}$, 29.5^{o}, 34^{o}, and 39^{o}, the π^{o} had higher energy and a smaller decay cone. This resulted in a higher efficiency and smaller errors. For large k, the errors became comparable with the $P \cdot \gamma$ errors. Figure 11 shows the high energy end of the distributions. The curves are the freehand fits to the $P \cdot \gamma$ cross sections from Part III A. The agreement between the points and the curves is excellent, indicating good agreement between the $P \cdot \gamma$ and $P \cdot 2\gamma$ results. This agreement is a welcome check on the rather complicated gamma efficiency calculation.

Figure 10

P $\cdot$ 2γ interpolated and averaged cross sections at $\theta_p^{lab} = 16^o$.

Figure 10

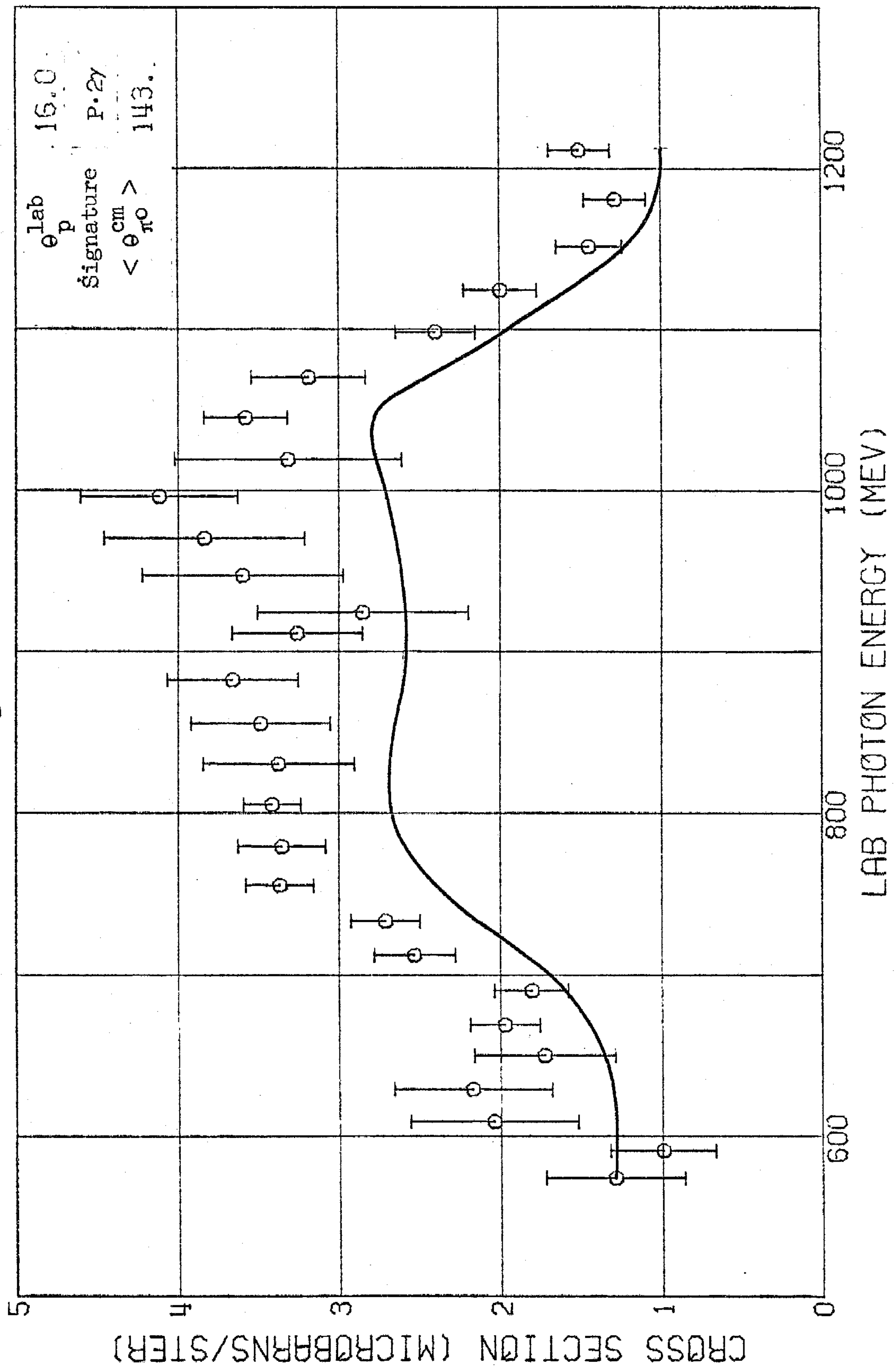

θ_p^{lab} 16.0
Signature P.2γ
$< \theta_{\pi^0}^{cm} >$ 143.
CROSS SECTION (MICROBARNS/STER)
0
1
2
3
4
5
LAB PHOTON ENERGY (MEV)
600
800
1000
1200

Figure 11

P · 2γ interpolated and averaged cross sections for large k at $\theta_p^{lab} = 25^o$, 29.5^o, 34^o, and 39^o.

Figure 11.1

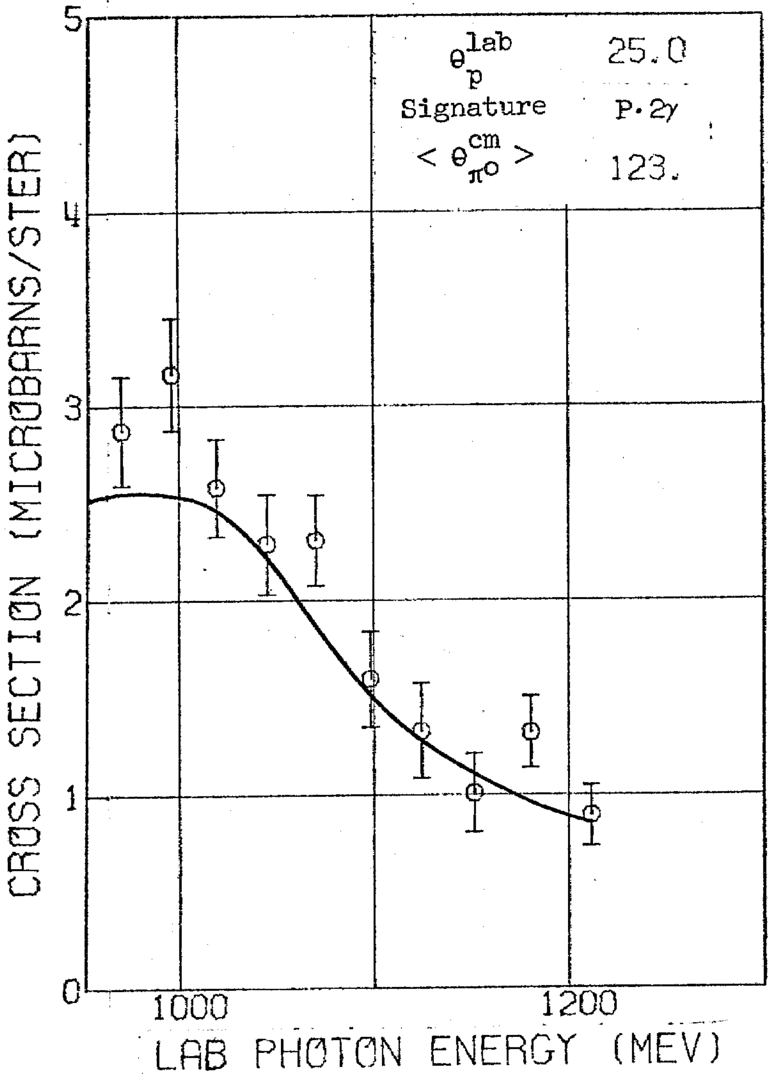

θ_p^{lab} 25.0
Signature P·2γ
$< \theta_{\pi^o}^{cm} >$ 123.
CROSS SECTION (MICROBARNS/STER)
LAB PHOTON ENERGY (MEV)
0
1
2
3
4
5
1000
1200

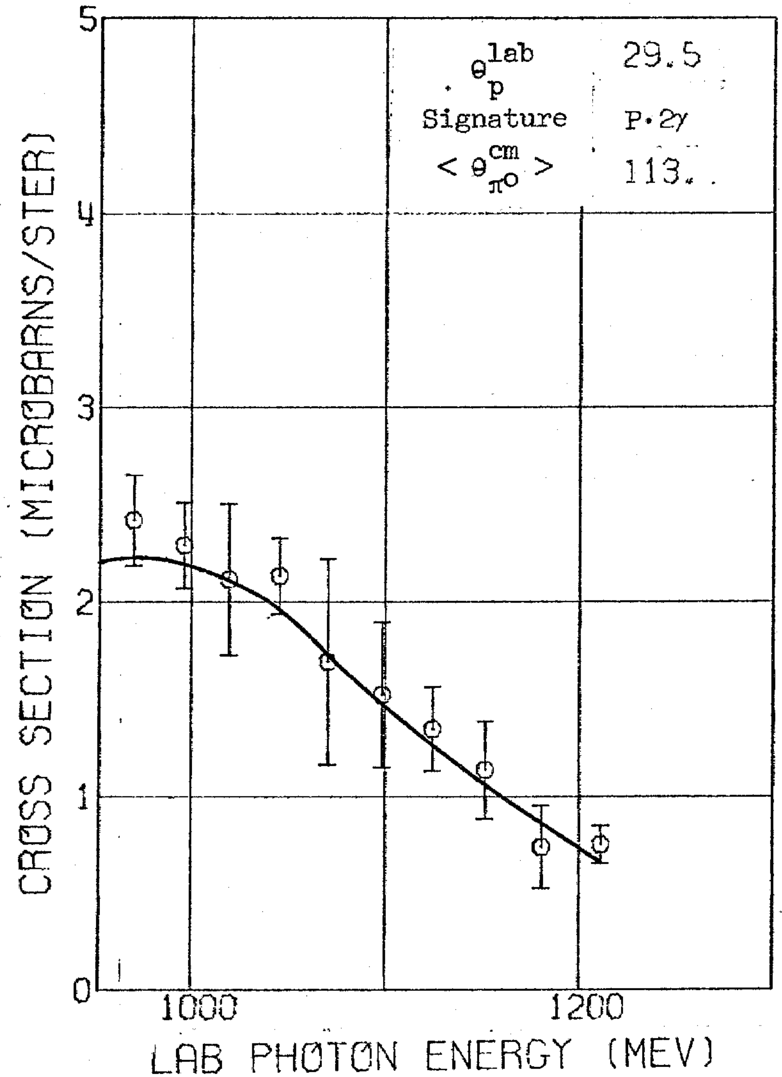

θ_p^{lab} 29.5
Signature P·2γ
$< \theta_{\pi^o}^{cm} >$ 113.
CROSS SECTION (MICROBARNS/STER)
LAB PHOTON ENERGY (MEV)
0
1
2
3
4
5
1000
1200

Figure 11.2

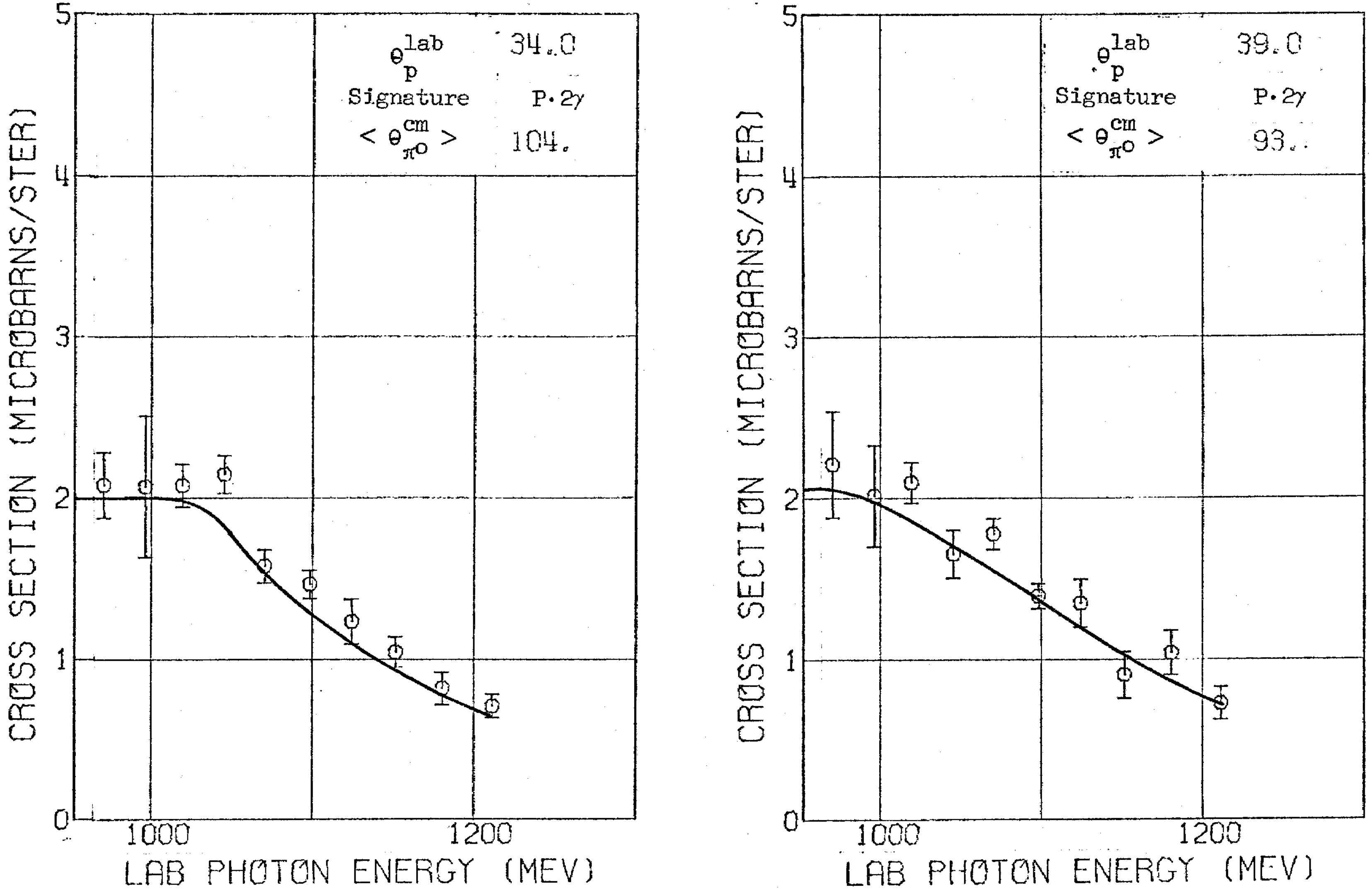
θ_p^{lab} 34.0
Signature P·2γ
$< \theta_{\pi^0}^{cm} >$ 104.
CROSS SECTION (MICROBARNS/STER)
LAB PHOTON ENERGY (MEV)
θ_p^{lab} 39.0
Signature P·2γ
$< \theta_{\pi^0}^{cm} >$ 93.
CROSS SECTION (MICROBARNS/STER)
LAB PHOTON ENERGY (MEV)

At 44^o the highest energy points are missing.

For $\theta_p^{lab} = 49^o$, 54^o the physical obstructions again made it difficult to measure 2γ events.

IV. CROSS SECTION ANGULAR DISTRIBUTION

The final cross sections were presented as energy distributions in Figure 7 of Part III A. They are presented here as angular distributions in Figure 12 and Table 2.

At energies up to 1124 MeV, forward angle points are added which were interpolated from the data of Highland and DeWire (17), Hatch (7), and Talman (1). At the three highest energies, angular distributions are added which were interpolated from Hatch's data. An approximate method was used to unfold the energy resolution from the Hatch data and the error bars were doubled to reflect the uncertainty in the unfolding and interpolation.

The data at 947 MeV and above were fit to linear combinations of Legendre polynomials up to 5^{th} order. The data below that energy were not fit, because of the error in the cross sections near 90^{o} at the 2^{nd} resonance.

There are little forward angle data at the third resonance. Our fits are not accurate in that region, and do not indicate the peak that probably exists at 30^{o}.

There is a clear peak at 140^{o} extending over a wide energy range around 1045 MeV. This peak has been expected from previous phenomenological fitting (18), but has not previously been measured.

Below 1000 MeV, as the data approach 180^{o}, they appear to drop more rapidly than the 5^{th} order polynomials can follow. This point is considered in more detail in Part V, where comparisons are made with other data near 180^{o}.

Figure 12

Angular distributions of final cross sections.

D	This experiment
J, X	Interpolated from other experiments

Figure 12.1

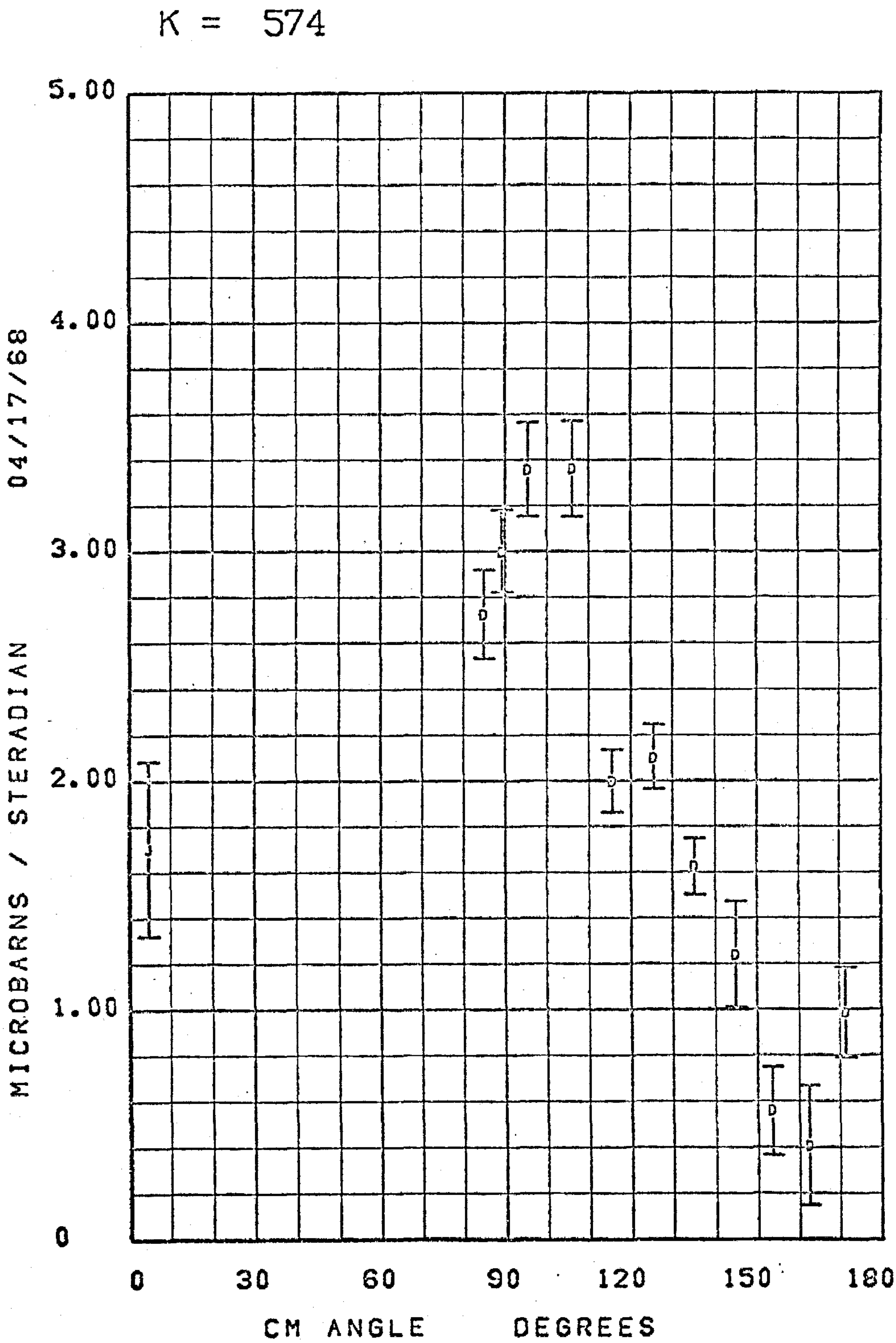
K = 574
5.00
4.00
3.00
2.00
1.00
0
04/17/68
MICROBARNS / STERADIAN
0
30
60
90
120
150
180
CM ANGLE DEGREES

Figure 12. 2

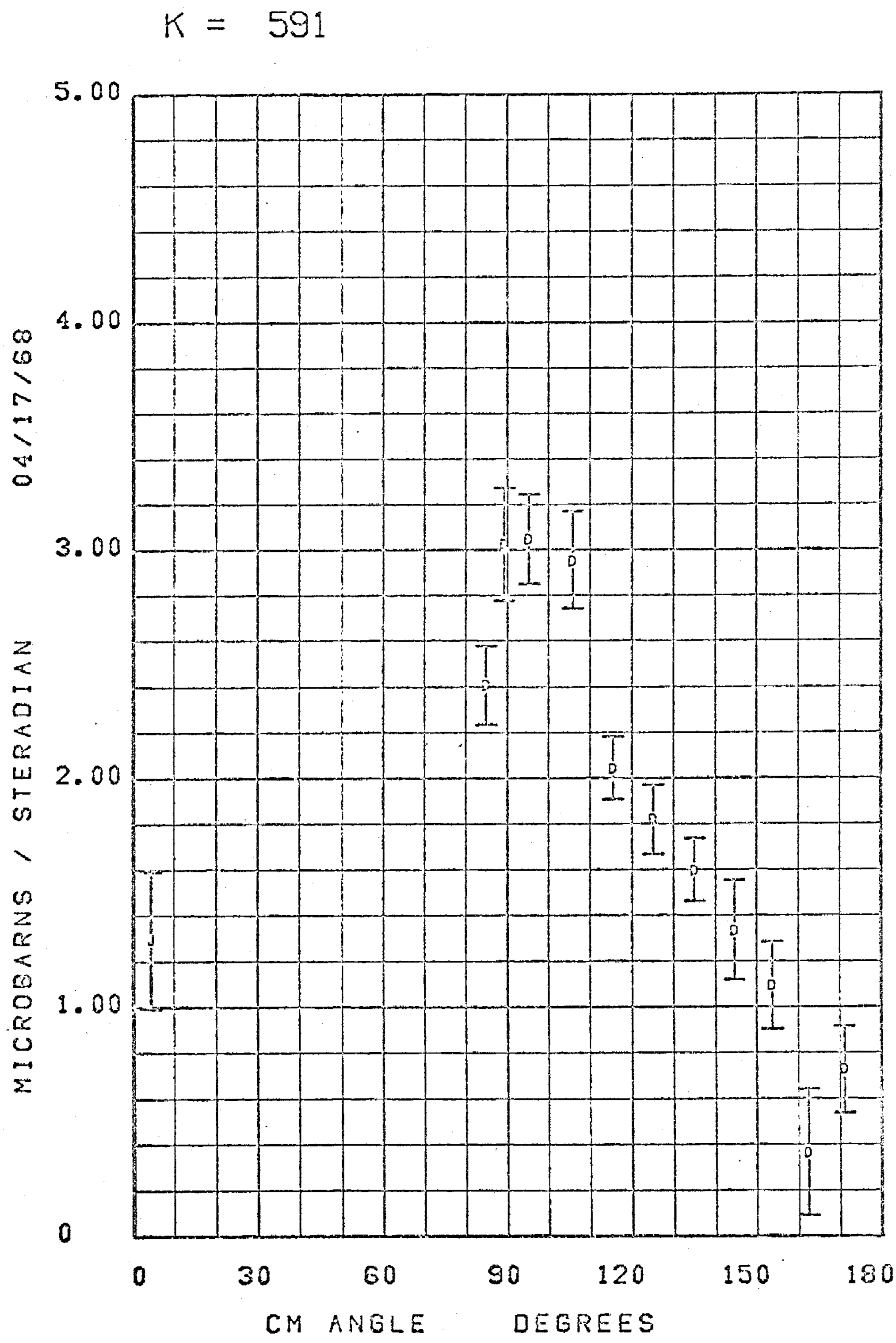
K = 591
5.00
4.00
3.00
2.00
1.00
0
04/17/68
MICROBARNS / STERADIAN
0
30
60
90
120
150
180
CM ANGLE DEGREES

Figure 12. 3

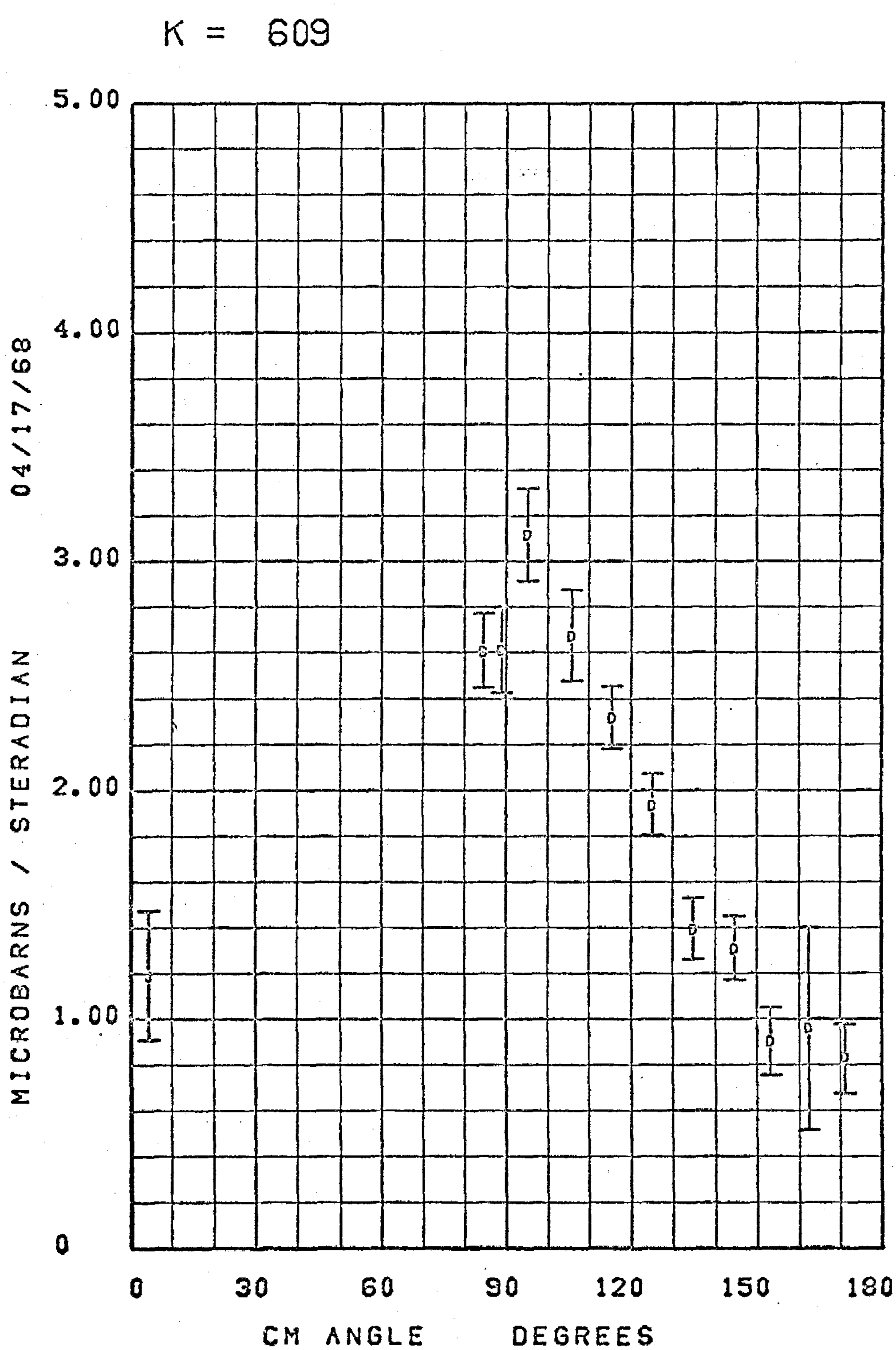
K = 609
5.00
4.00
3.00
2.00
1.00
0
04/17/68
MICROBARNS / STERADIAN
0
30
60
90
120
150
180
CM ANGLE DEGREES

Figure 12.4

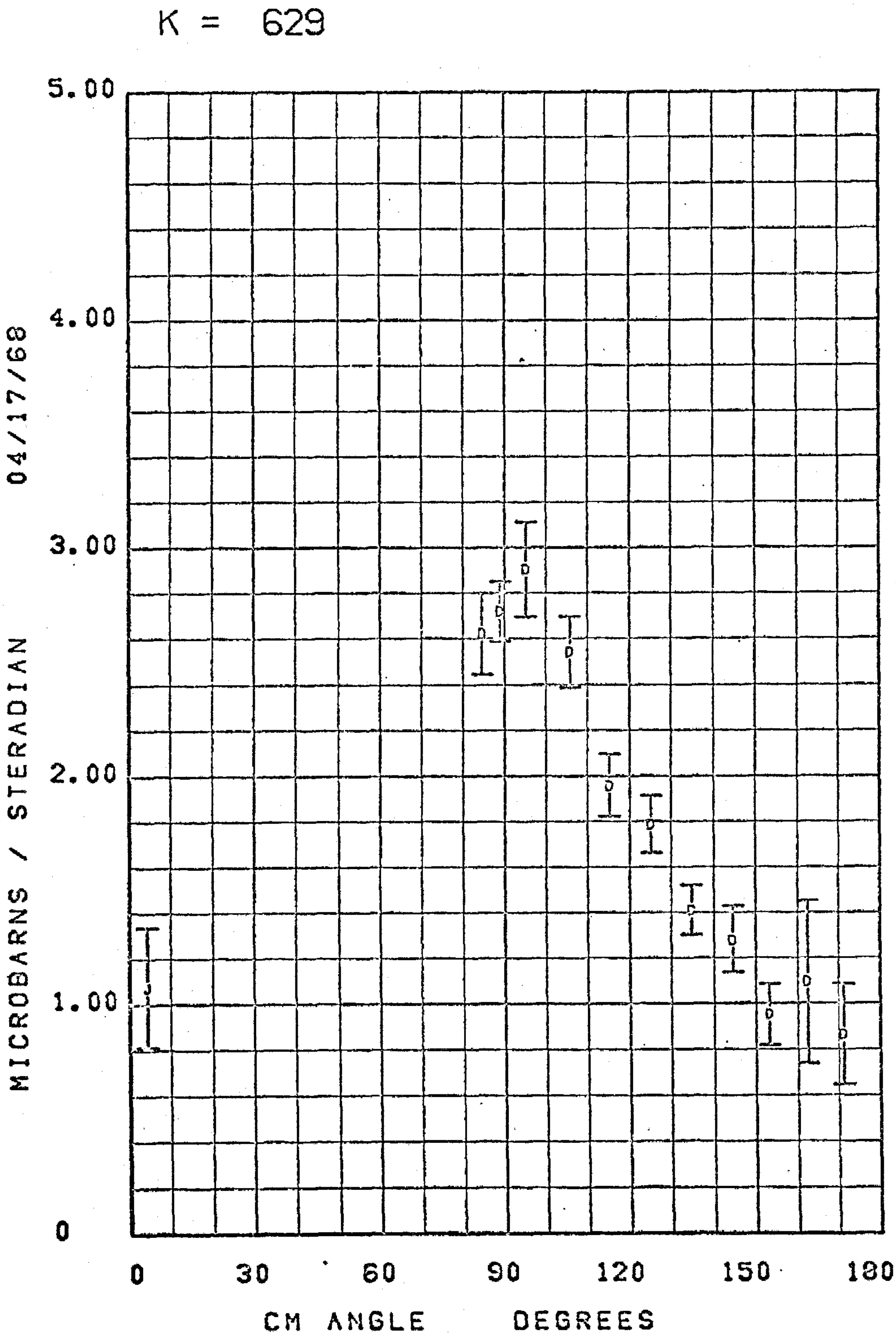
K = 629
5.00
4.00
3.00
2.00
1.00
0
MICROBARNS / STERADIAN
04/17/68
0
30
60
90
120
150
180
CM ANGLE DEGREES

Figure 12.5

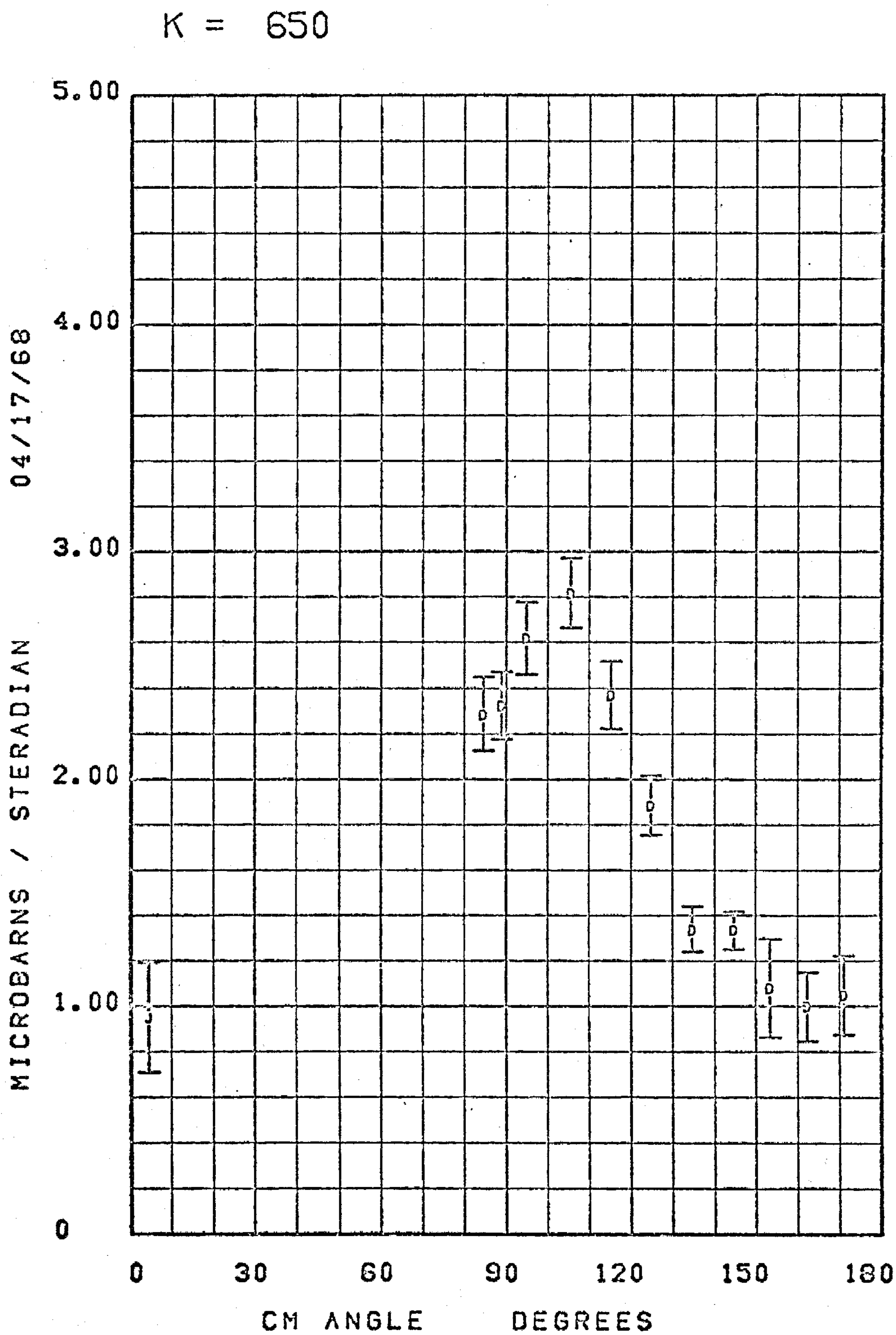
K = 650
5.00
4.00
3.00
2.00
1.00
0
04/17/68
MICROBARNS / STERADIAN
0
30
60
90
120
150
180
CM ANGLE DEGREES

Figure 12. 6

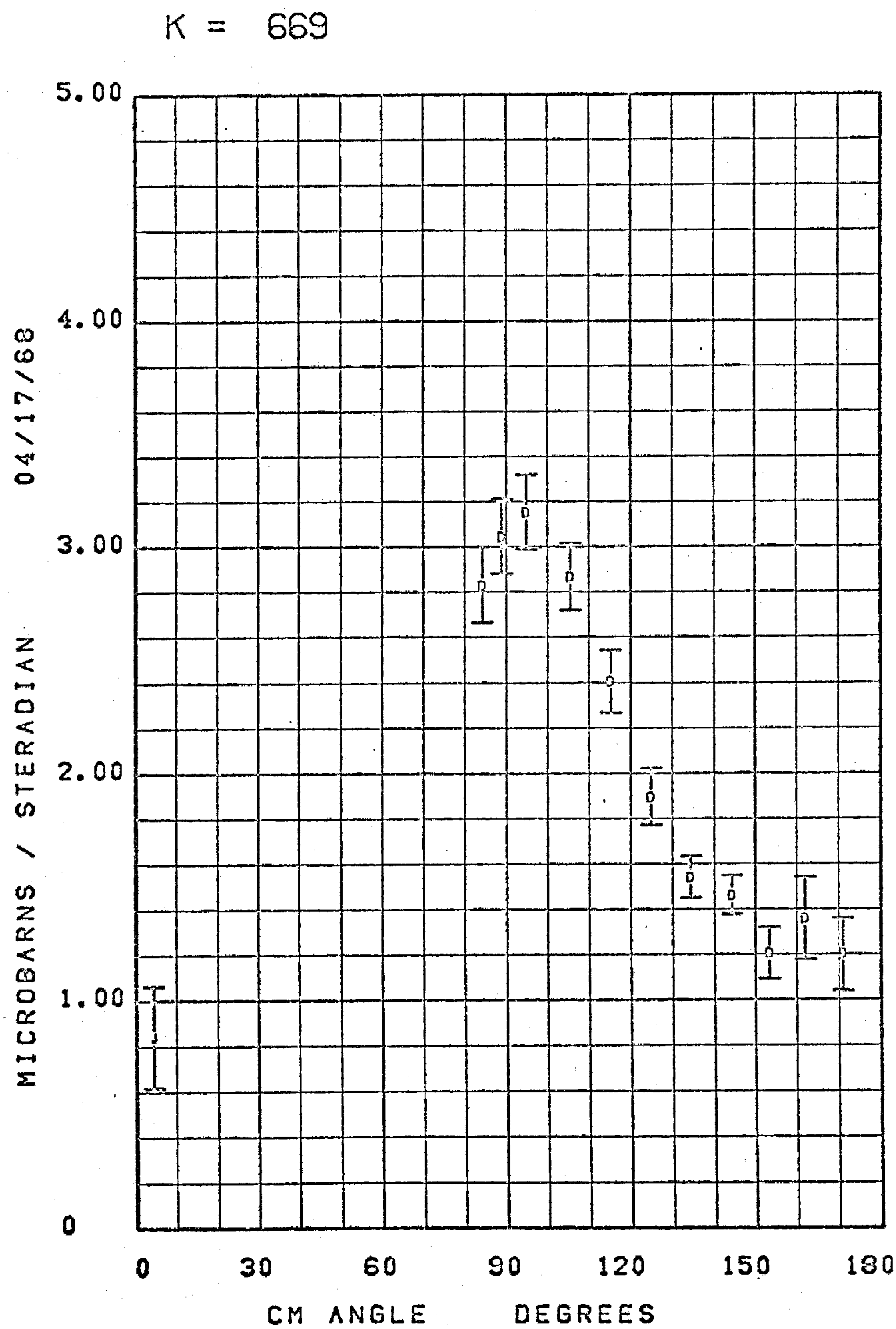
K = 669
5.00
4.00
3.00
2.00
1.00
0
04/17/68
MICROBARNS / STERADIAN
0
30
60
90
120
150
180
CM ANGLE DEGREES

Figure 12.7

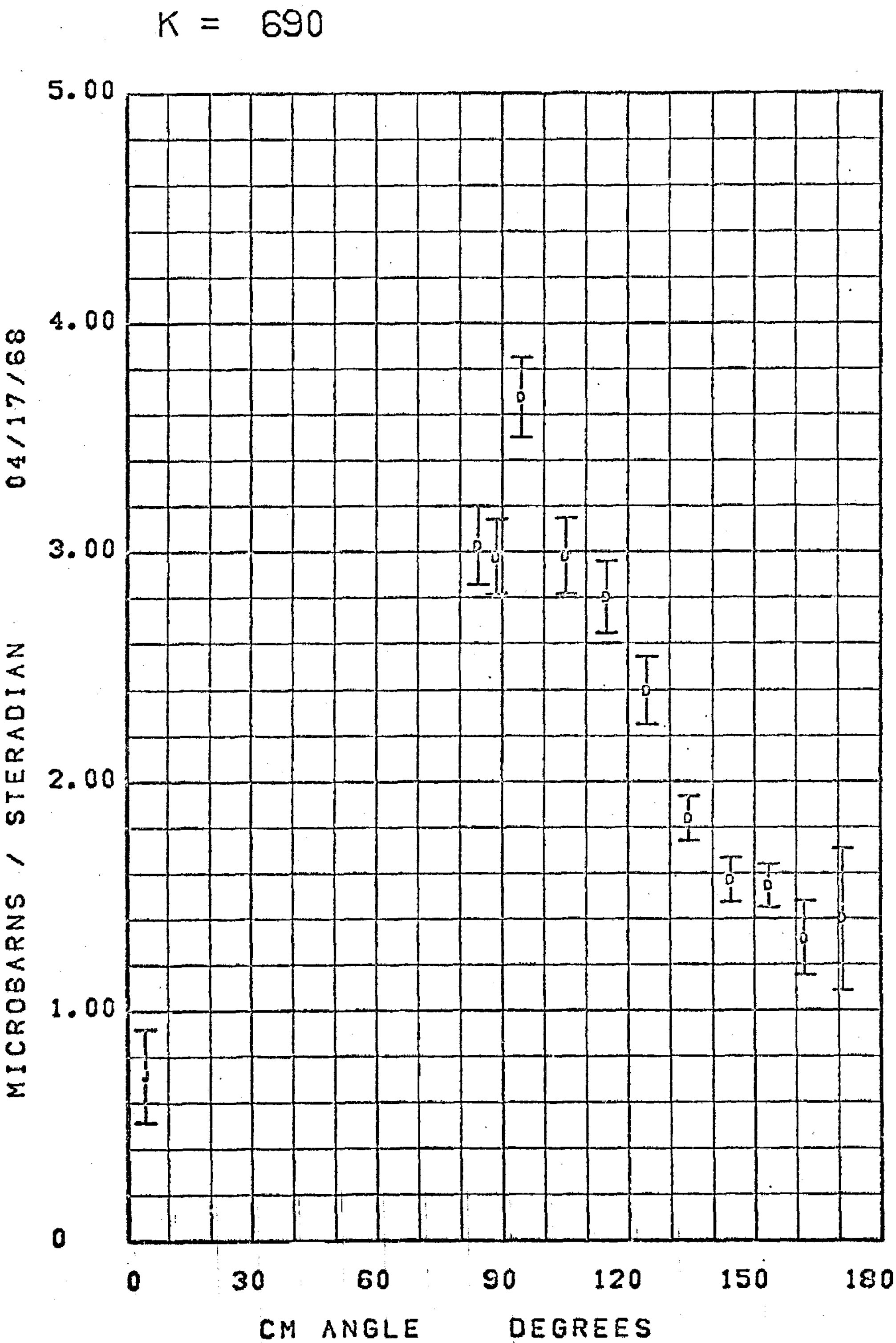
K = 690
04/17/68
MICROBARNS / STERADIAN
5.00
4.00
3.00
2.00
1.00
0
0
30
60
90
120
150
180
CM ANGLE DEGREES

Figure 12.8

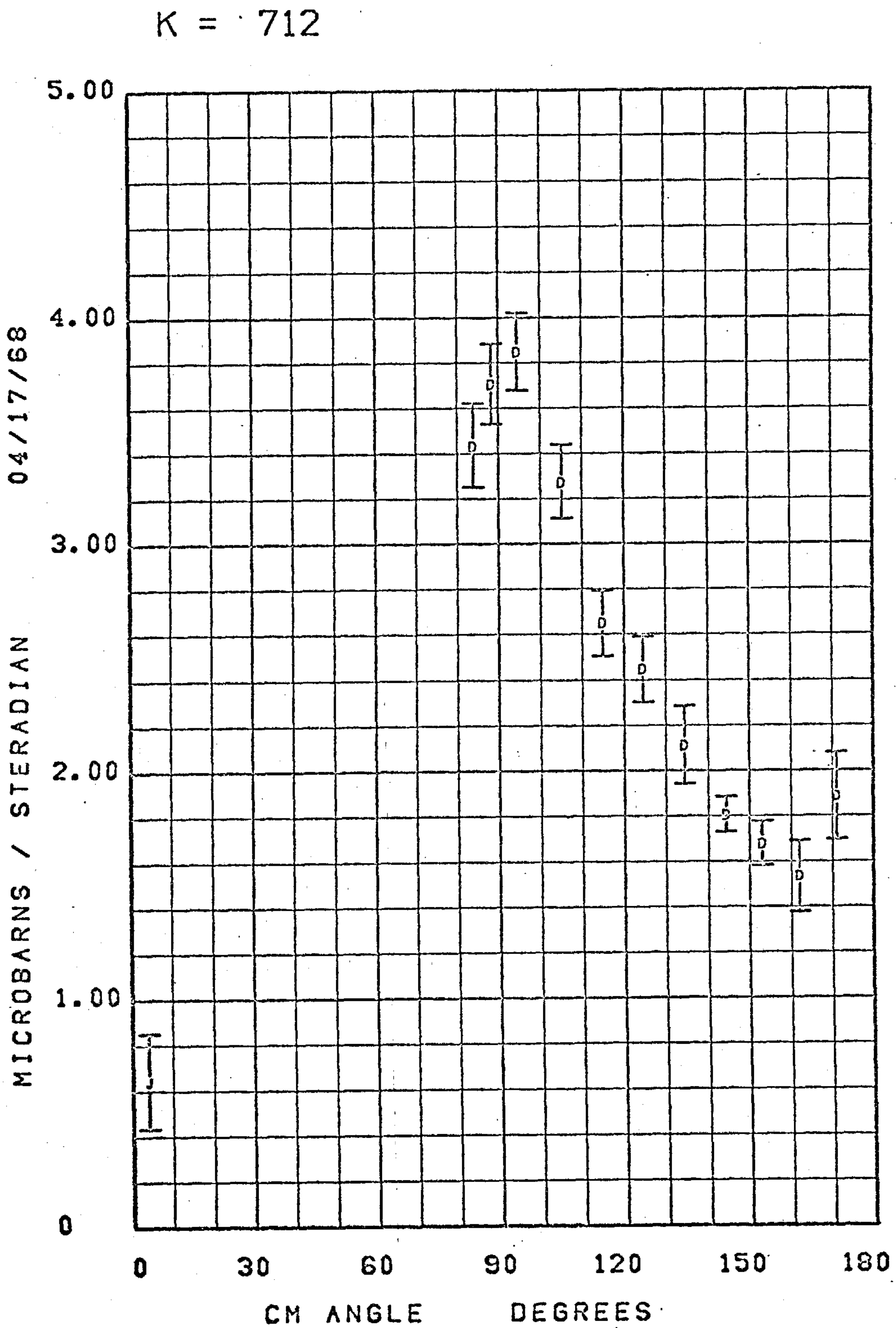
K = 712
5.00
4.00
3.00
2.00
1.00
0
MICROBARNS / STERADIAN
04/17/68
0
30
60
90
120
150
180
CM ANGLE DEGREES

Figure 12.9

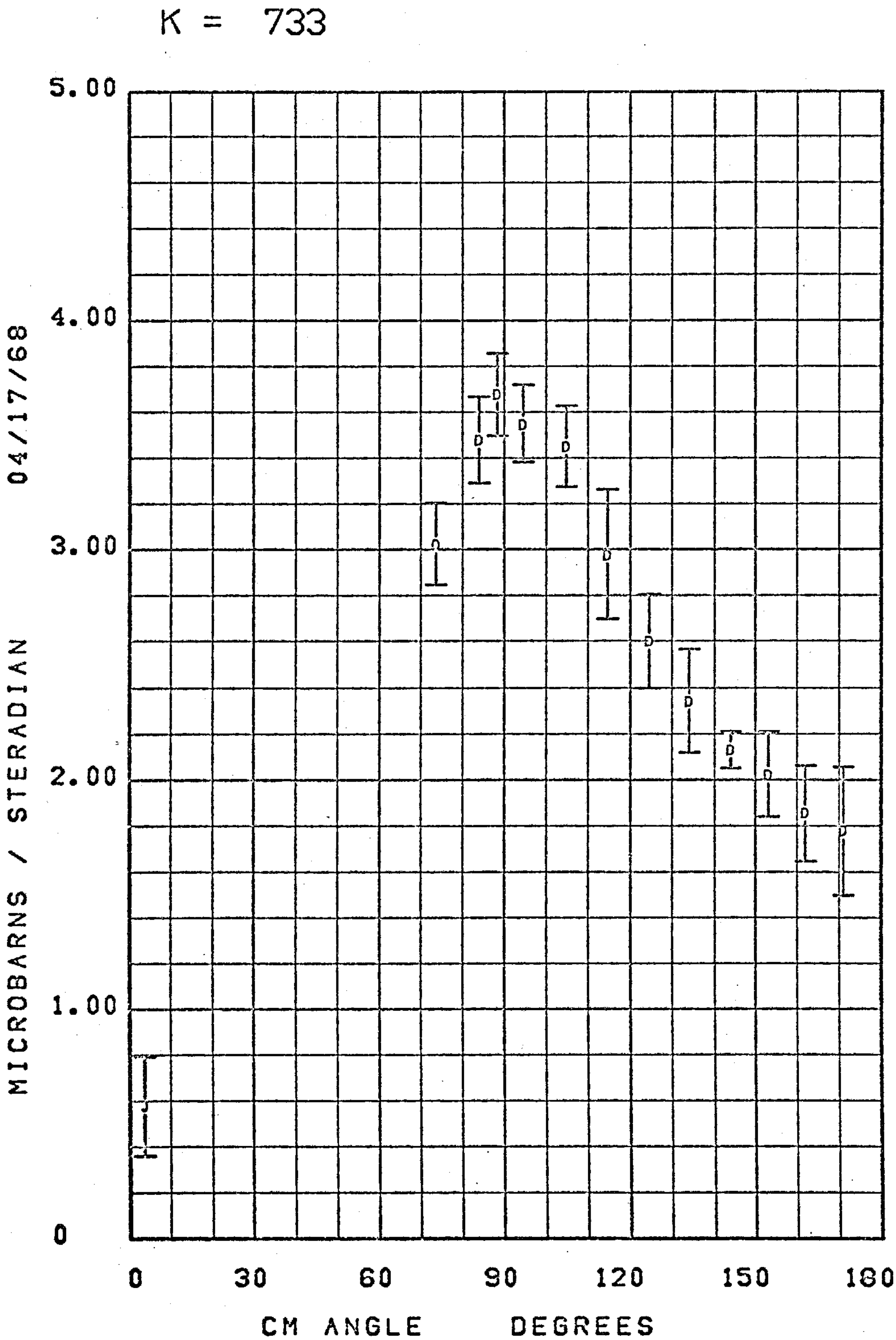
K = 733
5.00
4.00
3.00
2.00
1.00
0
04/17/68
MICROBARNS / STERADIAN
0
30
60
90
120
150
180
CM ANGLE DEGREES

Figure 12.10

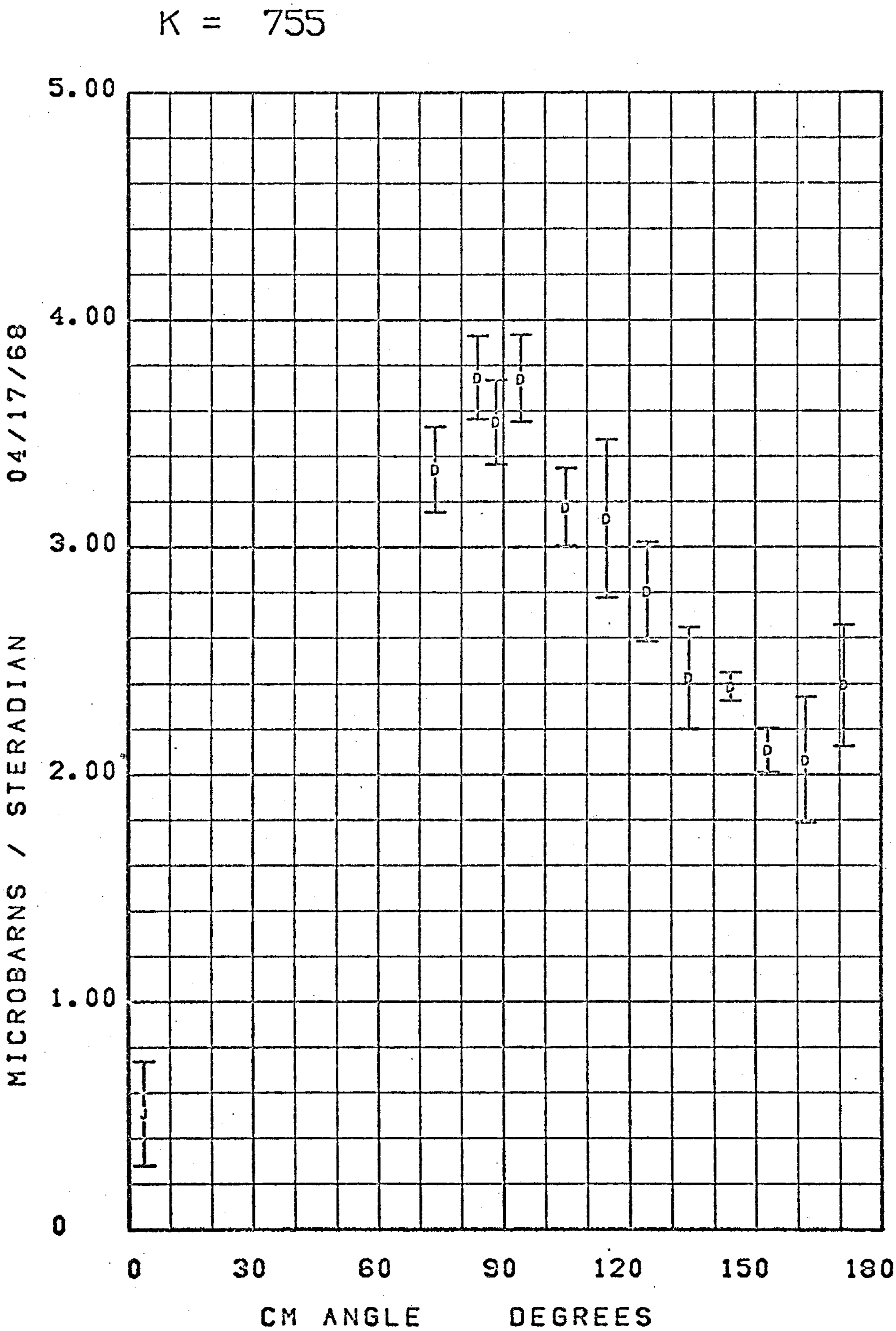
K = 755
5.00
4.00
3.00
2.00
1.00
0
04/17/68
MICROBARNS / STERADIAN
0
30
60
90
120
150
180
CM ANGLE DEGREES

Figure 12.11

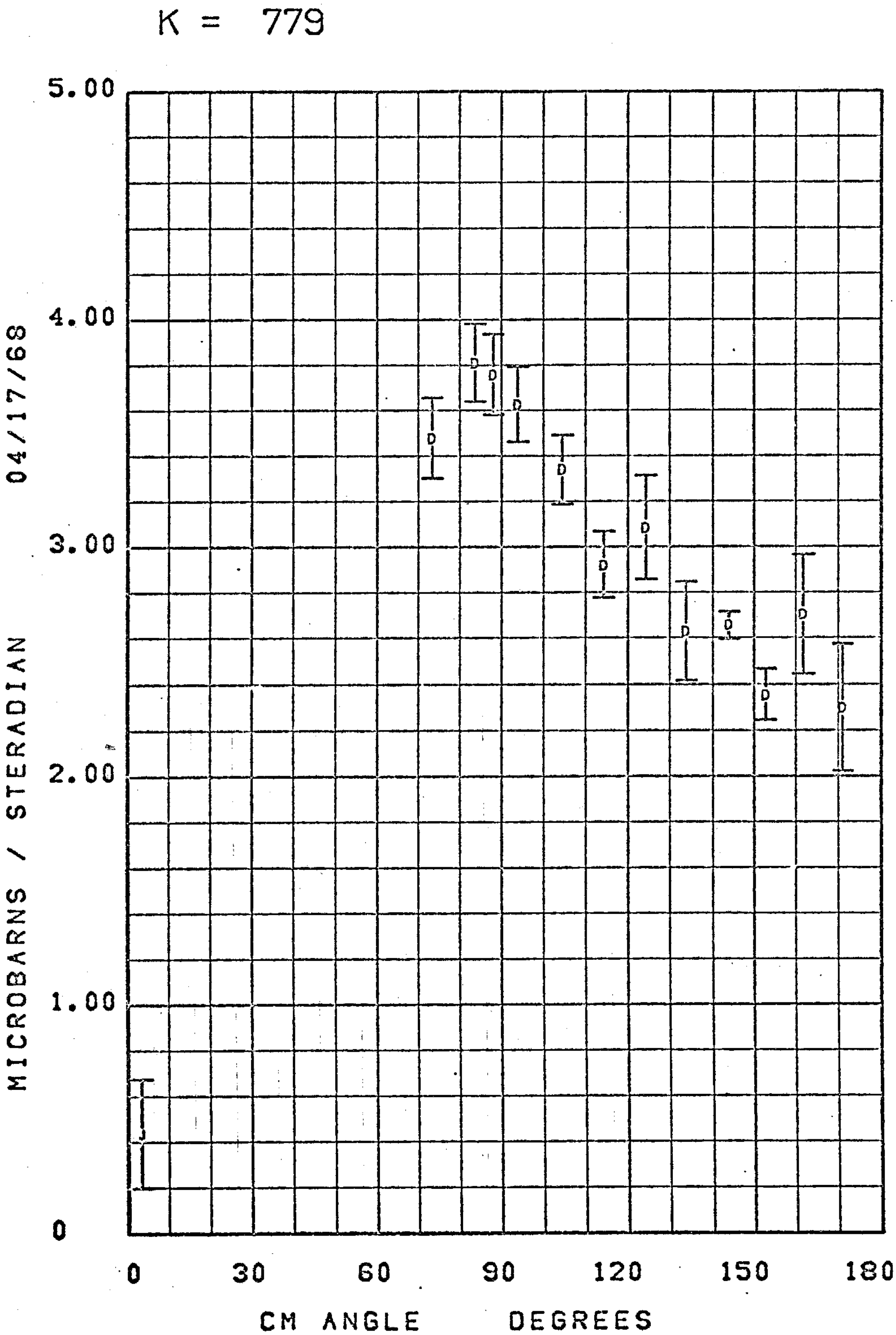
K = 779
5.00
4.00
3.00
2.00
1.00
0
04/17/68
MICROBARNS / STERADIAN
0
30
60
90
120
150
180
CM ANGLE DEGREES

Figure 12.12

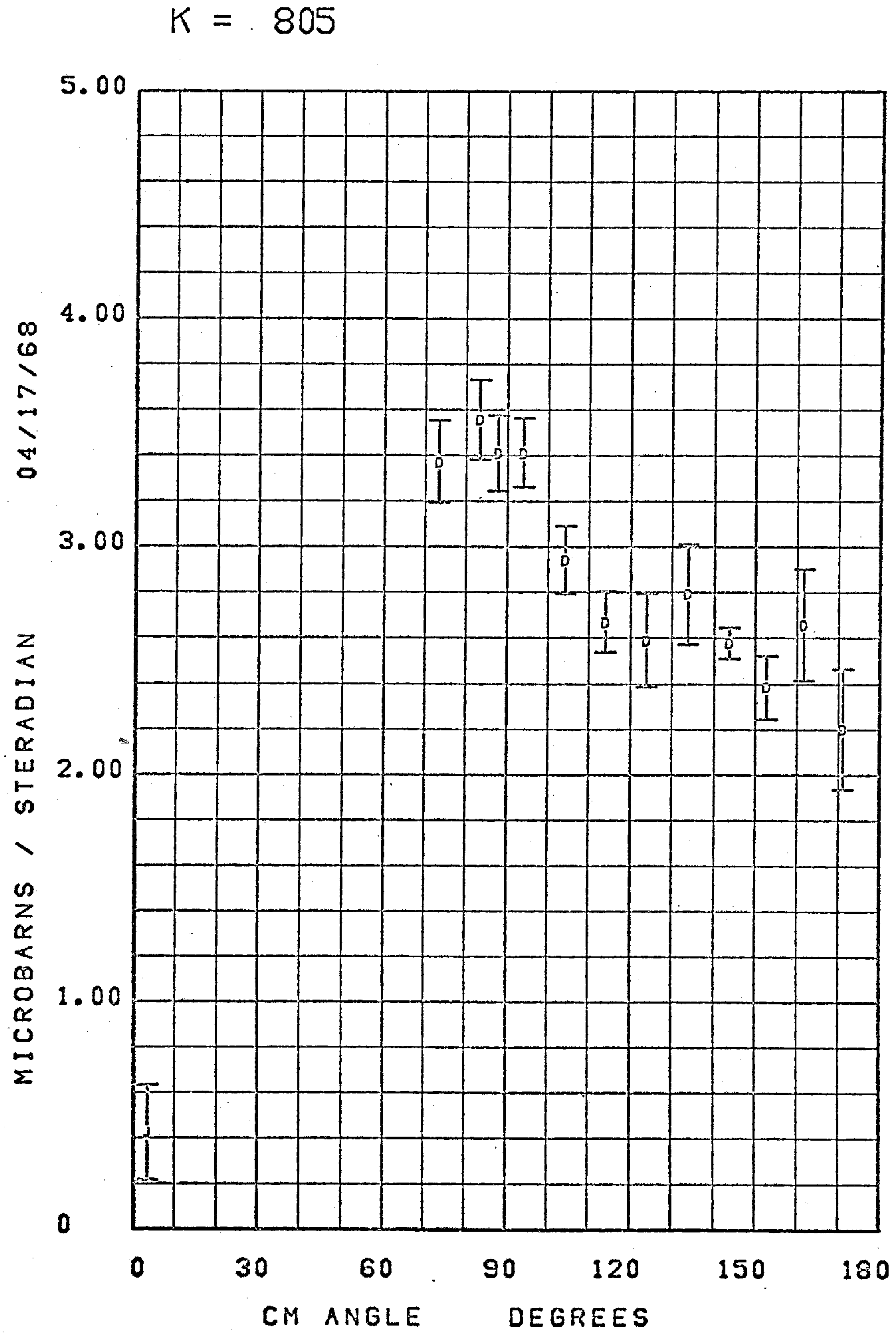
K = 805
5.00
4.00
3.00
2.00
1.00
0
04/17/68
MICROBARNS / STERADIAN
0
30
60
90
120
150
180
CM ANGLE DEGREES

Figure 12.13

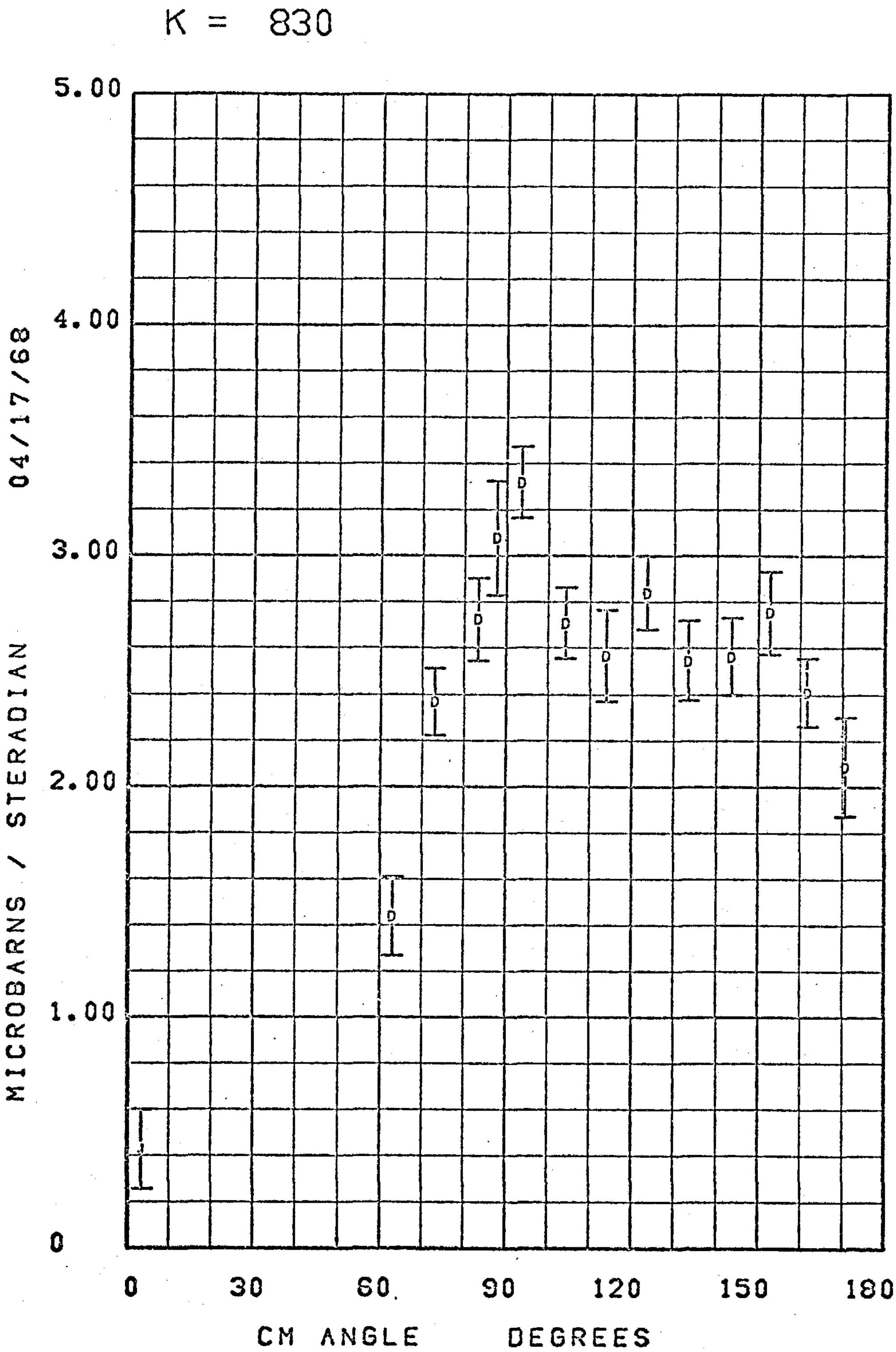
K = 830
5.00
4.00
3.00
2.00
1.00
0
04/17/68
MICROBARNS / STERADIAN
0
30
60
90
120
150
180
CM ANGLE DEGREES

Figure 12.14

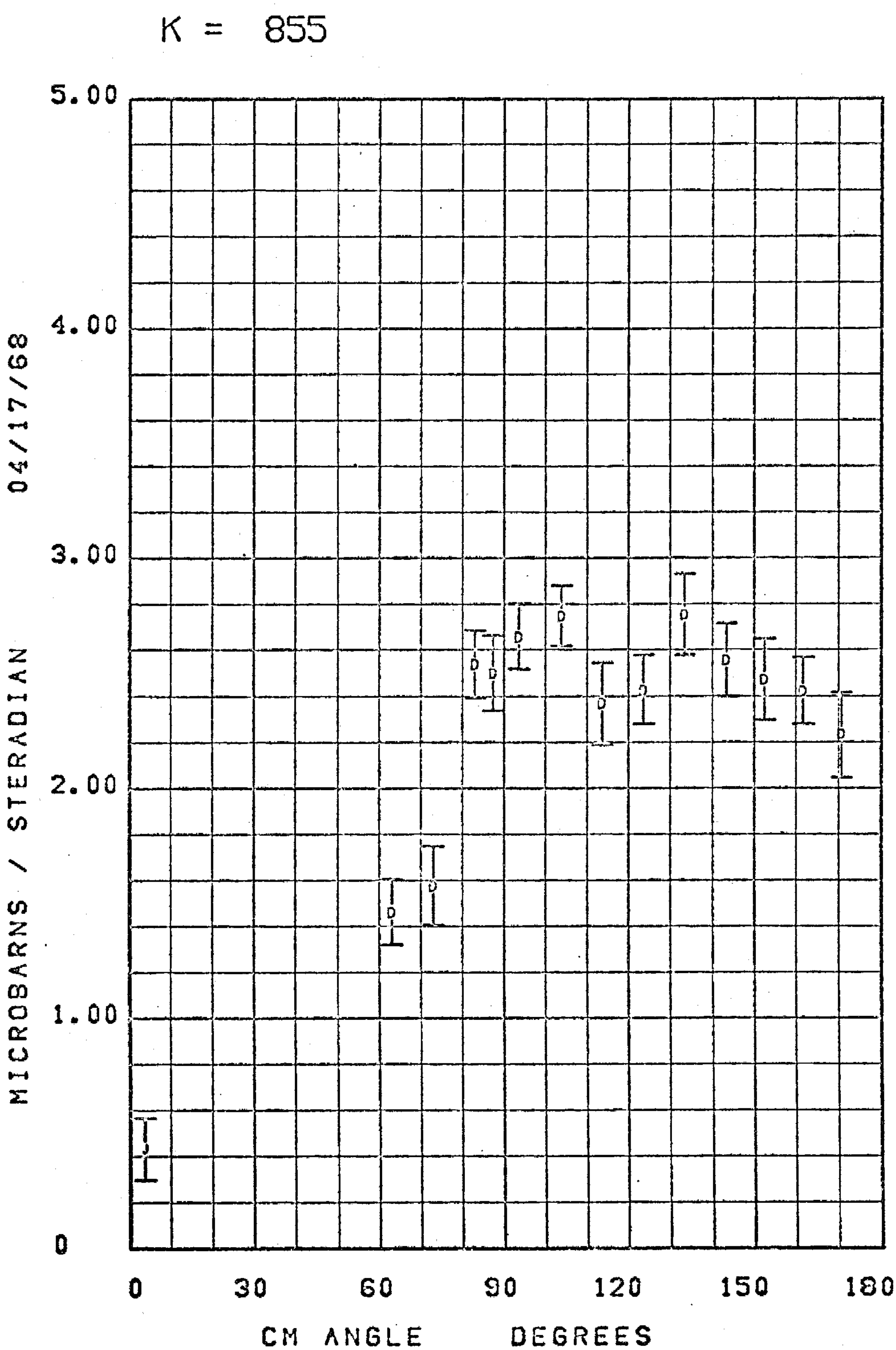
K = 855
5.00
4.00
3.00
2.00
1.00
0
04/17/68
MICROBARNS / STERADIAN
0
30
60
90
120
150
180
CM ANGLE DEGREES

Figure 12.15

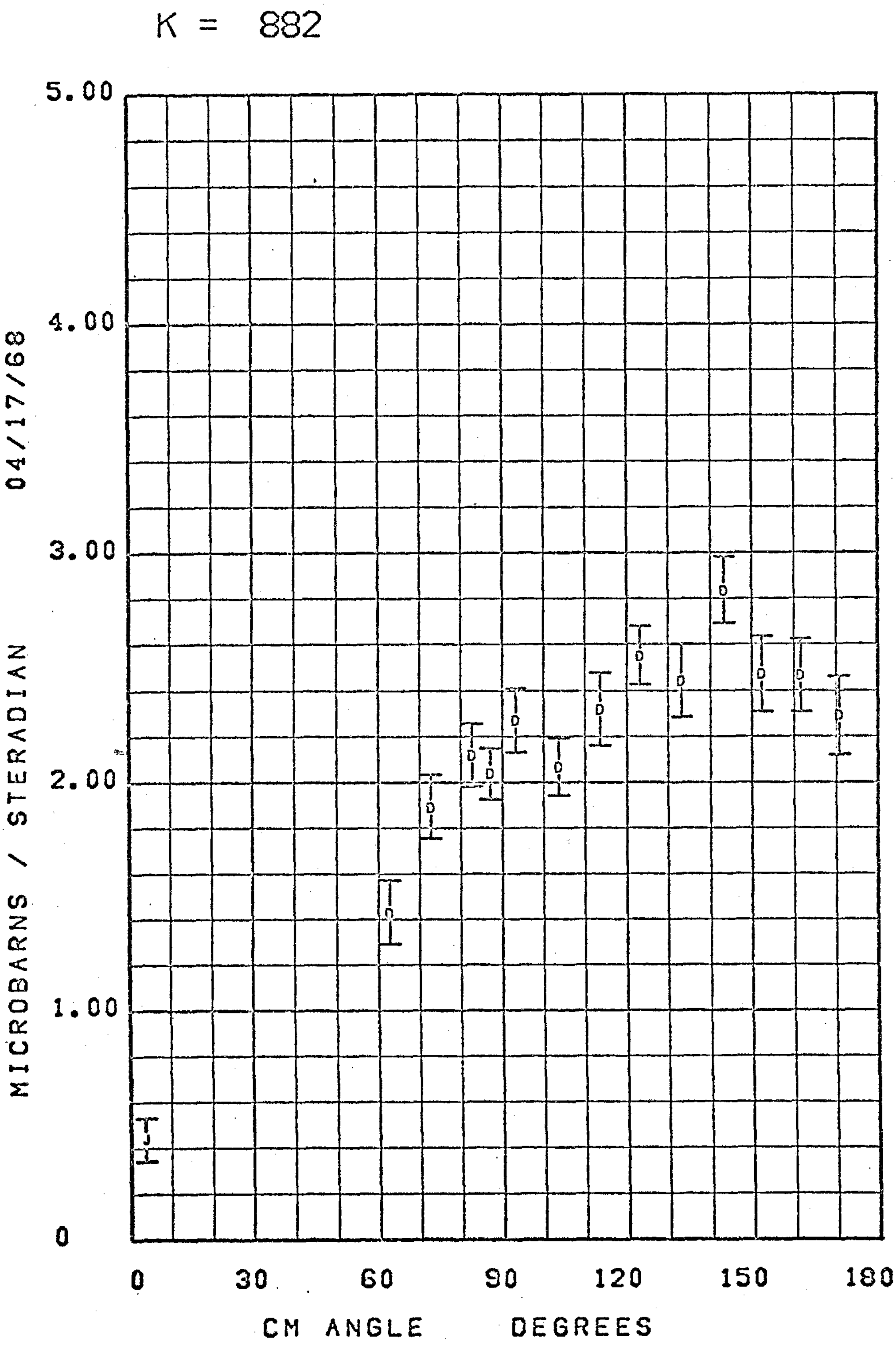
K = 882
5.00
4.00
3.00
2.00
1.00
0
04/17/68
MICROBARNS / STERADIAN
0
30
60
90
120
150
180
CM ANGLE DEGREES

Figure 12.16

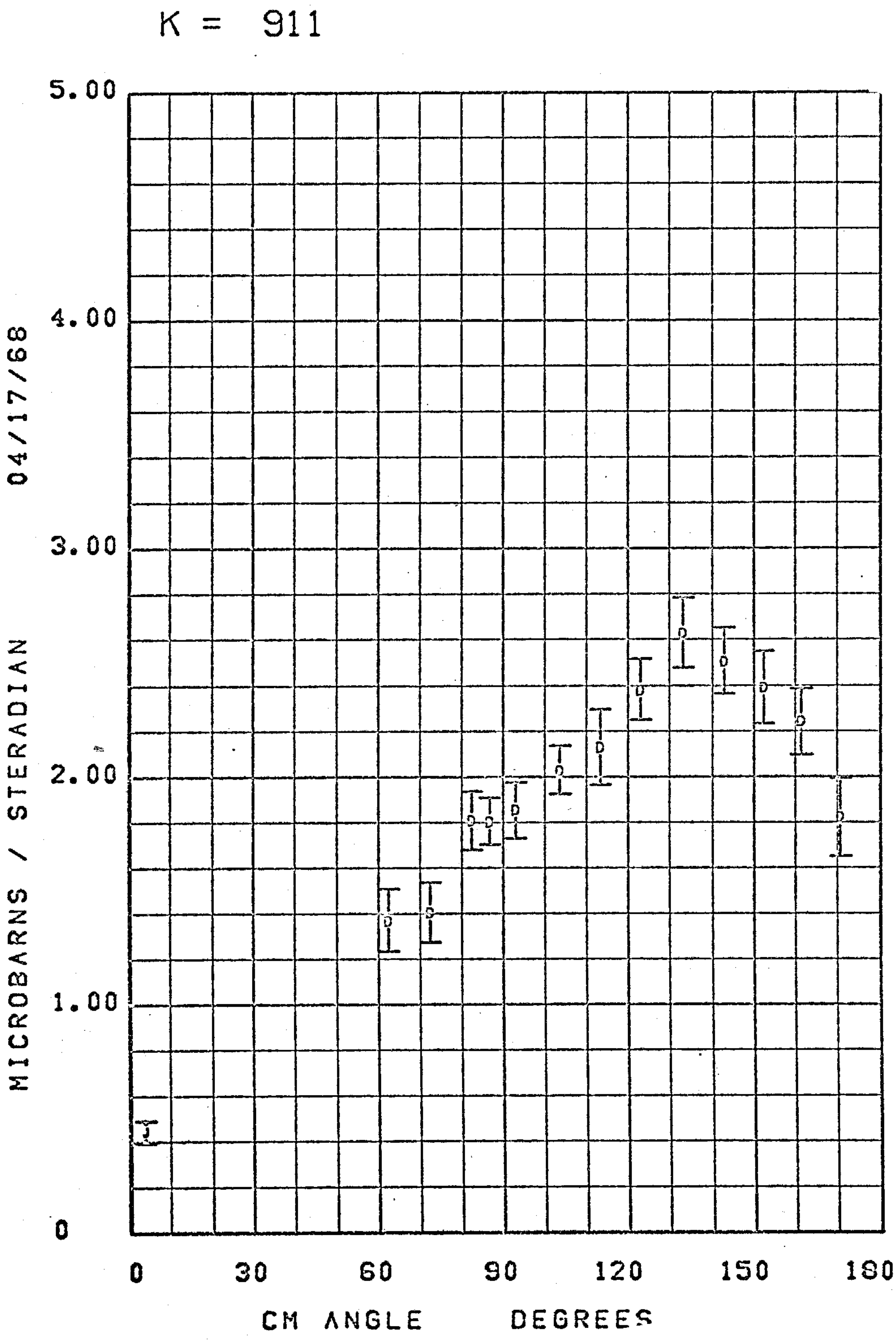
K = 911
5.00
4.00
3.00
2.00
1.00
0
MICROBARNS / STERADIAN   04/17/68
0
30
60
90
120
150
180
CM ANGLE   DEGREES

Figure 12.17

K = 924

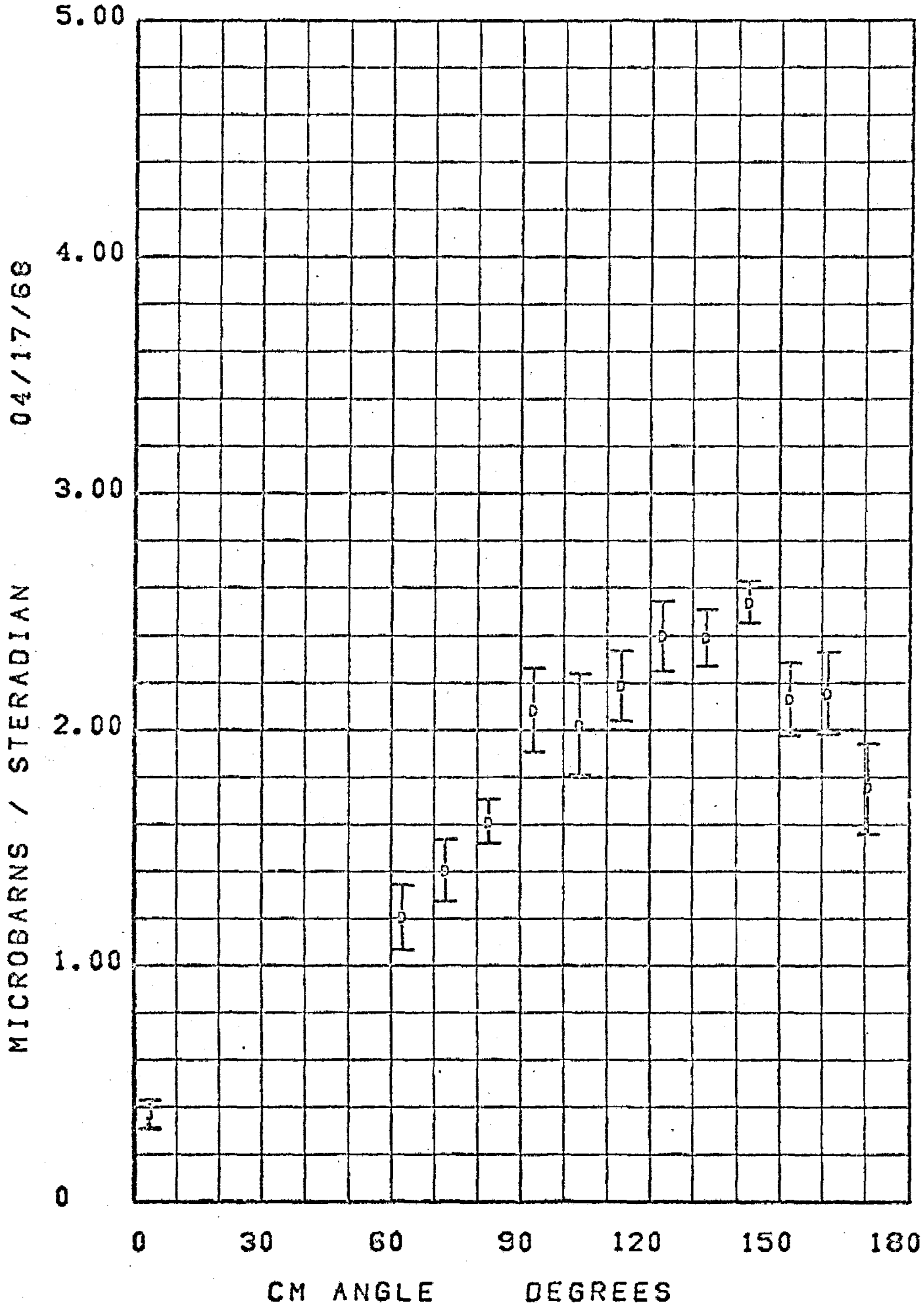

Figure 12.18

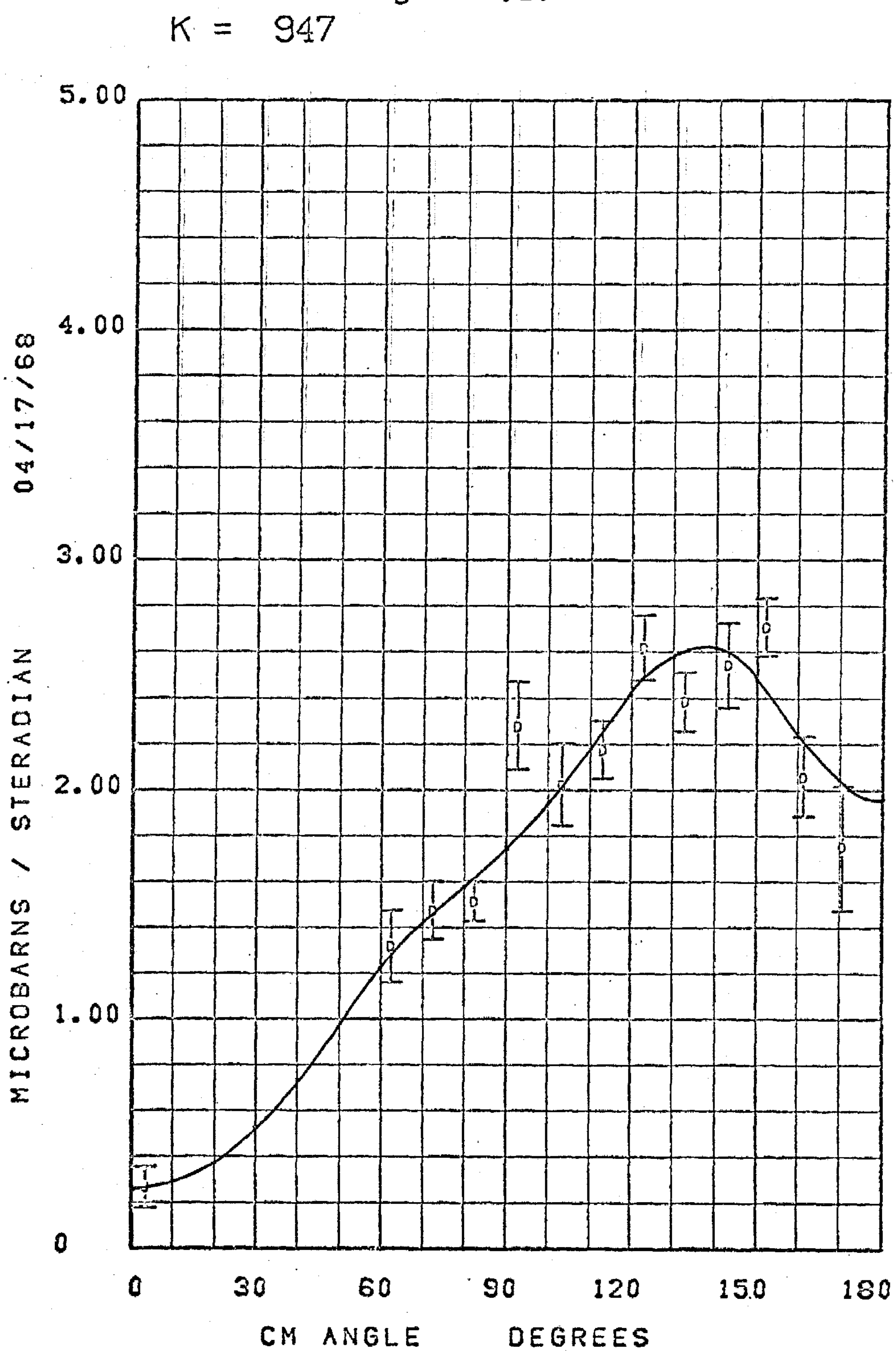
K = 947
MICROBARNS / STERADIAN
04/17/68
5.00
4.00
3.00
2.00
1.00
0
0
30
60
90
120
150
180
CM ANGLE DEGREES

Figure 12.19

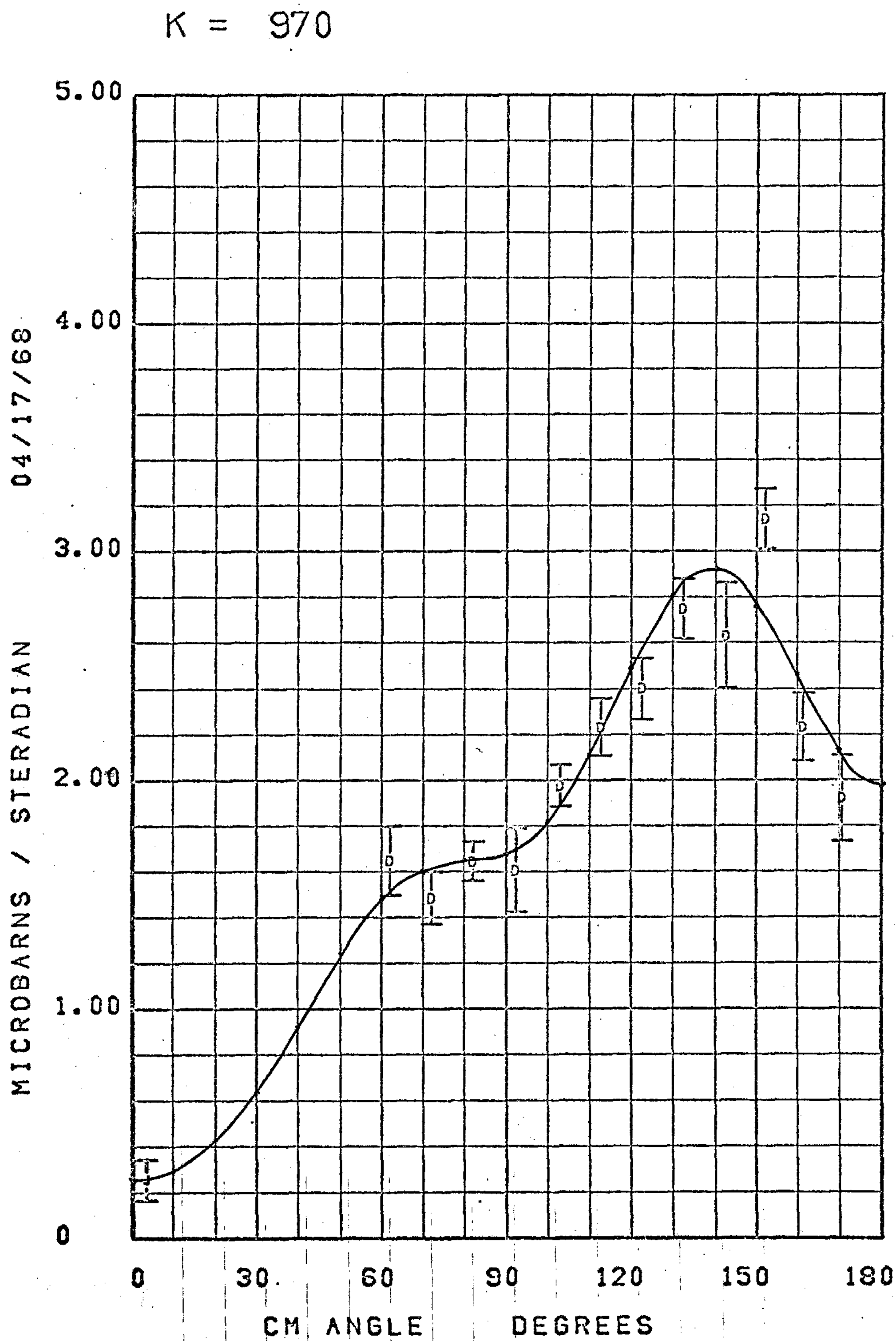
K = 970
5.00
4.00
3.00
2.00
1.00
0
04/17/68
MICROBARNS / STERADIAN
0
30
60
90
120
150
180
CM ANGLE DEGREES

Figure 12.20

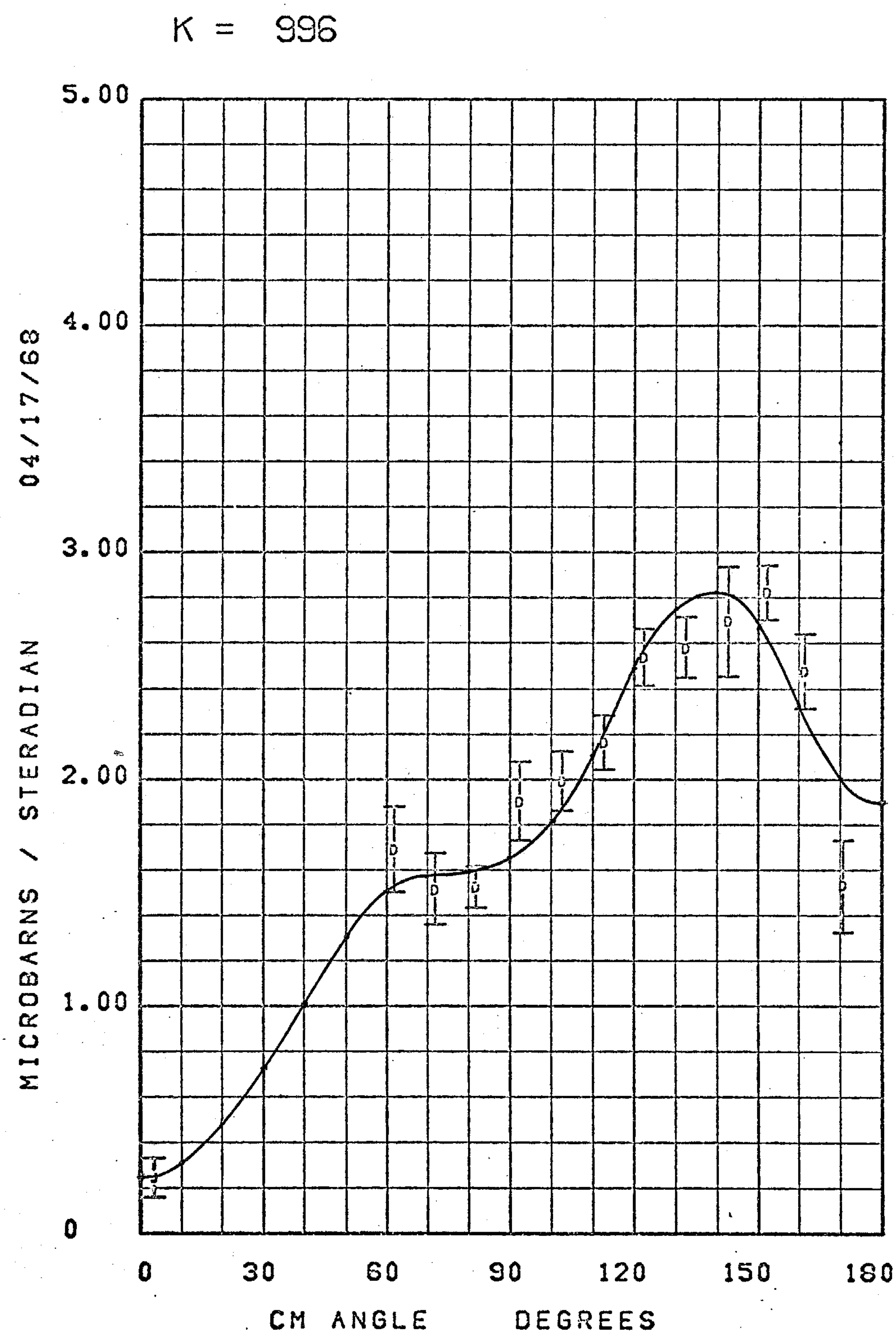
K = 996
5.00
4.00
3.00
2.00
1.00
0
04/17/68
MICROBARNS / STERADIAN
0
30
60
90
120
150
180
CM ANGLE DEGREES

Figure 12.21

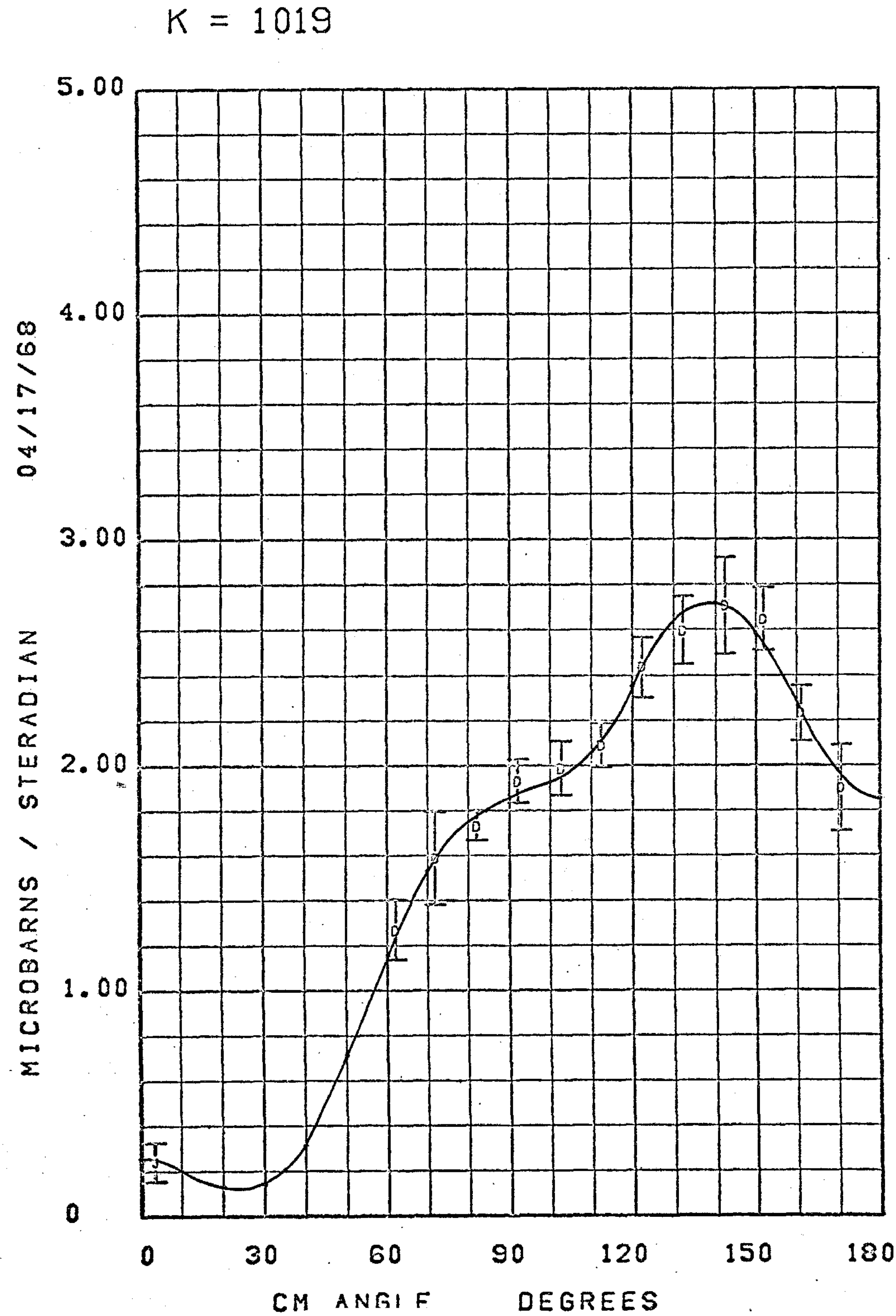
K = 1019
5.00
4.00
3.00
2.00
1.00
0
04/17/68
MICROBARNS / STERADIAN
0
30
60
90
120
150
180
CM ANGLE DEGREES

Figure 12. 22

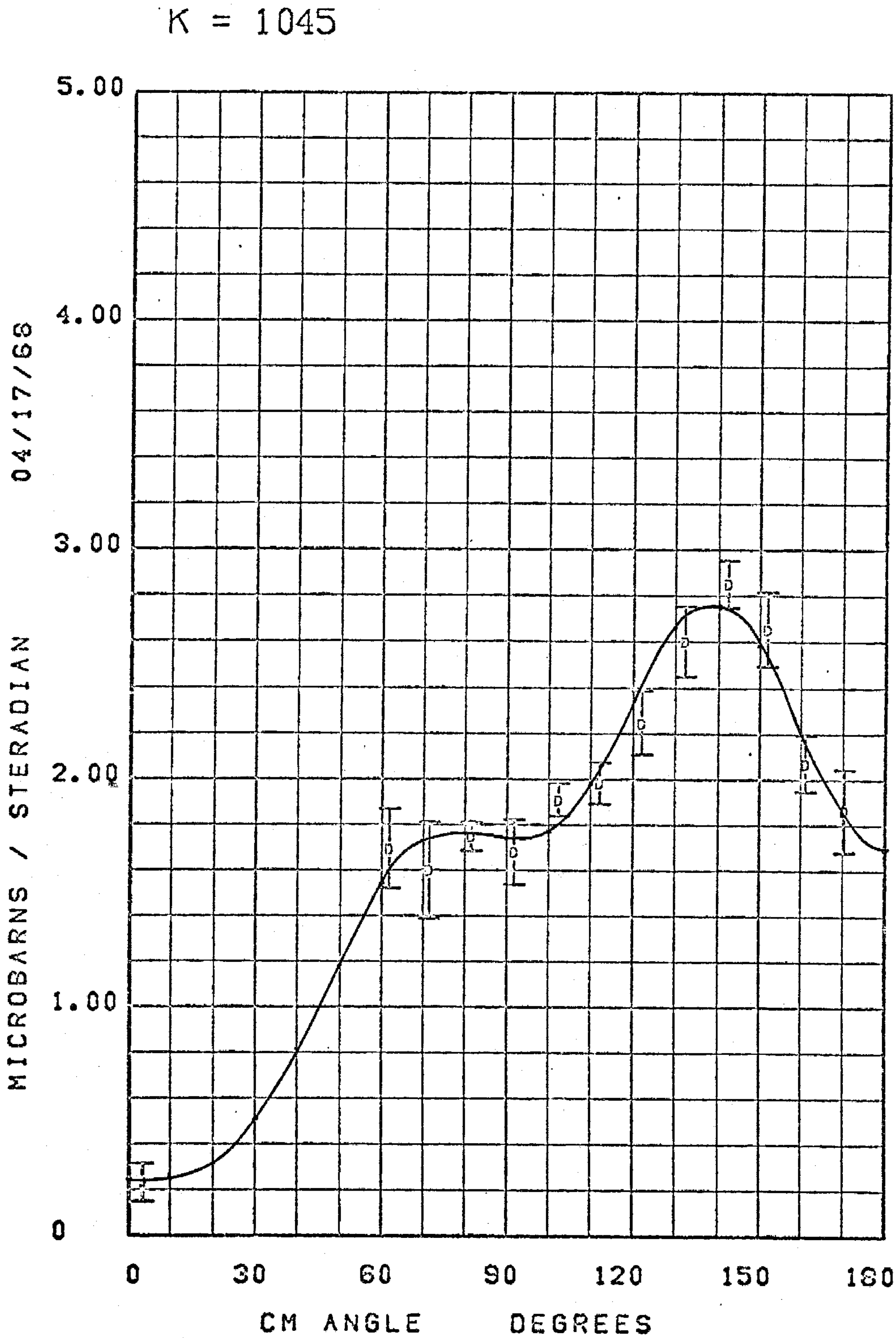
K = 1045
5.00
4.00
3.00
2.00
1.00
0
04/17/68
MICROBARNS / STERADIAN
0
30
60
90
120
150
180
CM ANGLE DEGREES

Figure 12.23

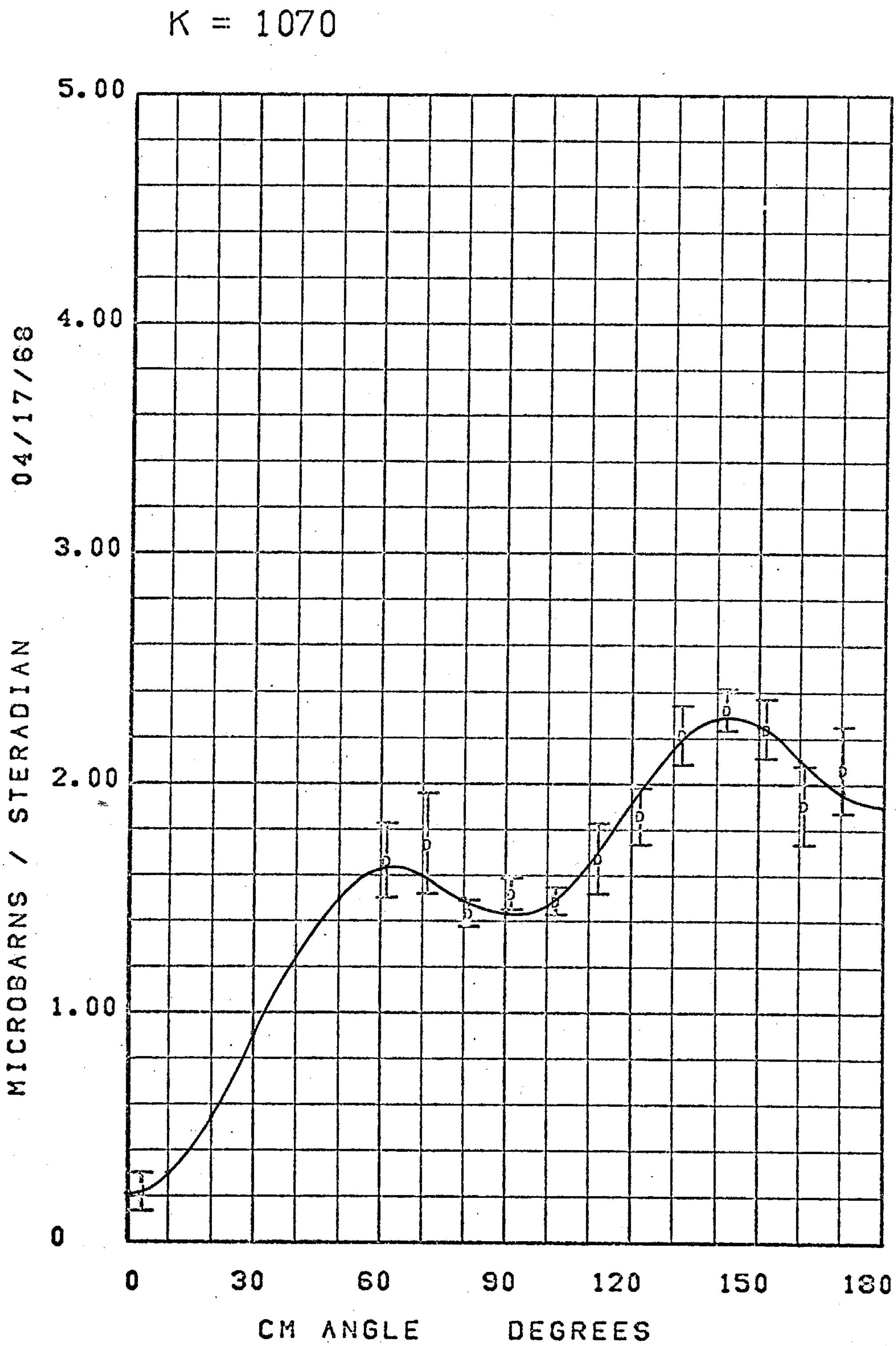
K = 1070
5.00
4.00
3.00
2.00
1.00
0
MICROBARNS / STERADIAN
04/17/68
0
30
60
90
120
150
180
CM ANGLE DEGREES

Figure 12.24

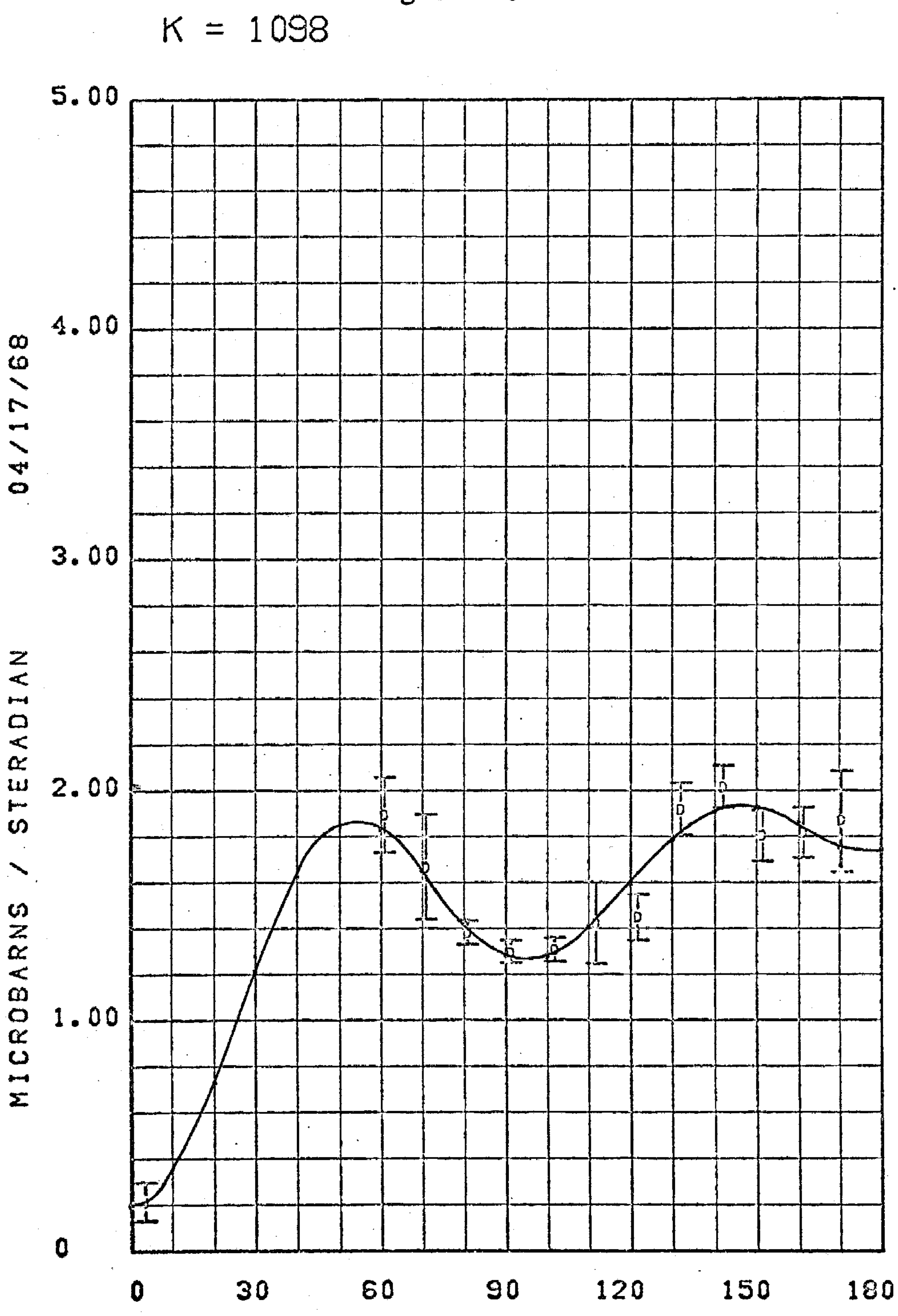
K = 1098
5.00
4.00
3.00
2.00
1.00
0
MICROBARNS / STERADIAN
04/17/68
0
30
60
90
120
150
180
CM ANGLE DEGREES

Figure 12.25

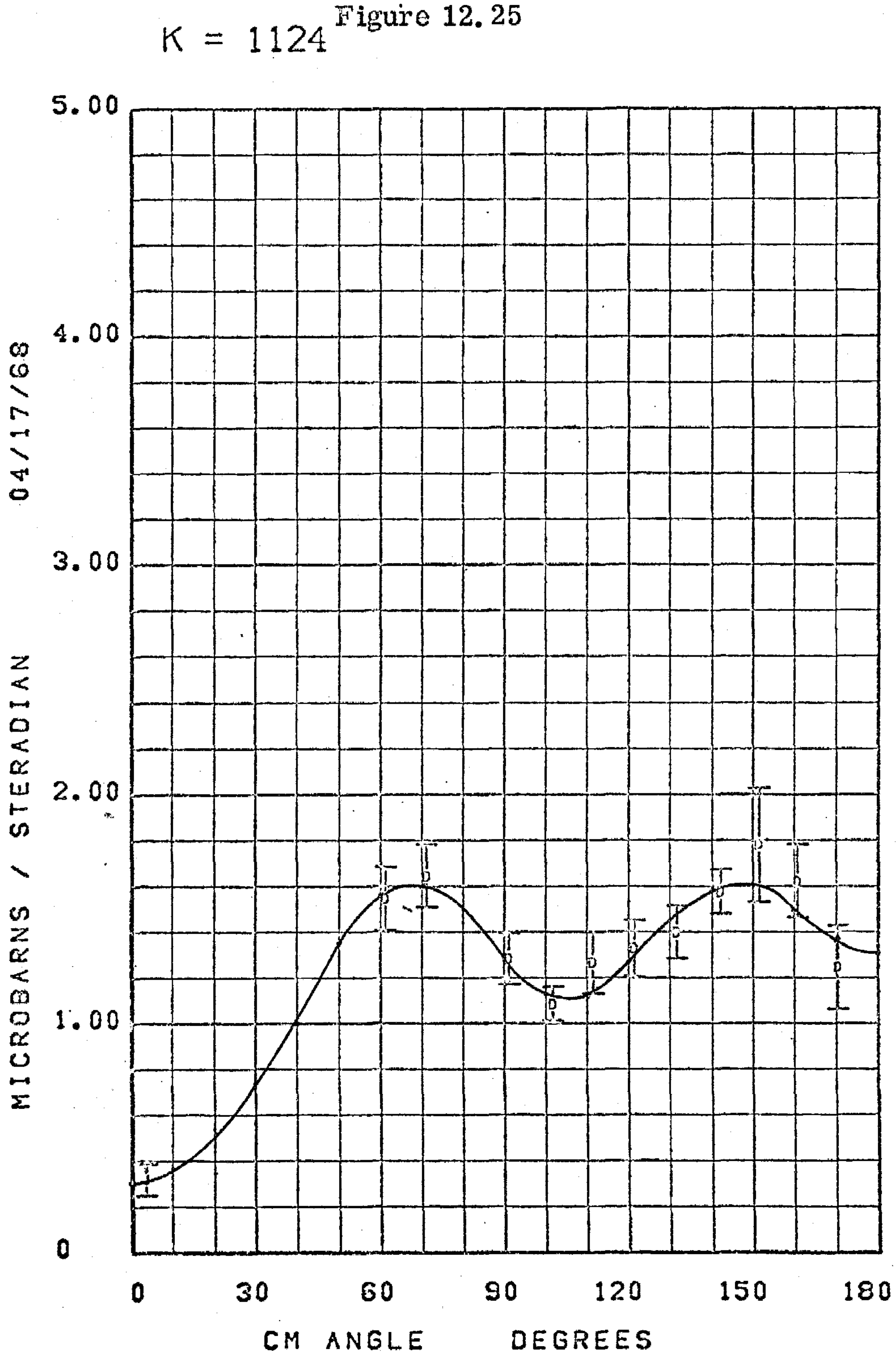
K = 1124
04/17/68
MICROBARNS / STERADIAN
5.00
4.00
3.00
2.00
1.00
0
0
30
60
90
120
150
180
CM ANGLE DEGREES

Figure 12.26

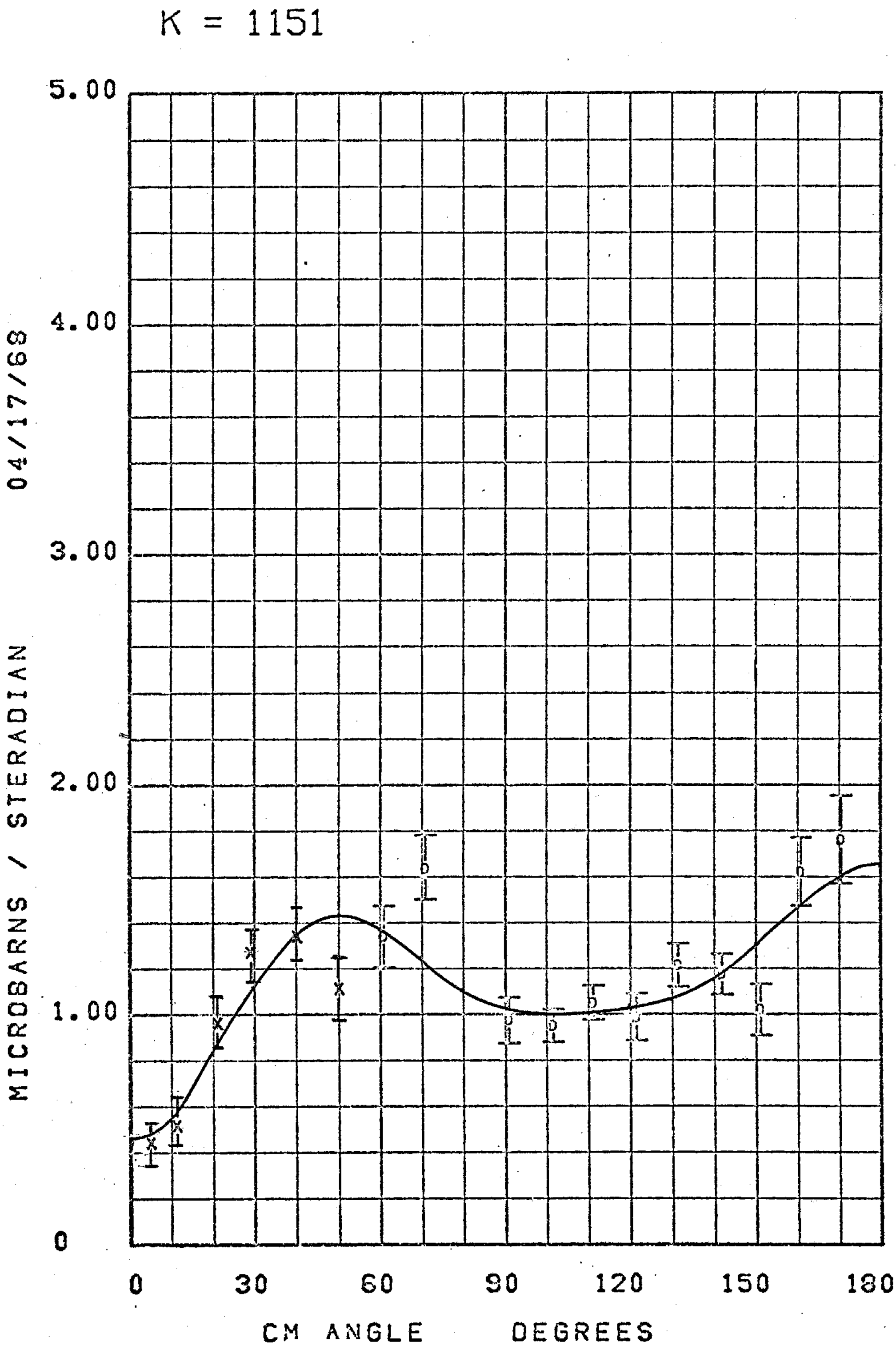
K = 1151
5.00
4.00
3.00
2.00
1.00
0
04/17/68
MICROBARNS / STERADIAN
0
30
60
90
120
150
180
CM ANGLE DEGREES

Figure 12.27

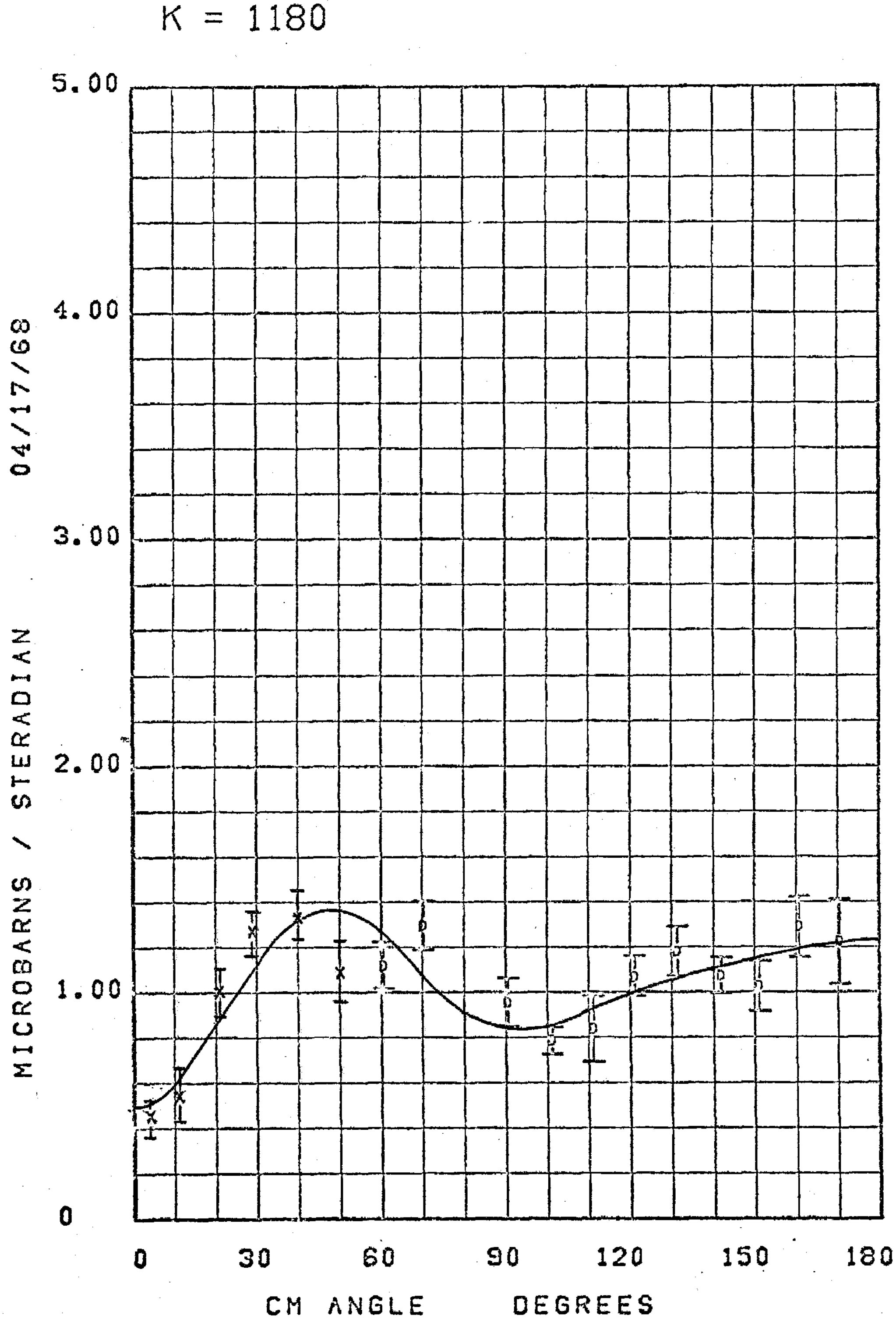
K = 1180
5.00
4.00
3.00
2.00
1.00
0
04/17/68
MICROBARNS / STERADIAN
0
30
60
90
120
150
180
CM ANGLE DEGREES

Figure 12.28

K = 1211

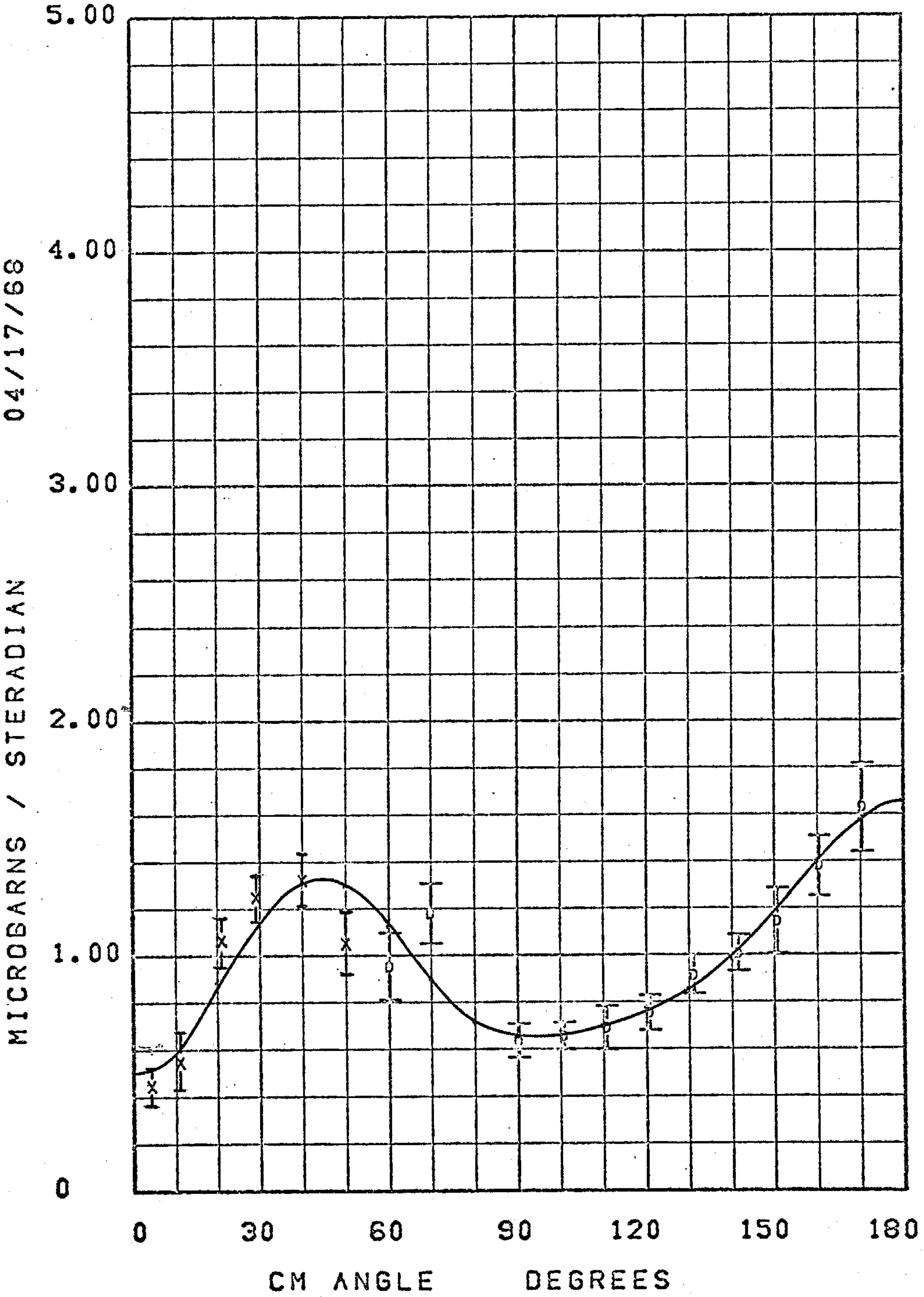

Table 2

Angular distributions of final cross sections. K is the laboratory photon energy. The cross sections and errors in microbarns/steradian are given versus the π^0 c.m. angle in degrees.

K = 574

CM PI ANGLE	CROSS SECTION	
84.6	2.73	0.19
89.0	3.00	0.18
95.2	3.36	0.20
105.8	3.36	0.21
115.4	2.00	0.14
125.1	2.10	0.14
134.8	1.63	0.12
144.7	1.24	0.23
153.5	0.56	0.19
162.3	0.41	0.26
171.1	0.98	0.20

K = 591

CM PI ANGLE	CROSS SECTION	
84.6	2.41	0.17
89.0	3.03	0.25
95.1	3.05	0.20
105.7	2.96	0.21
115.3	2.05	0.14
125.0	1.82	0.15
134.8	1.60	0.14
144.6	1.33	0.21
153.4	1.09	0.19
162.3	0.36	0.27
171.1	0.72	0.19

K = 609

CM PI ANGLE	CROSS SECTION	
84.5	2.61	0.16
88.9	2.61	0.19
95.0	3.12	0.20
105.6	2.68	0.20
115.2	2.32	0.14
124.9	1.94	0.14
134.7	1.39	0.13
144.5	1.31	0.14
153.3	0.90	0.15
162.2	0.96	0.44
171.1	0.83	0.15

K = 629

CM PI ANGLE	CROSS SECTION	
84.4	2.62	0.18
88.8	2.72	0.13
94.9	2.91	0.21
105.4	2.54	0.16
115.1	1.96	0.14
124.8	1.79	0.12
134.6	1.41	0.11
144.4	1.28	0.15
153.3	0.95	0.13
162.2	1.09	0.36
171.1	0.86	0.22

K = 650

CM PI ANGLE	CROSS SECTION	
84.3	2.28	0.16
88.7	2.32	0.15
94.8	2.62	0.16
105.3	2.82	0.15
115.0	2.37	0.15
124.7	1.88	0.13
134.5	1.34	0.10
144.4	1.33	0.08
153.2	1.08	0.22
162.1	1.00	0.15
171.0	1.05	0.17

K = 669

CM PI ANGLE	CROSS SECTION	
84.2	2.83	0.17
88.6	3.05	0.17
94.7	3.16	0.17
105.2	2.87	0.15
114.8	2.41	0.14
124.5	1.90	0.13
134.4	1.54	0.09
144.3	1.46	0.09
153.2	1.20	0.11
162.1	1.36	0.18
171.0	1.20	0.16

K = 690

CM PI ANGLE	CROSS SECTION	
84.1	3.03	0.17
88.4	2.98	0.16
94.5	3.68	0.17
105.0	2.98	0.16
114.7	2.81	0.16
124.4	2.40	0.15
134.2	1.84	0.10
144.2	1.57	0.10
153.1	1.55	0.09
162.0	1.31	0.16
171.0	1.40	0.31

K = 712

CM PI ANGLE	CROSS SECTION	
83.9	3.44	0.18
88.3	3.71	0.18
94.3	3.85	0.17
104.9	3.28	0.16
114.5	2.65	0.14
124.2	2.45	0.15
134.1	2.11	0.17
144.1	1.80	0.08
153.0	1.68	0.10
162.0	1.53	0.16
171.0	1.89	0.19

K = 733

CM PI ANGLE	CROSS SECTION	
73.6	3.03	0.18
83.9	3.48	0.19
88.2	3.68	0.18
94.2	3.55	0.17
104.8	3.45	0.18
114.4	2.98	0.28
124.1	2.60	0.20
134.0	2.34	0.23
144.0	2.13	0.08
152.9	2.02	0.18
161.9	1.85	0.21
170.9	1.77	0.28

K = 755

CM PI ANGLE	CROSS SECTION	
73.4	3.34	0.19
83.7	3.75	0.18
88.0	3.55	0.19
94.1	3.74	0.19
104.6	3.18	0.17
114.2	3.13	0.35
124.0	2.81	0.22
133.9	2.42	0.23
143.9	2.38	0.06
152.8	2.10	0.10
161.8	2.06	0.28
170.9	2.39	0.27

K = 779

CM PI ANGLE	CROSS SECTION	
73.3	3.48	0.18
83.5	3.81	0.17
87.8	3.76	0.18
93.8	3.63	0.16
104.4	3.34	0.15
114.0	2.92	0.15
123.8	3.09	0.23
133.7	2.63	0.22
143.7	2.66	0.06
152.7	2.35	0.11
161.8	2.70	0.26
170.9	2.30	0.27

K = 805

CM PI ANGLE	CROSS SECTION	
73.0	3.38	0.18
83.2	3.56	0.17
87.6	3.41	0.16
93.6	3.42	0.15
104.1	2.94	0.15
113.8	2.67	0.13
123.6	2.59	0.20
133.5	2.80	0.22
143.6	2.58	0.07
152.6	2.38	0.14
161.7	2.66	0.25
170.8	2.20	0.26

K = 830

CM PI ANGLE	CROSS SECTION	
63.0	1.44	0.17
73.0	2.37	0.15
83.2	2.73	0.18
87.5	3.08	0.25
93.5	3.32	0.15
104.0	2.71	0.15
113.7	2.57	0.20
123.5	2.84	0.16
133.4	2.55	0.17
143.5	2.56	0.17
152.5	2.76	0.18
161.6	2.41	0.15
170.8	2.08	0.21

K = 855

CM PI ANGLE	CROSS SECTION	
62.8	1.46	0.14
72.8	1.58	0.17
82.9	2.54	0.15
87.3	2.50	0.17
93.3	2.66	0.14
103.8	2.75	0.13
113.4	2.37	0.18
123.3	2.43	0.15
133.2	2.76	0.18
143.3	2.56	0.16
152.4	2.47	0.18
161.6	2.42	0.15
170.8	2.23	0.19

K = 882

CM PI ANGLE	CROSS SECTION	
62.6	1.43	0.14
72.5	1.89	0.14
82.7	2.12	0.13
87.0	2.03	0.11
93.0	2.27	0.14
103.5	2.07	0.13
113.2	2.32	0.16
123.0	2.55	0.13
133.0	2.44	0.16
143.2	2.84	0.15
152.3	2.47	0.17
161.5	2.46	0.16
170.7	2.29	0.17

K = 911

CM PI ANGLE	CROSS SECTION	
62.3	1.37	0.14
72.3	1.40	0.13
82.4	1.81	0.13
86.7	1.80	0.10
92.7	1.85	0.12
103.2	2.03	0.10
112.9	2.13	0.16
122.8	2.38	0.13
132.8	2.63	0.15
143.0	2.51	0.15
152.2	2.39	0.16
161.4	2.24	0.14
170.7	1.82	0.17

K = 924

CM PI ANGLE	CROSS SECTION	
62.5	1.21	0.14
72.4	1.40	0.13
82.5	1.61	0.09
92.8	2.08	0.18
103.3	2.02	0.22
112.9	2.19	0.15
122.8	2.40	0.15
132.8	2.39	0.12
143.0	2.54	0.09
152.1	2.13	0.15
161.4	2.15	0.18
170.7	1.75	0.19

K = 947

CM PI ANGLE	CROSS SECTION	
62.2	1.32	0.16
72.2	1.47	0.13
82.2	1.51	0.09
92.5	2.28	0.19
103.1	2.02	0.18
112.7	2.17	0.13
122.6	2.62	0.14
132.6	2.38	0.13
142.9	2.54	0.19
152.0	2.71	0.13
161.3	2.06	0.17
170.6	1.74	0.27

K = 970

CM PI ANGLE	CROSS SECTION	
62.0	1.65	0.15
71.8	1.48	0.12
81.9	1.64	0.09
92.3	1.60	0.18
102.8	1.97	0.09
112.5	2.23	0.13
122.4	2.40	0.13
132.4	2.75	0.13
142.7	2.63	0.23
151.9	3.14	0.13
161.2	2.23	0.15
170.6	1.92	0.19

K = 996

CM PI ANGLE	CROSS SECTION	
61.6	1.69	0.19
71.5	1.51	0.16
81.6	1.52	0.09
92.0	1.90	0.17
102.5	1.99	0.13
112.3	2.16	0.12
122.2	2.54	0.13
132.2	2.58	0.14
142.5	2.70	0.24
151.8	2.82	0.12
161.2	2.48	0.17
170.6	1.53	0.20

K = 1019

CM PI ANGLE	CROSS SECTION	
61.9	1.27	0.13
71.7	1.59	0.20
81.8	1.73	0.06
92.0	1.93	0.10
102.5	1.99	0.12
112.2	2.09	0.10
122.1	2.43	0.14
132.2	2.60	0.15
142.5	2.71	0.21
151.7	2.65	0.14
161.1	2.23	0.12
170.5	1.90	0.19

K = 1045

CM PI ANGLE	CROSS SECTION	
61.6	1.69	0.17
71.4	1.60	0.21
81.4	1.75	0.06
91.7	1.68	0.14
102.2	1.91	0.07
111.9	1.98	0.09
121.8	2.24	0.14
132.0	2.60	0.15
142.3	2.85	0.10
151.6	2.65	0.16
161.0	2.07	0.12
170.5	1.86	0.18

K = 1070

CM PI ANGLE	CROSS SECTION	
61.2	1.66	0.16
71.0	1.74	0.22
81.1	1.43	0.06
91.4	1.52	0.07
101.9	1.48	0.06
111.6	1.67	0.15
121.6	1.86	0.12
131.8	2.21	0.13
142.2	2.32	0.09
151.5	2.24	0.13
160.9	1.91	0.17
170.5	2.06	0.19

K = 1098

CM PI ANGLE	CROSS SECTION	
60.9	1.89	0.16
70.6	1.67	0.23
80.6	1.38	0.05
91.0	1.30	0.05
101.6	1.31	0.05
111.3	1.42	0.18
121.4	1.45	0.10
131.6	1.92	0.11
142.0	2.01	0.09
151.4	1.80	0.11
160.9	1.81	0.11
170.4	1.86	0.22

K = 1124

CM PI ANGLE	CROSS SECTION	
61.2	1.54	0.14
70.9	1.64	0.14
91.0	1.28	0.11
101.6	1.09	0.07
111.3	1.26	0.13
121.2	1.33	0.12
131.4	1.40	0.11
141.9	1.58	0.10
151.3	1.78	0.25
160.8	1.62	0.16
170.4	1.24	0.18

K = 1151

CM PI ANGLE	CROSS SECTION	
60.8	1.34	0.13
70.6	1.64	0.14
90.7	0.97	0.10
101.3	0.95	0.07
111.0	1.05	0.07
121.0	0.99	0.10
131.2	1.21	0.10
141.7	1.17	0.09
151.1	1.02	0.11
160.7	1.62	0.15
170.3	1.76	0.19

K = 1180

CM PI ANGLE	CROSS SECTION	
60.4	1.12	0.10
70.1	1.30	0.11
90.4	0.96	0.10
101.0	0.79	0.06
110.7	0.84	0.15
120.8	1.07	0.09
131.0	1.18	0.11
141.5	1.07	0.08
151.0	1.02	0.11
160.6	1.29	0.13
170.3	1.22	0.19

K = 1211

CM PI ANGLE	CROSS SECTION	
60.0	0.95	0.14
69.7	1.18	0.13
90.1	0.64	0.07
100.7	0.66	0.05
110.5	0.69	0.09
120.5	0.76	0.07
130.8	0.92	0.08
141.4	1.00	0.08
150.9	1.14	0.14
160.5	1.38	0.13
170.2	1.63	0.19

V. COMPARISON WITH OTHER EXPERIMENTS

Since the present experiment covers many angles and many energies, comparisons with other experiments are most conveniently made by interpolating the data of this experiment to find values where other experiments have data. Each interpolated point is a linear interpolation between the two nearest measured points. The errors are interpolated similarly. For convenience, the data for $\theta_p^{lab} = 41.9^o$ are not used in the interpolation because they did not cover the full energy range.

Each experiment appears either in energy distributions or in angular distributions, whichever is most appropriate for that experiment. No experiment, except the present one, appears in both.

The coding of the points is the same as that used in Beale et al. (19). New symbols have been assigned to data not in that report. Where more recent values have been used for experiments cited in Beale, a new symbol has been used.

Figure 13 shows energy distributions of most of the data at 60, 67.5, 75, 90, 105, 125, 135, and 147 degrees.

At 60^o, the present experiment only goes down to 830 MeV. The agreement with Diebold's data (code C) is excellent except for the 830 MeV point. The Bloom data (code B) have fairly large errors around 975 MeV, but seem to agree reasonably well. The data of Stein and Rogers (code S) and Vette (code X) seem to be higher around 925 MeV, but the effect could be statistical. It is interesting to note that these two experiments did not require a decay gamma ray, while the others did. The remaining point of Vette agrees very well with present data.

Figure 13

Energy distributions for $\theta_{\pi^o}^{cm} = 60^o, 67.5^o, 75^o, 90^o, 105^o, 120^o, 125^o, 135^o$, and 147^o. The symbol code is as follows:

B	Bloom (11)
C	Diebold (1)
E	Buschhorn et al. (12)
K	Bacci et al. (8)
L	Deutsch et al. (1)
M	Belletini et al. (6)
N	Nagashima
P	Jackson et al. (2)
Q	Alvarez et al. (3)
R	Cortellesa and Reale (1)
S	Stein and Rogers (1)
X	Vette (1)
3	De Wire et al. (1)
⊙	This experiment

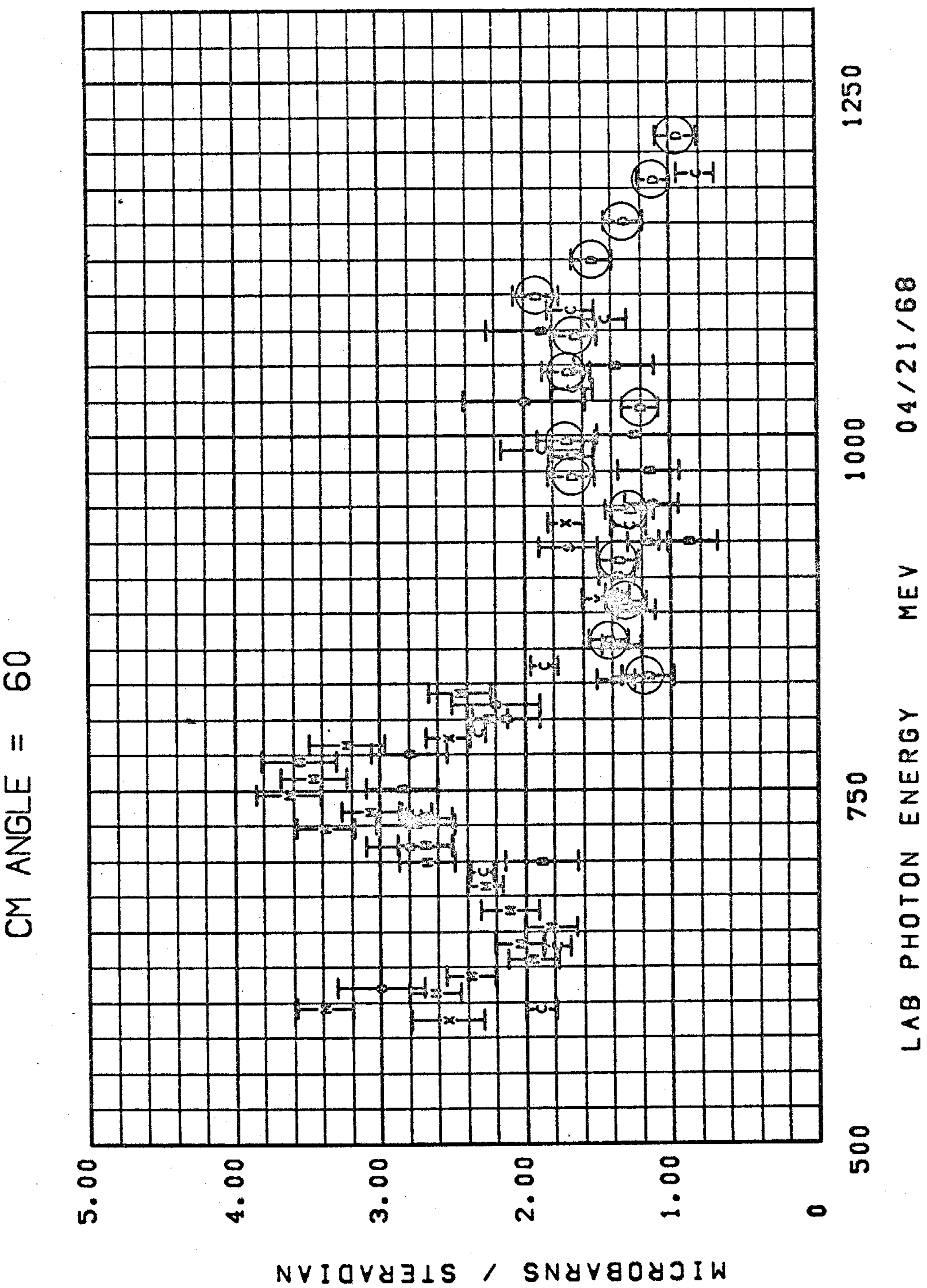
CM ANGLE = 60
LAB PHOTON ENERGY MEV
04/21/68
MICROBARNS / STERADIAN
500
750
1000
1250
0
1.00
2.00
3.00
4.00
5.00

Figure 13.1

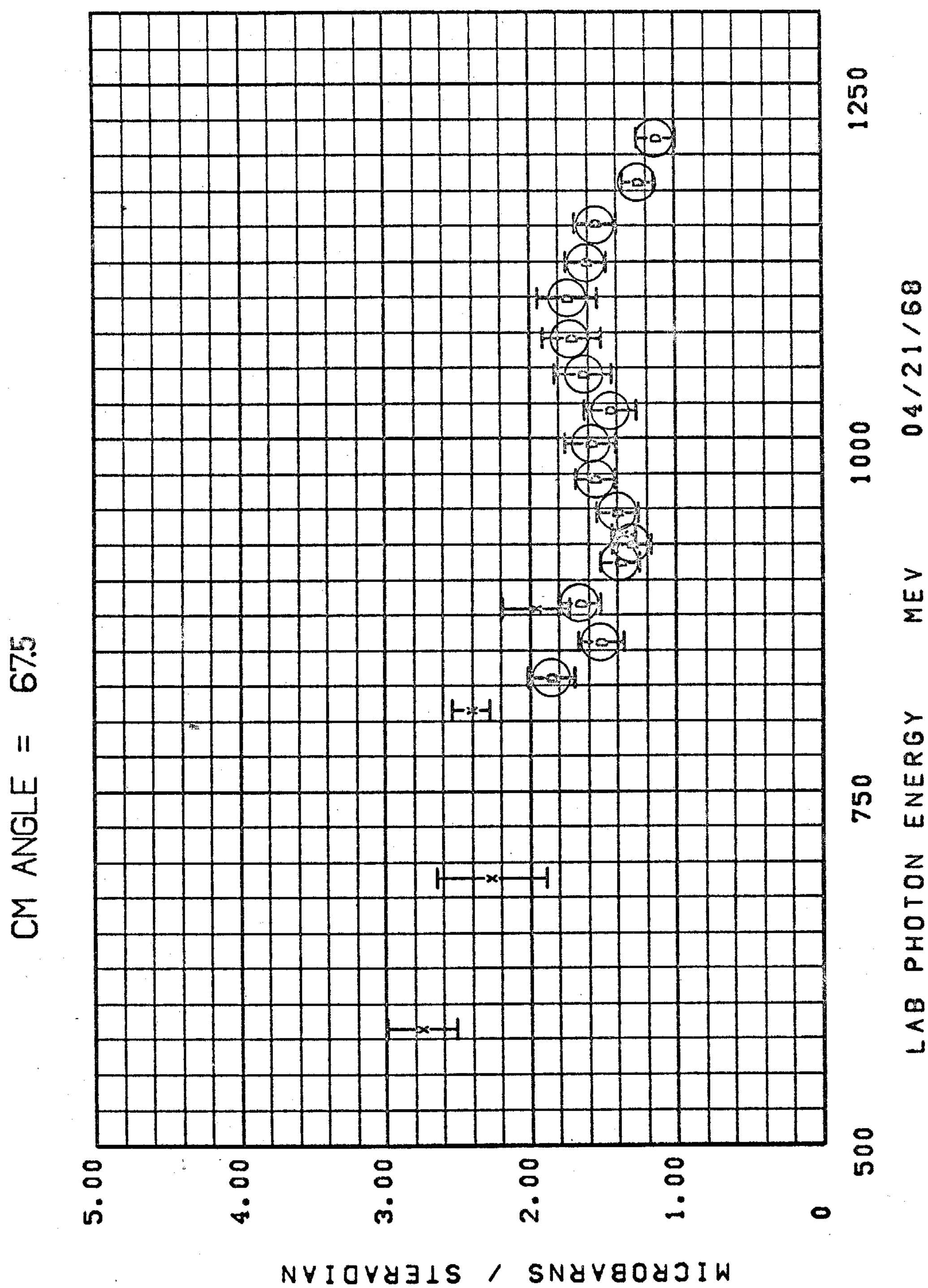
CM ANGLE = 67.5
MICROBARNS / STERADIAN
5.00
4.00
3.00
2.00
1.00
0
500
750
1000
1250
LAB PHOTON ENERGY MEV
04/21/68

Figure 13.2

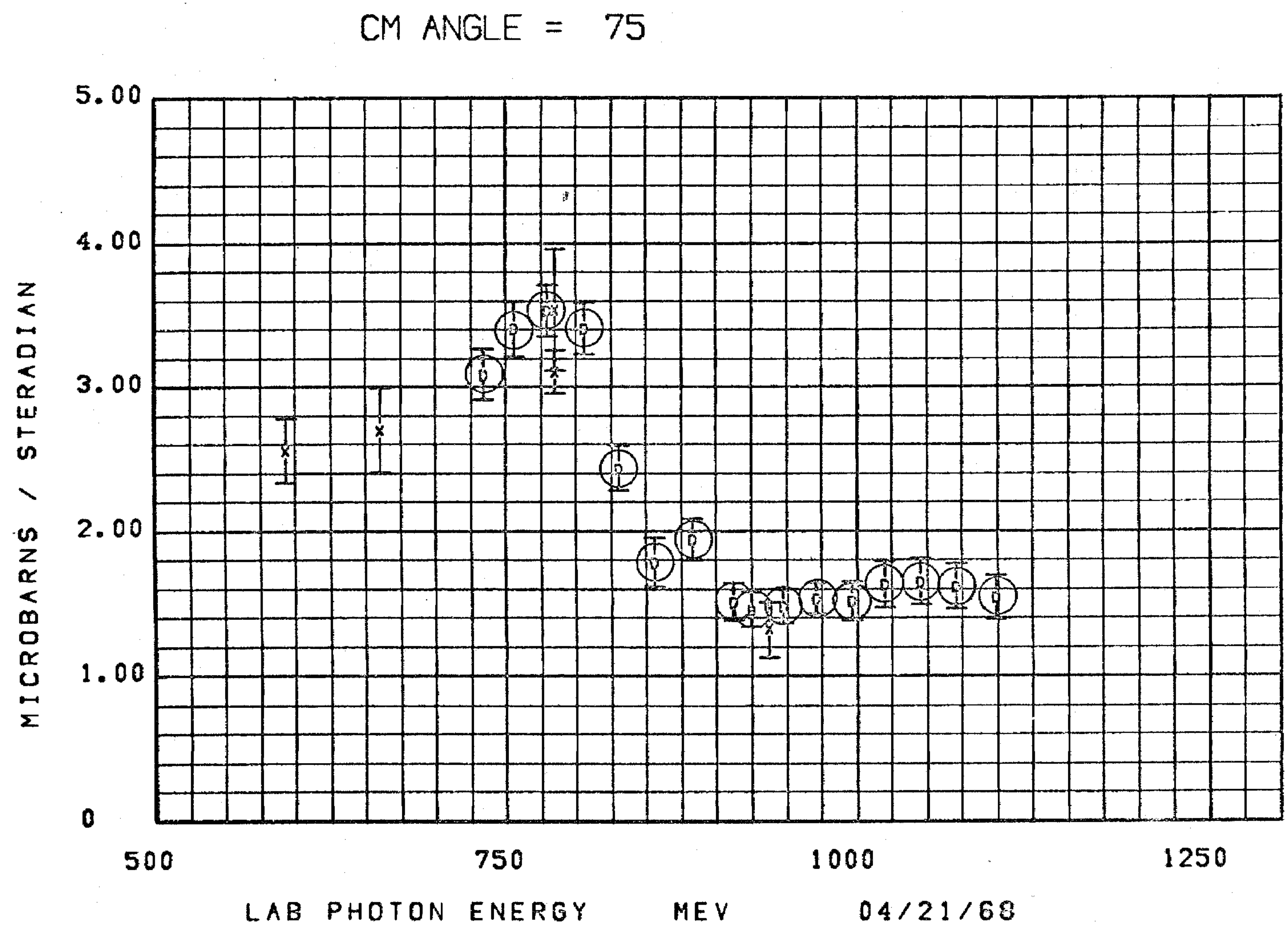
CM ANGLE = 75
5.00
4.00
3.00
2.00
1.00
0
MICROBARNS / STERADIAN
500
750
1000
1250
LAB PHOTON ENERGY MEV 04/21/68

Figure 13.3

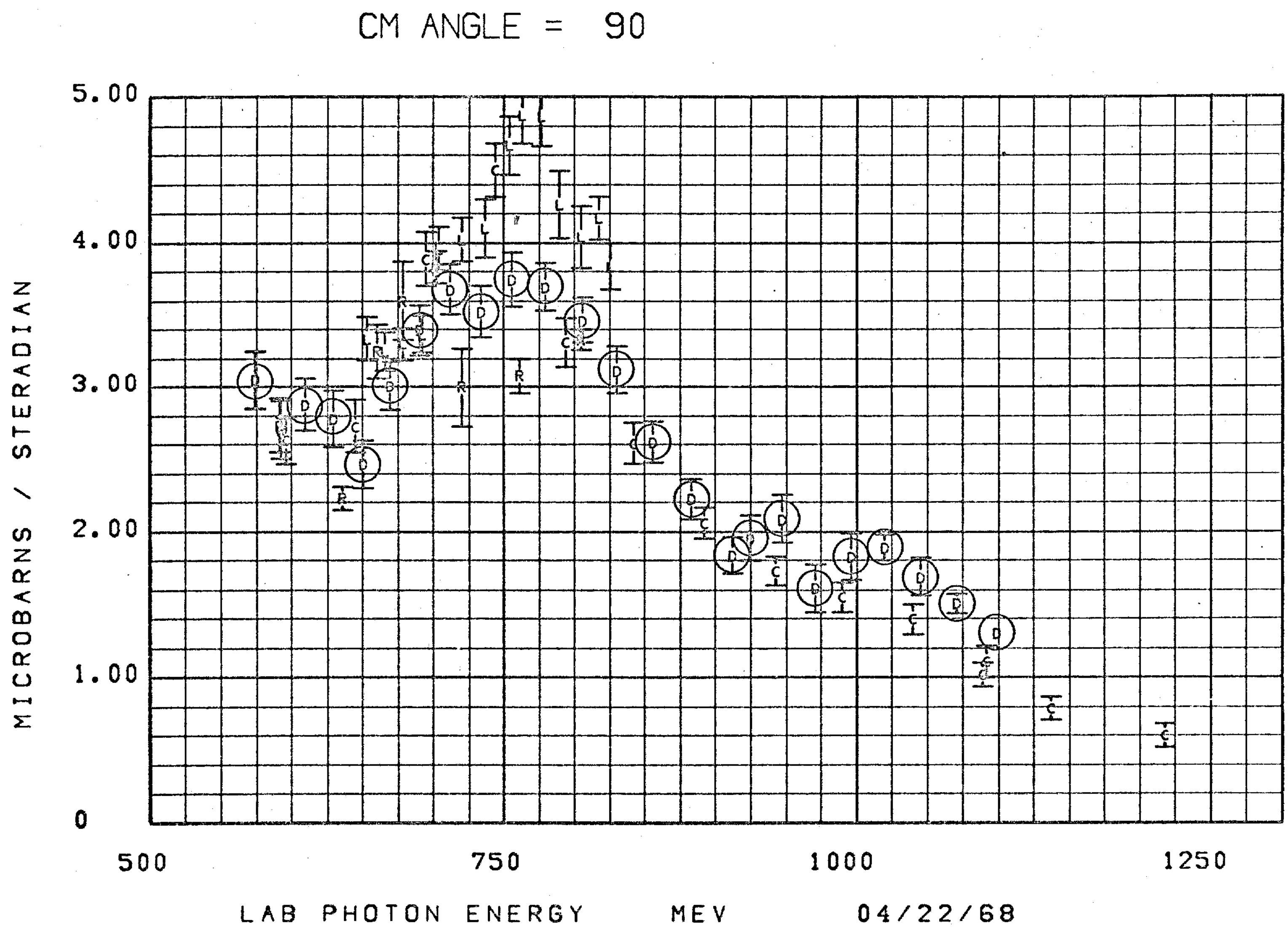
CM ANGLE = 90
MICROBARNS / STERADIAN
5.00
4.00
3.00
2.00
1.00
0
500
750
1000
1250
LAB PHOTON ENERGY MEV 04/22/68

Figure 13.4

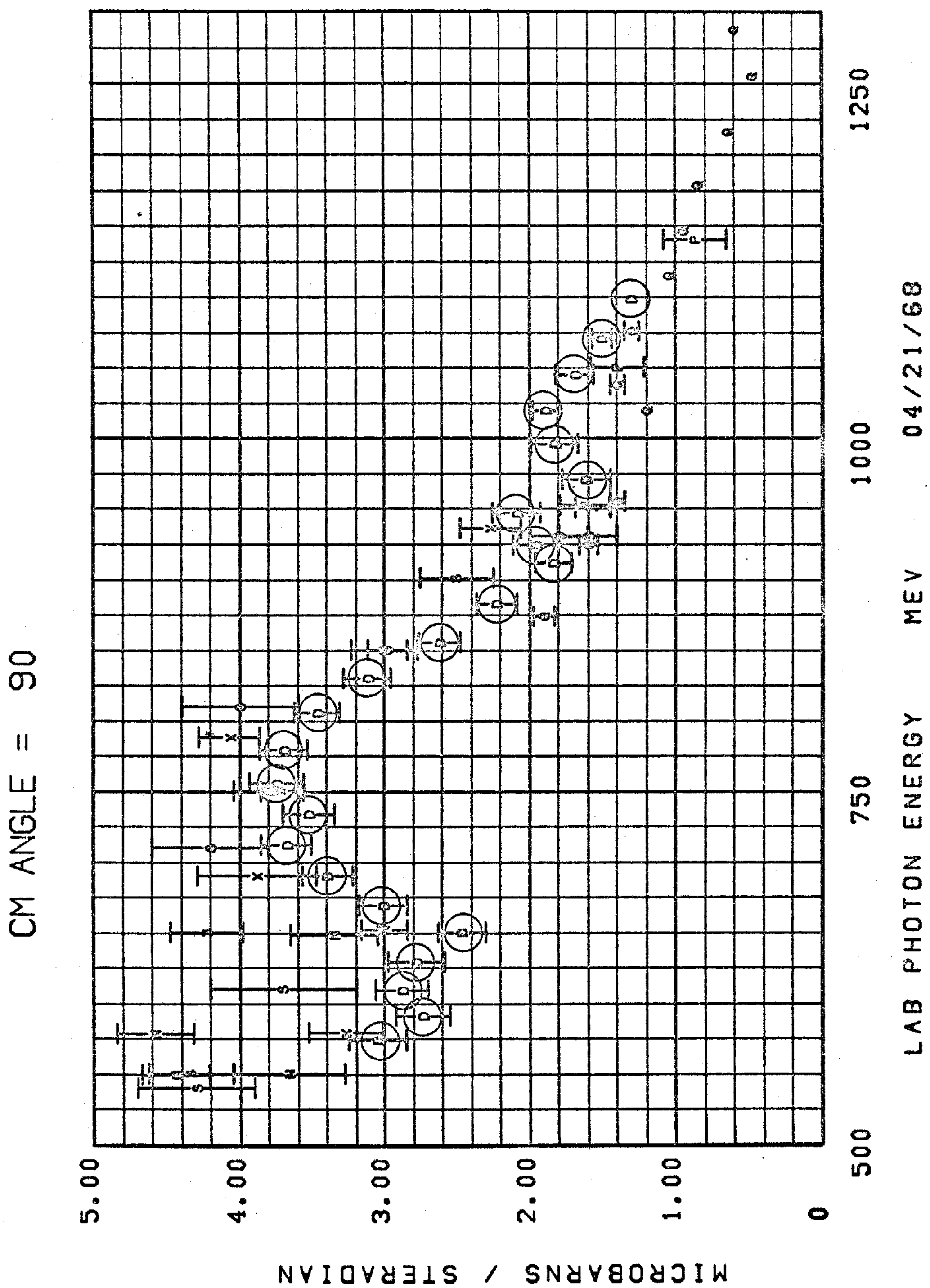

CM ANGLE = 90
5.00
4.00
3.00
2.00
1.00
0
MICROBARNS / STERADIAN
500
750
1000
1250
LAB PHOTON ENERGY MEV 04/21/68

Figure 13.5

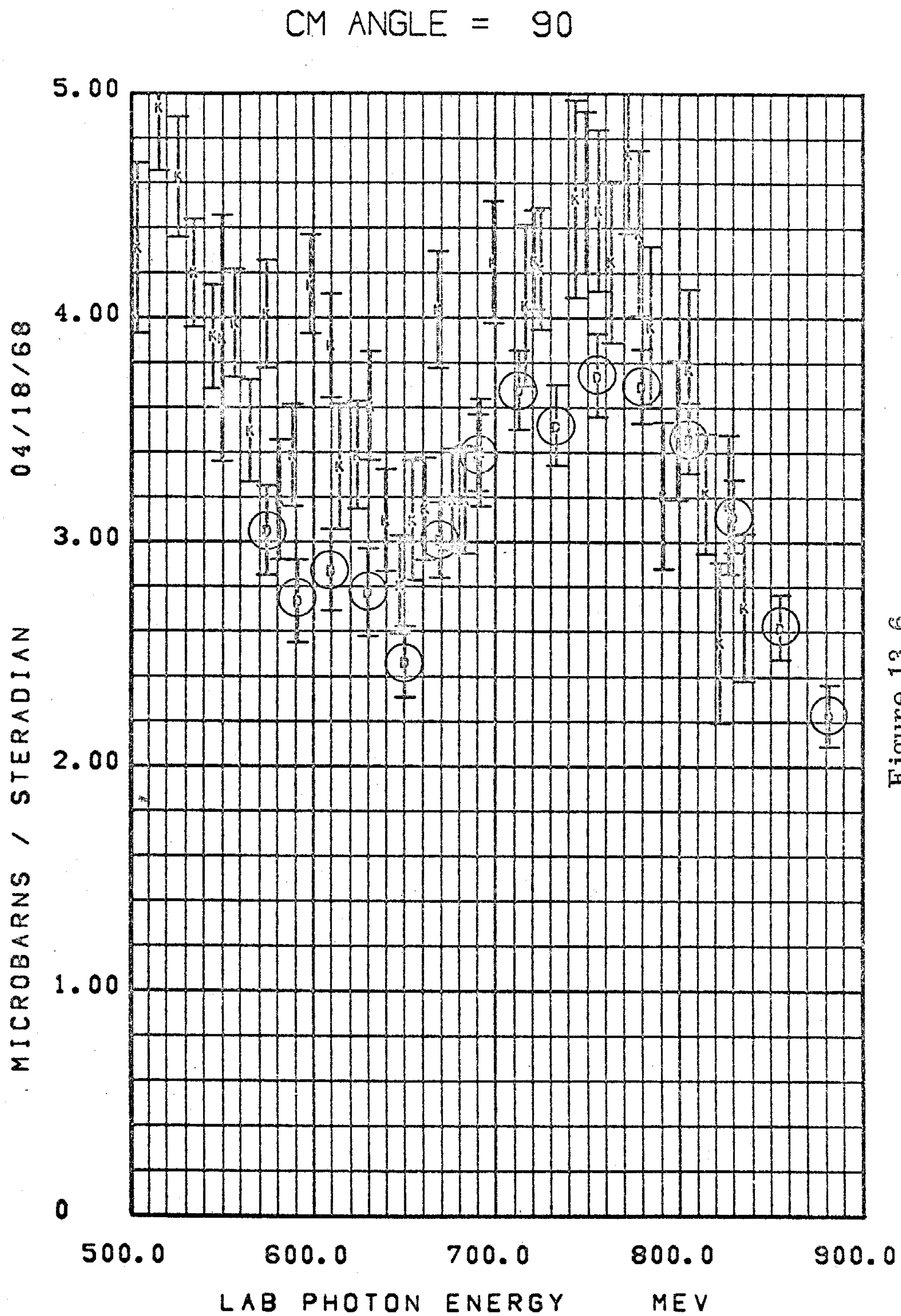
CM ANGLE = 90
04/18/68
MICROBARNS / STERADIAN
5.00
4.00
3.00
2.00
1.00
0
500.0
600.0
700.0
800.0
900.0
LAB PHOTON ENERGY MEV

Figure 13.6

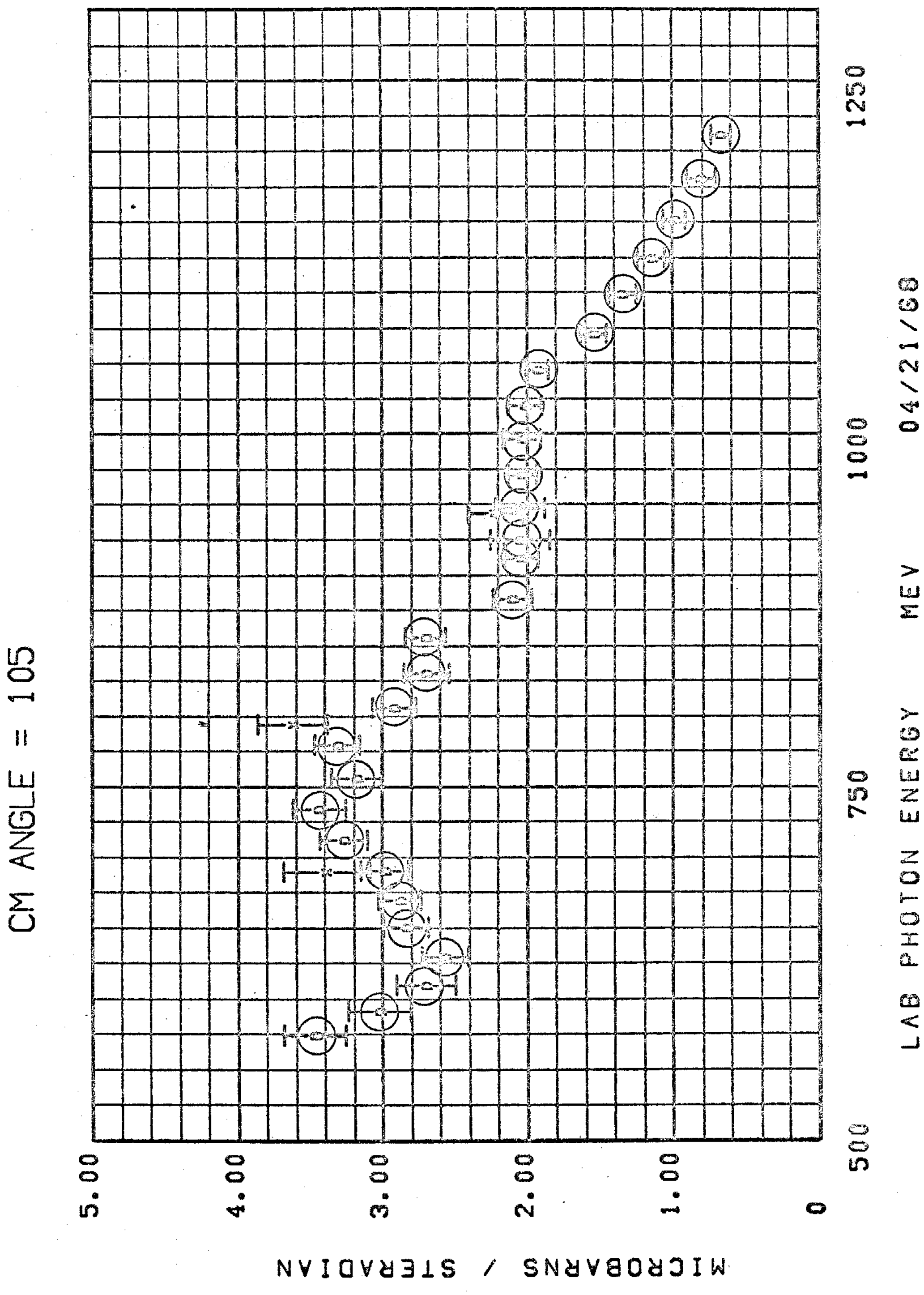
CM ANGLE = 105
LAB PHOTON ENERGY MEV
04/21/68
500
750
1000
1250
MICROBARNS / STERADIAN
5.00
4.00
3.00
2.00
1.00
0

Figure 13.7

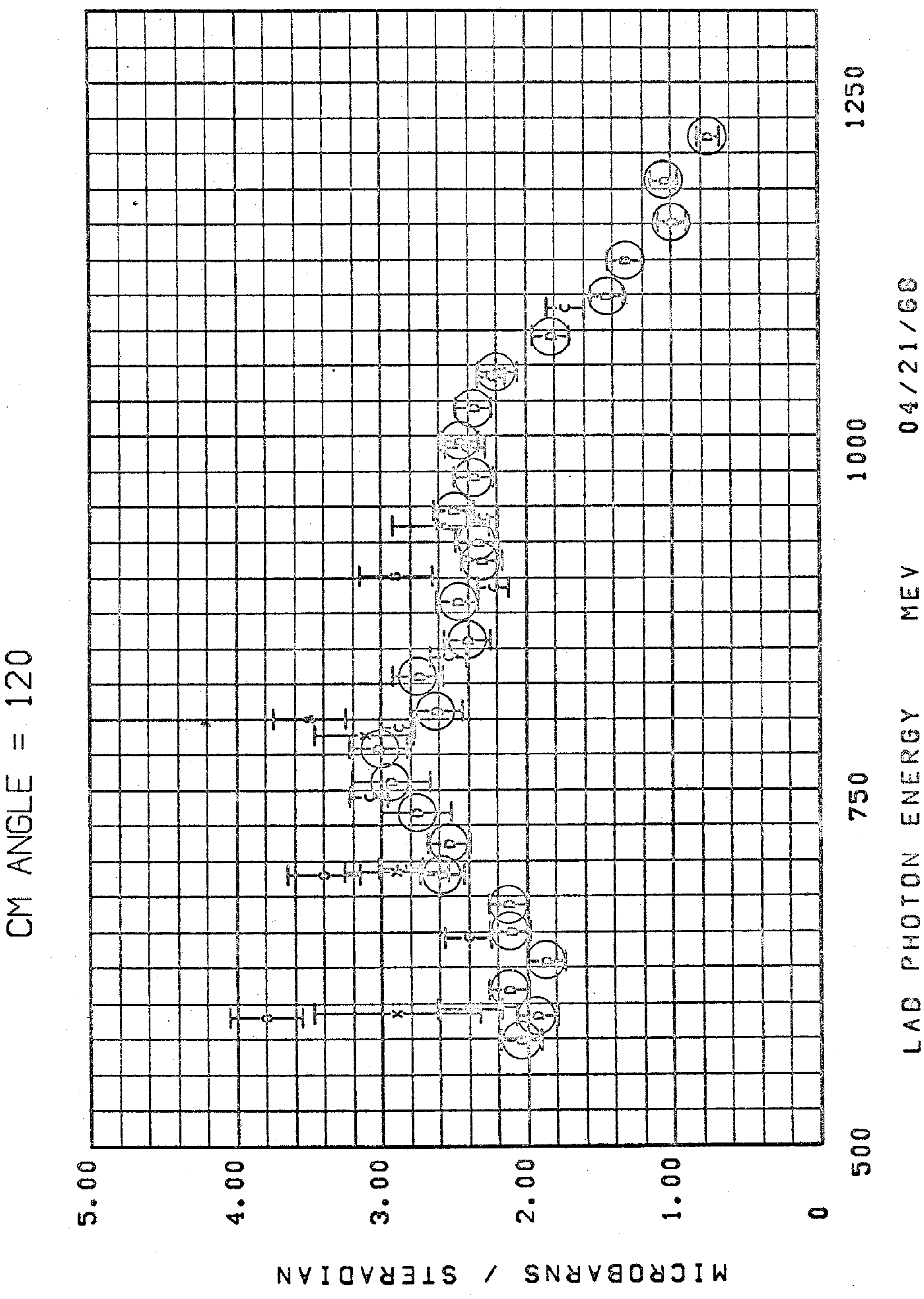
CM ANGLE = 120
5.00
4.00
3.00
2.00
1.00
0
MICROBARNS / STERADIAN
500
750
1000
1250
LAB PHOTON ENERGY MEV 04/21/68

Figure 13.8

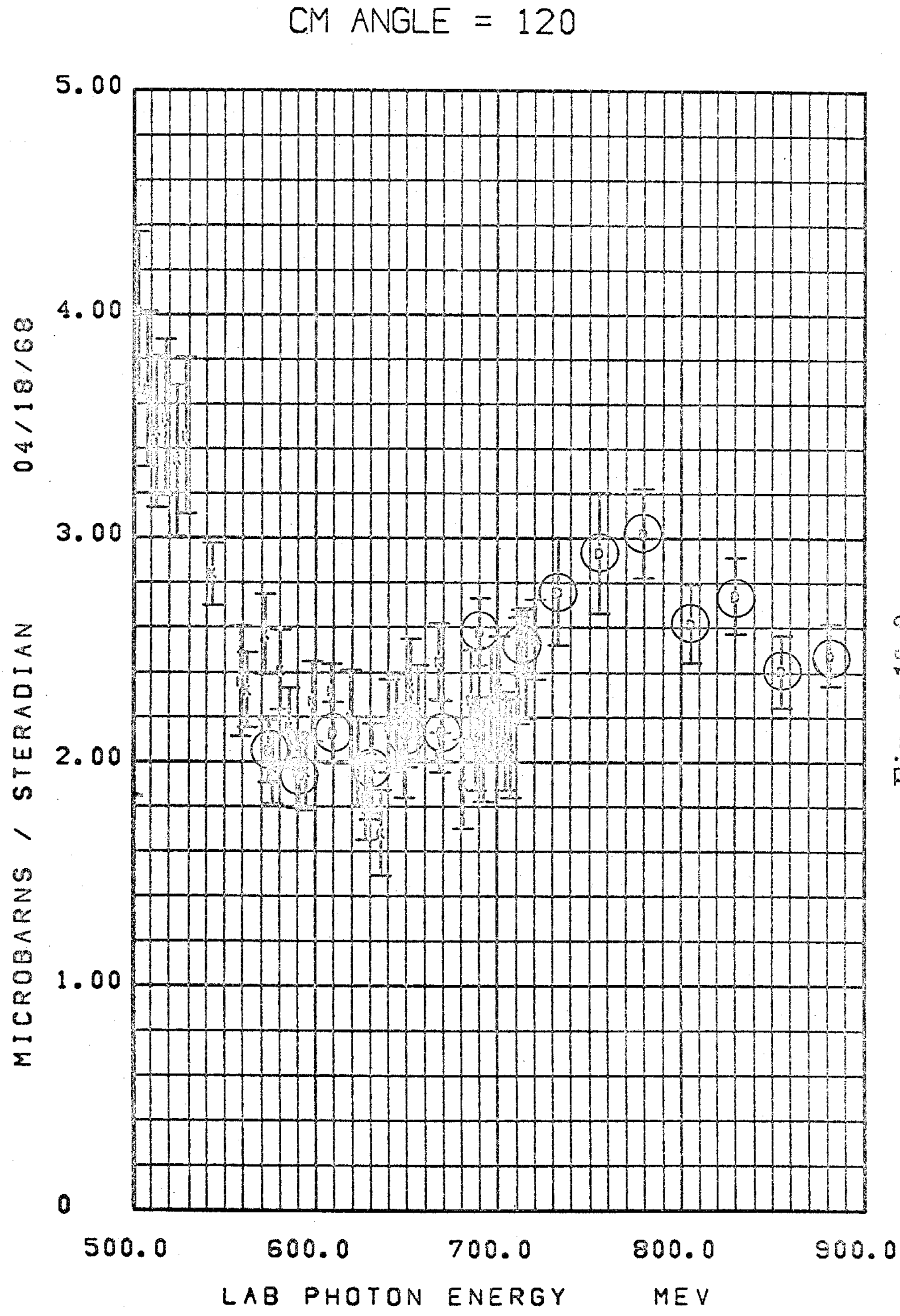
CM ANGLE = 120
5.00
4.00
3.00
2.00
1.00
0
04/18/68
MICROBARNS / STERADIAN
500.0
600.0
700.0
800.0
900.0
LAB PHOTON ENERGY MEV

Figure 15.9

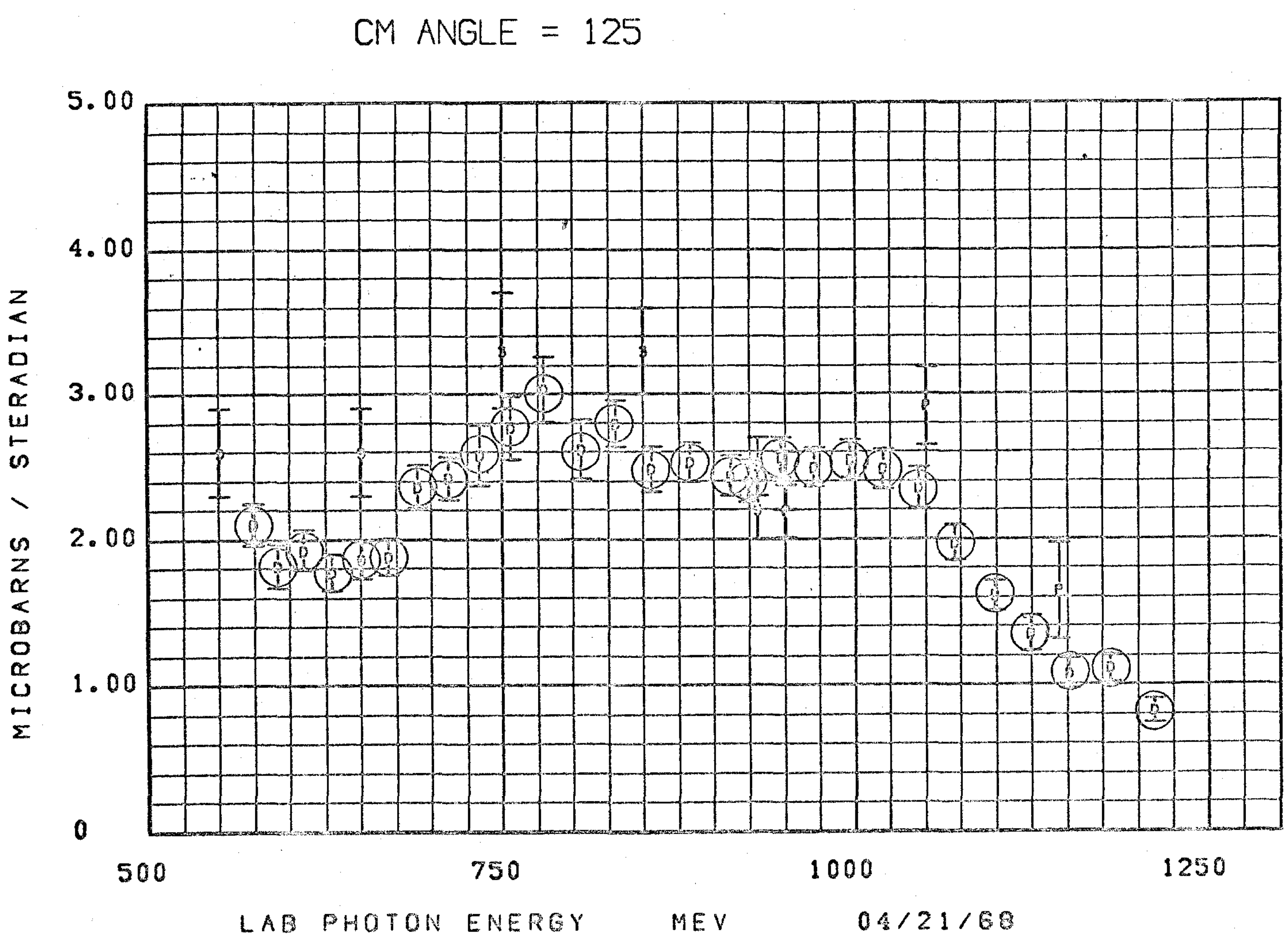
CM ANGLE = 125
5.00
4.00
3.00
2.00
1.00
0
MICROBARNS / STERADIAN
500
750
1000
1250
LAB PHOTON ENERGY MEV 04/21/68

Figure 13.10

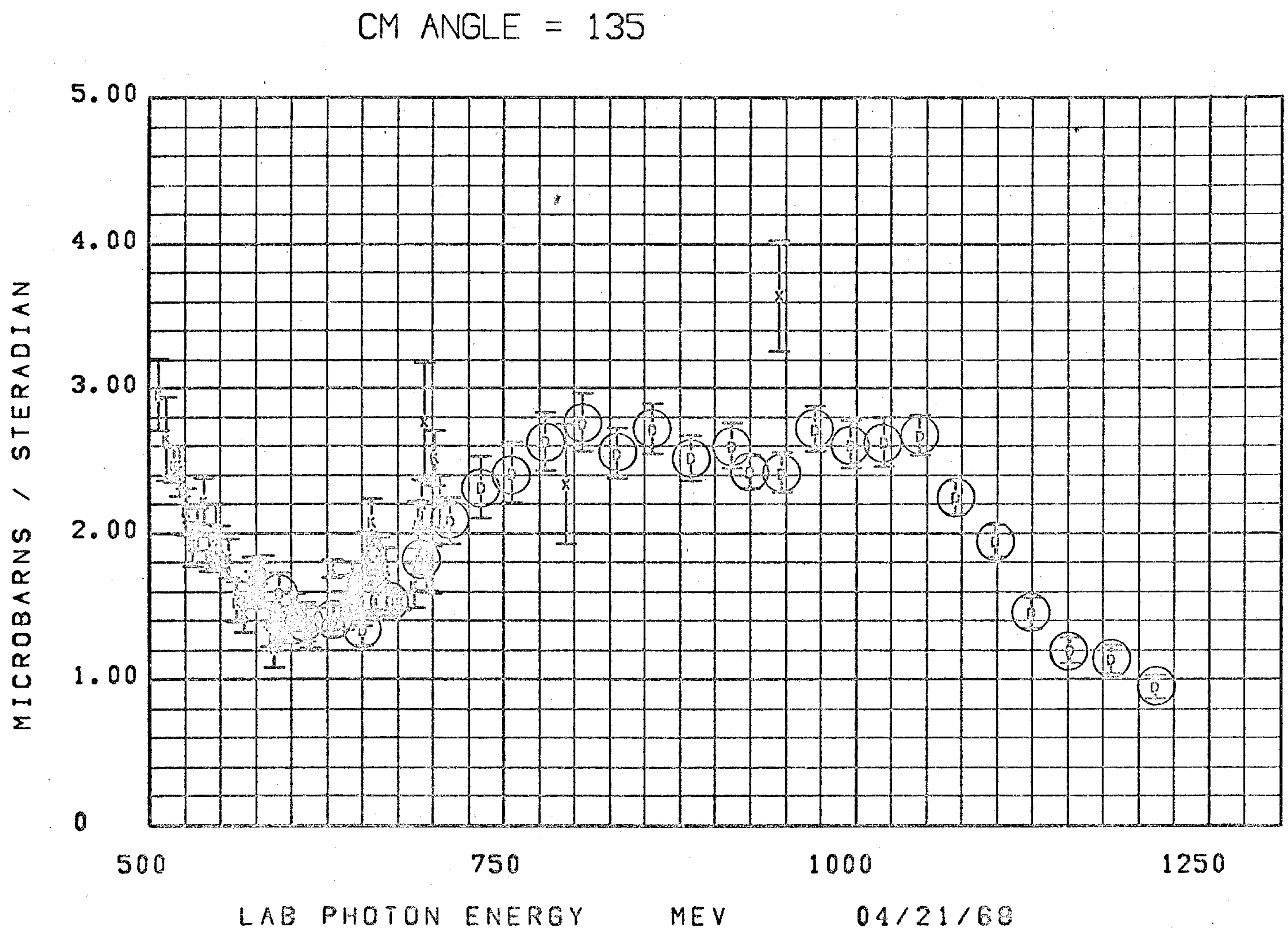
CM ANGLE = 135
5.00
4.00
3.00
2.00
1.00
0
MICROBARNS / STERADIAN
500
750
1000
1250
LAB PHOTON ENERGY MEV 04/21/68

Figure 13.11

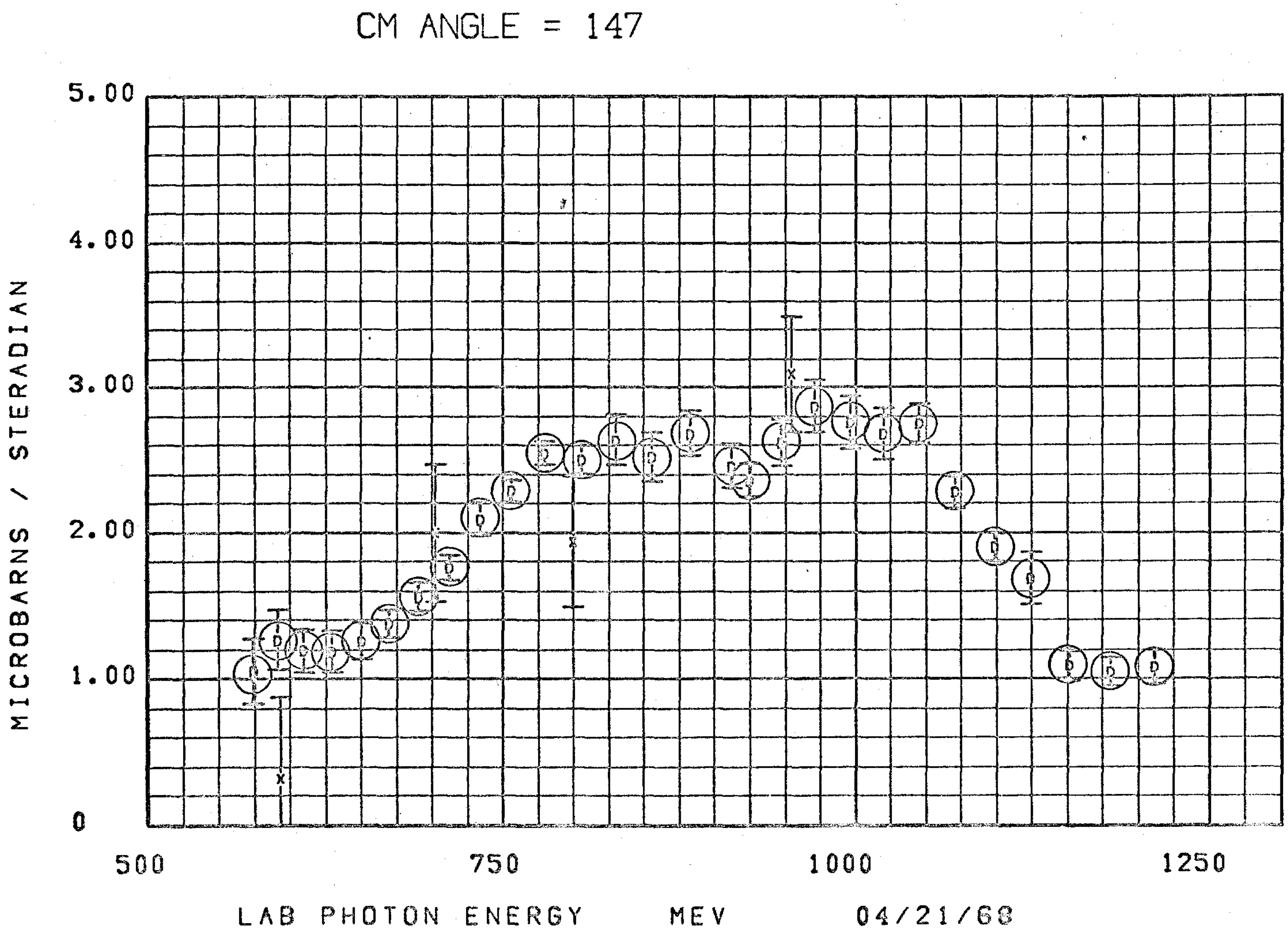
CM ANGLE = 147
5.00
4.00
3.00
2.00
1.00
0
MICROBARNS / STERADIAN
500
750
1000
1250
LAB PHOTON ENERGY MEV 04/21/68

Figure 13.12

The few points at 67.5° agree within statistics, as do the points at 75°.

The 90° data have been plotted on 3 graphs due to the large amount of data at that angle. Looking at the first graph, there is a discrepancy of about 17% between the data of this experiment and that of Diebold (code C) at the second resonance peak. A small part of this difference can be attributed to k resolution, but not all of it. The effect of wide k resolution is shown in Figure 8 of Reference 1. The resolution of the present experiment would have to be at least a factor of two wider than the calculated resolution of about $\Delta k/k = .06$ in order to explain the discrepancy. The results of this experiment are somewhat higher than those of Diebold but in agreement with data of other experiments at higher energies. The discrepancy with the Deutsch results at the second resonance (code L) is even larger. Neither the present experiment nor any other agrees with the data of Cortellesa (code R).

Turning to the second graph, the present results appear to agree with the data of DeWire et al. (code 3) at the peak. But the two should not have the same measured value because the DeWire experiment had much wider resolution.

Looking at the third graph, the data of Bacci et al. (code K) also say that the present results are too low at the peak. They seem to be low at the lower energies also.

The conclusion seems to be that the results of the present experiment are too low at 90° at the second resonance. Note that even the P signature data from this experiment indicated that the cross section should be higher at the peak. In fact, the P signature data would agree quite well with the other experiments.

At 105°, the two points of Vette (code X) near the second resonance lie above the present results. The third point is consistent.

At 120°, the data appear on two graphs. The agreement with Diebold's data (code C) at high energy is excellent. On the bottom side of the second resonance, his points lie above ours. Vette's data (code X) also tend to be larger, but with large statistical errors. The data of Stein and Rogers (code S) are far too high. They detected only the proton and therefore their results may be contaminated with pi pairs which are copious in this region. Referring to the second graph, which is hard to read, due to the density of data points, the consistency with the data of Bacci et al. (code K) is seen to be good.

At 125°, DeWire et al. (code 3) results are higher than those of the present experiment at low energies, but with large errors. Jackson et al. (code P) results are higher at high energies. Both experiments detect a decay photon. Curiously, both experiments agree with the present experiment at 950 MeV.

At 135°, the agreement with the data of Bacci et al. is excellent.

At 135° and 147°, Vette's data (code X) have large errors, but the results are consistent with this experiment within statistics.

In summary, Figure 13 shows that, except near 90° at the second resonance, this experiment agrees fairly well with the other data most of the time. A given experiment will agree at one angle and not at another.

Figure 14 shows a comparison with the data taken by Ward et al. (code G). They attempted a survey similar to the one being

Figure 14

Energy distributions for $\theta_{\pi^o}^{cm} = 59^o$, 74^o, 83^o, 91^o, 106^o, 121^o, and 134^o. Symbol code is as follows:

G	Ward et al. (5)
+	Kenton (9)
Ⓓ	This experiment

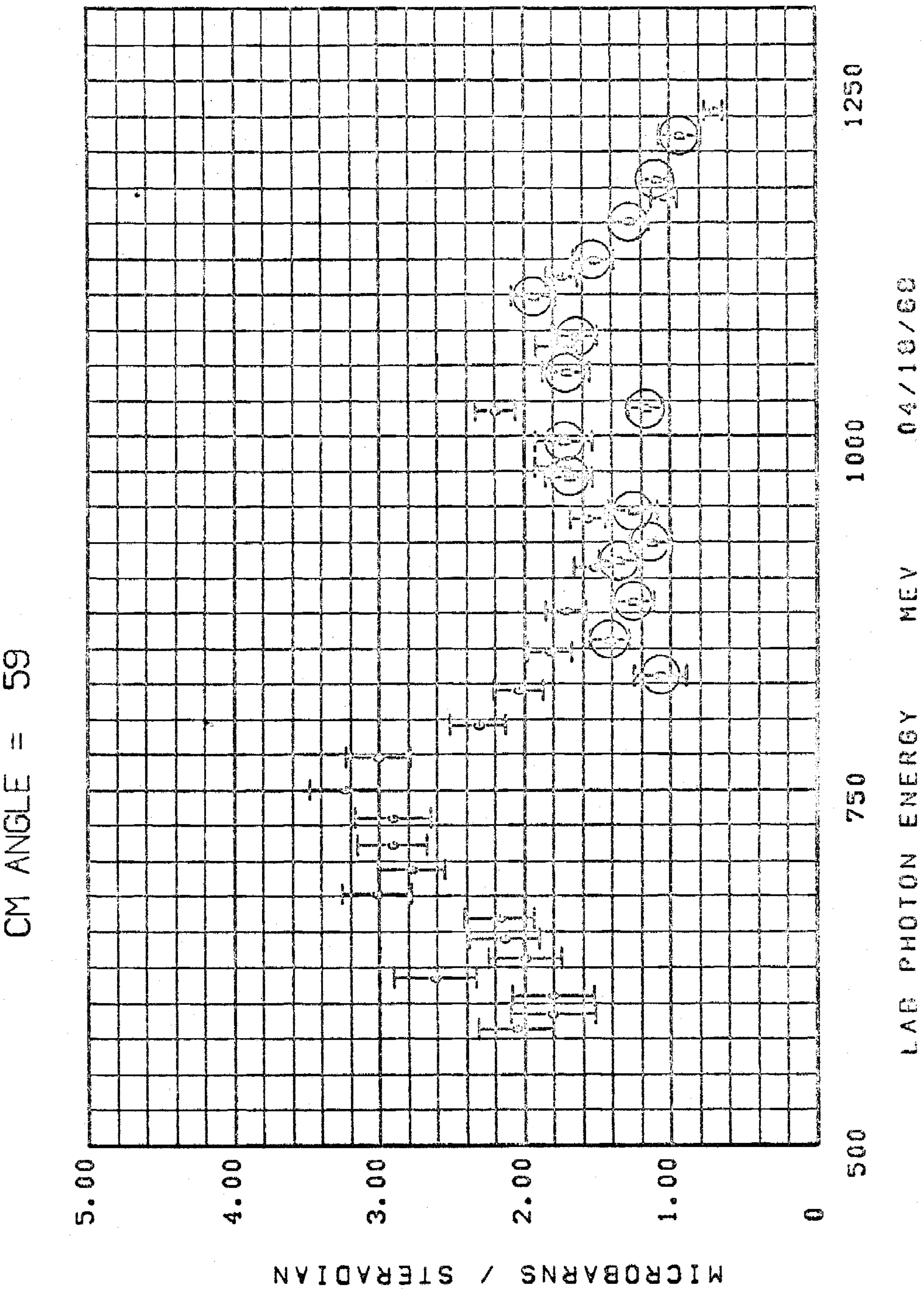
CM ANGLE = 59
MICROBARNS / STERADIAN
5.00
4.00
3.00
2.00
1.00
0
500
750
1000
1250
LAB PHOTON ENERGY MEV
04/18/68

Figure 14.1

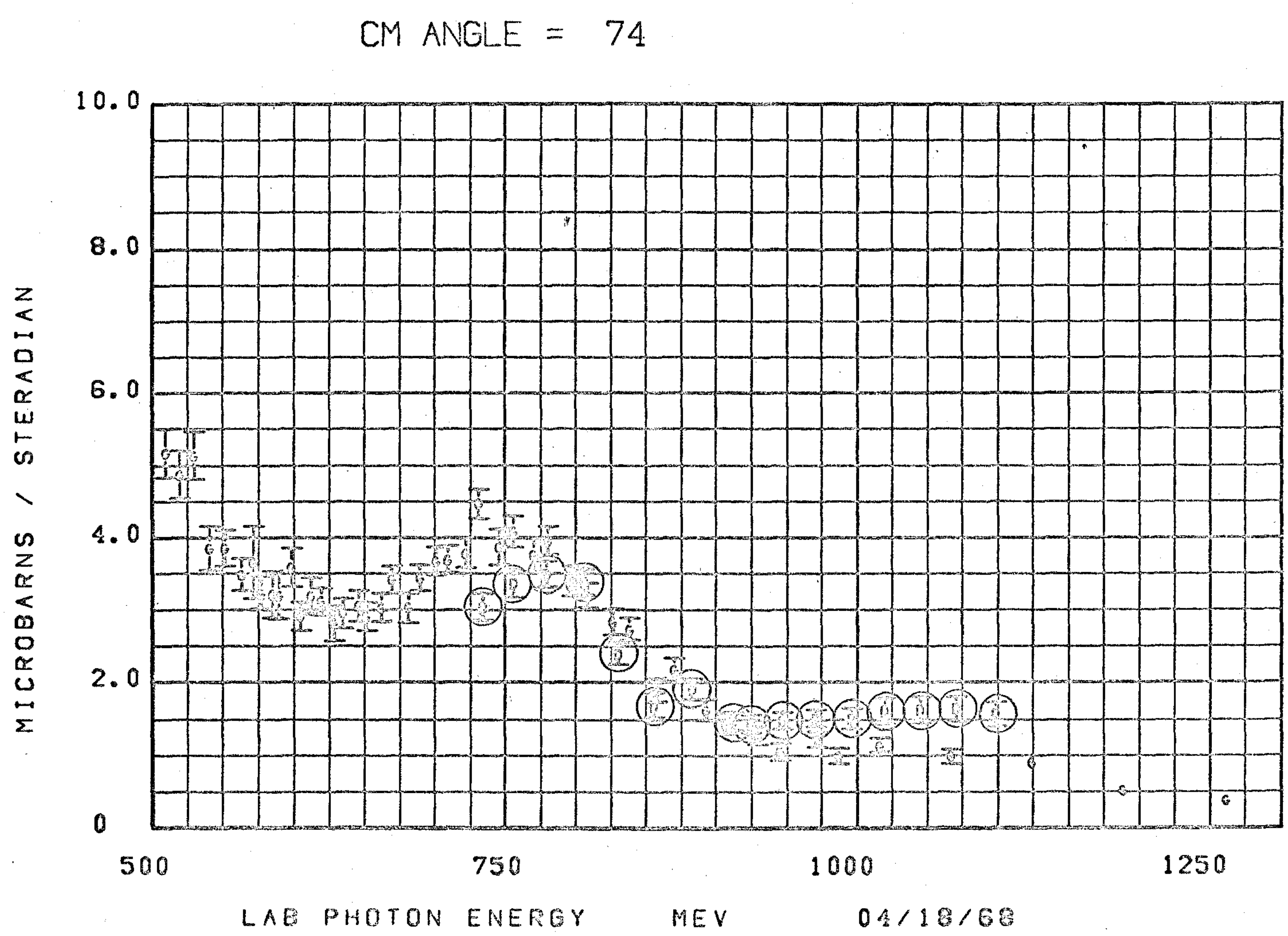
CM ANGLE = 74
MICROBARNS / STERADIAN
10.0
8.0
6.0
4.0
2.0
0
500
750
1000
1250
LAB PHOTON ENERGY MEV 04/18/68

Figure 14.2

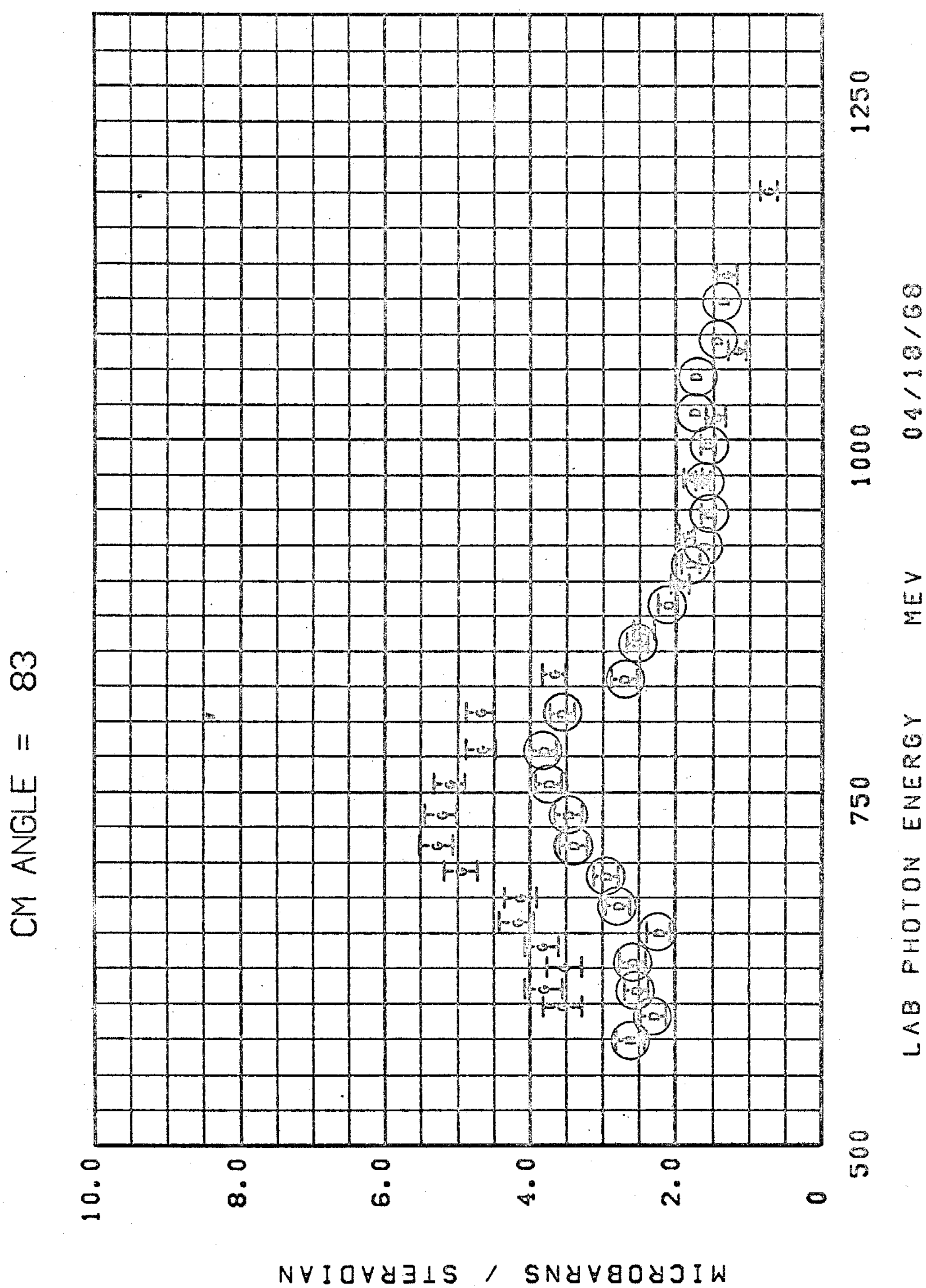
CM ANGLE = 83
LAB PHOTON ENERGY MEV
04/18/68
MICROBARNS / STERADIAN
500
750
1000
1250
0
2.0
4.0
6.0
8.0
10.0

Figure 14.3

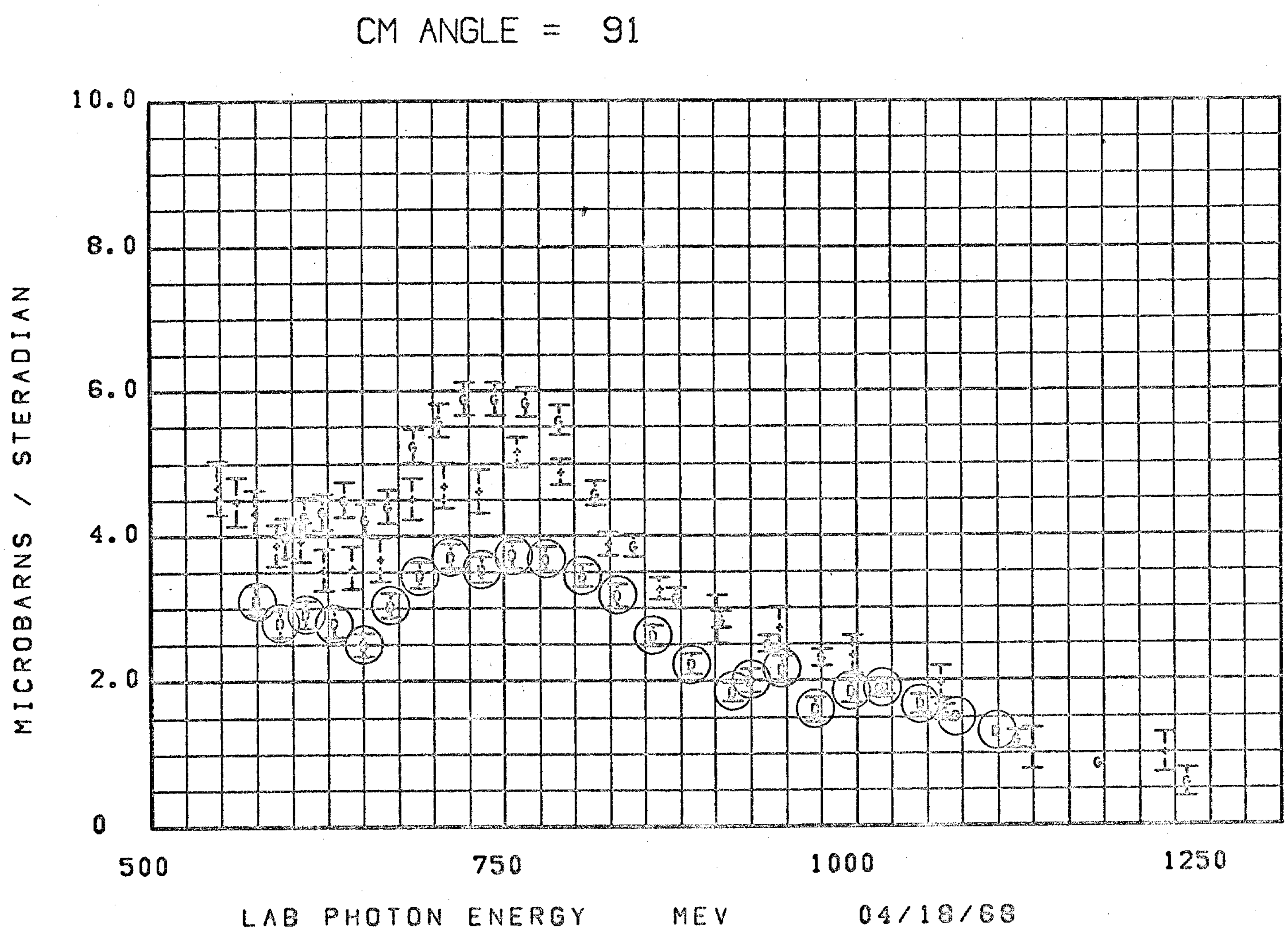
CM ANGLE = 91
10.0
8.0
6.0
4.0
2.0
0
MICROBARNS / STERADIAN
500
750
1000
1250
LAB PHOTON ENERGY MEV 04/18/68

Figure 14.4

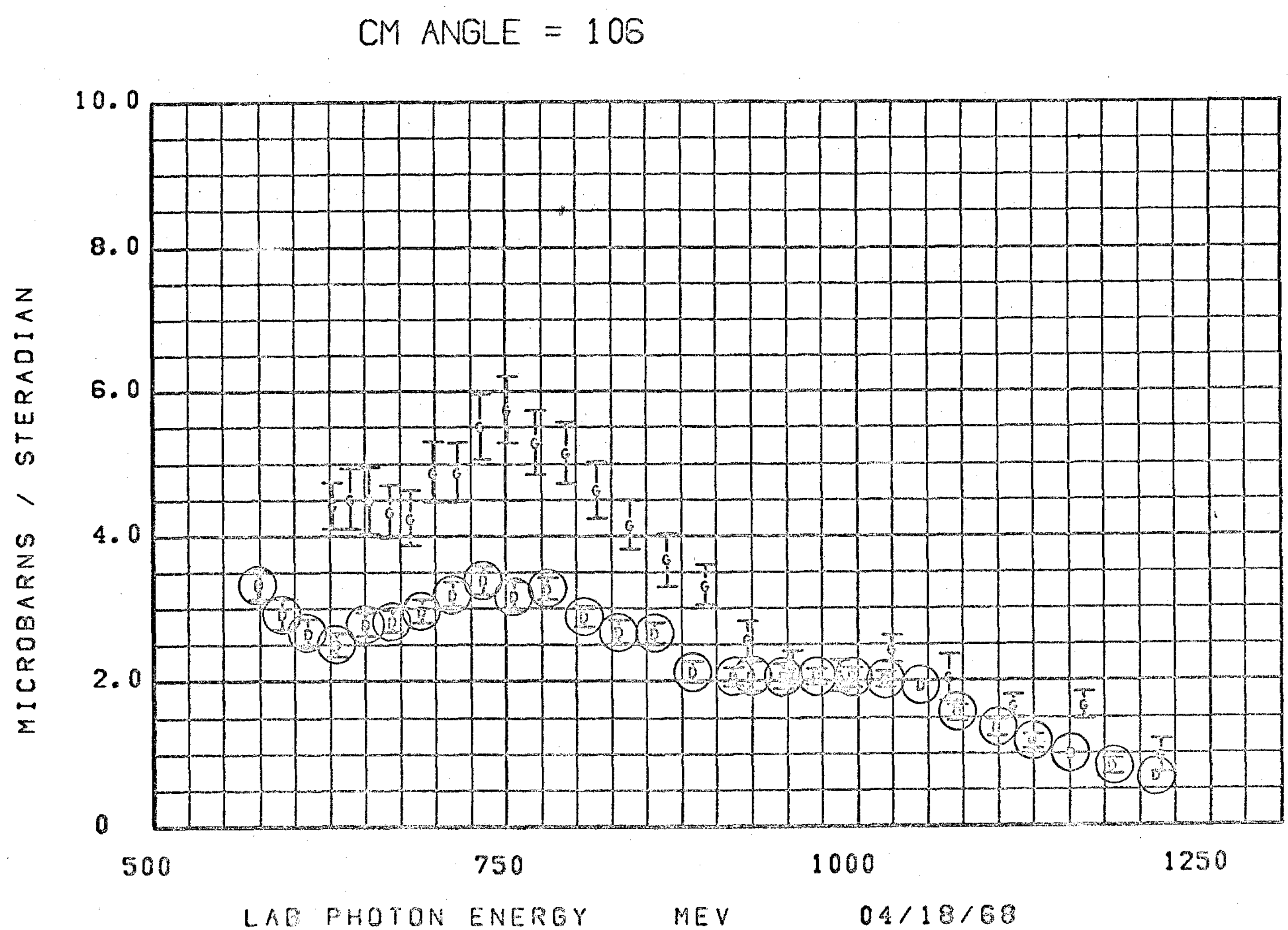
CM ANGLE = 106
MICROBARNS / STERADIAN
10.0
8.0
6.0
4.0
2.0
0
500
750
1000
1250
LAB PHOTON ENERGY MEV 04/18/68

Figure 14.5

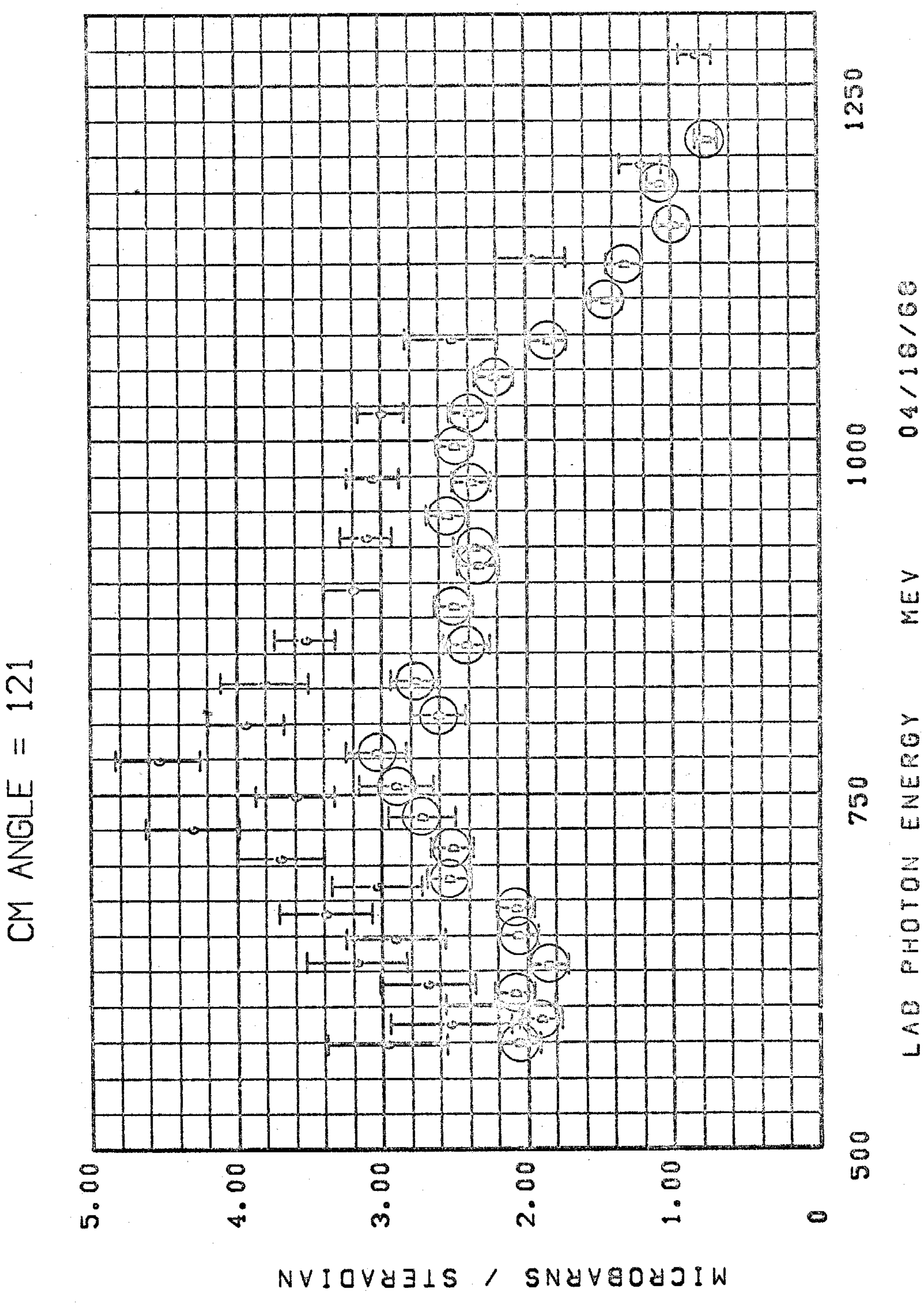

CM ANGLE = 121
5.00
4.00
3.00
2.00
1.00
0
MICROBARNS / STERADIAN
500
750
1000
1250
LAB PHOTON ENERGY MEV
04/18/66

Figure 14.6

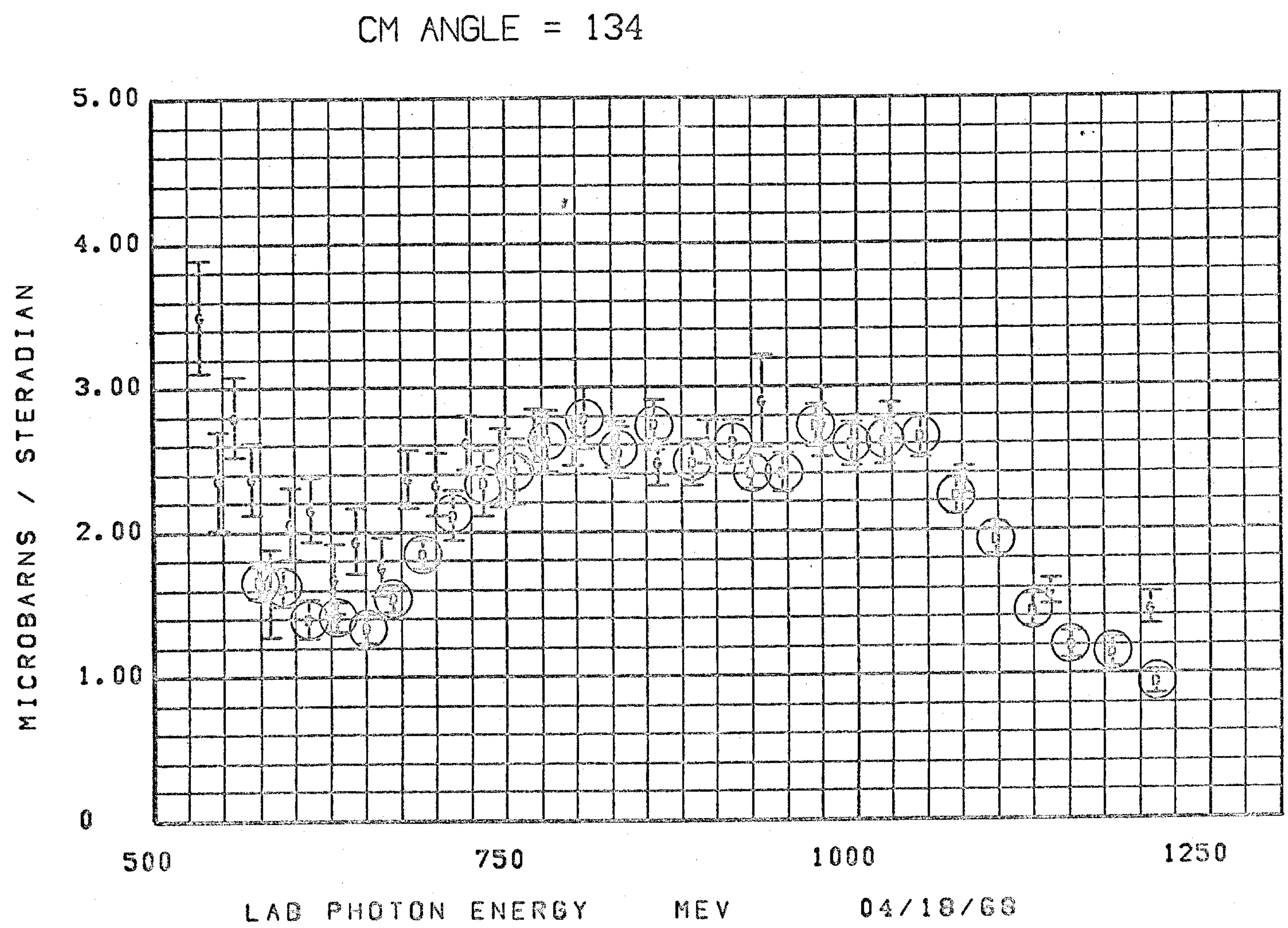
CM ANGLE = 134
5.00
4.00
3.00
2.00
1.00
0
MICROBARNS / STERADIAN
500
750
1000
1250
LAB PHOTON ENERGY MEV 04/18/68

Figure 14.7

reported here, but using a very different method. They measured many points with very small error bars and, taken alone, their data look very nice. But their cross sections are, in many cases, much larger than the existing data. In their paper, they attempt to explain the discrepancy as being due to their better resolution by referring to a figure of merit they define as being the product of the angular acceptance and the k resolution. They argue that a smaller figure of merit implies narrower resolution which in turn implies larger measured cross sections at peaks. While their argument may be correct qualitatively, it cannot explain the difference quantitatively. To check their hypothesis, one would need only fold the other experiments' resolutions into the Ward et al. data. Clearly this would not cause a large enough change to bring about agreement. The discrepancy with previous data is real and large, being as large as 30% in some cases.

When the data of Ward et al. are compared with the data of this experiment, the discrepancy is exaggerated because the region where they are too high is exactly the place that the present experiment is too low, near 90^{o} at the second resonance.

The agreement between the two experiments is quite good for the smallest and largest angles plotted. Except at 74^{o}, the agreement is fairly good at high energies. Ward et al. measured their cross sections by viewing both the proton and a decay gamma ray, with small apertures on both, and doing a precise time-of-flight measurement between them. To regain the counting rate they lost with the small apertures, they used many momentum channels with their k values extending down to half the endpoint energy. The veto on their gamma counter vetoed charged pairs, but they were still susceptible to neutral pi pairs. They claim to have checked for this but, Kenton (code +) using the same apparatus and the same data reduction programs got a smaller answer (see 91^o plot) when using a lower endpoint energy (20).

There is no apparent explanation for the Ward data being lower than this experiment near k = 1050, $\theta^{cm}_{\pi^o} = 74^o$. Unfortunately, there are no other data at this energy and angle. At this energy, the present experiment is higher than Diebold at 90^o, but agrees with Diebold at 60^o. It is possible, but not definite, that the present experiment is too high in this case.

Figure 15 shows angular distribution data at several energies. The plots from 600 to 800 MeV are near the second resonance and again show this experiment to be low at 90^o. The agreement with the data of DeStaebler et al. (code A) is good near 140^o at all the above energies. However, near 170^o the DeStaebler results drop below the present results, giving a value at 780 MeV about 60% of the present result. At 180^o DeStaebler has the same type of discrepancy with Buschhorn (12) (not shown). It is therefore assumed that the DeStaebler data are in error near 170^o.

At 920 MeV there appears to be a discrepancy between this experiment and the data of Hatch (code F), but such is not the case. The Hatch experiment had wide k resolution, due to not detecting the proton, and Hatch expects a difference of .38 μb/sr. between his results and an experiment such as Diebold's, to which this experiment is similar. The difference between the 60^o results after the correction is .1 μb/sr., which is smaller than the statistical error.

At 1175 MeV, there is some scatter in the points, but there is general agreement with Hatch (code F) and Talman (code H).

Figure 15

Angular distributions for k = 600, 660, 680, 700, 720, 740, 760, 780, 800, 920, and 1175 MeV. Symbol code is as follows:

A	DeStaebler (4)
F	Hatch (7)
H	Talman (1)
V	Worlock (1)
ⓓ	This experiment

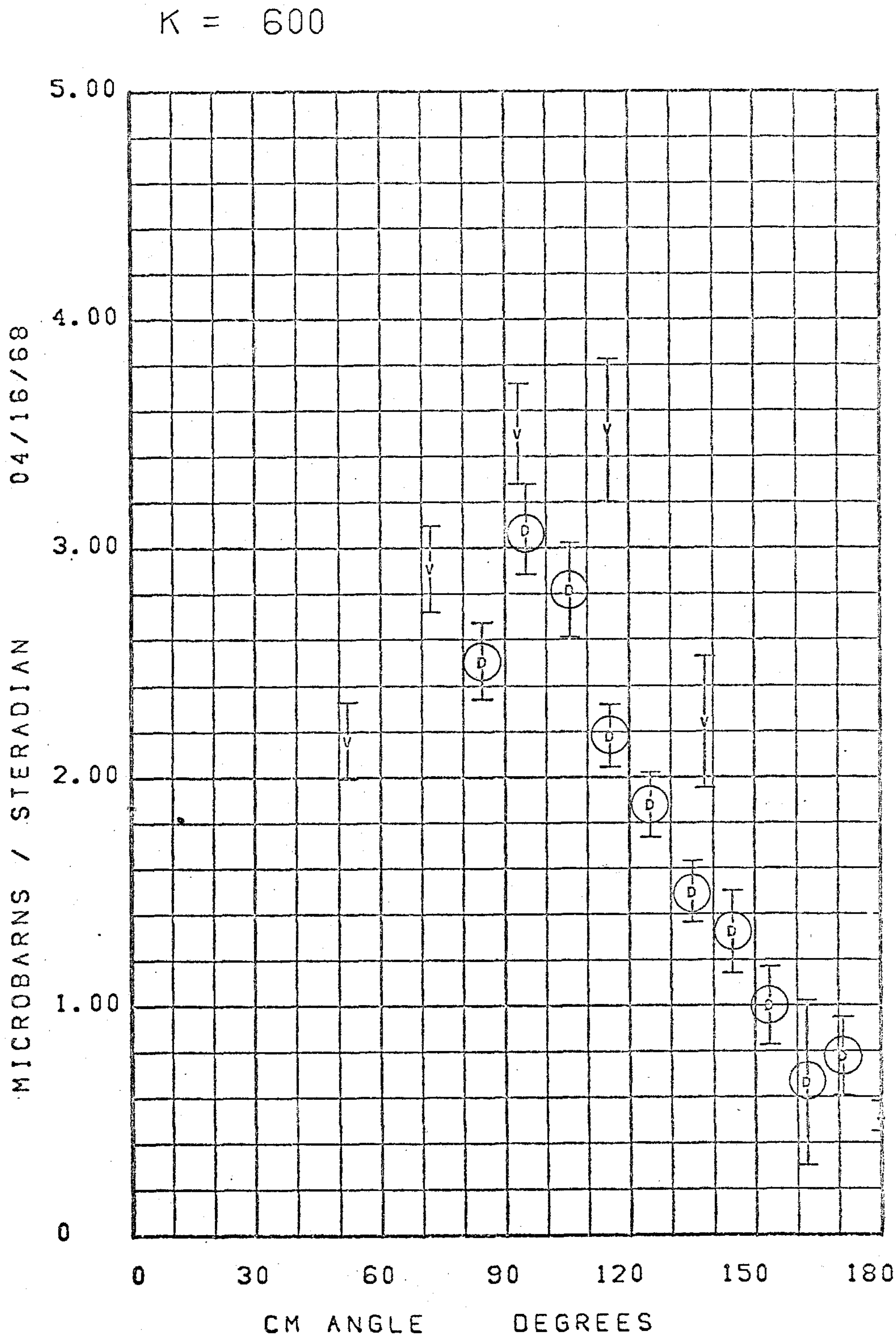
K = 600
04/16/68
MICROBARNS / STERADIAN
5.00
4.00
3.00
2.00
1.00
0
0
30
60
90
120
150
180
CM ANGLE DEGREES

Figure 15.1

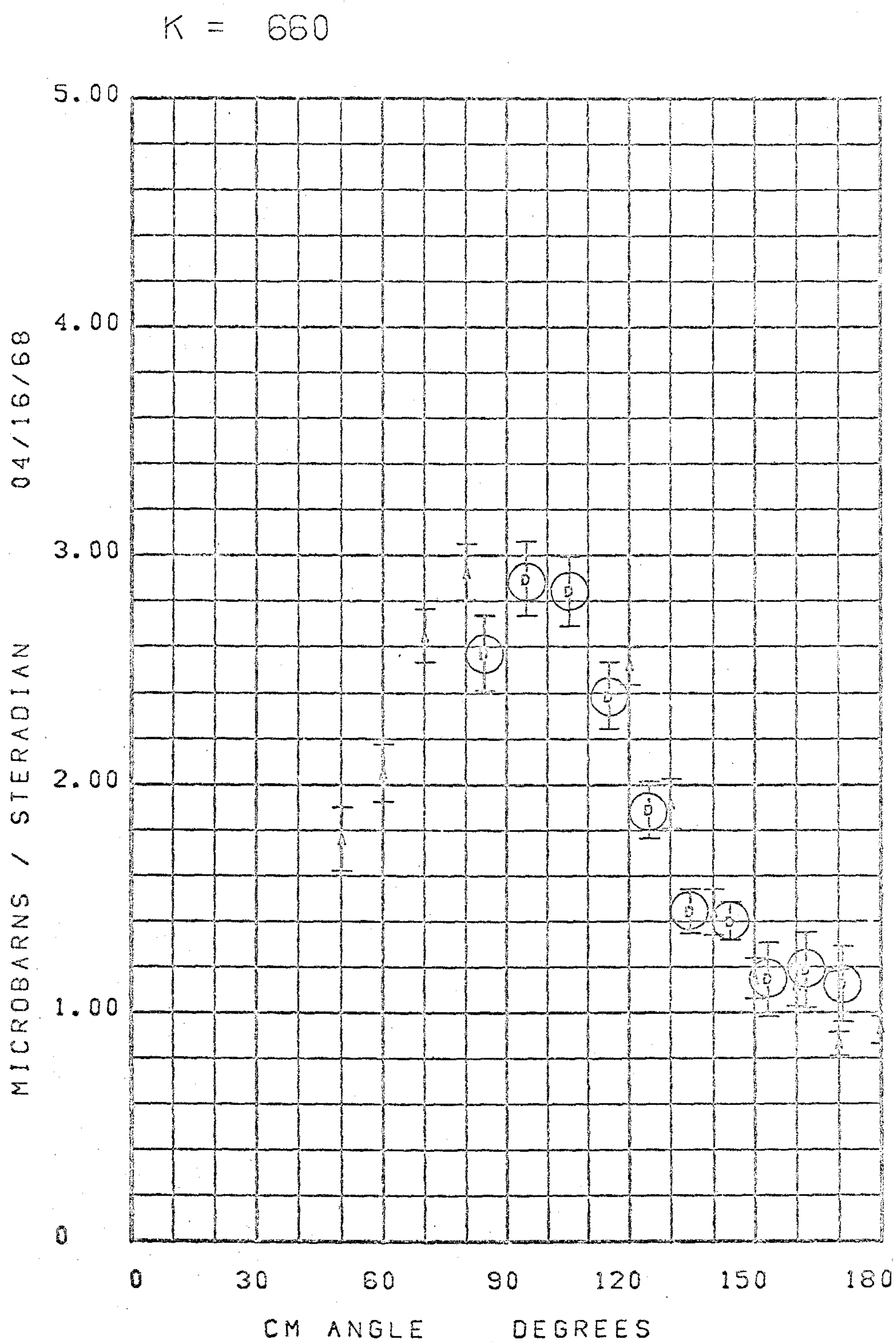
K = 660
5.00
4.00
3.00
2.00
1.00
0
04/16/68
MICROBARNS / STERADIAN
0
30
60
90
120
150
180
CM ANGLE DEGREES

Figure 15.2

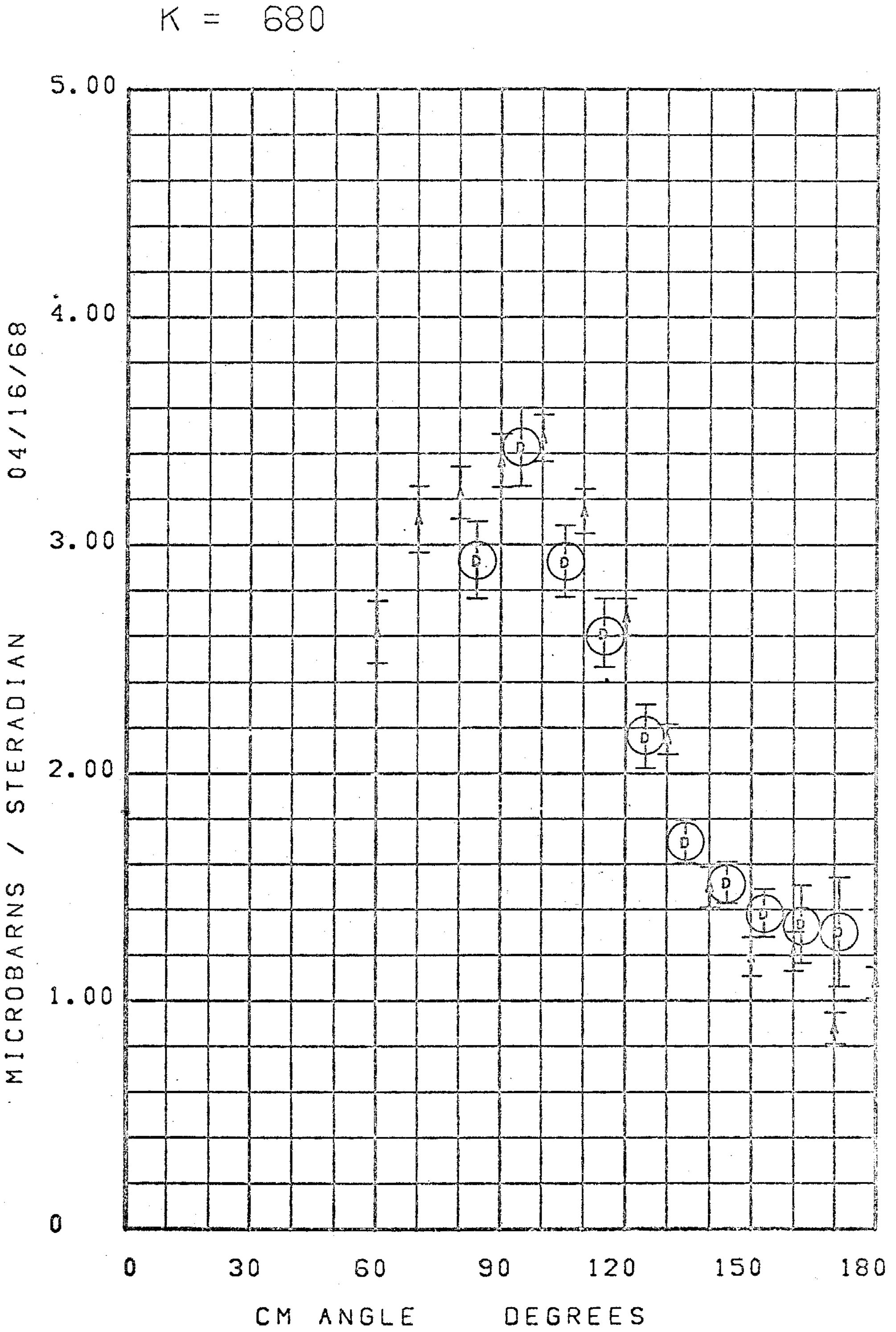

K = 680
5.00
4.00
3.00
2.00
1.00
0
04/16/68
MICROBARNS / STERADIAN
0
30
60
90
120
150
180
CM ANGLE DEGREES

Figure 15.3

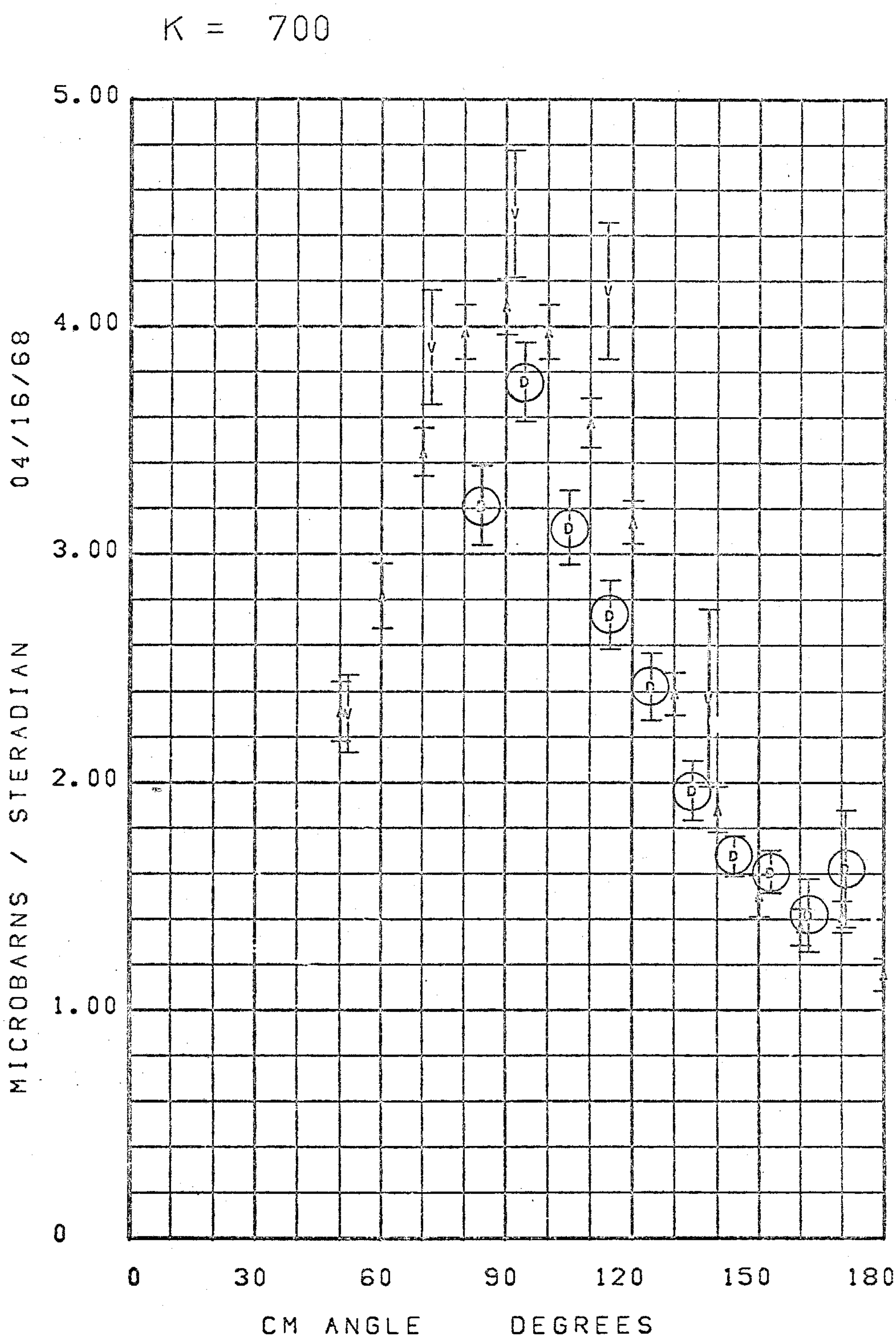
K = 700
5.00
4.00
3.00
2.00
1.00
0
04/16/68
MICROBARNS / STERADIAN
0
30
60
90
120
150
180
CM ANGLE DEGREES

Figure 15. 4

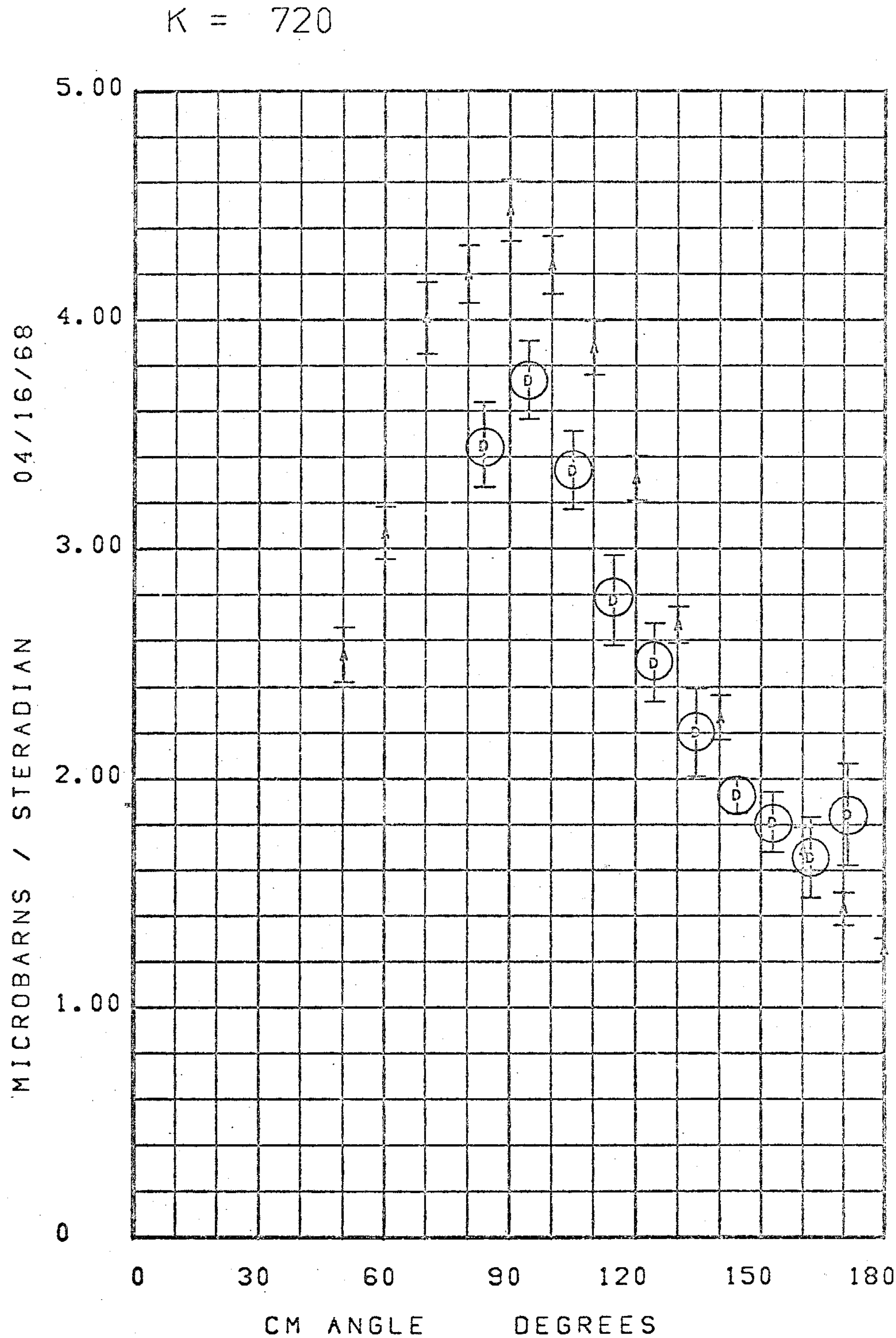
K = 720
5.00
4.00
3.00
2.00
1.00
0
MICROBARNS / STERADIAN
04/16/68
0
30
60
90
120
150
180
CM ANGLE DEGREES

Figure 15.5

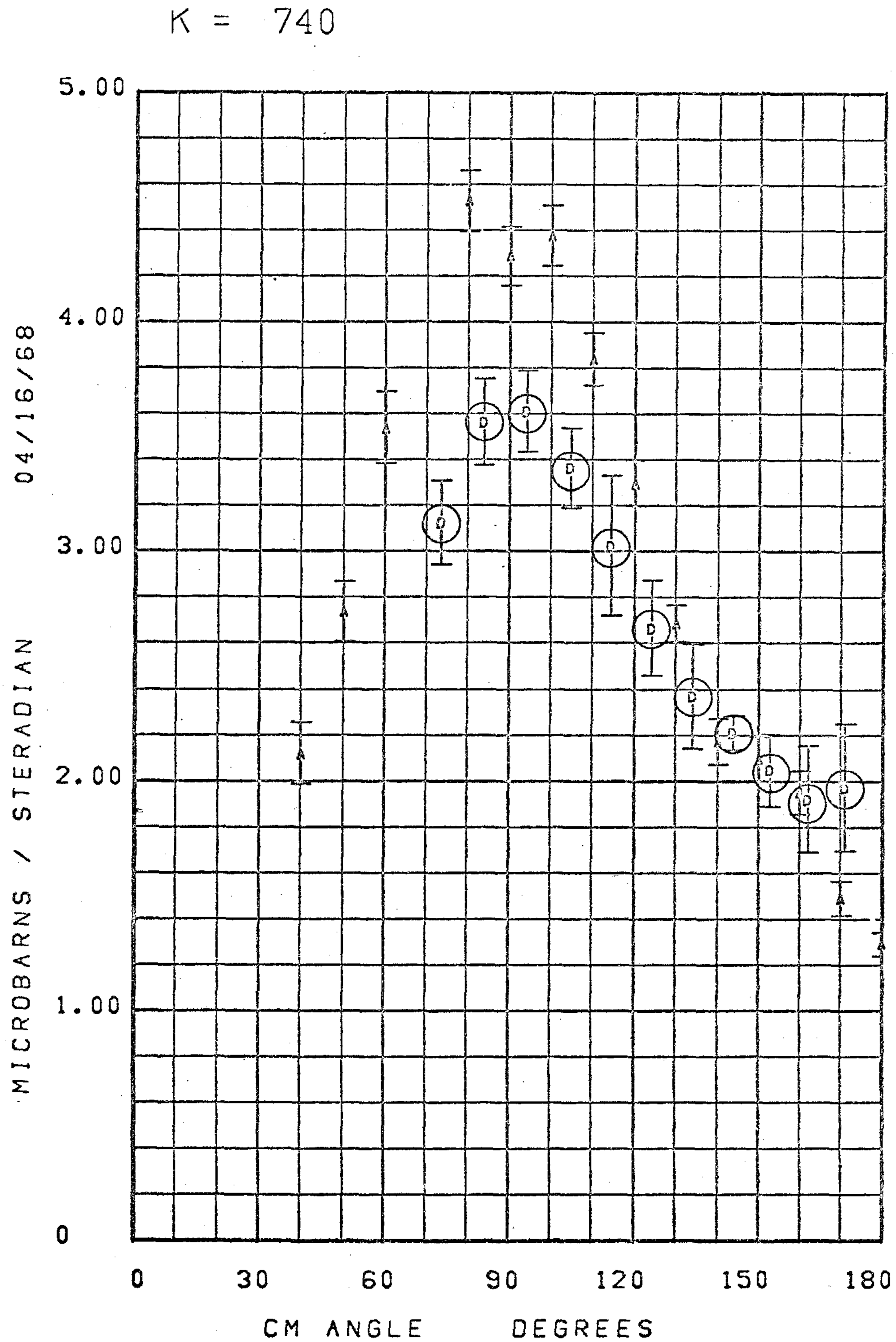
K = 740
5.00
4.00
3.00
2.00
1.00
0
0
30
60
90
120
150
180
CM ANGLE DEGREES
MICROBARNS / STERADIAN
04/16/68

Figure 15.6

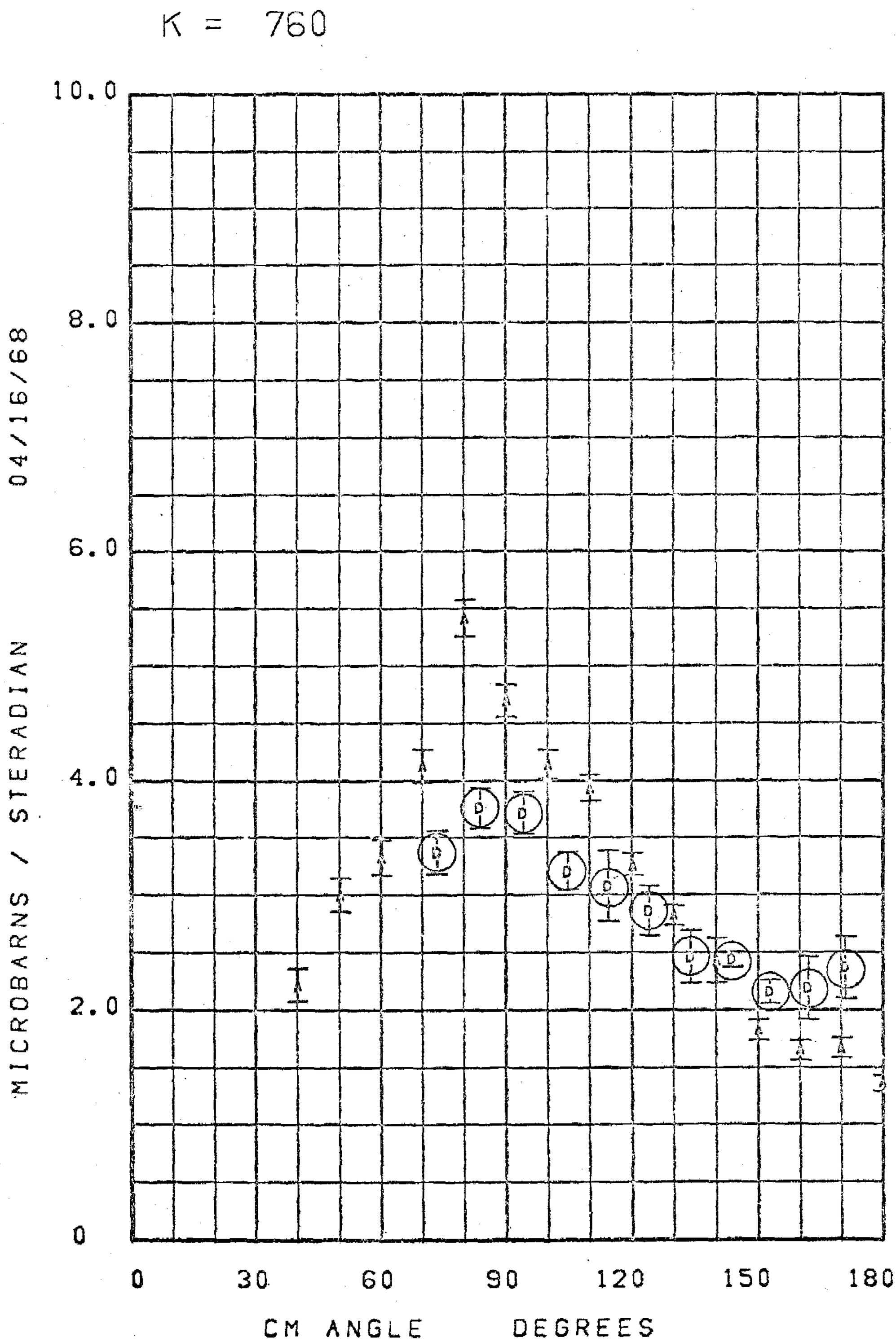
K = 760
10.0
8.0
6.0
4.0
2.0
0
0
30
60
90
120
150
180
CM ANGLE DEGREES
MICROBARNS / STERADIAN
04/16/68

Figure 15.7

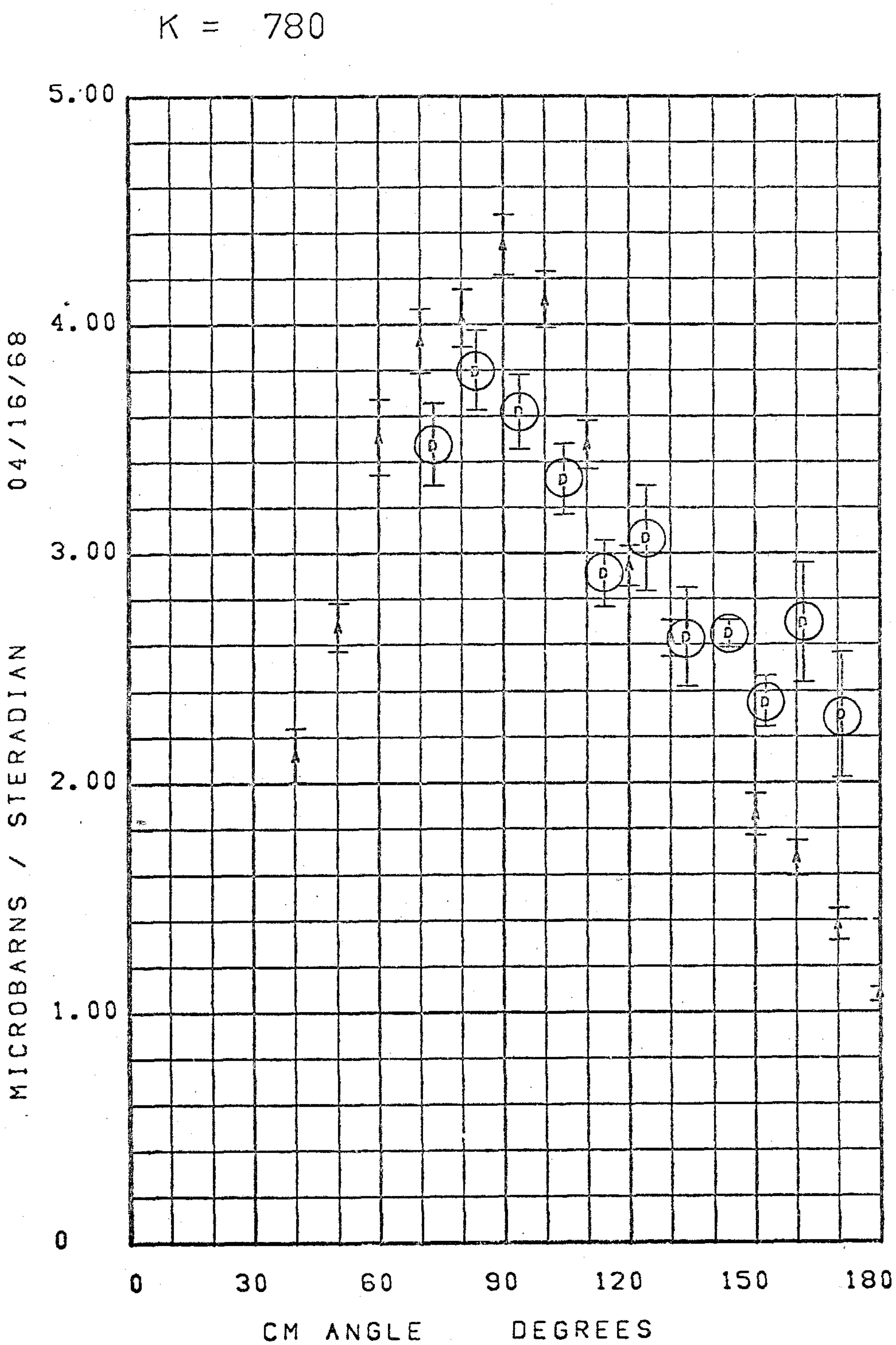

K = 780
5.00
4.00
3.00
2.00
1.00
0
MICROBARNS / STERADIAN
04/16/68
0
30
60
90
120
150
180
CM ANGLE DEGREES

Figure 15. 8

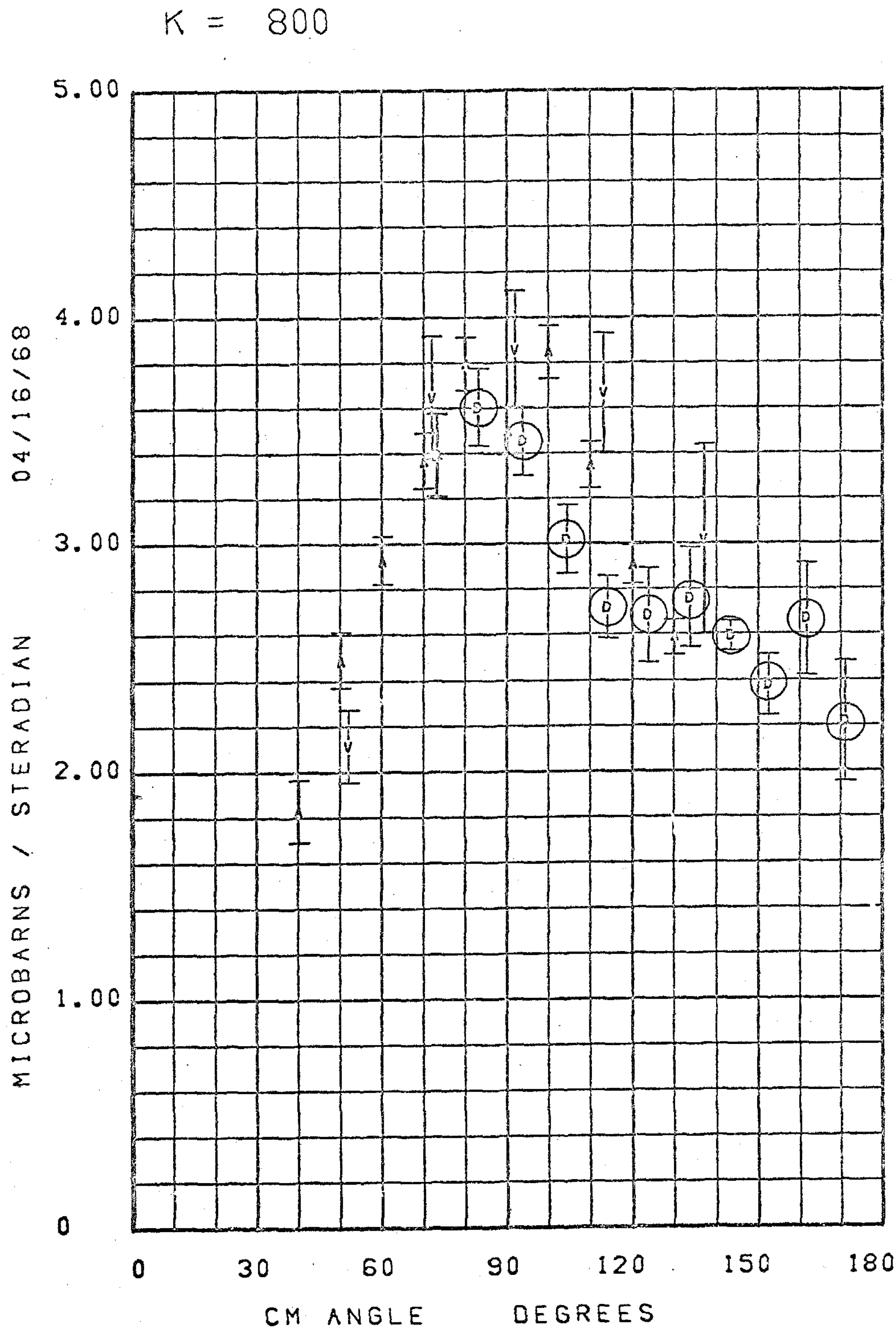
K = 800
5.00
4.00
3.00
2.00
1.00
0
MICROBARNS / STERADIAN
04/16/68
0
30
60
90
120
150
180
CM ANGLE DEGREES

Figure 15.9

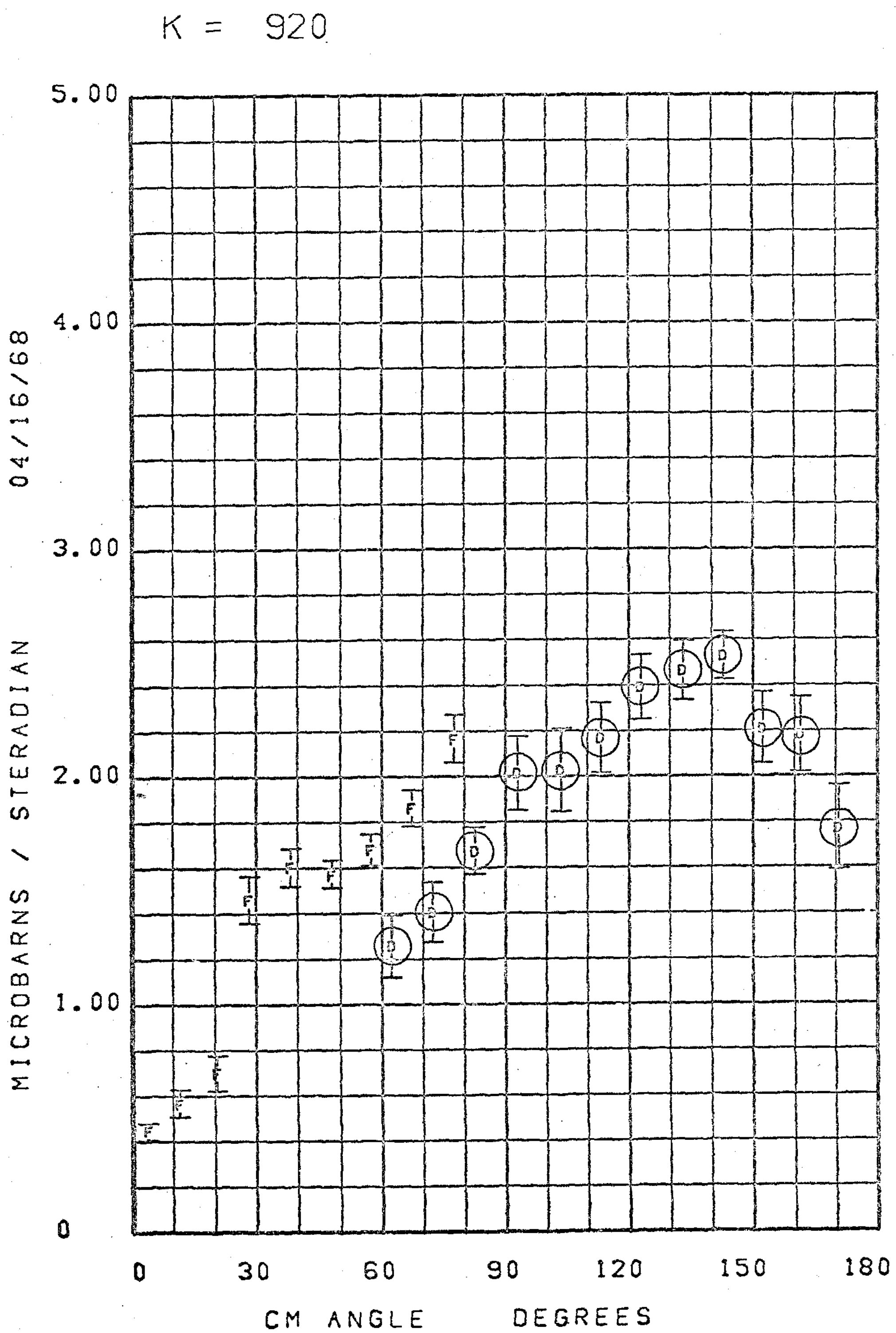
K = 920
5.00
4.00
3.00
2.00
1.00
0
04/16/68
MICROBARNS / STERADIAN
0
30
60
90
120
150
180
CM ANGLE DEGREES

Figure 15.10

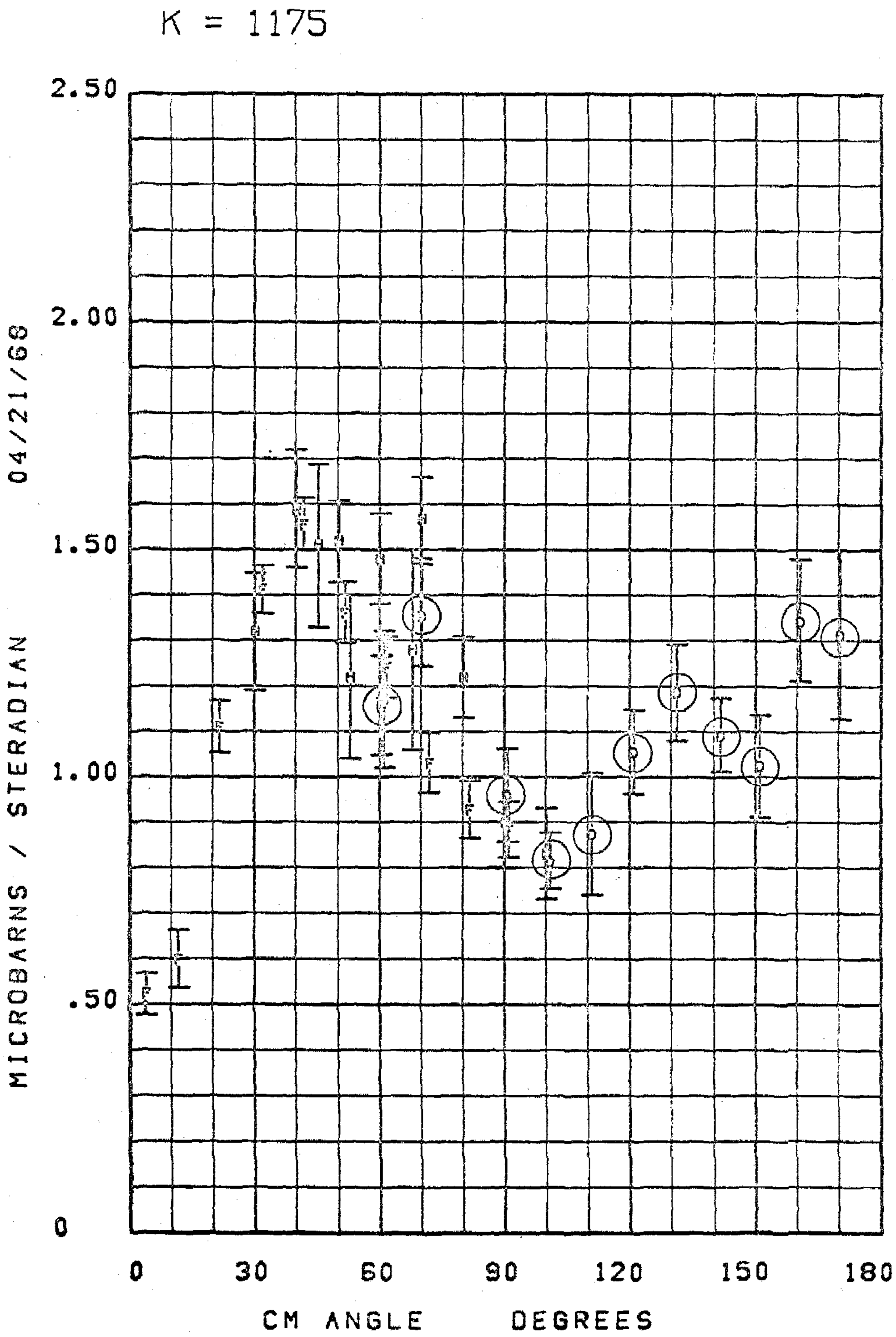
K = 1175
2.50
2.00
1.50
1.00
.50
0
MICROBARNS / STERADIAN
04/21/68
0
30
60
90
120
150
180
CM ANGLE DEGREES

Figure 15.11

Lundquist (code -) has measured cross sections at constant proton momentum, P_p. These are shown in Figure 16. The points are plotted versus k with the pi c. m. angle ranges indicated. For P_p = 684 MeV/c his data are higher in general than ours. Near k = 750 MeV this is understandable because ours are too low. But near k = 950 MeV there should be no such discrepancy. At P_p = 755 and 833 MeV/c, agreement is good, except near 90^o at the second resonance.

Although the data of the present experiment did not go to 180^o, it is interesting to compare the present results with the existing data near 180^o. Figure 17 shows a plot of the Buschhorn et al. (code E) and Loh et al. (code I) data. The data plotted for Loh et al. are preliminary results from a paper given before the final normalization of their data was determined. The final data, which are not yet published, are a little higher than that shown (13), but not as high as Buschhorn's. Also plotted for comparison are points ◎ showing the 180^o values of the polynomial fits to the angular distributions of this experiment. The data indicate either that this experiment disagrees with Buschhorn and Loh's between 800 and 1100 MeV, or that the cross section drops rapidly between 170 and 180 degrees. DeStaebler (code A), whose results appear to be too small at 180^o, did see this sort of a shape in the angular distribution near 180^o. It would be useful to have a measurement, in one experiment, of the cross section near and including 180^o over the range of at least 700 to 1200 MeV.

Figure 16

Distributions at constant momentum. The range of pi c.m. angles is indicated on each graph. The symbol code is as follows:

-	Lundquist (10)
Ⓓ	This experiment

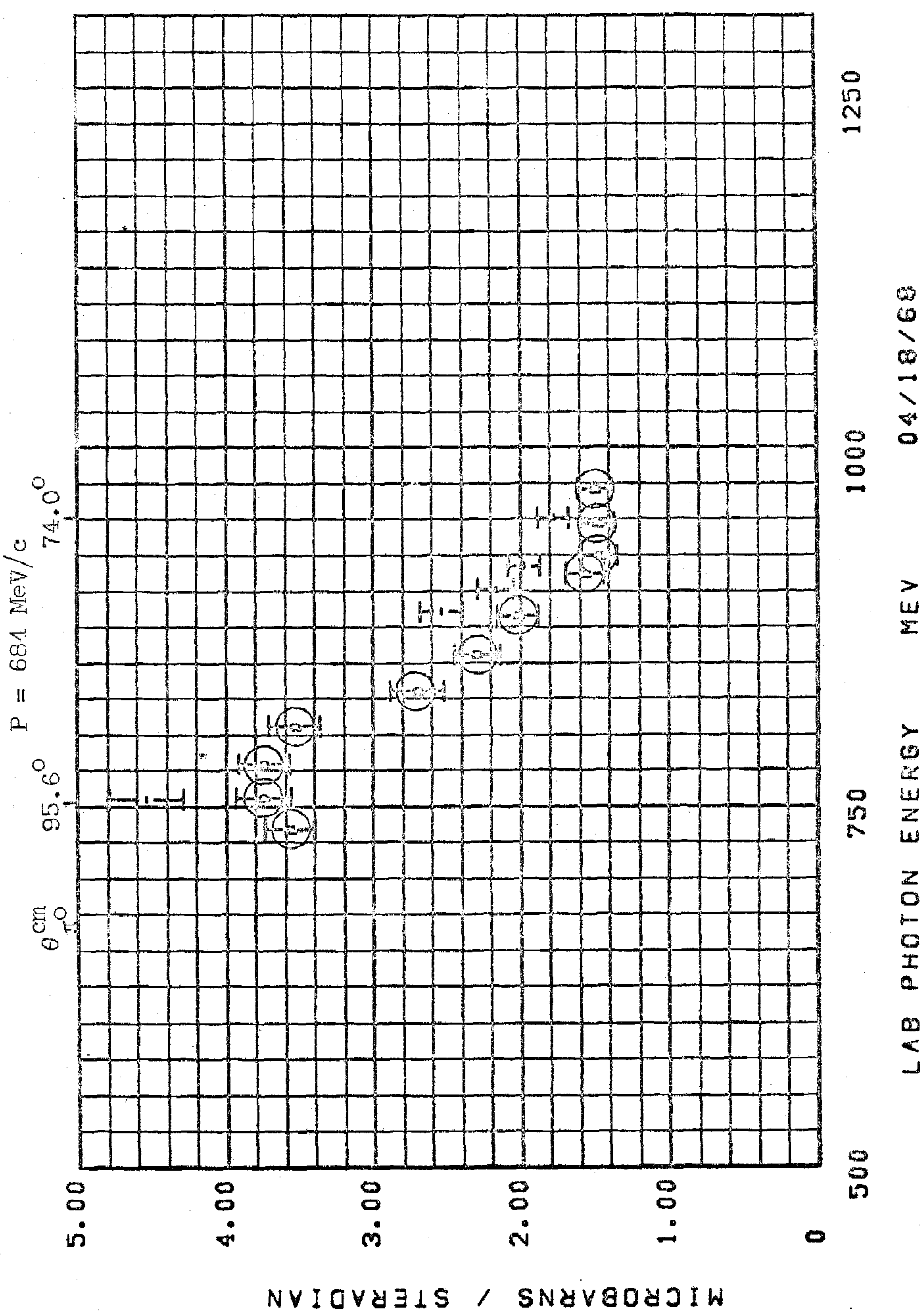
$\theta_{\pi^0}^{cm}$
95.6°
P = 684 MeV/c
74.0°
5.00
4.00
3.00
2.00
1.00
0
MICROBARNS / STERADIAN
500
750
1000
1250
LAB PHOTON ENERGY MEV
04/18/68

Figure 16.1

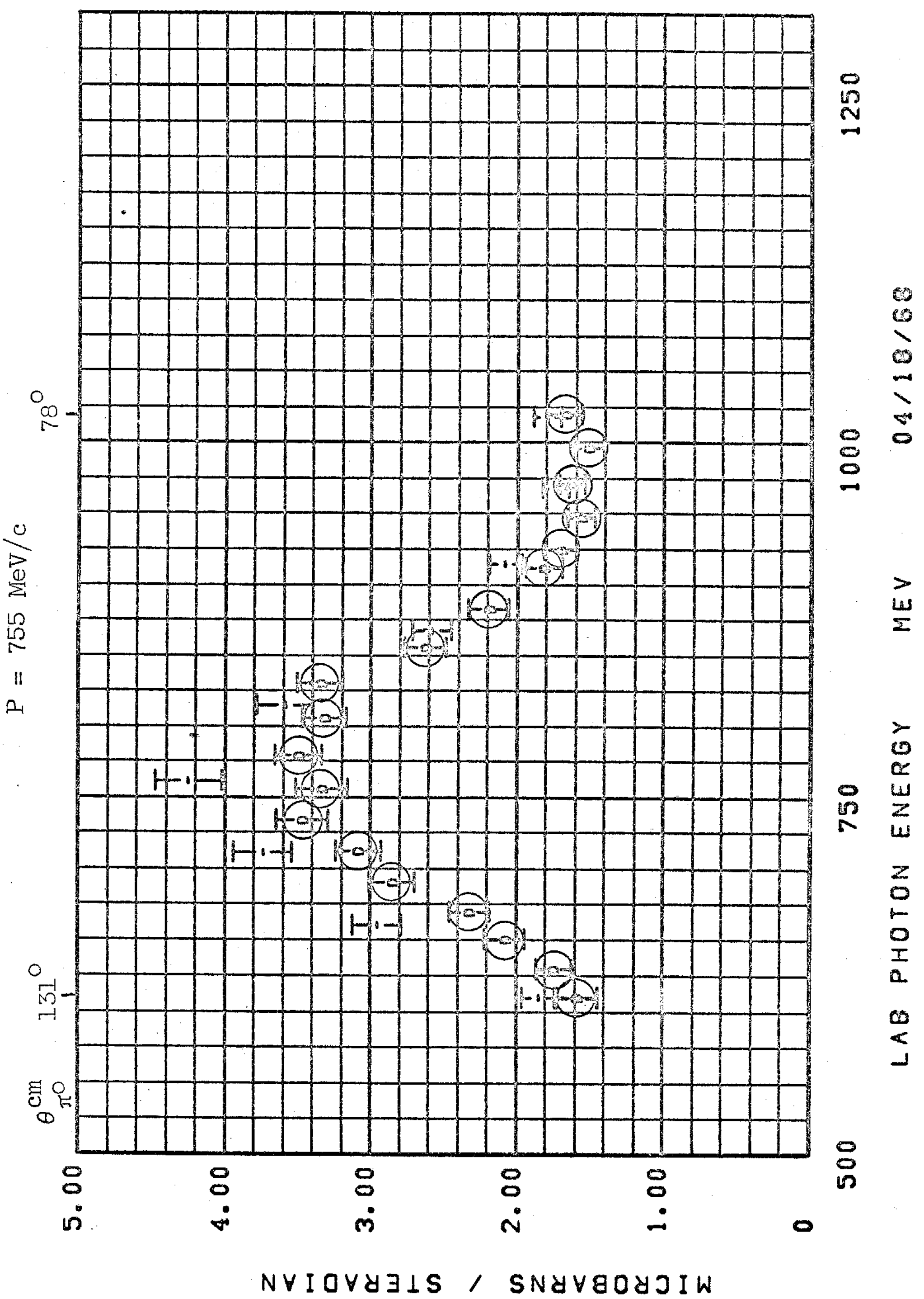
P = 755 MeV/c
78°
131°
θ cm π°
5.00
4.00
3.00
2.00
1.00
0
500
750
1000
1250
LAB PHOTON ENERGY MEV
04/18/68
MICROBARNS / STERADIAN

Figure 16.2

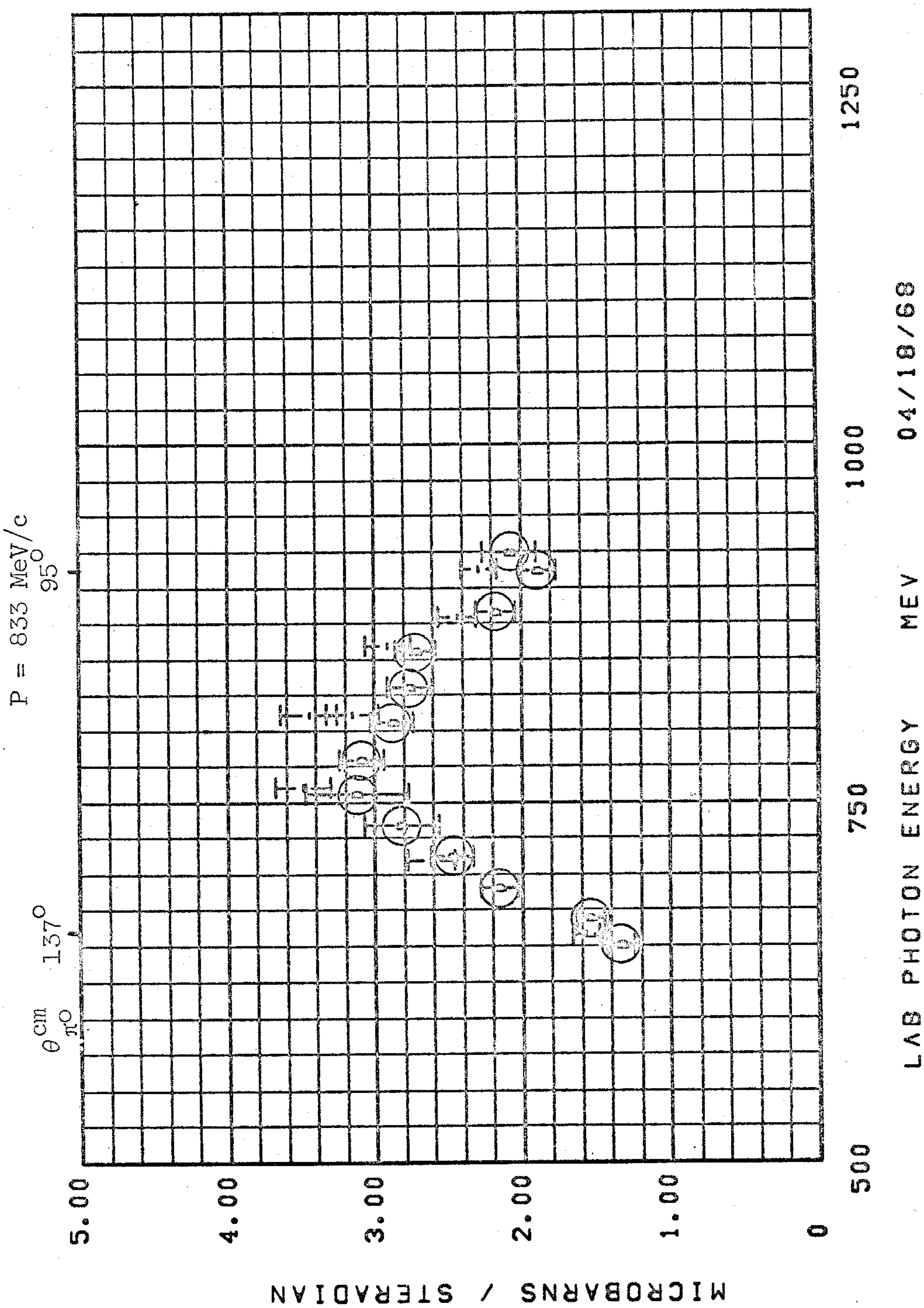
P = 833 MeV/c
$\theta_{\pi^0}^{cm}$
137°
95°
5.00
4.00
3.00
2.00
1.00
0
MICROBARNS / STERADIAN
500
750
1000
1250
LAB PHOTON ENERGY MEV
04/18/68

Figure 16.3

Figure 17

Energy distributions near 180°. The symbol code is as follows:

A	DeStaebler et al. (4) at 180°.
E	Buschhorn et al. (12) at 179°.
I	Loh et al. (13) at 180° (preliminary).
+	Polynomial fits to this experiment evaluated at 180°.
(D)	This experiment at $\sim 170^{\circ}$.

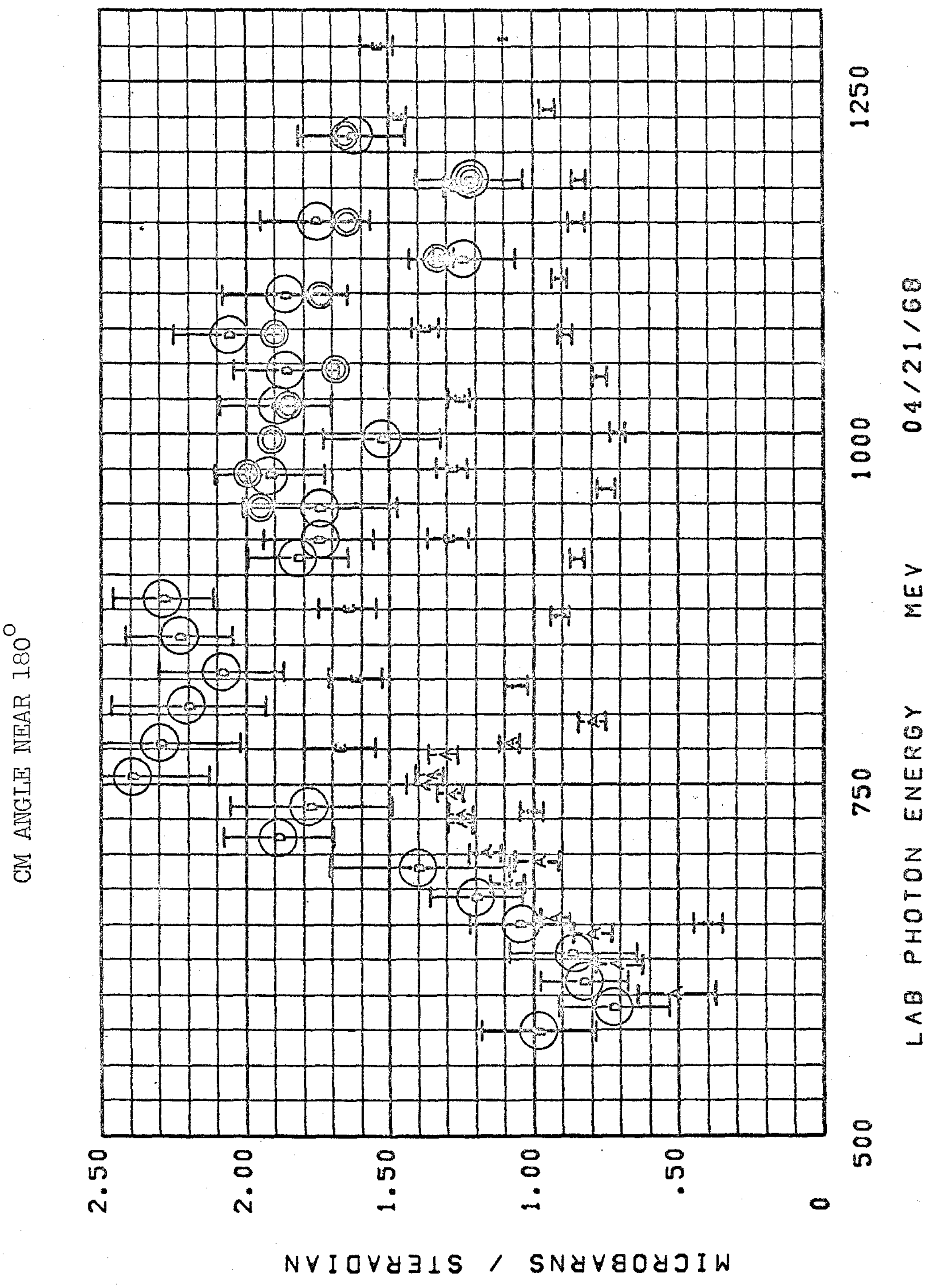
CM ANGLE NEAR 180°
2.50
2.00
1.50
1.00
.50
0
500
750
1000
1250
LAB PHOTON ENERGY MEV 04/21/68
MICROBARNS / STERADIAN

Figure 17

VI. CONCLUSIONS

The 328 cross sections measured in this report provided angular distributions from about 60° to 170° with points at least every 10° at energies from 574 MeV to 1211 MeV. There is a peak in the angular distribution at 140° in the third resonance region, which has been expected from phenomenological fitting, but has not been measured before (18).

Both internal inconsistency and comparison with other experiments indicate that the cross sections from the present experiment at 90° in the second resonance region are about 15% low. The problem, although not understood, seems to be connected with the veto data and does not seem to affect the majority of the data.

A comparison of the 170° data from this experiment with the data near 180° from other experiments indicates either a large discrepancy in the measured cross sections or a rapid decrease in the cross section between 170° and 180° for energies between 700 and 900 MeV. A careful investigation of the cross section near to and including 180° would be useful.

APPENDIX I. BEAM AND HYDROGEN TARGET

A. Beam line

This experiment was performed in the south beam of the CalTech Synchrotron, shown in Figure 1. After being produced by electron bremsstrahlung in a 0.2 radiation length tantalum radiator the beam passed through a rectangular lead collimator. The beam next passed through two scraping walls, a set of sweep magnets and a 6 inch liquid hydrogen target being used by a UCLA group. To remove all electrons produced in the UCLA target, the beam was swept with another magnet. The cleaned beam traveled through a 60 inch helium bag and through a 4 x 4 inch hole in a scraping wall. The primary purpose for the sweep magnet, the helium bag and this wall was to reduce background rates in the gamma counters for this experiment. Following the wall, the beam passed through a Mylar window to enter a vacuum snout extending upstream from the hydrogen target. The beam then passed through the target itself, which was a vertical 3 inch diameter cylinder of .005 inch Mylar filled with liquid hydrogen. At this point the beam was 408 inches from the radiator, 1.8 inches high and 1.3 inches wide. The beam then traveled through a vacuum snout on the downstream side of the target and exited through another Mylar window. After passing through several feet of air, the beam either hit the yoke and coils of the spectrometer, if it was set at a small angle, or was stopped in a thick plate ionization chamber enclosed in a cement "beam catcher".

The height of the beam could not be controlled and was found to vary both with time and with machine energy. However, the amount by which it varied resulted in very small corrections. If the difference between the beam height and the spectrometer calibration height is written as

$$\Delta h = a + b \left(\frac{E_o - 1000}{1000} \right),$$

then a was -.18 inches, and b was zero for the initial portion of the experiment and .00027 for the latter part.

The horizontal position of the beam was checked each time the endpoint energy was changed and was kept centered on the gamma counter center of rotation to within .05 inches.

Both the calibration of the beam energy meter and the thickness of the hydrogen target have been investigated in detail by Thiessen (21). The values used for this experiment were

$$(E_o)_{true} = (E_o)_{meter} \times 1.025$$

for the energy meter calibration and

$$3.162 \times 10^{23} \left(\frac{\bar{\ell}}{\ell}\right) \frac{\text{protons}}{\text{cm}^2}$$

for the thickness of the hydrogen target where $(\bar{\ell}/\ell)$ is the ratio of effective target length to the target diameter. This thickness has been corrected for the atmosphere of hydrogen gas left when the target is emptied. It corresponds to the amount of hydrogen producing the difference between the foreground and background rates.

B. Beam monitoring

The absolute reference for monitoring the intensity of the bremsstrahlung beam was a Wilson-type quantameter. This quantameter has been intercalibrated with other monitors and been found to be stable over periods of several months. The most likely source of instability in this type of monitor is leakage of gas into or out of the chamber. To check for changes in amount of gas, the temperature and pressure of the quantameter were measured frequently during the experiment. The rms deviation of the measurements was < 1% and the overall drift was found to be < 1%.

The absolute calibration of the quantameter was checked by H. A. Thiessen and J. Pine, using electrons from the Stanford Linear Accelerator (22). During that calibration, the intensity of the electron beam was measured with a Faraday cup. The calibration of the quantameter on electrons agreed with the theoretical calibration for electrons to within the experimental error (± 3%). Thus the data for the present experiment were analyzed using the theoretical calibration for photons

$$\frac{\text{coulombs}}{\text{MeV}} = (13.10 \times 10^{15}) \frac{P}{T}$$

where

P = absolute pressure in millimeters of mercury

T = absolute temperature in degrees Kelvin.

The charge from the quantameter was measured with a Model 4 ion current integrator designed by M. Sands. This same integrator has been used in previous experiments. The number of pulses from the integrator (BIPS) was multiplied by the calibration constant (coulombs/BIP) of the integrator to get the charge from the quantameter. The integrator constant changed by as much as 2.5% from day to day and was measured each day using an integrator calibrator designed by M. Sands. The accuracy of the calibrator has been checked by H. A. Thiessen and found to be accurate to ± .25%.

There were several reasons why the quantameter was not placed in the beam during the data runs. First, it could not be placed in the beam catcher because its sensitive area is too small to subtend the whole beam at that distance from the radiator and because it would have been blocked by the magnet when the magnet was at small angles. It could not be placed immediately following the hydrogen target, again, because of the small angle running. It could have been placed following the hydrogen target for large angle running, but this would have interferred with the external electron beam, which is created in the south beam catcher, and probably would have caused high backgrounds in the gamma counters for this experiment.

Thus it was necessary to use relative secondary monitors which could be used during the data runs. The two best monitors available for this purpose were:

(1) BCC, the amount of charge out of the beam catcher ionization chamber. (The charge was measured with the same integrator used for the quantameter, since the two chambers could never be used at the same time.)

(2) M1 and M2, two scalers counting the coincidence rate of a two scintillator monitor telescope placed beneath the hydrogen target to count particles produced at 90^{o} with respect to the beam (cf. Reference 14).

Because both the beam catcher ionization chamber and the quantameter absorb the photon beam, the ionization chamber could not be calibrated directly. Since it was feared that backscatter from the quantameter would affect the monitor telescope if the quantameter were placed downstream of the hydrogen target, the monitor telescope was not calibrated directly either.

Two other monitors were used to intercalibrate BCC, M1, and M2 with the quantameter. These were

(1) 40 MC, an induction probe inside the synchrotron, which measured the 40 mc. signal created by the circulating electron beam just before the beam was dumped.

(2) TC-1, a thin ionization chamber placed downstream of the primary collimator.

These two monitors had the advantage of being in the beam at all times. They had the disadvantage of not being as stable as the other monitors. Both 40 MC and TC-1 were critically dependent on beam lineup. Also 40 MC was affected at low E_o by phase oscillations of the circulating electron beam. 40 MC and TC-1 were compared to BCC, M1 and M2 during the data runs and with quantameter during short monitor runs interspersed among the data runs.

Because the UCLA target could convert 1.3% of the beam to electrons and because the sweep magnet could sweep these out of the beam, the various monitors were corrected for whether the UCLA target was full and whether the sweep magnet was on.

For monitor calibration purposes, the runs were divided into groups with each group being run at the same E_o on the same day. Separate calibrations were computed for each group. Consider one group and let Σ_d denote a sum over all data runs in that group and Σ_m denote a sum over all monitor runs in that group. The number of quantameter bips per beam catcher ionization chamber coulomb, Q/BCC, was determined using TC-1 and 40 MC as follows:

$$\left(\frac{Q}{BCC}\right)_{40\ MC} = \frac{\Sigma_m Q / \Sigma_m 40\ MC}{\Sigma_d BCC / \Sigma_d 40\ MC}$$

$$\left(\frac{Q}{BCC}\right)_{TC-1} = \frac{\Sigma_m Q / \Sigma_m TC-1}{\Sigma_d BCC / \Sigma_d TC-1}$$

$$\left(\frac{Q}{BCC}\right) = \frac{1}{2}\left[\left(\frac{Q}{BCC}\right)_{40\ MC} + \left(\frac{Q}{BCC}\right)_{TC-1}\right]$$

(Q/M1) and (Q/M2) were found in a similar way. Then, for each data run in the group, the effective number of quantameter bips was found as follows:

$$Q = \frac{1}{2} \left\{ \left(\frac{Q}{BCC}\right) BCC + \frac{1}{2} \left[\left(\frac{Q}{M1}\right) M1 + \left(\frac{Q}{M2}\right) M2 \right] \right\}$$

From Q, the integrator calibration, and the quantameter calibration, the total number of MeV in the beam was found for each run.

Because there were usually two or more monitor runs in each group and because calibrations using 40 MC and TC-1 were averaged together, the fluctuations in TC-1 and 40 MC tended to average out and give calibrations of BCC, M1, and M2 which had much more stability than TC-1 and 40 MC themselves.

To aid in evaluating the degree of stability in the calibrations and to check for systematic drifts, fits were made of BCC/(10^{17} MeV) and (M1 + M2)/(10^{17} MeV). The fits allowed a quadratic dependence on the endpoint energy and were of the form

$$a_o + a_1 \left(\frac{E_o - 1000}{1000} \right) + a_2 \left(\frac{E_o - 1000}{1000} \right)^2$$

where a_0, a_1, and a_2 were constants determined by the least squares fit. In order not to skew the fits, the few points with deviations of more than 10% from the fits were eliminated in the final fits. These data only constituted about 3% of the data, and, in nearly every case, the error was traceable to an obvious mistake. In no case did these mistakes affect the analysis of the data used for the final cross sections.

Table 3 shows the fitting constants and rms per cent deviations obtained in the fits of the foreground and background runs, i.e. the runs with liquid hydrogen or gaseous hydrogen in the target. Figure 18 shows the per cent deviations of the rates for the individual runs as a function of run number. BCC is the most stable monitor, having rms deviations of 1.2% and 1.5% for foreground and background runs. The plots show no systematic drifts in BCC. The (M1 + M2) foreground fit has an rms deviation of 2.1% with no long term systematic drifts. However, (M1 + M2) on backgrounds has twice as large an rms deviation and shows some systematic drifts. That (M1 + M2) was unstable with only gas in the hydrogen target is not surprising, since the monitor telescope monitored the rate from the target. With only gas in the target the statistical errors were large and rates were more dependent on beam lineup.

In estimating the accuracy of the beam monitoring for the final data, we must use the monitor with the larger error, i.e. (M1 + M2), because both monitors were not available for all runs. The upper limit on the foreground error is thus 2.1%. Since the backgrounds were typically 5% for the P · γ signature, the uncertainty in the background monitoring contributes a negligible error to the final cross sections. The overall rms error is thus 2.1%.

The monitor calibrations for the Lucite runs were done in a simpler and less accurate way. Normally, the only runs at the Lucite calibration energy on a given day were the Lucite run and one monitor calibration run. Thus the Lucite runs were calibrated using only 40 MC and TC-1 from the nearest monitor

Table 3. Monitor Calibration Fits for Data Runs

	FOREGROUND coefficients	FOREGROUND rms deviation	BACKGROUND coefficients	BACKGROUND rms deviation
BCC	.1566 - .0181 - .0058	1.2%	.1574 - .0193 - .0144	1.5%
M1 + M2	0.1592×10^6 0.0105×10^6 -0.1673×10^6	2.1%	0.0114×10^6 0.0017×10^6 -0.0096×10^6	3.8%

Figure 18

Monitor deviations for data runs.

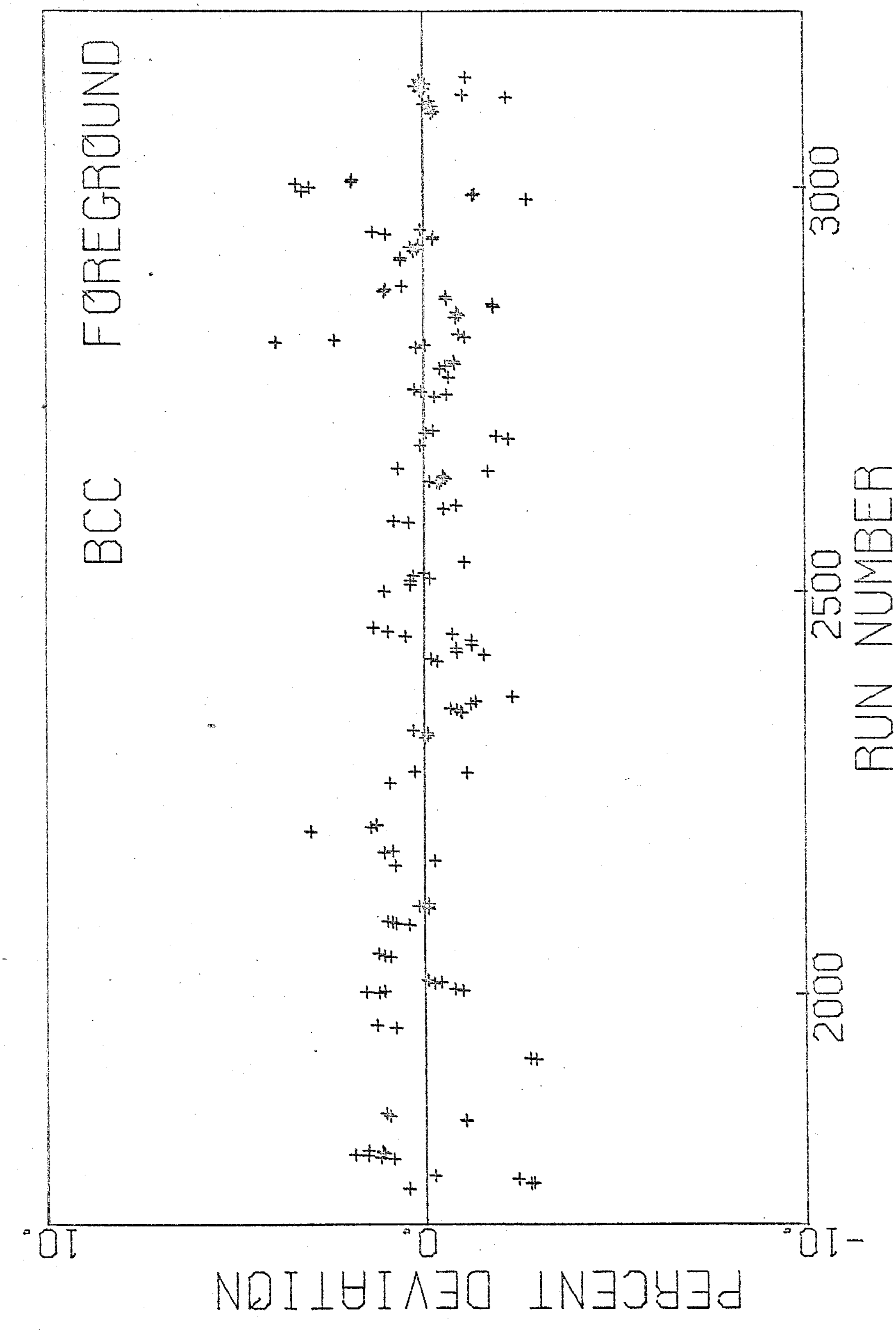
BCC FØREGROUND
RUN NUMBER
2000
2500
3000
PERCENT DEVIATION
10.
0.
-10.

Figure 18.1

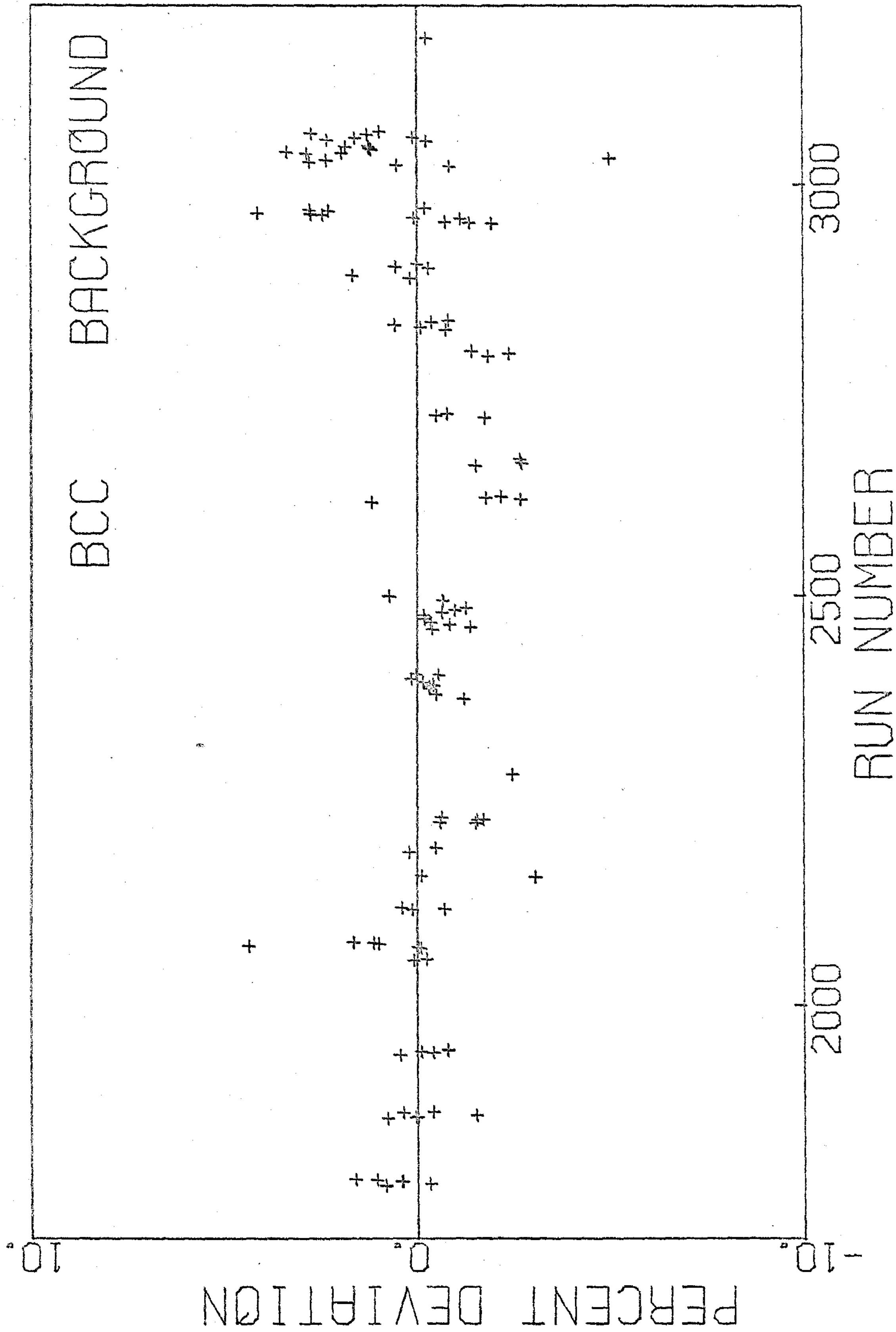
BCC
BACKGROUND
PERCENT DEVIATION
10.
0.
-10.
RUN NUMBER
2000
2500
3000

Figure 18.2

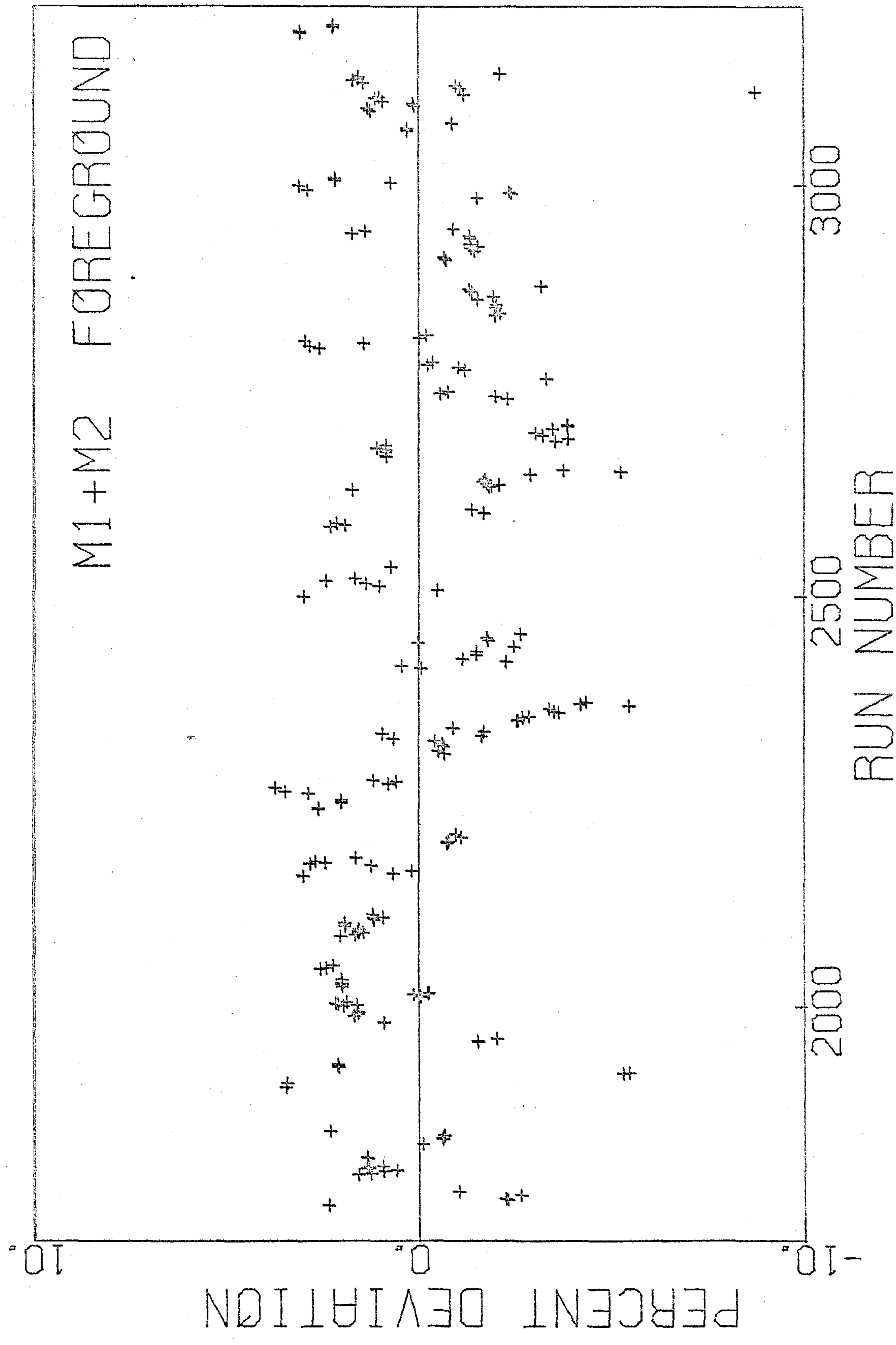
M1+M2 FØREGRØUND
RUN NUMBER
2000
2500
3000
PERCENT DEVIATIØN
10.
0.
-10.

Figure 18.3

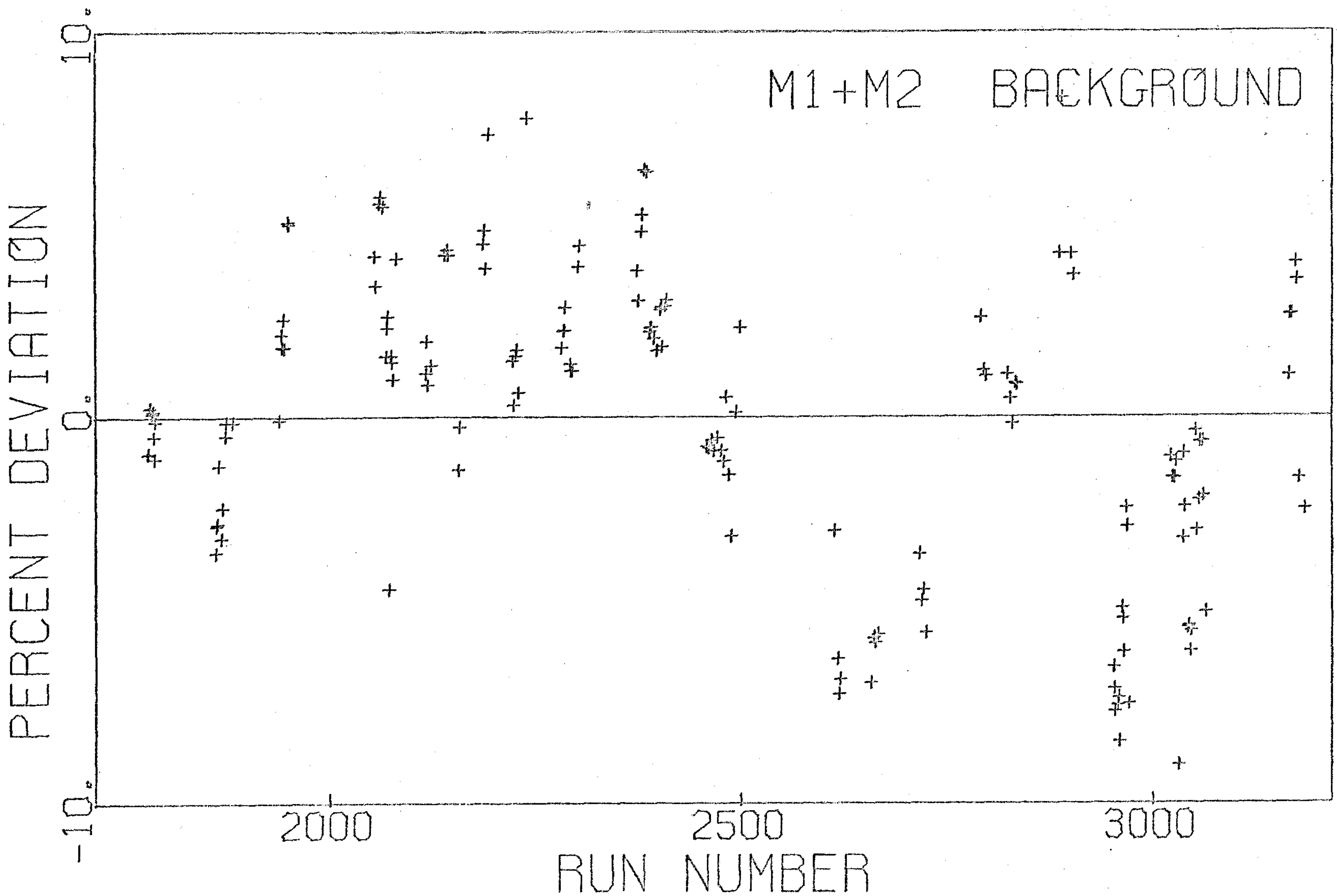
M1+M2 BACKGROUND
PERCENT DEVIATION
10.
0.
-10.
2000
2500
3000
RUN NUMBER

Figure 18.4

run. The calibration did not involve BCC, M1 or M2, even though they were recorded. Table 4 and Figure 19 show the results of the fits for the Lucite runs. The rms deviations are larger than for the foreground runs. (M1 + M2) shows systematic variations that are larger than for any other fit. It is possible that these variations are due to vertical motions of the beam. As the beam moved vertically, it changed the solid angle subtended by the monitor telescope. The effect could have been hidden in the fit of (M1 + M2) to the foreground data because that fit was allowed a functional dependence on E_o.

Since neither BCC, M1, nor M2 was used in the calibrations, it is legitimate to use the smaller value as the estimate of the random error, i.e. 2%. Considering the inherent instabilities in 40 MC and TC-1 individually, this random error is remarkably small.

Table 4. Monitor Calibration Fits for Lucite Runs

	coefficients	deviation
BCC	0.1386 -0.0246	2.0%
M1 + M2	0.9251×10^6 0.2288×10^6 -1.018×10^6	3.3%

Figure 19

Monitor deviations for Lucite runs.

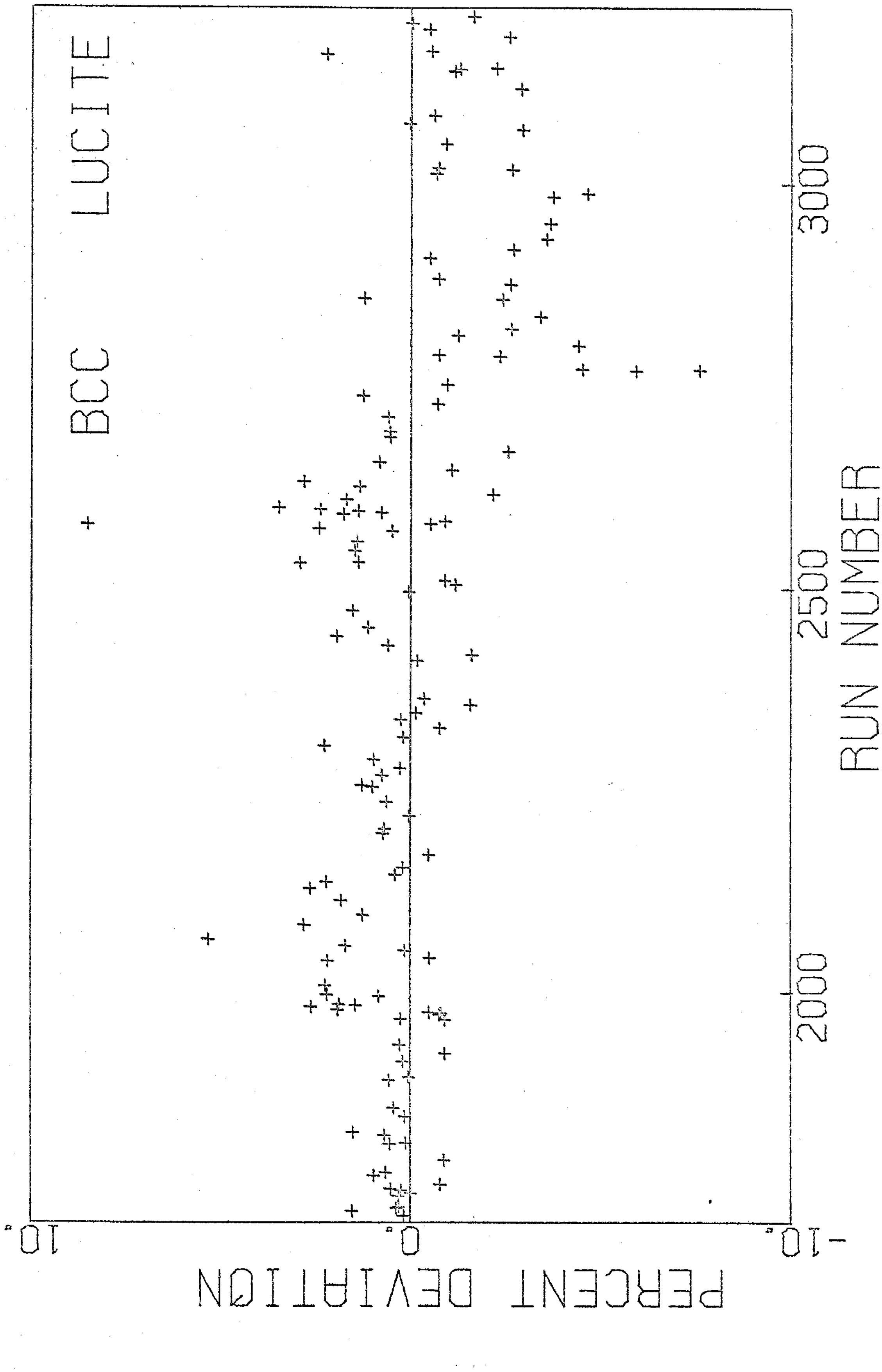
BCC LUCITE
RUN NUMBER
2000
2500
3000
PERCENT DEVIATION
10.
0.
-10.

Figure 19.1

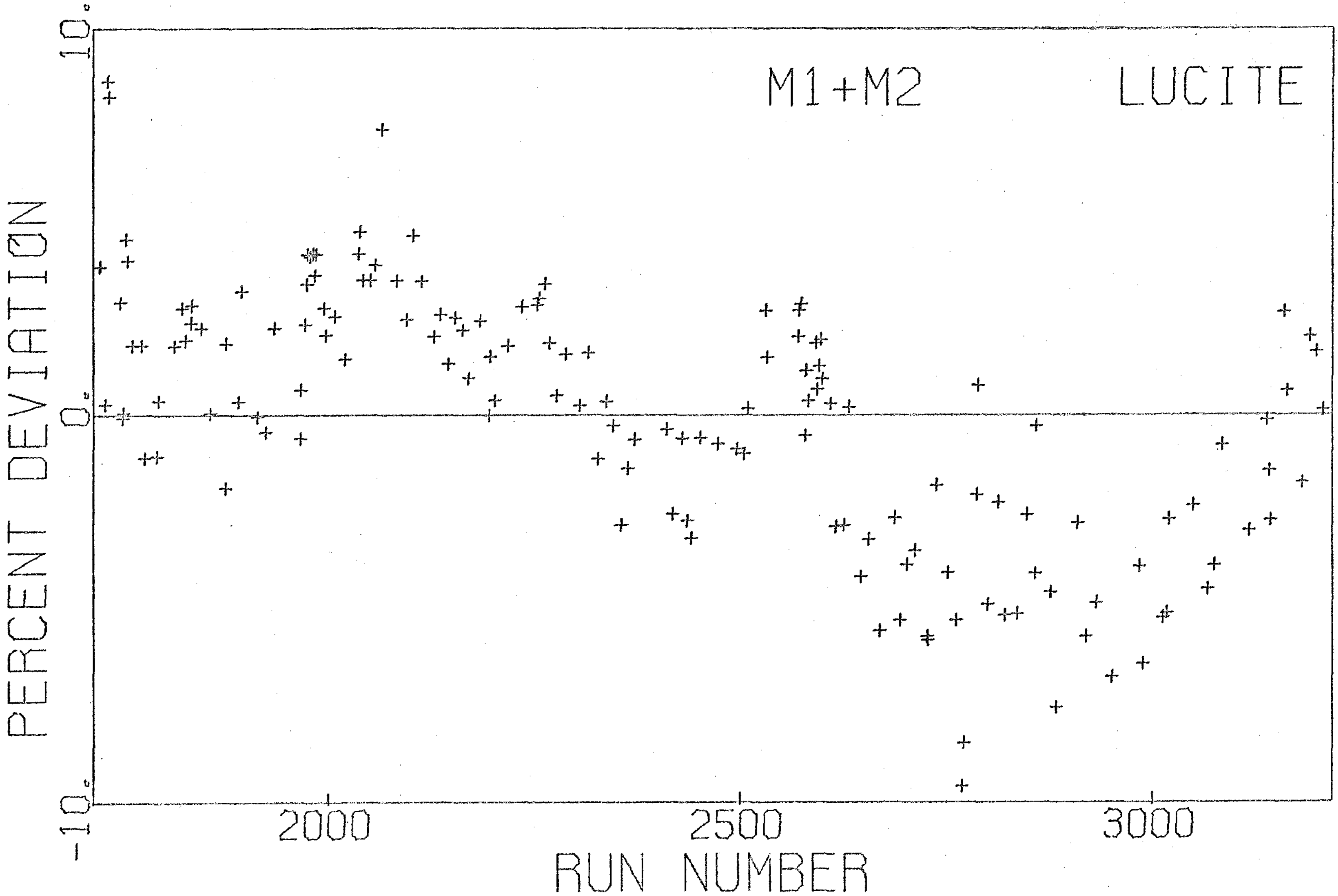
M1+M2
LUCITE
PERCENT DEVIATION
10.
0.
-10.
2000
2500
3000
RUN NUMBER

Figure 19.2

APPENDIX II. SPECTROMETER

A. Configurations

In this experiment, the spectrometer was used in two configurations. Overlapping data points taken with the two configurations showed excellent agreement between them. The HEMA configuration had a maximum momentum of 1200 MeV/c. The OUTR configuration had a maximum momentum of 1670 MeV/c, but was limited to angles less than 39.1°. The calibration of these configurations is described in detail by the present author in Reference 15. Only the results of that report are given here.

In order to detect the high momentum, forward going, protons in backward π^o production, it was desired to have a configuration of the spectrometer which would go to a higher momentum than the previous maximum of 1200 MeV/c. The highest momentum protons from π^o production by 1500 MeV photons have a momentum of about 1800 MeV/c. Measurements indicated that the 1800 MeV/c focus of the spectrometer was under the laboratory floor. A compromise configuration was chosen with a fairly good 1st order focus and a maximum momentum of 1670 MeV/c. The momentum defining counters were held in place by an outrigger which bolted to the back of the magnet carriage and rolled on its own set of wheels. Hence the name "outrigger" or "OUTR" for this configuration.

Although the configuration had a good 1st order focus, floating wire measurements indicated a severe 2nd order aberration. The momentum, which should have been independent of the angle of the proton out of the target, decreased as the square of the vertical angle. To correct this, pieces, shown in Figure 20, were added to the pole tip extensions at the magnet entrance. These additions increased the bending of rays at large positive and negative vertical angles, removing nearly all the 2nd order aberration. The floating wire measurements indicated that the added pieces also improved the 1200 MeV/c configuration focusing. Thus it was decided to create a new 1200 MeV/c configuration to be termed HEMA (HEM for the old HEM focus position and A for the additions to the magnet).

For both configurations, the central ray started horizontally from a point directly over the magnet pivot at a height of 57.85 inches above an aluminum plate epoxied to the magnet tongue. The two configurations differed only in the position of the focus. For HEMA, the focus was 23.51 inches above a labeled aluminum plate epoxied to the laboratory floor, when the magnet was placed at the lineup angle. The OUTR focus was 6.13 inches above another aluminum plate.

The momentum calibration of the spectrometer, i.e. the momentum of the central ray, P_o, in MeV/c as a function of the proton resonance magnetometer frequency, f, in megacycles per second, was given in the form

$$P_o/f = \begin{cases} A_o & f \leq 30 \\ A_o + A_1 \left(\frac{f - 30}{100}\right) + A_2 \left(\frac{f - 30}{100}\right)^2 & f > 30 . \end{cases}$$

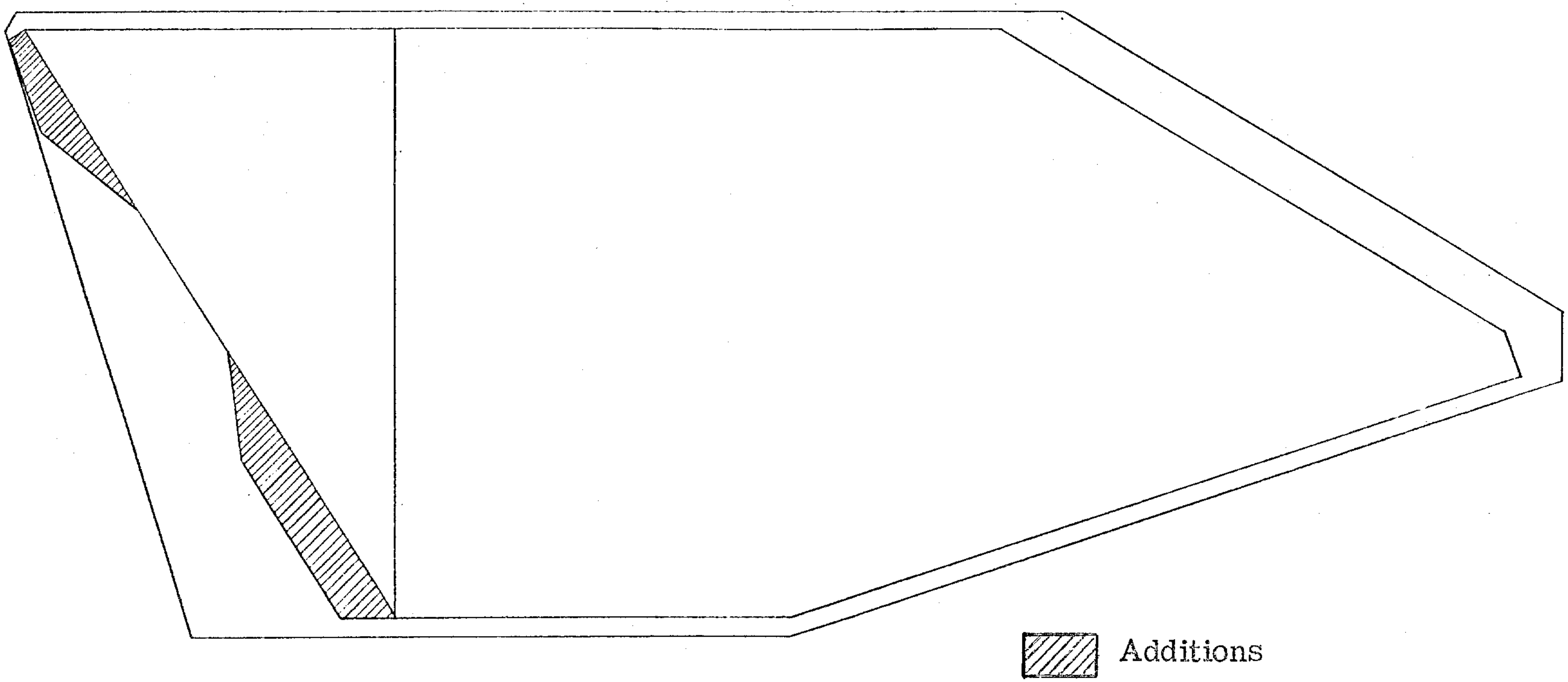

Figure 20. Pole tip extension additions

The values of A_o, A_1, A_2 are 18.812, - .12, - 4.9 for the HEMA configuration and 26.243, - .32, - 6.5 for the OUTR configuration. The break in the functional form at f = 30 is intended to fit the onset of magnet saturation at about that frequency.

The correction to the central momentum for departures of the actual beam height from the arbitrary central ray height can be found from

$$\left(\frac{\Delta p_o}{p_o}\right)_{HEMA} = .018\ \Delta h$$

and

$$\left(\frac{\Delta p_o}{p_o}\right)_{OUTR} = .024\ \Delta h$$

The momentum resolution functions for the HEMA configuration, including only effects of finite beam size, finite counter size and magnet optics, are given in Table 5 and Figure 21 as a function of $Q = (P - P_o)/P_o$. Similar functions for OUTR are given in Table 6 and Figure 22. The overlap of the channels was, in both cases, predominantly due to the vertical beam size (1.8 inches). Better resolution could have been obtained by using a smaller beam collimator, at the cost of decreased counting rate.

The HEMA acceptance properties are presented in Table 7. β, θ, and Ω denote vertical angle, horizontal angle, and solid angle, respectively. The OUTR acceptance properties are contained in Table 8.

Table 5

HEMA RESOLUTION FUNCTIONS
(STERADIANS * 10**-4)

CHA		CHB		CHC		CHD	
Q		Q		Q		Q	
0.008	0.	-0.024	0.	-0.054	0.	-0.082	0.
0.010	2.4	-0.022	0.6	-0.052	0.3	-0.080	0.1
0.012	26.5	-0.020	3.8	-0.050	2.1	-0.078	1.2
0.014	69.9	-0.018	9.8	-0.048	5.7	-0.076	3.8
0.016	120.4	-0.016	24.3	-0.046	12.6	-0.074	8.9
0.018	171.3	-0.014	47.8	-0.044	24.3	-0.072	17.3
0.020	231.7	-0.012	82.4	-0.042	41.3	-0.070	29.5
0.022	296.3	-0.010	131.0	-0.040	64.1	-0.068	45.7
0.024	364.5	-0.008	188.9	-0.038	93.5	-0.066	66.6
0.026	439.1	-0.006	252.3	-0.036	130.2	-0.064	92.6
0.028	514.6	-0.004	319.7	-0.034	176.0	-0.062	124.2
0.030	584.5	-0.002	394.4	-0.032	233.6	-0.060	161.8
0.032	654.9	0.000	472.7	-0.030	301.3	-0.058	205.9
0.034	714.7	0.002	553.0	-0.028	373.3	-0.056	256.8
0.036	758.2	0.004	631.2	-0.026	449.9	-0.054	315.1
0.038	786.5	0.006	704.3	-0.024	528.7	-0.052	381.1
0.040	799.2	0.008	769.1	-0.022	604.9	-0.050	451.5
0.042	795.3	0.010	806.7	-0.020	676.5	-0.048	521.1
0.044	776.3	0.012	820.5	-0.018	736.2	-0.046	586.8
0.046	743.4	0.014	821.0	-0.016	780.5	-0.044	645.7
0.048	696.8	0.016	807.3	-0.014	805.7	-0.042	696.2
0.050	639.6	0.018	781.4	-0.012	810.6	-0.040	735.0
0.052	578.2	0.020	723.5	-0.010	796.6	-0.038	758.4
0.054	515.0	0.022	655.1	-0.008	764.3	-0.036	763.1
0.056	451.4	0.024	582.2	-0.006	715.3	-0.034	746.9
0.058	388.9	0.026	504.4	-0.004	645.0	-0.032	711.5
0.060	328.7	0.028	431.9	-0.002	564.2	-0.030	662.1
0.062	272.1	0.030	361.5	0.000	484.2	-0.028	601.4
0.064	221.0	0.032	294.1	0.002	404.9	-0.026	525.6
0.066	176.7	0.034	233.7	0.004	329.2	-0.024	444.8
0.068	138.7	0.036	178.1	0.006	260.3	-0.022	366.4
0.070	106.5	0.038	127.7	0.008	198.0	-0.020	290.5
0.072	79.8	0.040	85.3	0.010	141.5	-0.018	220.3
0.074	58.1	0.042	52.8	0.012	90.6	-0.016	160.2
0.076	40.8	0.044	29.0	0.014	45.9	-0.014	107.0
0.078	27.7	0.046	15.3	0.016	12.1	-0.012	61.8
0.080	18.1	0.048	8.8	0.018	2.5	-0.010	28.9
0.082	11.4	0.050	4.5	0.020	0.3	-0.008	7.3
0.084	7.1	0.052	1.8	0.022	0.	-0.006	0.2
0.086	4.2	0.054	0.4	0.024	-0.0	-0.004	0.
0.088	2.1	0.056	0.	0.026	-0.0	-0.002	-0.0
0.090	0.8	0.058	-0.0	0.028	-0.0	0.000	-0.0
0.092	0.	0.060	-0.0	0.030	-0.0	0.002	-0.0

Figure 21. HEMA resolution functions

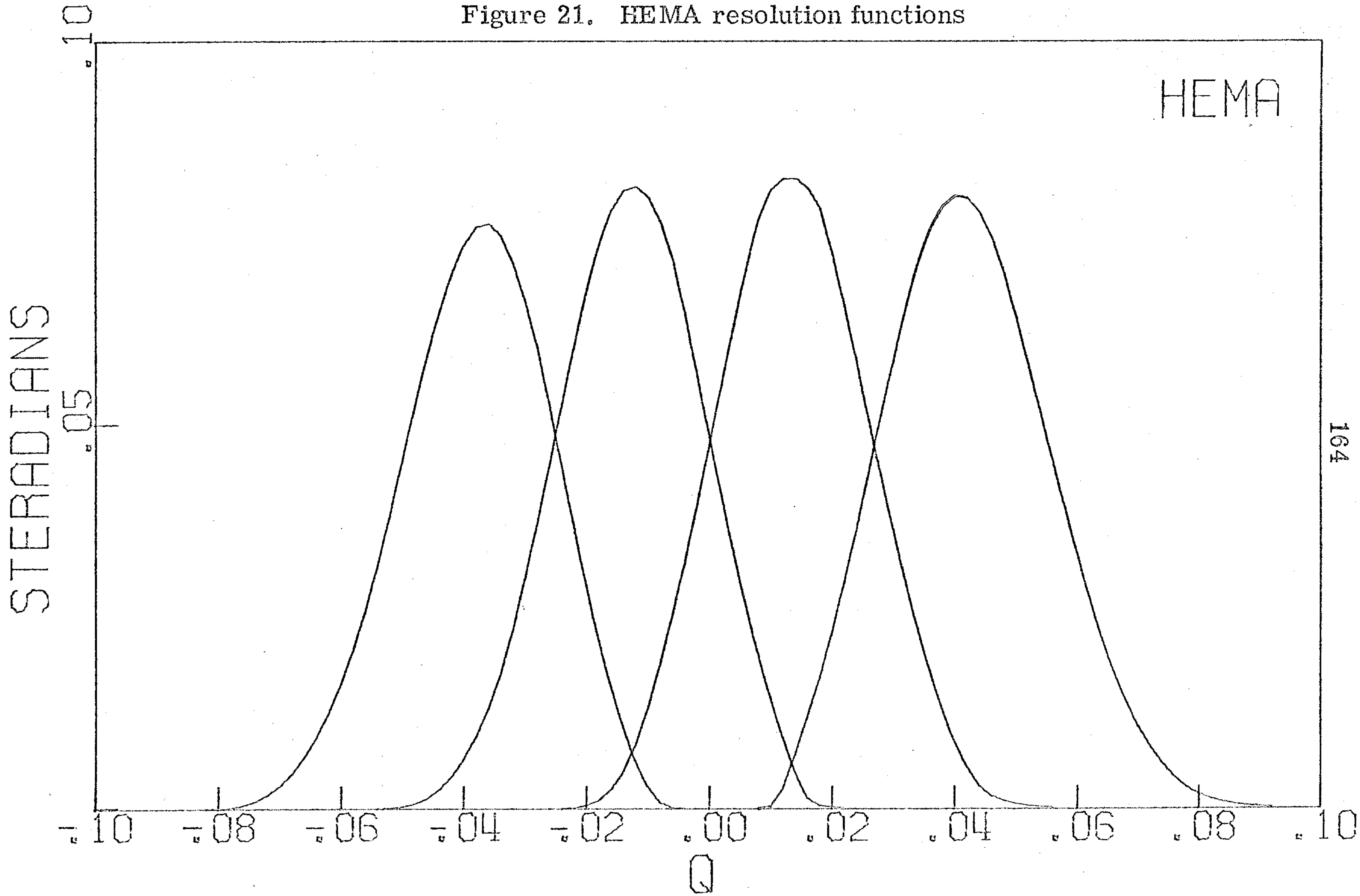

Table 6
OUTR RESOLUTION FUNCTIONS
(STERADIANS * 10**-4)

CHA Q		CHB Q		CHC Q		CHD Q	
-0.012	0.	-0.036	0.	-0.058	0.	-0.080	0.
-0.010	0.8	-0.034	0.3	-0.056	0.3	-0.078	0.1
-0.008	2.6	-0.032	1.4	-0.054	1.3	-0.076	0.8
-0.006	5.6	-0.030	3.4	-0.052	3.2	-0.074	2.2
-0.004	11.0	-0.028	6.4	-0.050	5.8	-0.072	4.3
-0.002	21.8	-0.026	11.0	-0.048	9.8	-0.070	7.3
0.000	41.1	-0.024	18.5	-0.046	15.9	-0.068	11.8
0.002	71.5	-0.022	29.4	-0.044	24.5	-0.066	18.5
0.004	107.2	-0.020	45.3	-0.042	35.8	-0.064	27.4
0.006	146.1	-0.018	69.5	-0.040	50.1	-0.062	38.6
0.008	187.5	-0.016	104.1	-0.038	68.1	-0.060	52.6
0.010	233.2	-0.014	143.6	-0.036	91.7	-0.058	69.3
0.012	278.9	-0.012	186.0	-0.034	125.1	-0.056	88.7
0.014	327.1	-0.010	230.2	-0.032	165.9	-0.054	111.4
0.016	370.5	-0.008	277.2	-0.030	208.7	-0.052	139.2
0.018	411.7	-0.006	325.5	-0.028	253.6	-0.050	177.5
0.020	440.7	-0.004	370.5	-0.026	298.3	-0.048	219.8
0.022	463.3	-0.002	411.5	-0.024	343.2	-0.046	262.5
0.024	477.5	0.000	440.1	-0.022	386.3	-0.044	305.4
0.026	487.1	0.002	461.0	-0.020	424.4	-0.042	347.9
0.028	489.6	0.004	476.7	-0.018	450.3	-0.040	388.7
0.030	486.3	0.006	484.8	-0.016	467.5	-0.038	425.8
0.032	477.0	0.008	486.9	-0.014	479.2	-0.036	454.8
0.034	459.5	0.010	481.6	-0.012	484.8	-0.034	471.2
0.036	437.3	0.012	469.4	-0.010	480.4	-0.032	480.0
0.038	410.8	0.014	451.1	-0.008	470.0	-0.030	481.8
0.040	379.9	0.016	426.3	-0.006	453.8	-0.028	475.3
0.042	345.2	0.018	395.8	-0.004	427.4	-0.026	461.0
0.044	304.7	0.020	361.3	-0.002	397.8	-0.024	438.7
0.046	262.3	0.022	320.4	0.000	361.7	-0.022	408.9
0.048	220.9	0.024	272.2	0.002	316.0	-0.020	374.2
0.050	182.5	0.026	226.1	0.004	266.0	-0.018	332.0
0.052	148.2	0.028	183.0	0.006	217.4	-0.016	282.2
0.054	118.6	0.030	145.2	0.008	173.6	-0.014	230.1
0.056	91.0	0.032	111.4	0.010	133.5	-0.012	183.7
0.058	66.9	0.034	80.5	0.012	96.6	-0.010	140.3
0.060	46.3	0.036	54.6	0.014	65.4	-0.008	101.0
0.062	29.4	0.038	32.4	0.016	38.9	-0.006	68.2
0.064	16.1	0.040	15.5	0.018	16.8	-0.004	38.9
0.066	8.7	0.042	6.7	0.020	3.4	-0.002	15.6
0.068	4.9	0.044	2.6	0.022	0.1	0.000	0.
0.070	2.4	0.046	0.6	0.024	0.	0.002	-0.0
0.072	0.9	0.048	0.0	0.026	-0.0	0.004	-0.0
0.074	0.1	0.050	0.	0.028	-0.0	0.006	-0.0
0.076	0.	0.052	-0.0	0.030	-0.0	0.008	-0.0

Figure 22. OUTR resolution functions

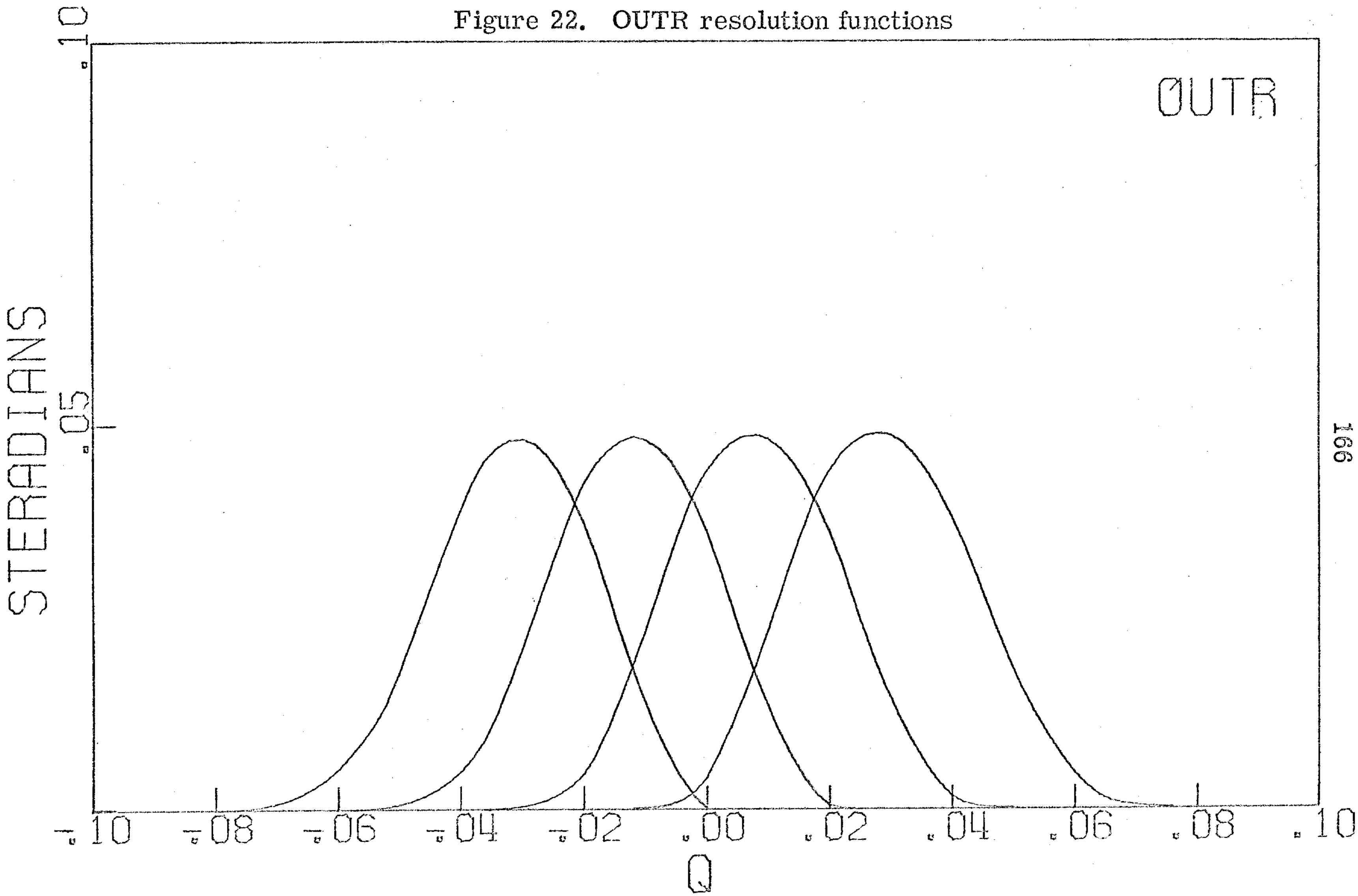

Table 7

HEMA Acceptance Properties

12 x 2.75 inch aperture counter

1.18 inch momentum counters

Momentum channel	Mean Q	$\Delta\beta$ radians	ΔQ	$\Delta\beta\Delta Q$ radians	$\Delta\theta$ radians	$\Delta\Omega$ steradians	$\Delta Q\Delta\Omega$ steradians
A	.0423	.1022	.0266	.00272	.0158	1.614×10^{-3}	4.30×10^{-5}
B	.0138	.1026	.0252	.00258	.0158	1.620	4.08
C	-.0129	.1030	.0239	.00246	.0158	1.628	3.89
D	-.0380	.1033	.0228	.00236	.0158	1.633	3.73

Table 8

OUTR Acceptance Properties

12 x 2.75 inch aperture counter

1.18 inch momentum counters

Momentum channel	Mean Q	$\Delta\beta$ radians	ΔQ	$\Delta\beta\Delta Q$ radians	$\Delta\theta$ radians	$\Delta\Omega$ steradians	$\Delta Q\Delta\Omega$ steradians
A	.0292	.0913	.0199	.00182	.0164	1.497×10^{-3}	2.98×10^{-5}
B	.0080	.0914	.0189	.00173	.0164	1.499	2.84
C	-.0122	.0915	.0182	.00167	.0164	1.501	2.74
D	-.0316	.0916	.0178	.00163	.0164	1.503	2.67

The results presented so far are from Reference 15, which ignores the effects of ionization loss by the protons while leaving the target and traversing the spectrometer. The significant quantity to consider in evaluating the effects of this loss is the difference in momentum between the protons at their source and at the center of the magnet. In the target, the protons passed through an average of about 1.5 inches of liquid hydrogen and a negligible amount of material in the form of heat shields. To exit from the target they left through a mylar window or through a 1/16 inch aluminum vacuum jacket. They then traveled through about 100 inches of air to reach the magnet center.

The momentum loss changed the central momentum of the magnet and also the resolution and acceptance properties. The change in central momentum was calculated using ionization loss values given by a Fortran computer program of D. E. Groom (23). The results are plotted in Figure 23 as a function of the magnet momentum, P_{MAG}, $(= P_o)$. The effect on the resolution and acceptance came from the difference in momentum loss rate between protons at their source and at the magnet. Clearly,

$$\frac{dP_{MAG}}{dP_{SOURCE}} = \frac{dP_{SOURCE}}{dP_{SOURCE}} - \frac{dP_{LOST}}{dP_{SOURCE}} = 1 - \frac{dP_{LOST}}{dP_{SOURCE}} \; .$$

dP_{LOST}/dP_{SOURCE} is simply the slope of the curves in Figure 23. dP_{MAG}/dP_{SOURCE} computed in this way is plotted in Figure 24. The variation of this factor over the width of the momentum channels was ignored and the reciprocal of the value at P_o for each magnet setting was used as a multiplicative correction to the acceptance.

Figure 23

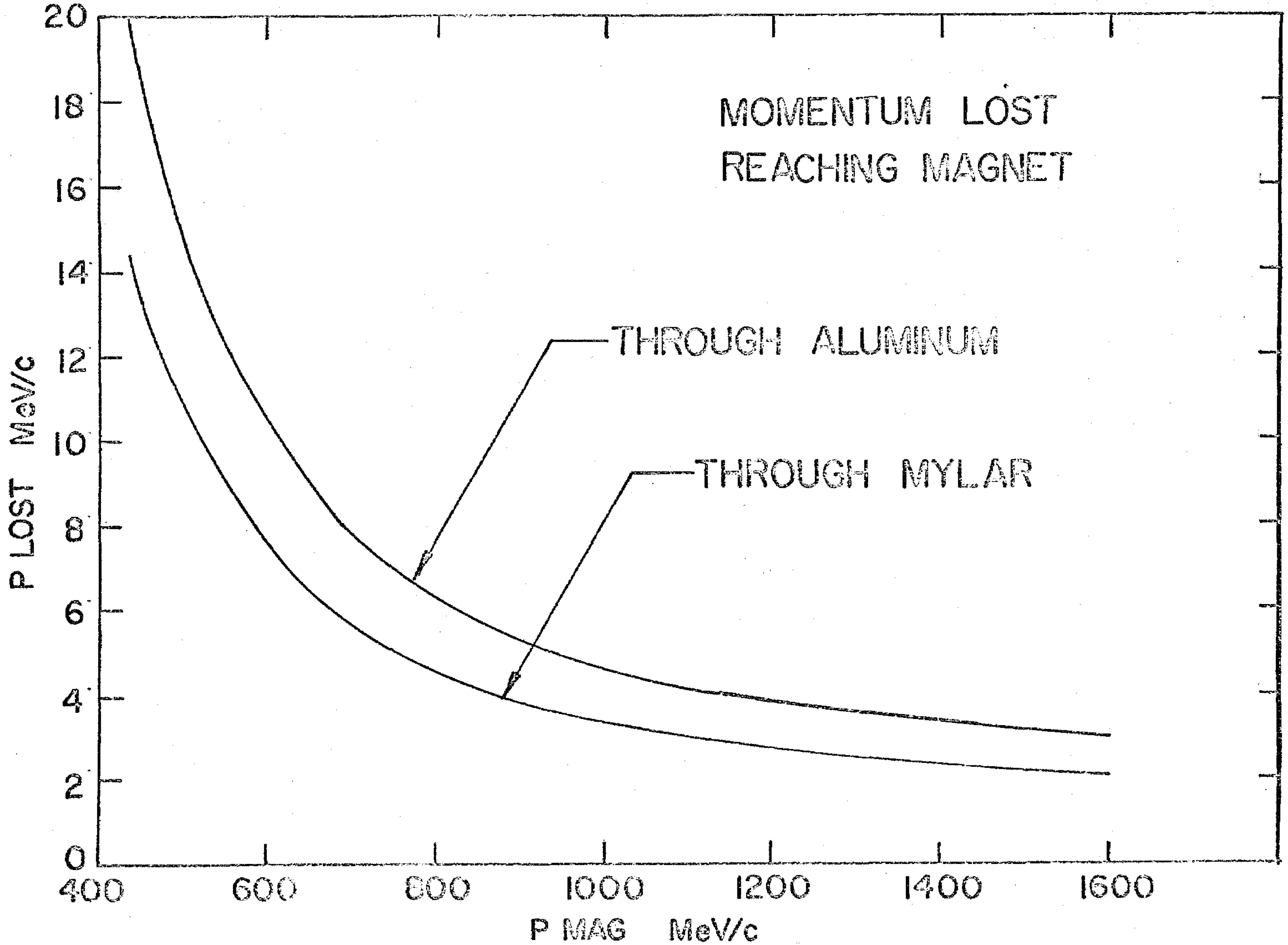

MOMENTUM LOST
REACHING MAGNET
THROUGH ALUMINUM
THROUGH MYLAR
P LOST MeV/c
P MAG MeV/c
20
18
16
14
12
10
8
6
4
2
0
400
600
800
1000
1200
1400
1600

Figure 24

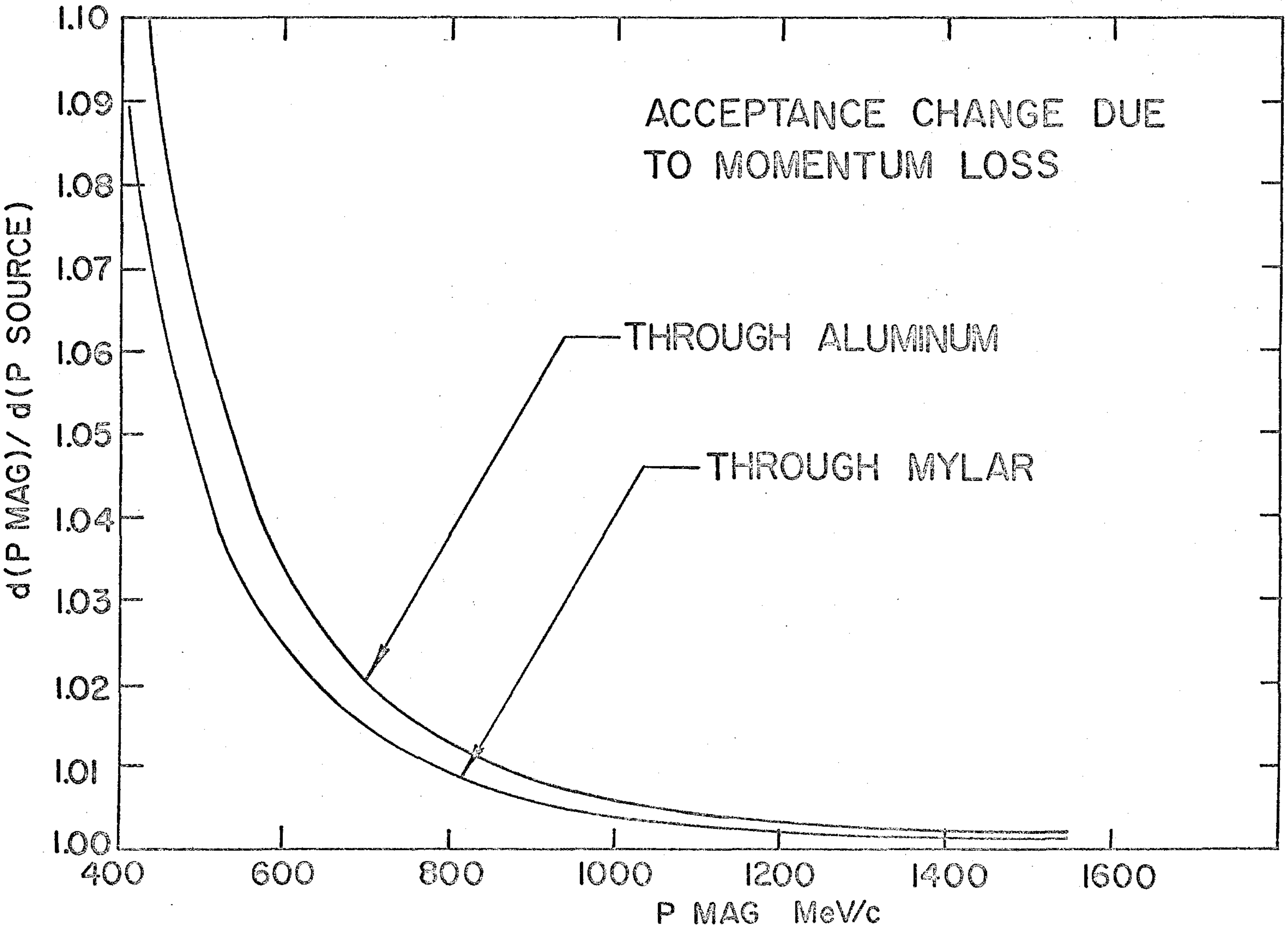
ACCEPTANCE CHANGE DUE
TO MOMENTUM LOSS
THROUGH ALUMINUM
THROUGH MYLAR
d(P MAG)/ d(P SOURCE)
1.10
1.09
1.08
1.07
1.06
1.05
1.04
1.03
1.02
1.01
1.00
400
600
800
1000
1200
1400
1600
P MAG MeV/c

The effect of energy loss on the shapes of the resolutions functions was ignored. The change in P_{LOST} as a function of momentum would make the resolution narrower. But the variation of P_{LOST} with position in the hydrogen target would make it wider. The two effects became a few per cent of the total width at the lowest momentum, but partially cancelled since they were of opposite sign.

Multiple scattering of the protons as they passed through the spectrometer, particularly scattering in A1 and A2, widened the momentum resolution. This effect, although not shown in Figures 21 and 22, was included in the data analysis.

In Figure 1, the downstream snout of the hydrogen target is shown to be asymmetric about the beam direction. On the east side of the beam the vacuum flange prevents measurements at angles near 20 degrees. On the west side, it prevents measurements at very small angles. Using both sides of the beam it was possible to measure at all angles with the HEMA configuration. Due to space limitations, the outrigger could not get to the west side of the beam. To get angles near 20 degrees with the outrigger, it was necessary to turn the target shield around, putting the large "horn" upstream. Points taken both ways showed agreement in cross sections.

B. Counters

The positions of the counters for the two spectrometer configurations are shown in Figures 2 and 3. The counter sizes are listed in Table 9.

Table 9. Spectrometer Counters

	Material	Dimensions (Height) (Width) (Thickness)
FANS	scintillator	irregular, 1/2 inch thick
A1	scintillator	(12", 9", 6") x 2.75" x .25"
A2	scintillator	13.5" x 5" x .25"
FC	Freon 12	~ 4-1/2 ft. active length
S1	scintillator	6.5" x 11" x .25"
LC	Lucite	5.75" x 11" x 1.5"
S2 A, B, C, D	scintillator	1.18" x 11" x .25"
S3	scintillator	6.5" x 11" x .375"

Two fan shaped counters lined the pole tips in the 4 inch gap of the magnet. These counters vetoed protons which scattered from the pole tips, typically 6% of the protons accepted by the rest of the system. The angular aperture was defined by the counter, A1, which had interchangeable 1/4 inch thick scintillators. The scintillator size, which was 12 inches high by 2-3/4 inches wide when the magnet was at wide angles, was reduced to 9 inches high at 8° and to 6 inches high at 4° in order to maintain good angular resolution. Another 1/4 inch scintillator, A2, improved the proton definition, but did not restrict the aperture. A five foot long threshold Cerenkov counter, FC, filled with one atmosphere of Freon gas discriminated against high energy electrons. Following the Freon counter was a four counter telescope. The first of these, S1, was a 1/4 inch scintillation counter used for fast coincidences with the FAN, A1, and A2. The second, LC, was a 1-1/2 inch thick Lucite threshold Cerenkov counter used to veto high energy pions and electrons. The third counter, S2, was a four counter hodoscope used to define the four momentum channels of the spectrometer. The center of this counter was placed at the focus of the spectrometer. The last counter, S3, was another 1/4 inch scintillator with a 1/4 inch thick sheet of lead placed in front of it to stop low energy electrons. The lead was necessary only at small angles and was removed at the wide angle low energy points where the proton had lower momentum and was more readily absorbed by the lead.

APPENDIX III. GAMMA COUNTERS

A. Design

In the four counter configuration, the gamma counters, γA, γB, γC, and γD, were placed side by side, each facing the hydrogen target as shown in Figure 4. Each 1/4 inch scintillation counter was preceded by a 1/2 inch lead converter. The aperture of each counter was determined by the size of the front surface of its converter. These surfaces were 14.60 inches high, 5.24 inches wide, and 21.7 ± .05 inches from the center of the hydrogen target. So that no gammas entering the front surface of a converter would be lost out the edge, the edges of each of the converters were tapered, making the back larger than the front, and each of the scintillators was made 1/16 inch larger than its converter on all sides, making them 15.00 inches by 5.50 inches. The counters were mounted, two counters to a cart, on two carts riding on a circular track around the hydrogen target. Normally, the four counters were kept together and the array was centered on the central direction of the π^o before decay. Because of the vacuum snouts surrounding the beam, it was necessary to place the array off center for the most forward and backward points. For the two most backward π^o angles, one cart was placed on each side of the beam. To reduce singles rates in the counters, they were surrounded by 1 inch of polyethylene as shown in Figure 4.

To gain a qualitative understanding of how the gamma rays distributed over the four counters, consider a surface which, in the center of mass of the π^o, was a plane normal to the direction of travel. In the laboratory, this plane was a cone of half-angle

$\cos^{-1}(\beta_{\pi^0})$. One gamma went inside the cone and its mate went outside the cone. In most of the cases for this experiment, the two center counters subtended the entire cone, except for the crack between the counters. In these cases, the efficiency of the two center counters for seeing at least one gamma ray depended largely on the detection efficiency of the lead-scintillator combination (~ 80%, depending on the gamma ray energy). In these cases, the side counters γA and γD contributed little to the efficiency (~ 10%) but they tended to count pi pairs as readily as the center counters.

The veto configuration differed from the four counter configuration only in that the lead convertors were removed from γA and γD, γA was placed in front of γB, and γD was placed in front of γC, as shown in Figure 5. In this configuration γA and γD were 21.2 inches from the target center. No change in the electronics was necessary in going from one configuration to the other. Since the rates were recorded for all possible combinations of gamma counters firing in coincidence with the proton, the computer could select veto events as easily as coincidence events. There was a significant practical advantage to requiring a fast coincidence instead of a fast veto. Requiring a veto with the fast electronics would have necessitated a longer resolution time and would have increased the accidental veto rate.

The calculation of the gamma counter efficiency involved knowing the probability that a gamma ray which was aimed toward a gamma counter would convert to charged particles, which then would count in the scintillator.

B. Conversion efficiency measurement

The laboratory energies of the decay photons depended both on the pion energy, which in turn depended on the kinematic point, and on the angle between the pion and the gamma ray. The gamma ray energies ranged from 35 to 950 MeV although no final cross sections depended on energies below 100 MeV. Gamma rays in this energy range convert primarily by pair production. The probability that a gamma ray converts in T radiation lengths of lead is

$$1 - e^{-\sigma_{pp}(k)T} ,$$

where $\sigma_{pp}(k)$ = pair production probability per radiation length for gamma rays of energy k. $\sigma_{pp}(k) \cong 7/9$ for large k. If the lead is thick, there is a higher conversion probability, but if it is too thick, the electrons shower and may produce little or no pulse height in the counter. For the signal bias used in this experiment (.25 × minimum uinizing pulse height), the optimum thickness for the 200 MeV gamma rays is .6 inches of lead. One-half inch was chosen as the thickness for the actual convertors.

Instead of performing a complicated calculation to determine the conversion efficiency, including the effects of showering, the efficiency was measured directly using the Caltech Synchrotron's tagged gamma beam. The design of the beam is described in detail in a report by C. Prescott (24). Briefly, the beam works as follows. Positrons produced by showering in the south beam catcher ion chamber are momentum analyzed and focused with an alternating gradient magnet to form a mono-energetic positron beam. This beam strikes a thin radiator (.025 r.l. for these measurements) and recoil positrons from bremsstrahlung in this radiator are momentum analyzed with a wedge magnet. The difference in energy between the incoming and recoil positrons determines the energy lost by bremsstrahlung. Usually there is only one gamma ray, making the beam highly monochromatic. But, in an appreciable number of cases, there are two gamma rays sharing the energy between them. An approximate calculation of the resulting spectrum has been described by the present author in a separate report (25).

The beam was carefully aligned and the existing counters were augmented by four additional counters to discriminate against events where the positron scattered in the second magnet or where there was pair production in the radiator or in the air in the magnet.

To test the efficiency of the gamma trigger, a shower counter was placed in the gamma beam and its output was pulse height analyzed whenever a trigger occurred. This counter was a lead-scintillator counter of the type described by Heusch and Prescott (26). It consisted of 10 sheets of lead, .5 r.l. thick, separated by 1/4 inch sheets of scintillator. The light from all the scintillators was gathered onto one 5 inch photomultiplier tube. To the extent that the output pulse height was proportional to gamma energy, the output from two gamma events was the same as from one gamma event, making this an ideal instrument for testing the trigger. The tagged gamma spectra showed that 2% of the events gave little or no pulse in the shower counter. It is not known whether the 2% of small pulse heights was due to a contamination in the trigger or a 2% probability that the photons converted in the lead by a process other than pair production, such as neutron production.

Only one of the gamma counters for this experiment, γB, was tested in detail in the tagged gamma beam. It was assumed representative of the four counters. Pulse height distributions from the counter were taken with gamma beam energy set at 50, 100, 150, 200, 300, 400, 500, and 700 MeV.

In order to evaluate the effect of the two gamma events on the distributions, it was necessary to make an assumption about the pulse height distributions in γB for gamma ray energies below 50 MeV. The distribution is expected to shift toward small pulse heights in some complicated way, resulting in a decrease in the efficiency for a given bias. As an approximation, it was assumed that the efficiency goes linearly to zero below 50 MeV for any given bias. In terms of the distribution, this implies that the fraction of pulses in any given channel goes linearly to zero, except in the zero pulse height channel. Clearly this is not correct; it is an approximation. An IBM 7094 program to unfold the effect of the two gamma events from the pulse height distributions was written by Paul Scheffler. The correction to the measured efficiency computed from the unfolded spectra was less than 1% at most energies and less than 2% at all energies. This correction was not included in the final data analysis because of the size and uncertainty of the correction.

The measured conversion efficiency for a bias of .25 times minimum ionizing pulse height is plotted in Figure 25. The solid curve through the points was drawn freehand and was used to obtain conversion efficiency values for the analysis of the data.

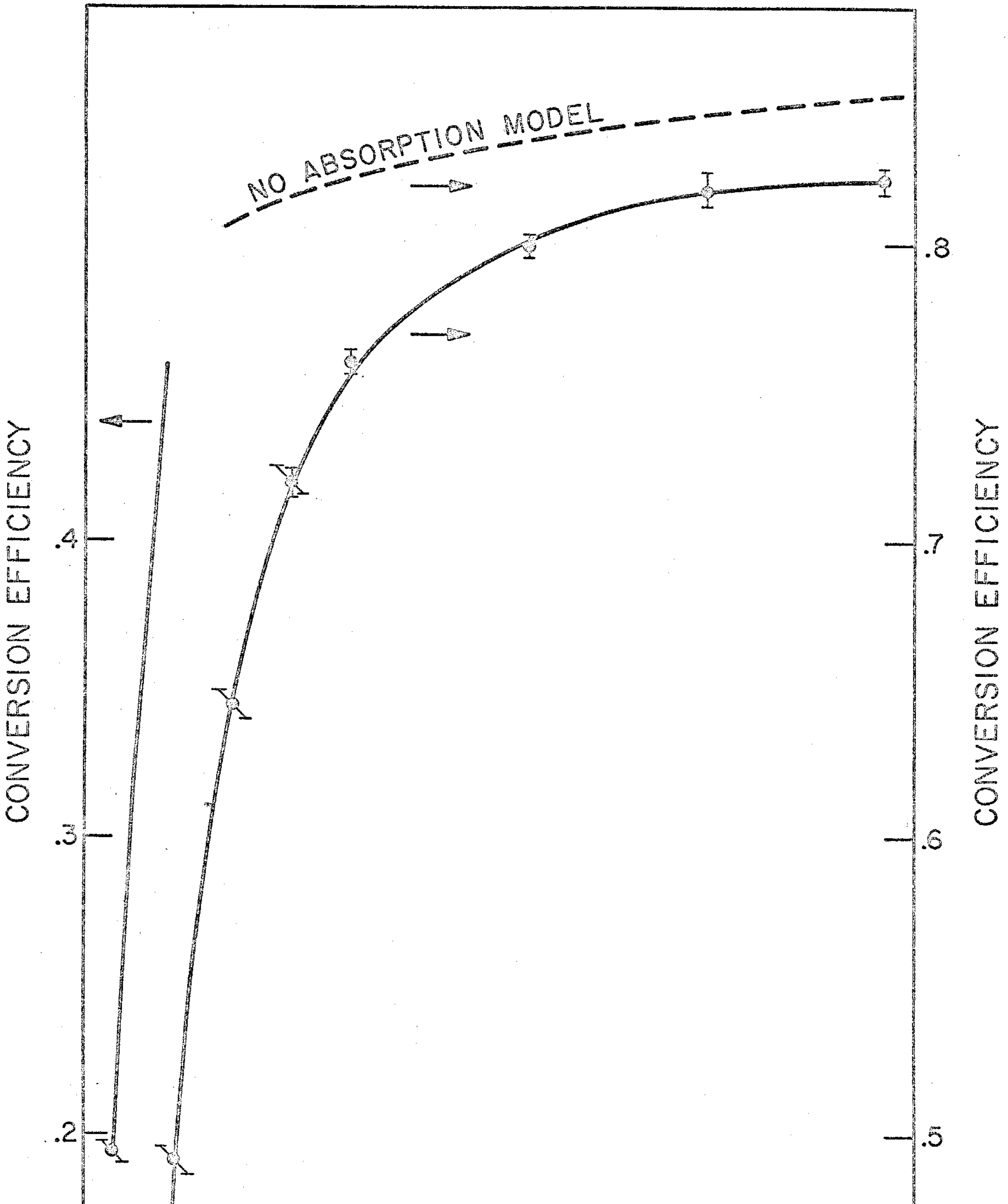
NO ABSORPTION MODEL
CONVERSION EFFICIENCY
.4
.3
.2
CONVERSION EFFICIENCY
.8
.7
.6
.5
100
200
300
400
500
600
700
GAMMA RAY ENERGY (MeV)

Figure 25

It is interesting to compare the measured counter efficiency with the efficiency for converting the original gamma. That efficiency has been evaluated using the pair production absorption coefficient given by Rossi and Greisen (27) and has been plotted as a dashed curve in Figure 25. The measured efficiency is 2.5% below the formula at high energy and drops off more quickly at low energy due to showering.

In all the tagged gamma beam measurements, the gamma rays were incident normally on the convertor. In the experiment, however, gamma rays that struck the top or bottom of the convertor entered at an angle of 19 degrees. They traveled through more lead than gamma rays hitting the center. The efficiency for a gamma entering at angle θ depends on the derivative of the efficiency with respect to thickness (in inches) as follows:

$$\epsilon(k) + \frac{.5}{\cos\theta} \frac{d\epsilon(k)}{dt} .$$

Of course the particles from the shower enter the scintillator at an angle, but that doesn't matter. Since low energy ones stop in the scintillator, their light output is independent of incident angle. Since the high energy ones were well above the bias, it did not matter that they put out more light. The derivative of the efficiency was found by measuring the change in efficiency caused by an extra piece of lead 1/16 inch thick in front of the regular convertor. The correction to the efficiency of the whole counter from this effect was found to be negligible compared to the other uncertainties.

C. Detection efficiency calculation

The measured conversion efficiency was used as input to a Monte Carlo computer program which computed the probability that a proton in the spectrometer would be accompanied by a count in each of the combinations of gamma counters.

The program chose randomly a reaction location in the target, a position for the proton trajectory to cross A1, a horizontal multiple scattering angle and a height (measured perpendicular to the central ray) for the proton to cross S2. Since vertical multiple scattering was ignored, this completely determined the proton orbit and momentum.

The horizontal position at S3 was calculated to determine whether the proton would count in S3. It was in this way that the S3 efficiency came as a side result of the gamma efficiency calculation.

The reaction kinematics determined the pion direction and energy. Choosing the pion center of mass decay angles randomly then determined the gamma ray energies and directions.

Consider the four counter arrangement. It was a simple matter to determine whether each gamma ray hit a counter and, if so, to decide, using the measured efficiency and another random variable, whether the counter counted. If both gamma rays hit the same counter, the counter was considered to count if and only if one of the gamma rays made a big enough pulse by itself to count. This method ignored the cases where two pulses, each below the bias, added to give a count above the bias. It can be shown that the number of cases omitted was negligible.

In calculating the detection efficiency, account had to be taken of gamma rays which converted in the hydrogen target or in the polyethylene absorbers. When the conversion efficiency was measured, materials were inserted to simulate the hydrogen target and absorbers. That took care of the conversion of gamma rays which were headed toward the lead. We can consider the possibility of detecting gamma rays that were not headed toward the lead. For instance, a gamma ray could have converted in the target or absorber and counted in the 1/16 inch of scintillator that extends beyond the lead. The border area is only 3% of the counter area. Since the conversion in this region is about 1/10 as much as where there is lead, the counts in the border region were only .3% of the total counts and were ignored.

Extra counts could have come from gamma rays which were not aimed at the counter, but which converted in the hydrogen target, and because of the finite pair production angles, sent an electron or positron toward the counter. Because the particles were usually on opposite sides of the gamma ray, we could not have lost many counts from this mechanism. We can estimate the per cent gained by considering the case where the electron and positron has equal energy. The angle between the gamma and either particle was of order m_e/E_γ. This means, letting L be the distance from the hydrogen target to the counter, the gamma could have been aimed of order $.5L/E_\gamma$ inches from the counter and have had a 50% chance of counting. At the lowest gamma ray energy, this was 0.2 inches, which added an area which was 10% of the counter area. Since the conversion efficiency was 1/50 as much in the target as in the lead, this was a 0.2% effect and was negligible.

Extra counts could have come from gammas which were not aimed at the counter and which converted in the hydrogen target, but whose electrons hit the counter because of multiple scattering. It was more probable that at least one of the pair produced particles scattered toward the counter than that both scattered away. Considering again the equal energy case, the rms multiple scattering angle was $30\sqrt{t}/E_\gamma$ where t was the scattering thickness. The average scattering thickness was one half the thickness of hydrogen and aluminum between the target center and the counter. That gave t = .01. Thus, the gamma aim could have missed by $3L/E_\gamma$. For the lowest energy gammas this was 1.4 inches, which added an area 80% of the counter area. Since the conversion in the counter was 1/50 the conversion in the lead, this was a 1.5% effect. The effect was only this big for the backward angle two gamma rates which had large statistical errors. For the one gamma rates in the two most efficient counters, the effect was .5% and was ignored.

At $\theta_p^{lab} = 4^o$, γC could catch electrons from photons converting in the upstream snout of the hydrogen target. A careful investigation of this effect showed it to be negligible.

For the veto configuration, the efficiency of the back counters was computed in the same way as described above since the 1/4 inch additional scintillator had a negligible effect on the conversion efficiency. For the front counters, the only conversion materials were the target, the 1 inch of polyethylene, and the counters themselves. The conversion efficiency was computed from the pair production absorption coefficient and was typically about 5%. The calculation was valid in this case because there was very little material in which the gamma rays could shower. It was assumed that any event which counted in a veto counter and was headed toward the counter behind it also counted in the counter behind. This assumption is good at high energies, but not at low energies. A precise calculation of the front and back counter correlation at low energies would be complicated. This correlation was not measured only because we had not decided to use the veto configuration at the time the measurements were being made in the tagged beam. Fortunately, most of the veto measurements were made at points where the energy was high.

D. Experimental check

The best experimental check on the gamma efficiency determination is the comparison between signatures discussed in Part III.

The agreement between the $P \cdot \gamma$ signature using the four counter configuration and the P signature is very good. As remarked in Part III, the $P \cdot \gamma$ signature using the veto configuration seems to be about 10% low near 90^o at the second resonance. It is possible that this error is due to an error in the veto configuration efficiency determination.

The agreement between the $P \cdot \gamma$ signature using the four counter configuration and the $P \cdot 2\gamma$ signature is good at high energy where the $P \cdot 2\gamma$ errors are small, but not at low energy where the $P \cdot 2\gamma$ errors are large. The discrepancy may be due to small effects which caused errors in the $P \cdot 2\gamma$ efficiency without bothering the $P \cdot \gamma$ efficiency, such as an error in the efficiency for very low energy gamma rays.

APPENDIX IV. ELECTRONICS

A. Logic

In Figure 26 is shown a simplified block diagram of the electronics used to obtain particles rates from coincidences between the counter signals. The electronic setup for the spectrometer was very nearly that used by S. Ecklund and described in Reference 14. The general features were as follows. The three counters with the highest backgrounds, FAN, A1, and A2 were each placed in fast coincidence ($\tau \sim 6$ ns.) with S1. Then these three signals, the logical sum of the signals from the four momentum counters, S2A, S2B, S2C, S2D and all the other spectrometer signals went into the 50 ns. and .5 μs logic network which defined various particles going through the spectrometer. In addition, each of the S2 signals was put in 50 ns coincidence with (A1 · S1) to provide signals which could be gated by the output of the slow logic to specify the number of particles in each momentum channel.

The FAN counters had very high background rates when the spectrometer was placed at 4^{o} due to electrons produced in the hydrogen target and in the coils and iron of the magnet, which at small angles are struck by the main beam. Instead of turning the FAN counters off under these conditions, we used base boost circuits as done by Hauser (28). But, instead of monitoring the accidentals by the delayed coincidence technique, we monitored them using the technique that was used for the gamma counters, which will be described presently.

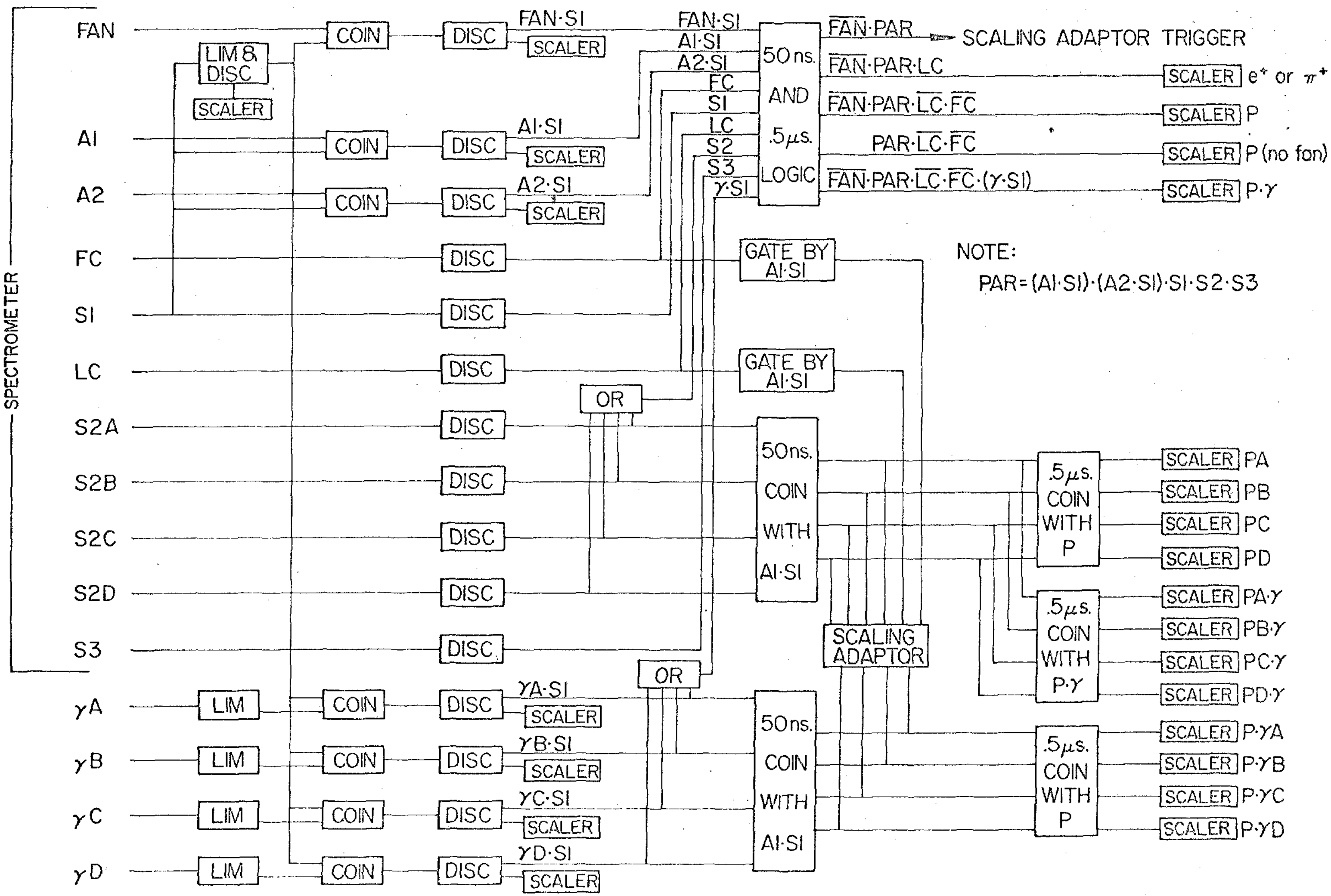

Figure 26. Electronics Block Diagram

Because of the high momentum of the protons from π^0 production, there was less than 10% background from pions at most angles. For this reason, the Lucite Cerenkov counter, which was used for vetoing pions, did not have to have a high efficiency. The bias on this counter was turned up to the point where the pion efficiency dropped to 97% in order to insure that small pulses from high energy protons would not be counted. It was found that when the gamma counters were used to help define a clean proton beam, less than 2% of the protons counted in the Lucite counter, even at the highest momentum.

Because of the high momentum, there were few electrons. The Freon Cerenkov counter, which was intended to veto electrons, had a significant accidentals rate when run with the bias too low. The accidentals were partly from phototube noise and partly from particle background. By raising the bias to the point where the efficiency was 98%, the accidentals were reduced to a negligible level.

Since we were interested in protons rather than pions, our slow logic differed from Ecklund's. If we use the shorthand

$$\mathrm{PAR} \equiv (\mathrm{A1} \cdot \mathrm{S1}) \cdot (\mathrm{A2} \cdot \mathrm{S1}) \cdot \mathrm{S1} \cdot \mathrm{S2} \cdot \mathrm{S3},$$

the rates that were defined for scaling were

(a) proton, $\mathrm{P} \equiv \overline{\mathrm{FAN}} \cdot \mathrm{PAR} \cdot \overline{\mathrm{LC}} \cdot \overline{\mathrm{FC}}$

(b) proton with at least one of the four gamma counters

$$\mathrm{P} \cdot \gamma \equiv \overline{\mathrm{FAN}} \cdot \mathrm{PAR} \cdot \overline{\mathrm{LC}} \cdot \overline{\mathrm{FC}} \cdot (\gamma \cdot \mathrm{S1})$$

(c) proton, with or without the FAN,

$$P_{\substack{no\\fan}} = PAR \cdot \overline{LC} \cdot \overline{FC}$$

(d) electron or pion,

$$(e^{+} \text{ or } \pi^{+}) \equiv \overline{FAN} \cdot PAR \cdot LC$$

Rate (c) was used to monitor the FAN veto rate. Rate (b) required the signal ($\gamma \cdot S1$) from the gamma counters, yet to be discussed. The P and $P \cdot \gamma$ signals were used to gate the momentum channel signals to provide PA, PB, PC, PD, and $PA \cdot \gamma$, $PB \cdot \gamma$, $PC \cdot \gamma$, $PD \cdot \gamma$. Note that the $P \cdot \gamma$ rates described here simply required a count in at least one gamma counter and are not the rates used to compute the $P \cdot \gamma$ signature cross sections.

The gamma counter electronics was added for this experiment and was a combination of fast modules designed by A. V. Tollestrup (29) and slow modules designed by C. Peck (30).

Since the γ counters directly viewed the hydrogen target and the hole in the scraping wall, the background rates in these counters were high. By careful shielding, the rate of pulses bigger than .25 times minimum ionizing was kept less than 1 Mhz. To keep the number of accidental coincidences between protons and gamma counter signals low, the four gamma signals were placed in fast coincidence with S1 to yield four signals $\gamma A \cdot S1$, $\gamma B \cdot S1$, $\gamma C \cdot S1$, and $\gamma D \cdot S1$ which had much lower background rates. The logical sum of these signals formed the $\gamma \cdot S1$ used in the 50 ns. logic. The resolution time of the fast coincidence circuits was about 8 ns. The resolution time could not be reduced without going to more elaborate electronics because the 10 ns. risetime of the phototube pulses and the wide range of pulse heights from the gammas caused a time jitter in the outputs from the limiters. The net effect was to put the gammas in coincidence with the protons with an effective resolution time equal to that of the fast coincidence circuits. Since in some cases this still left significant accidentals, it was necessary to monitor and correct for the accidentals. The method used for this is described in Appendix IV B.

As was done with the momentum channels, each of the gamma channels was placed in 50 ns. coincidence with (A1 · S1) and then gated by P to provide $P \cdot \gamma A$, $P \cdot \gamma B$, $P \cdot \gamma C$, $P \cdot \gamma D$. These rates were useful for comparing the gamma counters to one another.

It will be noticed that rates for protons in each momentum channel were scaled for only two reaction signatures, (a) proton only and (b) proton plus at least one of the four gamma counters. Scaling all the possible one and two gamma signatures on conventional scalers would have required many more scalers and more logic. Instead, use was made of a scaling adaptor designed by H. A. Thiessen (16). This adaptor, in conjunction with a 1024 channel Nuclear Data Analyzer, can be used to scale all possible logic combinations of ten input signals. In this application it was triggered on the signal $\overline{FAN} \cdot PAR$ and the ten inputs were

(a) the four momentum channels,

(b) the four gamma channels,

(c) FC,

(d) LC.

Each signal was first put in 50 ns. coincidence with $A1 \cdot S1$ to reduce the signal rates, since the adaptor has a .3 μs resolution time. Thus the scaling adaptor and analyzer recorded the rates for protons, pions and electrons, in each momentum channel for all gamma combinations. At the end of each run the counts in the analyzer were punched onto paper tape for analysis by computer.

B. Accidentals monitoring

Because of the high background rates in the gamma counters, it was necessary to correct the rates for accidental coincidences. The rather simple method used for doing this was based on the following observation. Since S1 did not view the particles passing through the gamma counters, most of the coincidences between S1 and the gamma counters were accidentals. Of course the π^o events were real coincidences, but these were a very small fraction of the total coincidence rate. Let γ_i denote the i^{th} gamma counter. Let α be the fraction of S1 signals which had a gamma counter signal accidentally in coincidence, that is,

$$\alpha = \frac{S1 \cdot \gamma_i}{S1} .$$

Then the measured $P \cdot \gamma_i$ rate can be expressed as follows:

$$P\cdot\gamma_i = (P\cdot\gamma_i)_{real} + \alpha\,(P\cdot\bar{\gamma}_i)_{real}$$

$$= (P\cdot\gamma_i)_{real} + \alpha P - \alpha\,(P\cdot\gamma_i)_{real}$$

This can be solved for the real coincidence

$$(P\cdot\gamma_i)_{real} = \frac{P\cdot\gamma_i - \alpha P}{1-\alpha} \qquad (1)$$

The method extends easily to rates involving two or more gamma counters. This method depends on knowing the number of S1 counts large enough to trigger the coincidence circuit. For this reason, the S1 signal was put through a limiter and a discriminator to make a digital S1 signal to put into the S1 scaler and all the gamma counter fast coincidence circuits.

In practice α was rarely larger than .02. Expanding the denominator of equation (1) and keeping only first order terms gives

$$(P\cdot\gamma_i)_{real} \cong P\cdot\gamma_i\left(1 - \alpha\,\frac{P - P\cdot\gamma_i}{P\cdot\gamma_i}\right) \qquad (2)$$

Where the gamma efficiency was high the quantity multiplying α was small. But at the very backward angles, where the efficiency was small, the accidentals correction rose to about 10%.

There was also a deadtime associated with the gamma coincidence circuits, but, as will be shown, the deadtime correction did not get as large as the accidentals correction. The deadtime correction was neglected in the data analysis. The main contribution to the deadtime came from the gamma counter limiters. The deadtime of these circuits was measured by observing the limiter output with the normal clipping stub replaced by a resistor. The width of the output was about 25 ns. Comparing this with twice the resolving time of the coincidence circuit, it was concluded that the fraction of counts lost due to deadtime was about 1.5α. Considering only the deadtime correction yields:

$$P\cdot\gamma_i = (P\cdot\gamma_i)_{real} - 1.5\alpha(P\cdot\gamma_i)_{real}$$

$$(P\cdot\gamma_i)_{real} = P\cdot\gamma_i[1 + 1.5\alpha] \qquad (3)$$

Comparing (3) to (2) shows that when the gamma efficiency is 40%, the deadtime correction cancels the accidentals correction. Below this the accidentals dominate. Above this the deadtime correction dominates, but is small.

APPENDIX V. LUCITE RUNS

At the beginning of each day of running and whenever major changes were made in the setup, one or more runs were taken at the $\theta_p^{lab} = 16^o$, $E_o = 870$ MeV, point with a 3 inch Lucite cylinder in place of the hydrogen target.

Since the Lucite run and its monitor calibration run were frequently the only runs at $E_o = 870$ MeV on a given day and since the presence of the Lucite target affected M1 and M2 and might have affected BCC, the Lucite runs were not included in the regular beam monitor calibrations. The Lucite runs were calibrated in a simpler, less accurate way described in Appendix I.

Average rates were computed for several of the Lucite rates for both magnet configurations. The average rates are given in Table 10 as counts per 10^{16} MeV total energy in the beam. Also given are the ratios of OUTR to HEMA rates. The deviations of the individual runs from the averages are plotted in Figure 27. The HEMA and OUTR points are plotted with squares and diamonds, respectively. Note that the per cent scale is not the same on all the plots. The error bars indicate statistical errors only. Any run sufficiently far from the average for a given rate so as to lie off the plot was eliminated from the calculation of the average. Only for the FAN VETO rate did this involve eliminating more than three runs.

The plot of the P rate deviations shows the same systematic variations that were seen in the deviations of $(M1 + M2)/(10^{17}$ MeV) in Appendix I. (Note that the P rate is the total proton rate for the

Table 10

Average Lucite Rates

per 10^{16} MeV

Rate		HEMA	OUTR	OUTR/HEMA
P		99810.	63770.	.64
e^+ or π^+		1055.	222.	.21
FAN VETO		3599.	1523.	.42
P A		20570.	13890.	.68
P B		24090.	15470.	.64
P C		26620.	16760.	.63
P D		28470.	17680.	.62
P· γA	FOUR COUNTER CONF.	2912.	1874.	.64
P· γB		5144.	3398.	.66
P· γC		5282.	3488.	.66
P· γD		3588.	2327.	.65
P· γA	VETO CONF.	3368.	2462.	.73
P· γB		5076.	3118.	.61
P· γC		5267.	3025.	.58
P· γD		3803.	2650.	.70

Figure 27

Deviations from the average for Lucite rates.

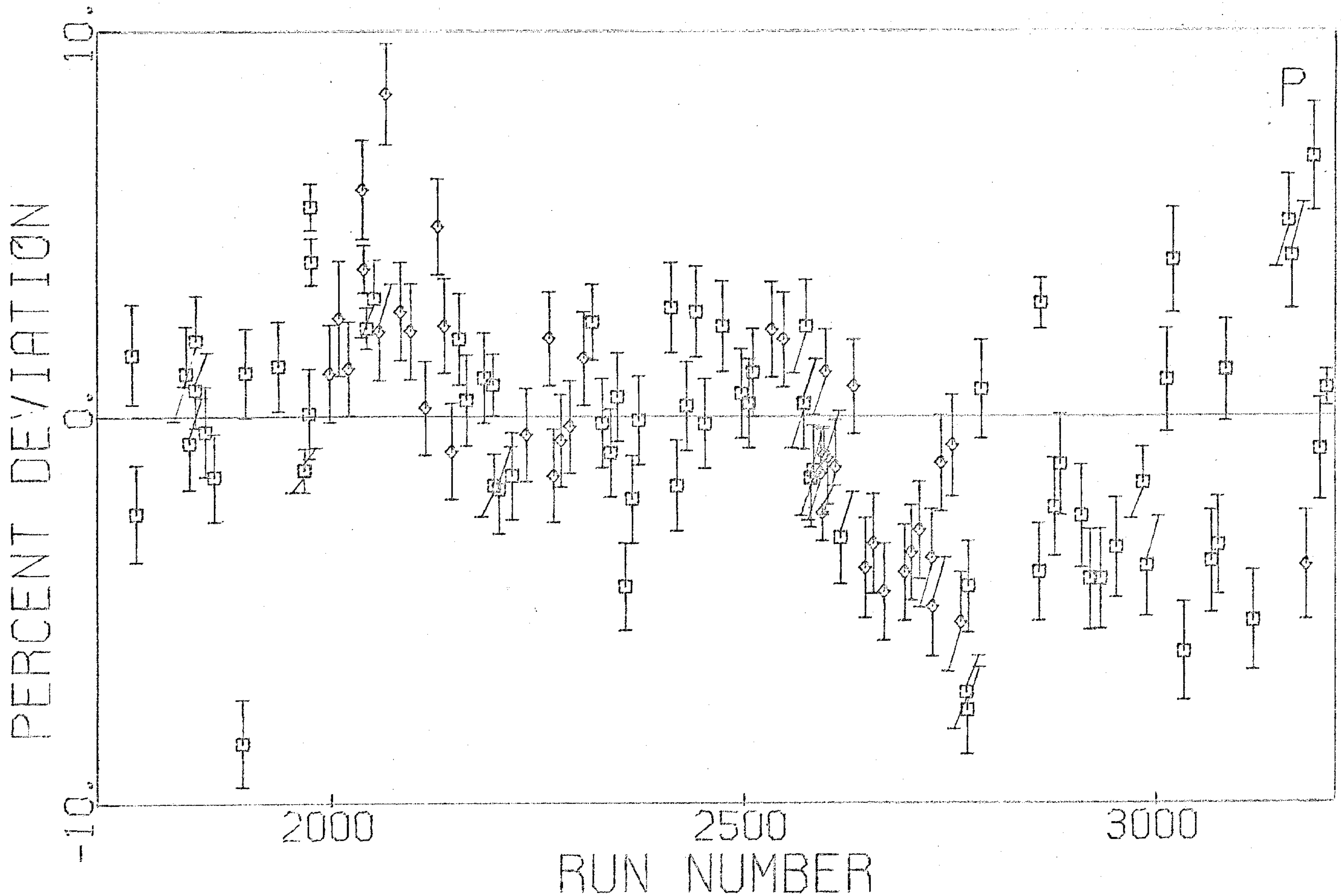

Figure 27.1

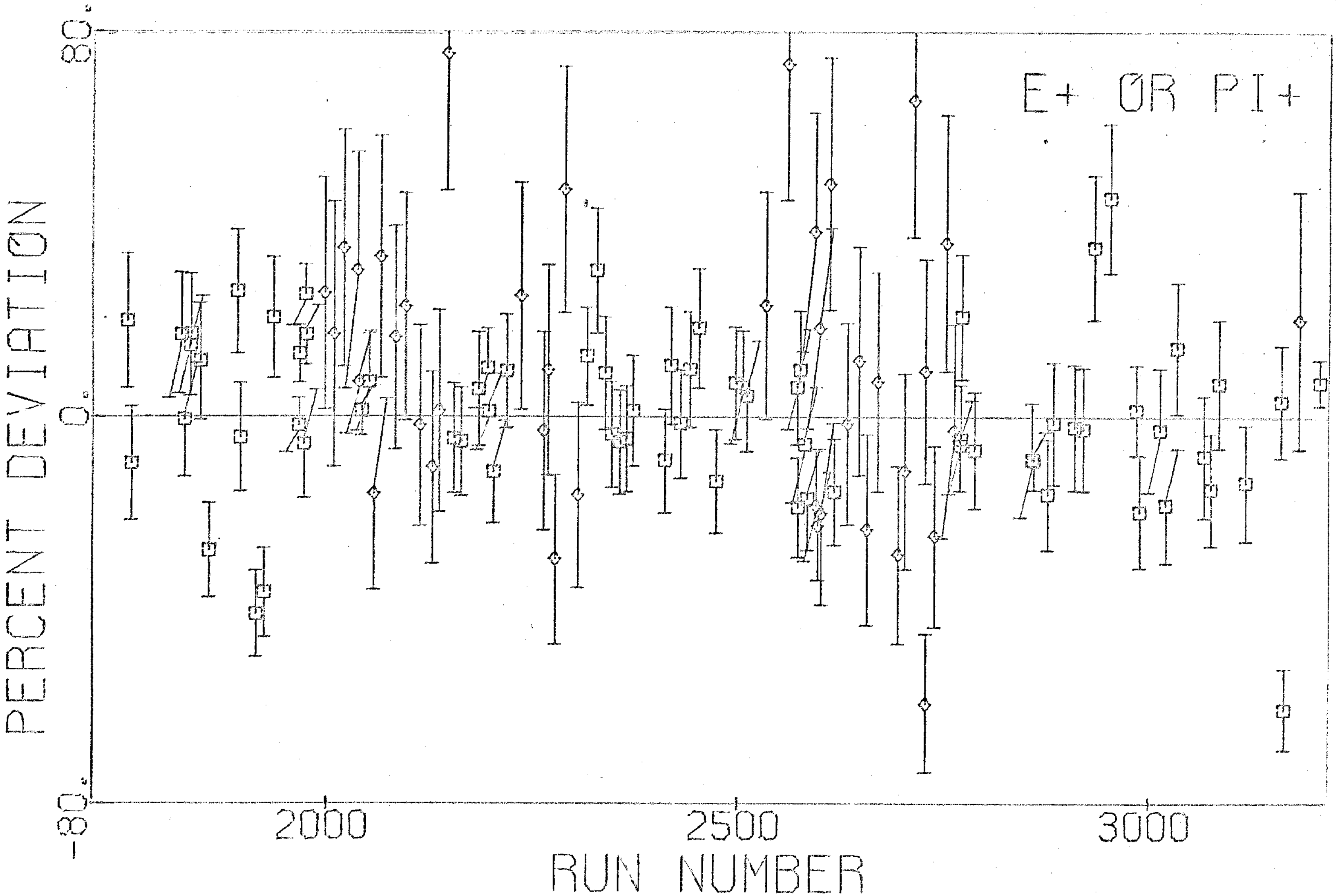

Figure 27.2

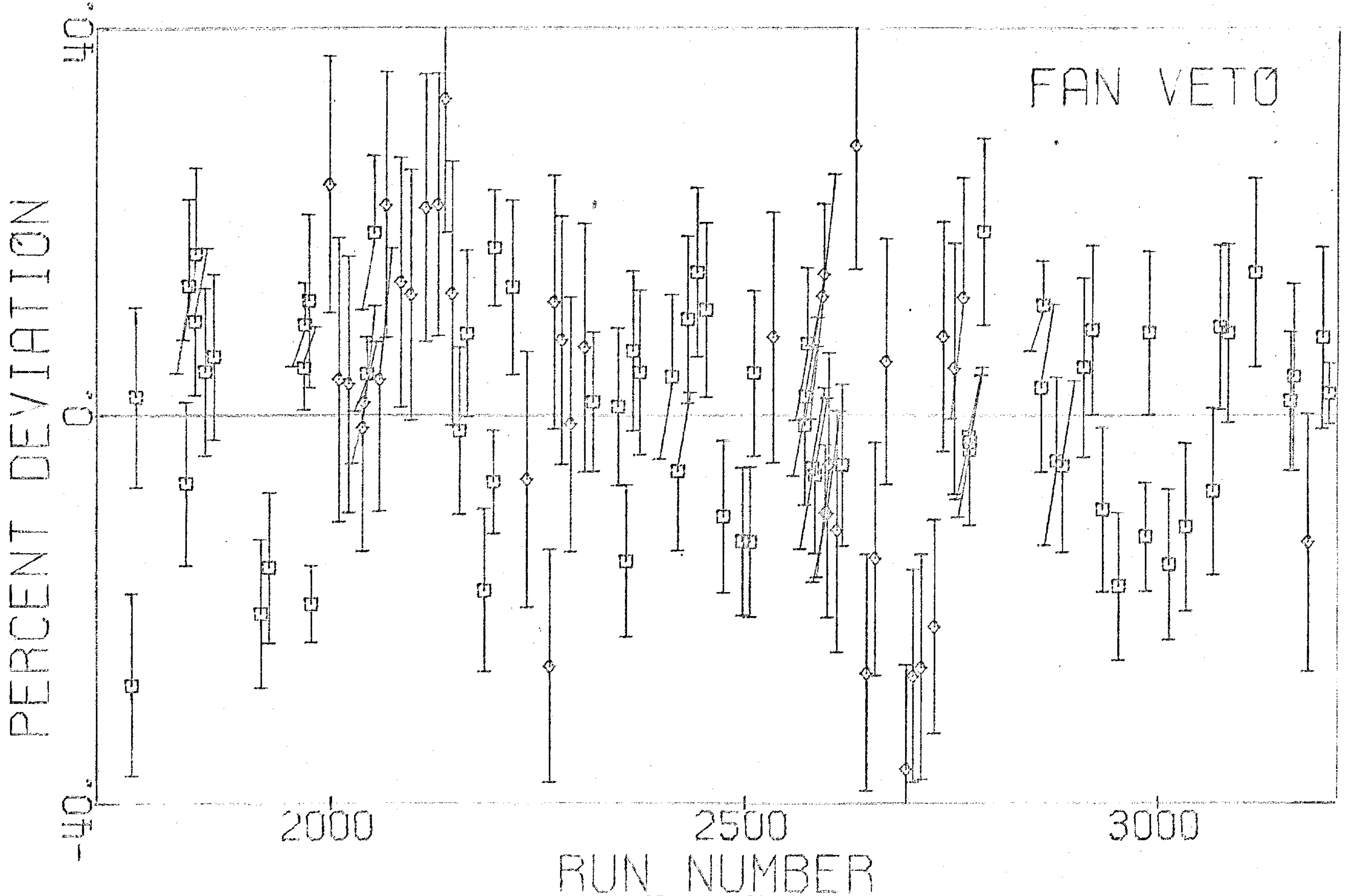

Figure 27.3

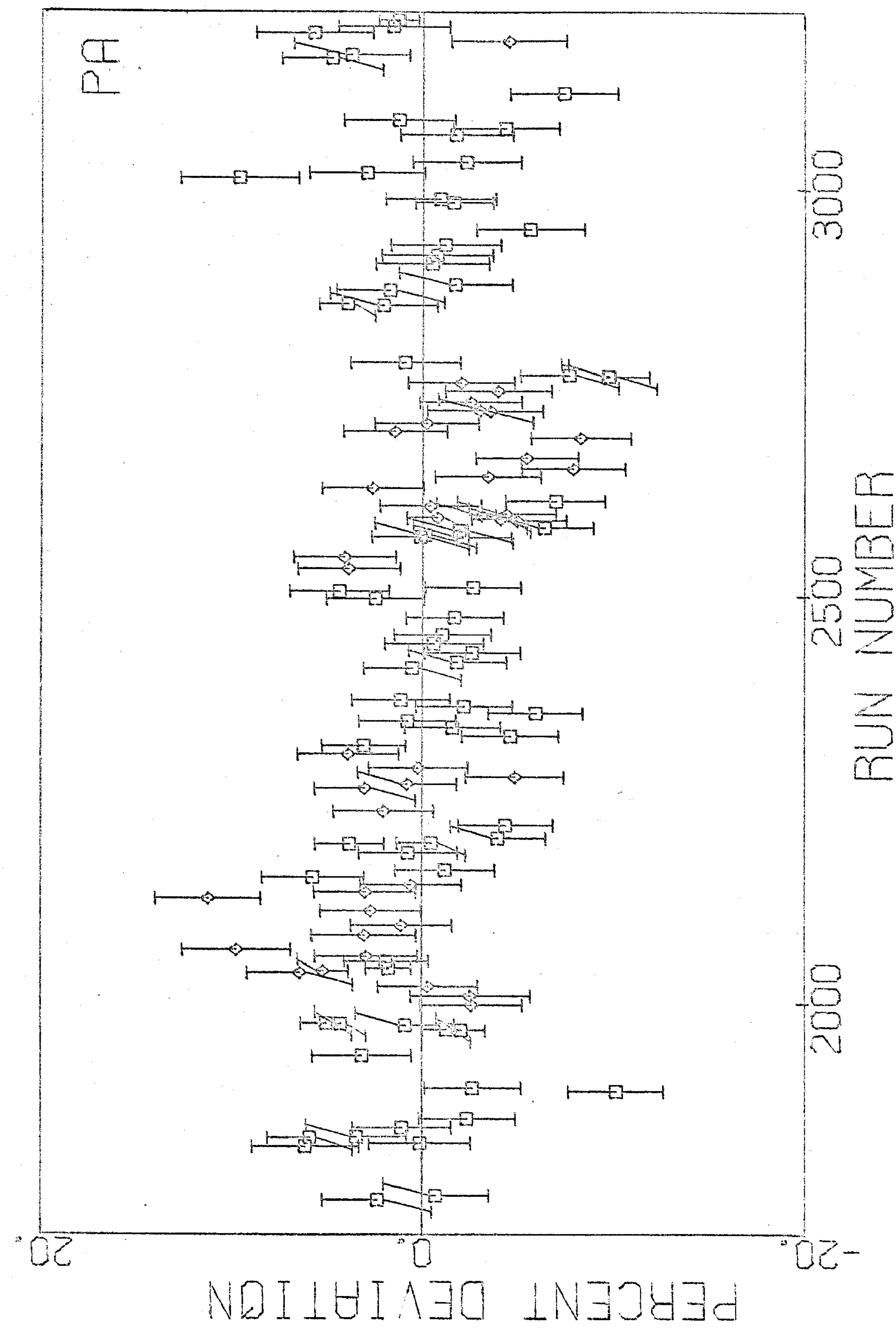

Figure 27.4

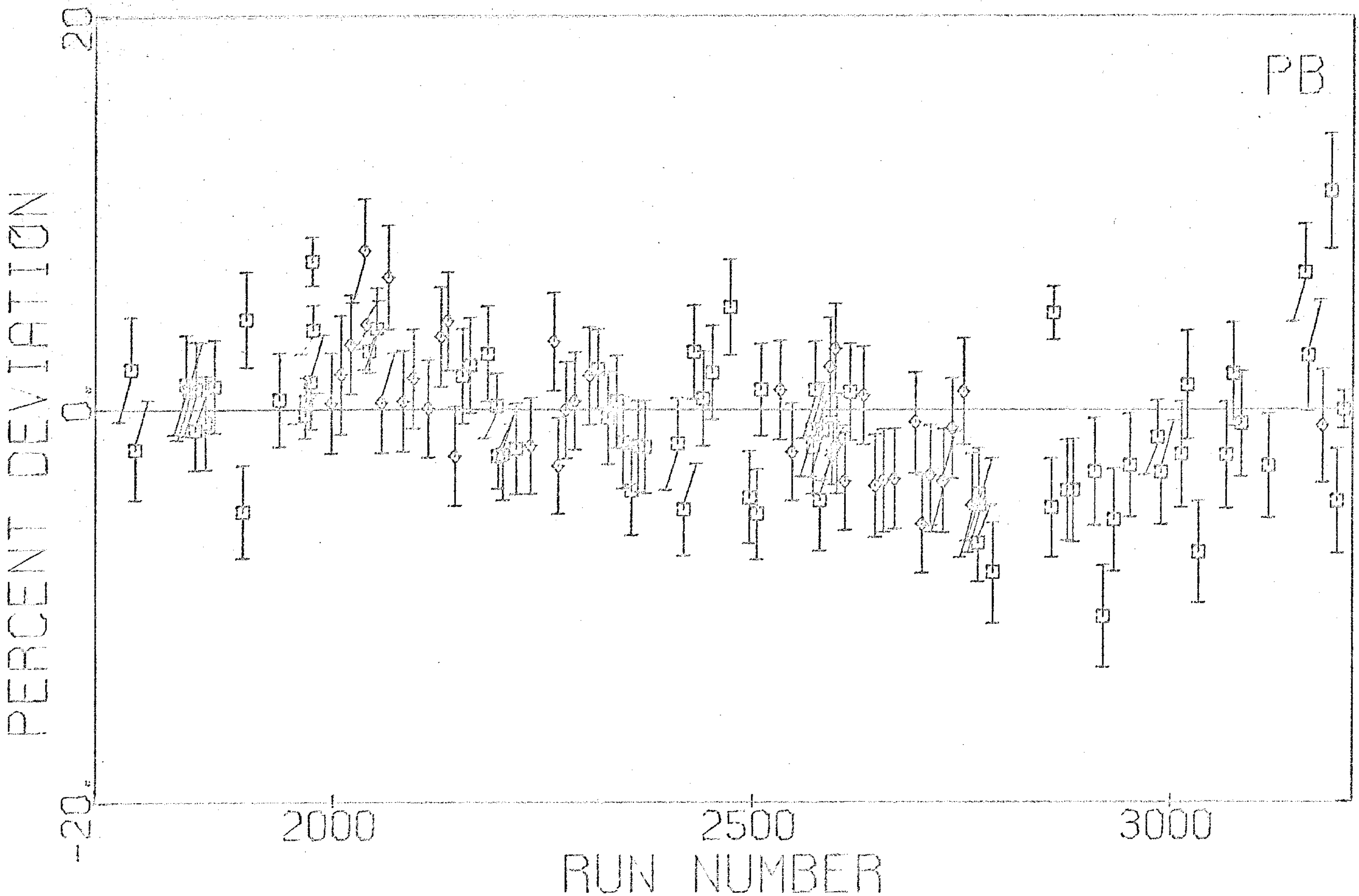

Figure 27.5

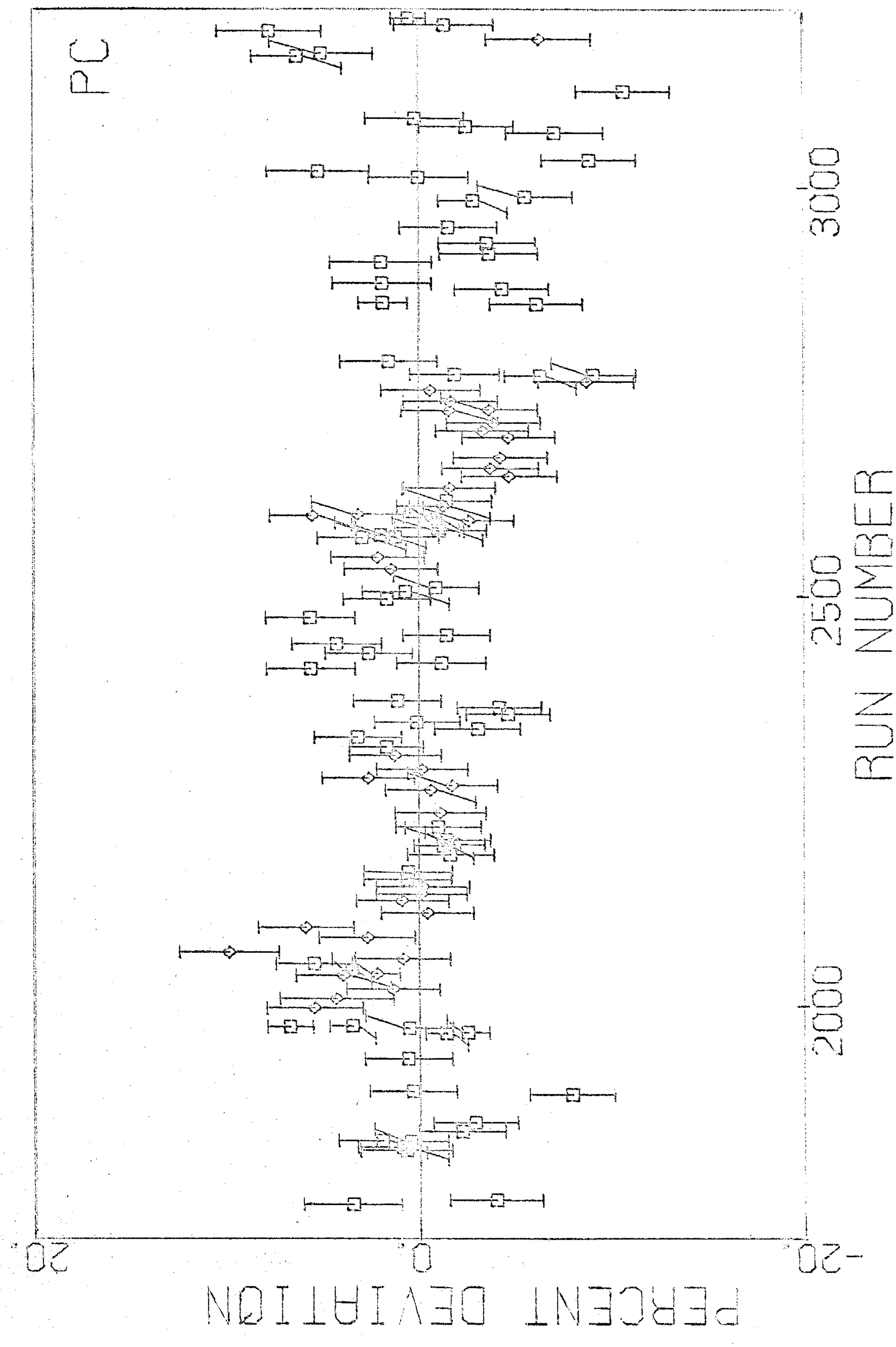

Figure 27.6

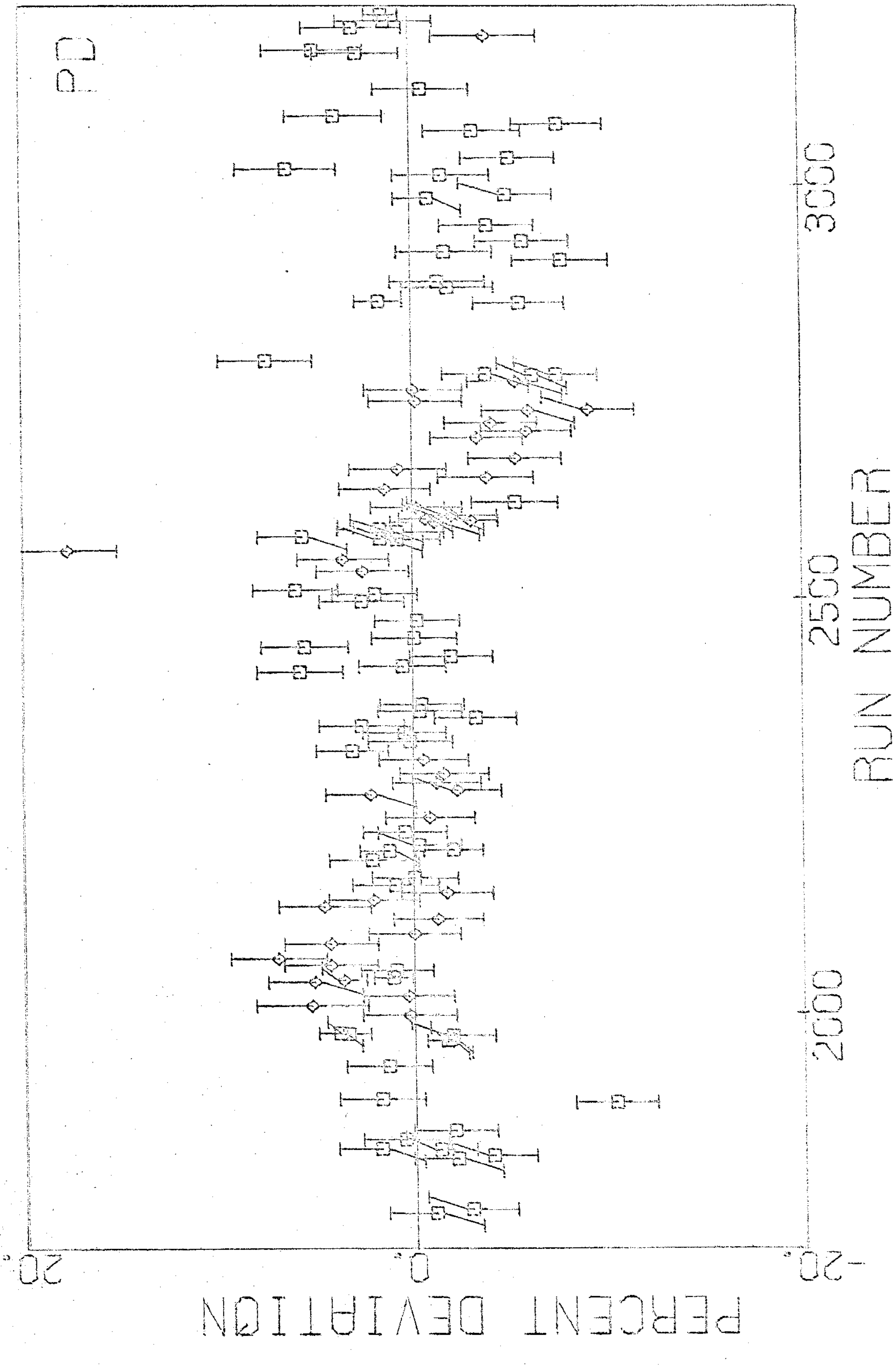

Figure 27.7

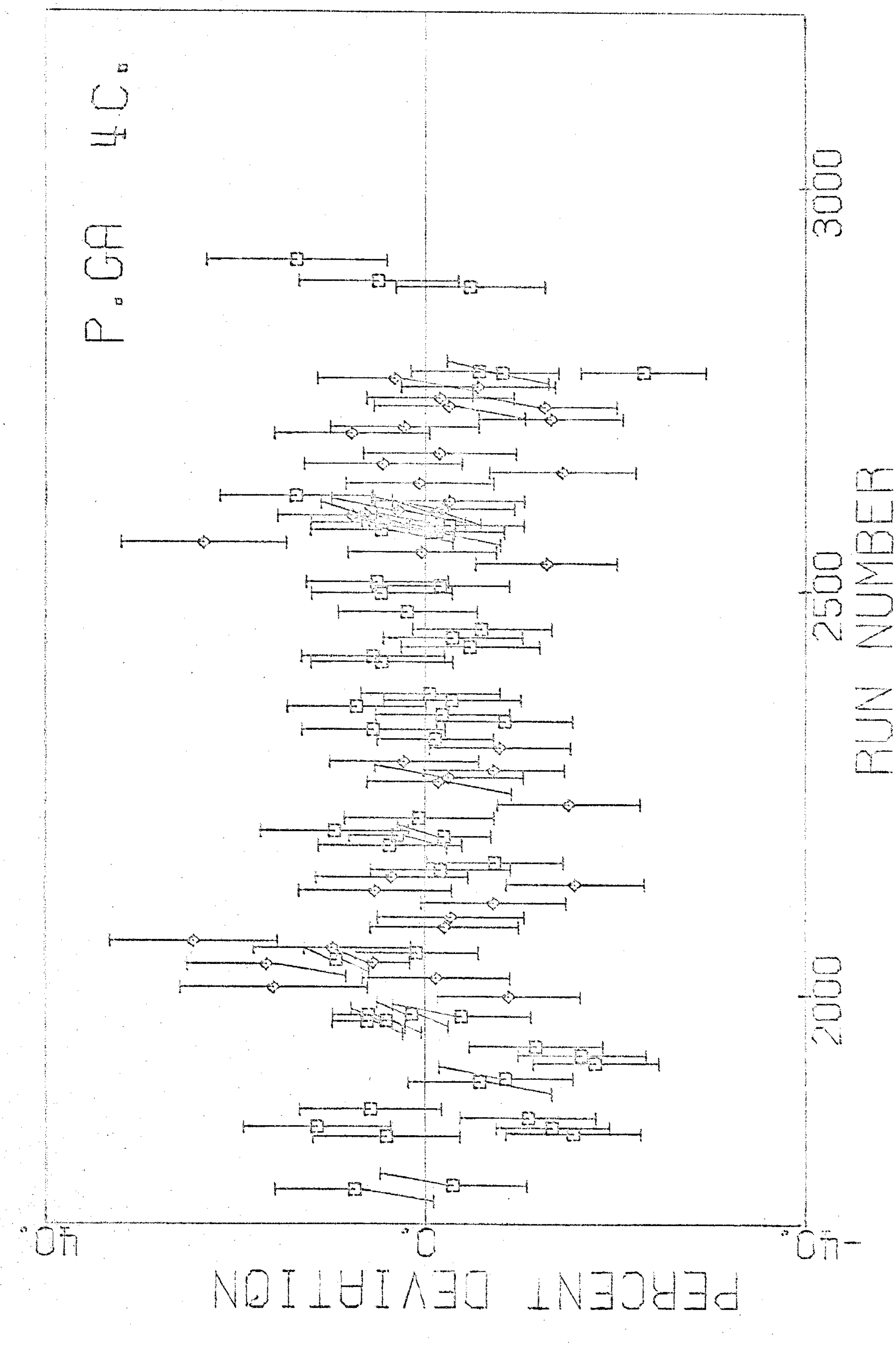

Figure 27.8

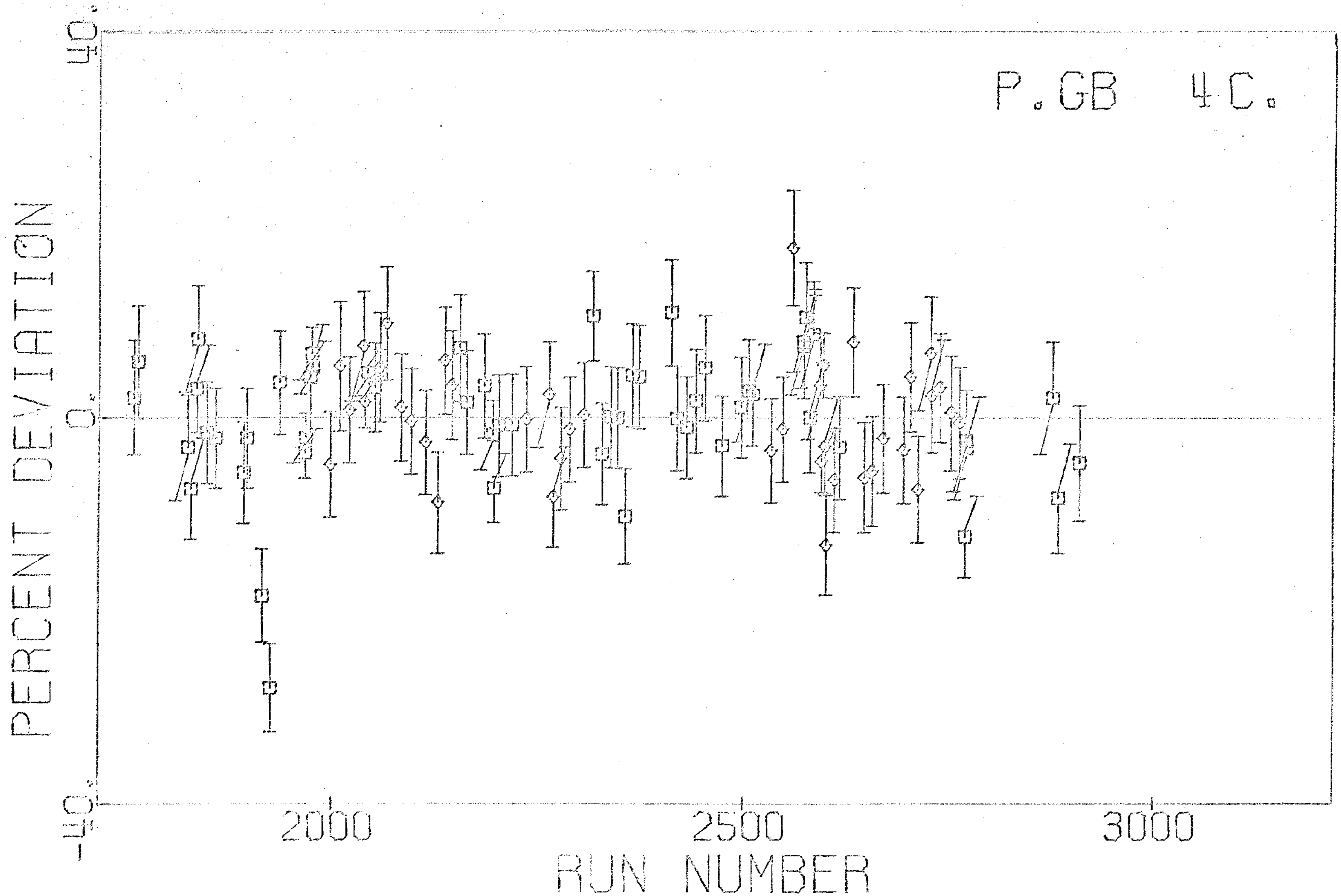

Figure 27.9

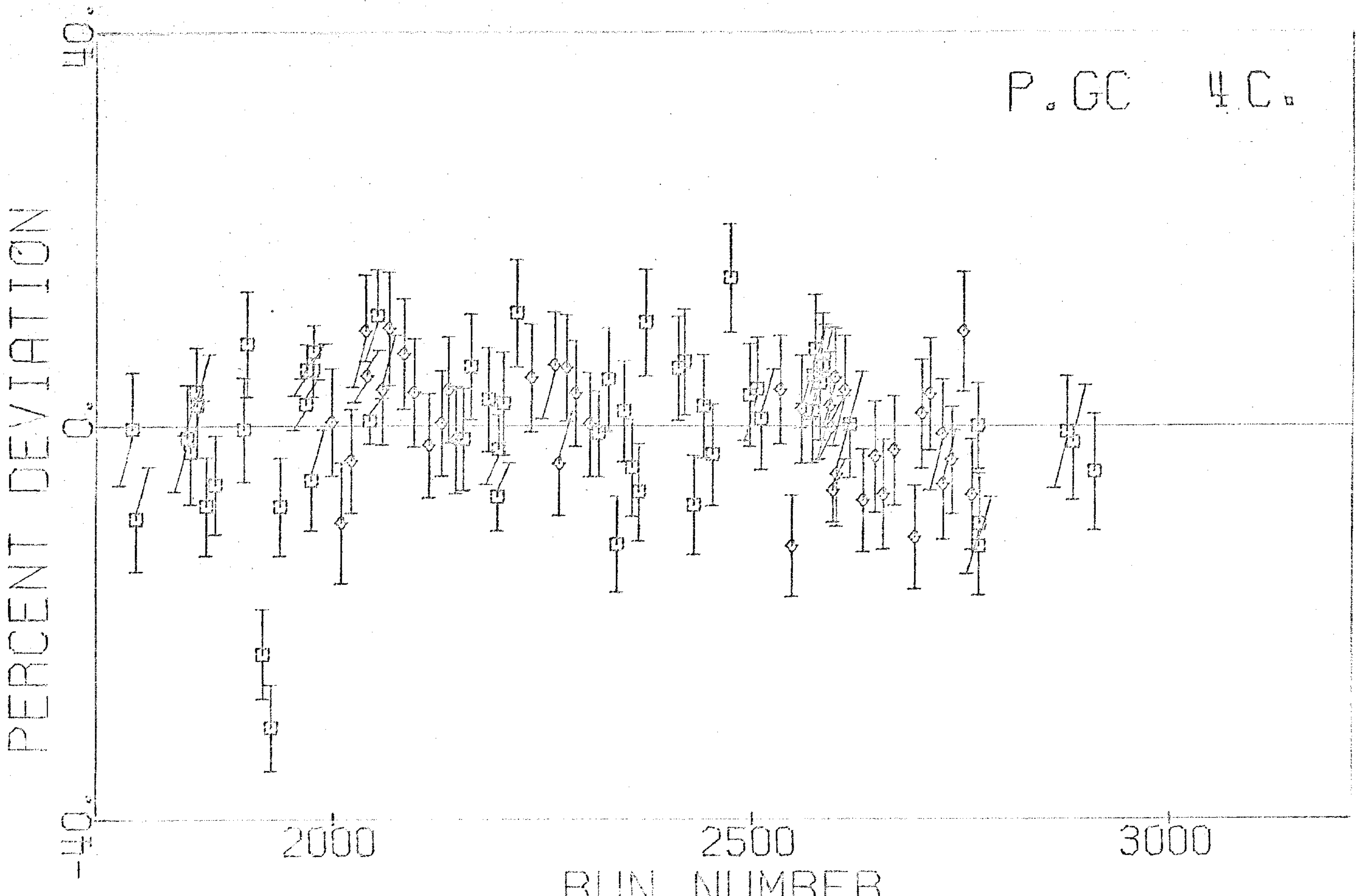

Figure 27.10

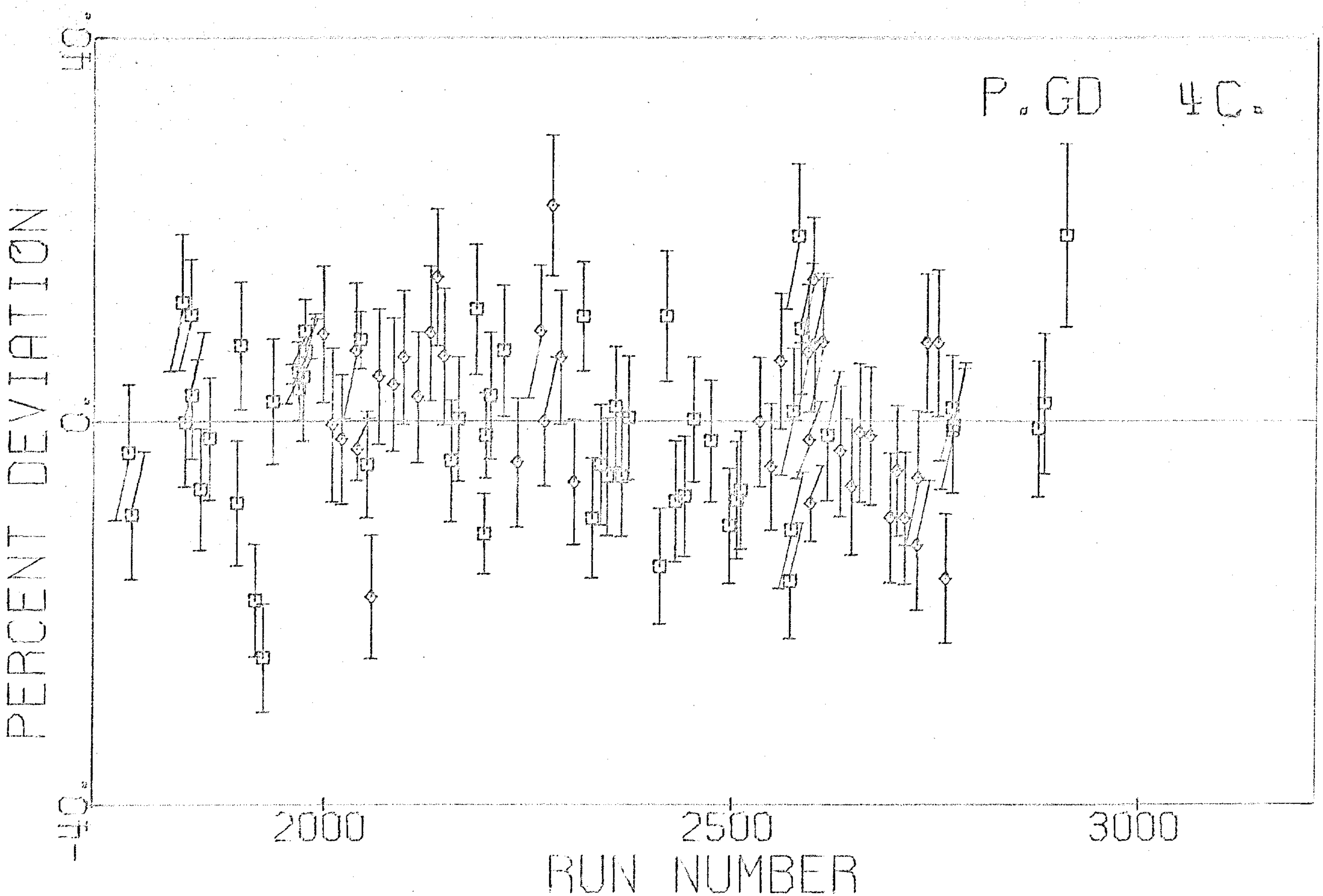

Figure 27.11

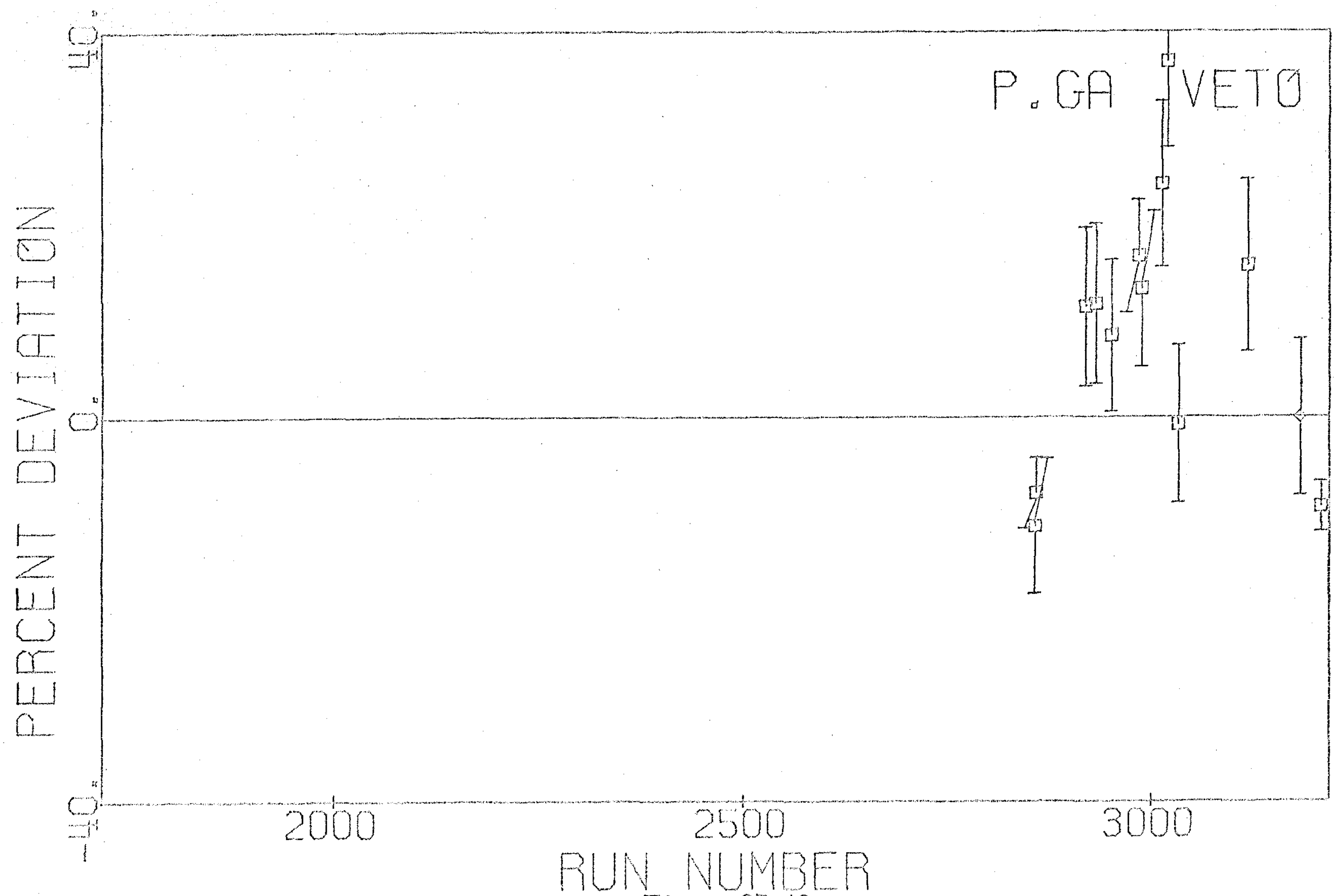

Figure 27.12

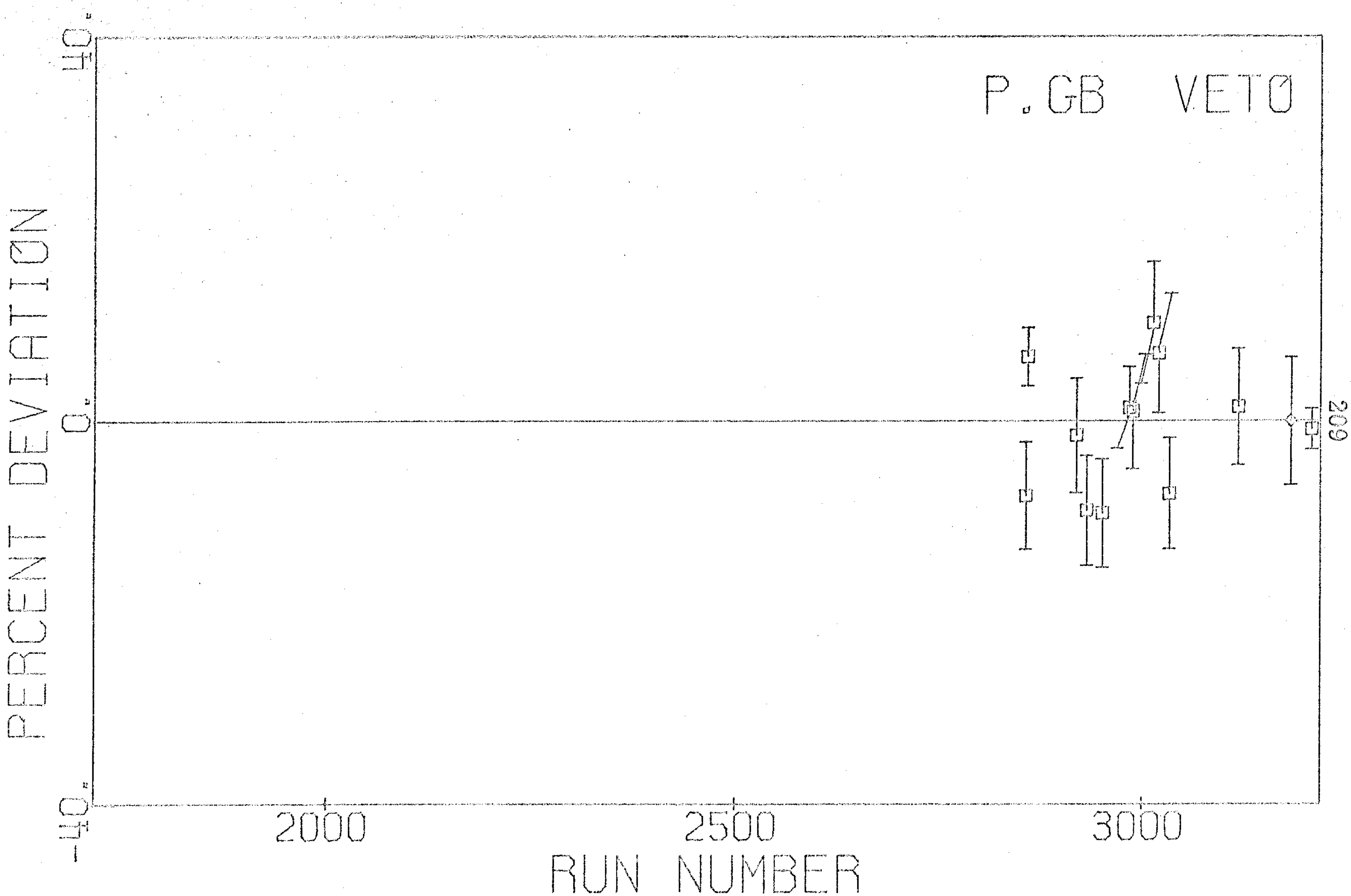
P.GB VETØ
PERCENT DEVIATIØN
40.
0.
-40.
RUN NUMBER
2000
2500
3000
209

Figure 27.13

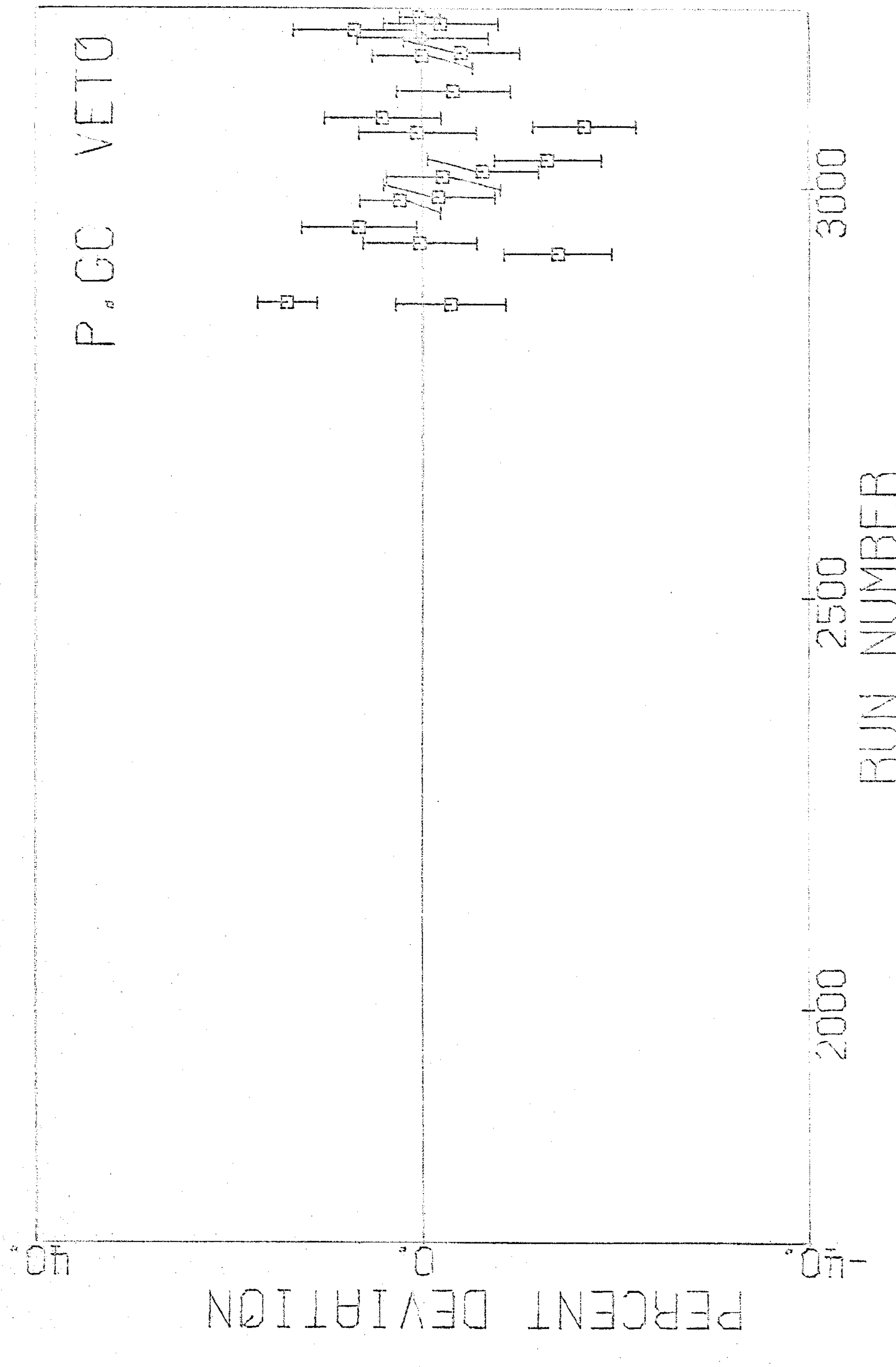

Figure 27.14

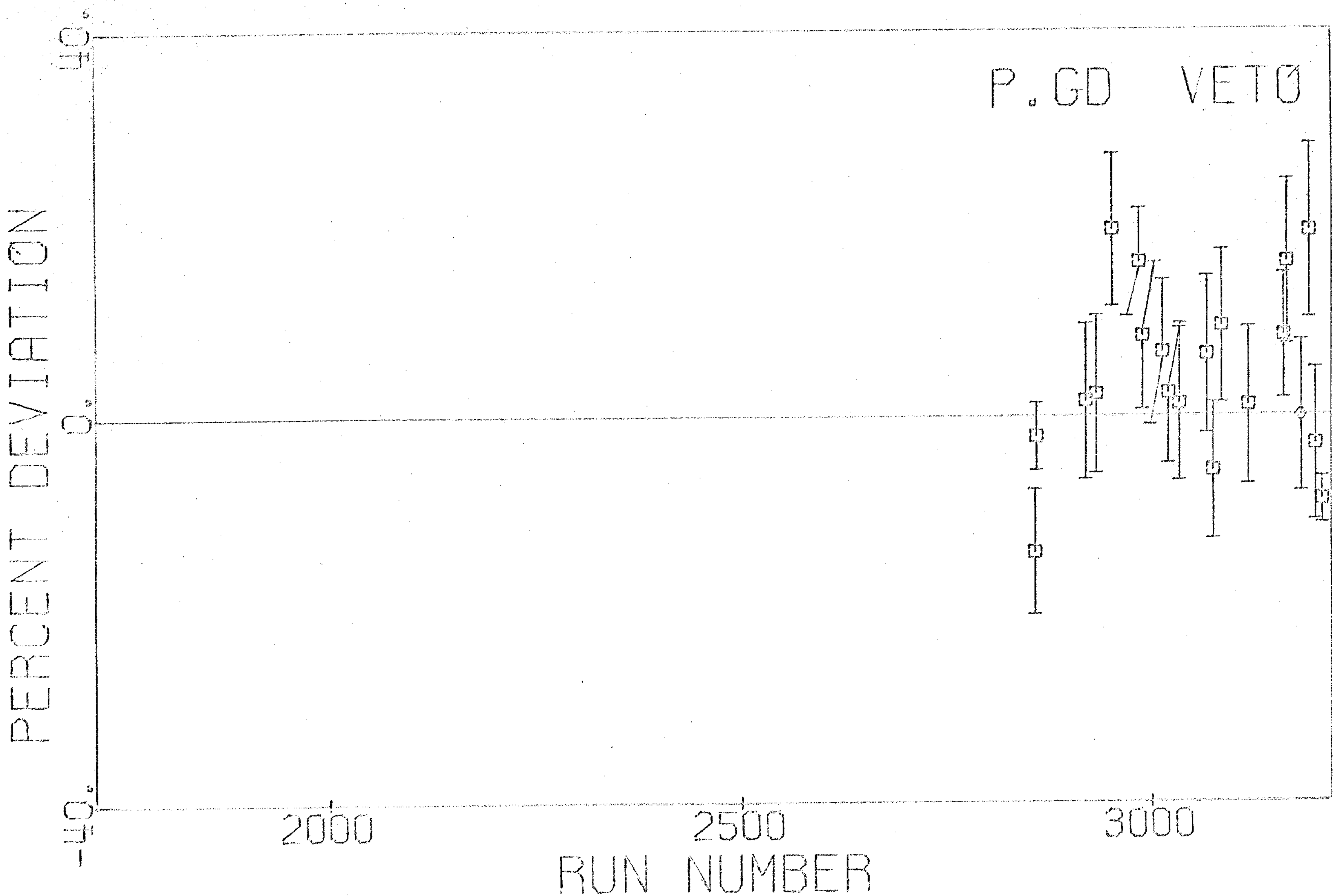

Figure 27.15

four momentum channels.) It is hypothesized in Appendix I that the variation is due to vertical motion of the beam. The same explanation works qualitatively for the P rate. As the beam moved up, the monitor telescope solid angle decreased and the spectrometer momentum increased causing both rates to drop. For the other rates, the variation is nearly lost in the statistical errors.

The expected ratio of OUTR to HEMA rates on the basis of a simple calculation, involving only the magnet acceptance and S3 counter loss, is .63. The ratio for the P rate is .64, which differs by only 2% from the expected value. The PA and PD ratios differ from .64, but this is expected because their momenta are different for the two configurations.

The ratios for the four counter $P \cdot \gamma B$ and $P \cdot \gamma C$ rates are 4% higher than for the P rate. This could be a geometric efficiency effect related to the difference in total momentum width of the two configurations.

In view of the problems with the veto cross sections, it is interesting to compare the veto and four counter Lucite rates. The $P \cdot \gamma A$ and $P \cdot \gamma D$ rates cannot be compared since these counters were in different situations in the two gamma counter configurations. The HEMA averages for $P \cdot \gamma B$ and $P \cdot \gamma C$ are about the same in the veto configuration as in the four counter configuration. This would indicate that the trouble was not a malfunction in either the spectrometer, γB, or γC. The OUTR averages have large errors in the veto configuration, but that is to be expected since there was only one such run and it had large statistical errors.

Both (e^+ or π^+) and FAN VETO have ratios that are much less than .63. Presumably, in the OUTR configuration, S3 is enough farther from the magnet that it picks up significantly fewer scattered particles.

APPENDIX VI. RATE CORRECTIONS

A. Background runs

In order to correct for photoproduction from the target materials, background runs were taken in which the target was filled with one atmosphere of hydrogen gas instead of liquid hydrogen. At least one background run was taken at each data point. Because of the well-known propensity of this hydrogen target to accumulate contamination over long periods of time, backgrounds were always taken within about a week of their mating foreground runs. The background runs were subtracted from the foreground runs and the difference rates were analyzed using a hydrogen density which was the difference between the liquid and gas densities.

When only the proton was required, the background rates at small proton angles became as much as one half the foreground rate, implying rates from the target materials that equalled the rates from the hydrogen.

When at least one gamma ray was required, the rate dropped to nearly the 3% expected from the hydrogen in the mylar and the hydrogen gas.

B. Pi Pairs

Figure 8 of Part III shows that, when only the proton was required at $\theta_p^{lab} = 16^o$, there was a pi pair contamination which was several per cent of the π^o rate. In the veto configuration, the veto counters eliminated the charged pairs, which turned out to be the majority of the pairs. In computing the veto rates, γB events were thrown out if they counted in γA, and γC events were thrown out if they counted in γD. In this configuration, no correction was possible for neutral pairs.

In the four counter configuration, the situation was more complicated. Simply requiring a count in at least one gamma counter reduced the pi pair contamination, but not enough. Requiring an event in one of the two most efficient gamma counters reduced the contamination still further. In order to finally get rid of all the pi pair contamination, the difference in the angular distribution of π^o and pi pair events was used as follows. All events where two counters fired were assumed to be π^o events. It was shown that the kinematic restrictions on the pi pair angular distributions made this a reasonable assumption. Next were considered R_A, the rate for events where only γA counted, and R_B, the rate for events where only γB counted. Assuming ϵ_A and ϵ_B were their π^o efficiencies and assuming their efficiencies for detecting pi pairs were equal, the π^o rate obtained for γB was

$$R_B^{\pi^o} = \frac{R_B - R_A}{1 - \epsilon_A/\epsilon_B}$$

Making similar assumptions for γC and γD implied

$$R_C^{\pi^o} = \frac{R_C - R_D}{1 - \epsilon_D/\epsilon_C} .$$

Assuming the pi pair rates were equal for A and B and equal for C and D amounted to assuming that the rates varied linearly across the array, which was probably a fairly good assumption.

The above method could not be used at $\theta_p^{lab} = 4^o$ and 8^o because of the physical restriction on the placement of counters. It was observed that the pi pair rate was nearly independent of angle for $\theta_p^{lab} = 12^o$, 16^o, and 20.5^o. Therefore, the pi pair rate in γB and γC, corrected for the change in A1 counter size, was subtracted from the 4^o and 8^o rates in γC and γD (which at 4^o and 8^o were nearly centered on the π^o). The 4^o and 8^o events where only γA or γB fired were not used because γA and γB were on the opposite side of the beam, where the π^o efficiency was low. The error assigned to the 4^o and 8^o correction was made large due to the uncertainty in the method. The lack of jumps every fourth channel in the 4^o and 8^o $P \cdot \gamma$ signature cross sections gives confidence in the method.

C. Nuclear scattering

Some protons with the proper momentum and direction to count in the spectrometer failed to count because they underwent nuclear scatters at sufficiently wide angles to cause them to miss S3, the last counter in the system.

In small angle scattering, such as multiple Coulomb scattering, there is a tendency for vertical (momentum plane) scattering to scatter as many particles into the system as it scatters out. But with nuclear scattering, where the angles are wider, this is not the case. For scatterers close to S3, there is no scattering material in the appropriate place to cause scattering in. For scatterers far from S3, most scattered particles receive enough horizontal angle to prevent hitting S3 regardless of the vertical angle. In the following, the possibility of scattering in will be ignored entirely.

The fraction of particles df which are lost due to nuclear interactions in a thickness of scatterer dx is

$$df = (6.023 \times 10^{-4}) \frac{\sigma_{total}(p)\, g(p, x)}{M} \rho \, dx$$

where

$\sigma_{total}(p)$ = total cross section per molecule for nuclear interaction in the scatterer,

$g(p, x)$ = geometric efficiency that a scattered proton misses S3,

M = molecular weight of the scatterer,

ρ = density of the scatterer.

Two things complicated what would otherwise have been a trivial integral over x to obtain f. First, the momentum, p, changed as a function of x because of ionization loss in the spectrometer. Second, the factor $g(p, x)$ was a complicated multiple integral involving the proton scattering angular distributions and the spectrometer geometry.

A Fortran program was written by C. Maxwell to perform the integration over x, given $\sigma_{total}(p)$ and $g(p, x)$. The program calculated $p(x)$ using loss rates from D. Groom's program (23) to calculate the losses in each of the materials in the spectrometer. The values of f were used to find $1 - \epsilon_{NA}$, the fraction of particles lost by nuclear absorption, using

$$\epsilon_{NA} = e^{-f} .$$

The per cent lost was typically 10 to 15%. Specific values are listed in Tables 16 and 17.

The remainder of this appendix is concerned with the method for obtaining $\sigma_{total}(p)$ and $g(p, x)$.

Table 11 lists the approximate per cent contribution to nuclear scattering made by each of the elements comprising the materials in the spectrometer. These would be the contributions to the loss rate if g were equal to 1. Elements not listed made negligible contributions. The calculations were based on the total interaction cross sections measured for 830 MeV/c protons by de Carvalho (31). The cross section for lead was obtained from scaling data on chlorine by $A^{2/3}$ to account for the difference in nuclear area.

Table 11

Contributions to Nuclear Scattering

Carbon	42%
Lead	26
Oxygen	13
Aluminum	8
Hydrogen	7
Nitrogen	4

From the table, it is clear that carbon and elements of very similar atomic number, oxygen and nitrogen, contributed over half (59%) of the scattering.

The next most important element was lead. Because lead occurred only one place in the system (before S3) and because its nearness to S3 made it difficult to compute $g(p, x)$, the contribution to f from the lead was measured directly. At 16°, where very little electromagnetic showering was expected in the spectrometer, protons were counted with and without S3 required, both with the lead in and with the lead out. From these measurements, it was deduced that the lead absorbed $1.4 \pm .4\%$ of the protons at 985 MeV/c. Since, on the basis of the cross section extrapolated from de Carvalho's data, about 5.1% of the protons scattered in the lead, apparently two thirds of the scattered protons still managed to count. For lack of detailed experimental information on the momentum dependence of the lead cross section, it was assumed to be proportional to the carbon cross section. This may not be an accurate approximation, but the amount of absorption by the lead was small.

With the lead handled as a special case, nearly all the remaining scattering was due to carbon or elements similar to carbon. For this reason, an approach was taken which handled carbon accurately and other elements approximately.

The total scattering cross section, $\sigma_{total}(p)$, on carbon has a minimum at about 800 MeV/c (carbon data is summarized by C. J. Batty (32)). It rises rapidly as the momentum decreases and slowly as the momentum increases. At 800 MeV/c, the scattering is about one third elastic and two thirds inelastic.

Geometric factors, $g(p, x)$, for elastic scattering were computed at four momenta using elastic scattering angular distributions measured by Dickson and Salter (33), Heiberg (34), and Batty, Lock, and March (35). The calculations took into account, in a crude way, the finite size of the proton beam and S3. The results are plotted as the four solid curves in Figure 28. The right hand side of the graph corresponds to the position of S3. The positions of S1, LC, and S2 are indicated because they contained much of the scattering material. The geometric factors changed rapidly in the region of these counters. As the distance from S3 increased, the geometric factors approached 1. At large distances from S3, $1 - g(p, x)$ varied as the inverse square of the distance from S3. At sufficiently large distances, $g(p, x)$ was nearly equal to 1, indicating that nearly all scattered particles were lost, as one would expect.

Although a majority of the scattering in carbon is inelastic, the data on inelastic scattering are less complete than on elastic scattering. For the calculation of the geometric factor for inelastic scattering, it was assumed that any heavy fragments from the scatters were stopped by ionization loss before reaching S3. The possibility of production of pions was more of a problem. Pions produced at very wide angles had no effect because they missed S3 anyway. Although it is possible that pions were produced at smaller angles, none were included in the calculation. The experimental information on even the scattered proton angular distributions was quite meager. There is a fair amount of information on inelastic scatters where the proton loses only a small amount of energy and excites the carbon nucleus to a low-lying excited state, but these only comprise a small fraction of the inelastic scatters. For

Figure 28

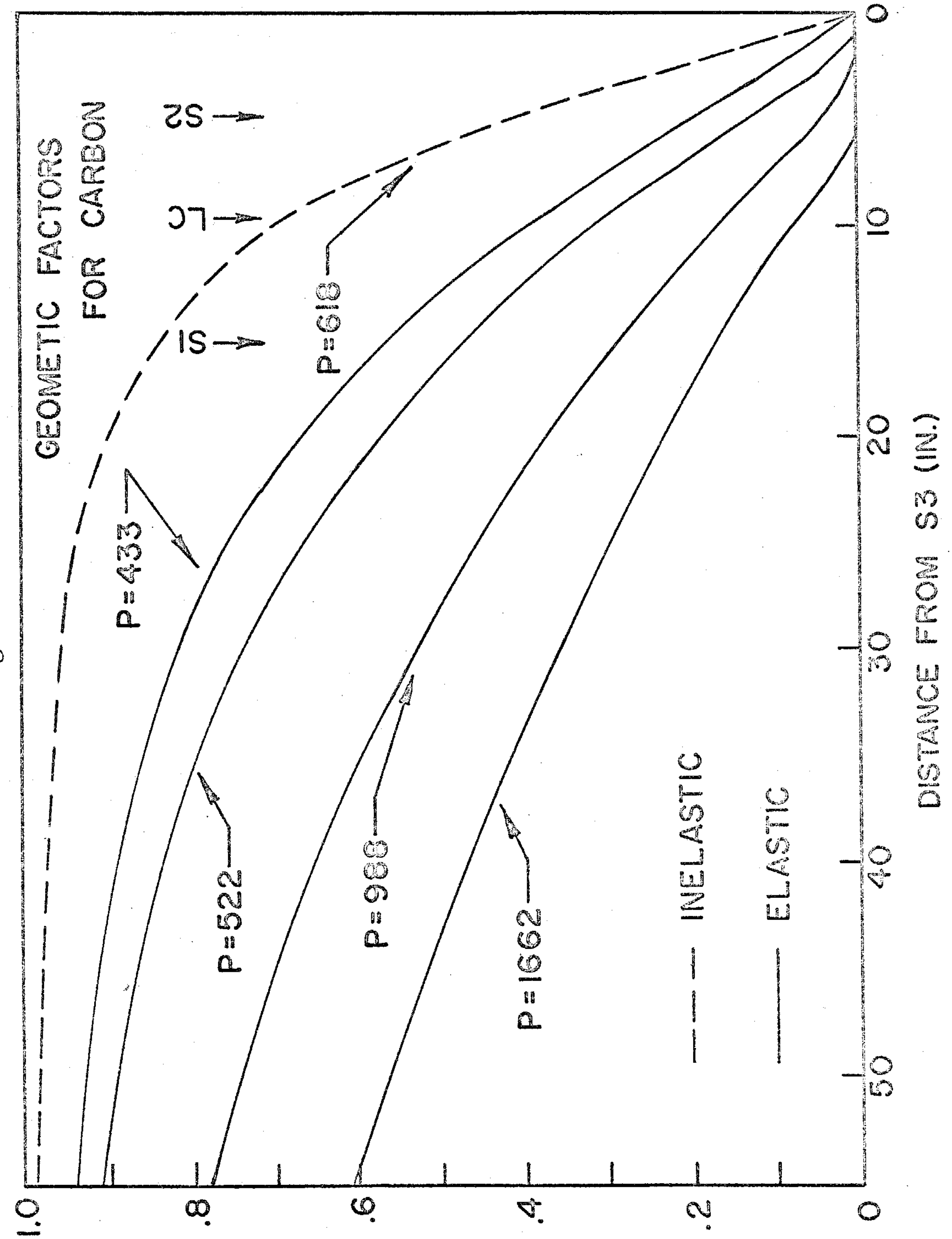
GEOMETIC FACTORS
FOR CARBON
S2
LC
S1
P=433
P=618
P=522
P=988
P=1662
INELASTIC
ELASTIC
DISTANCE FROM S3 (IN.)
0
10
20
30
40
50
1.0
.8
.6
.4
.2
0

instance, data of Caverzasio and Michalowicz (36) show that the outgoing energy distribution for the 30^{o} scattering of 155 MeV protons (P = 560 MeV/c) does not vary more than a factor of two from 50 to 155 MeV. Only the top end of this range corresponds to exciting low-lying nuclear levels. Although the evidence is rather scanty, the angular distribution of the inelastically scattered protons seems to be roughly independent of the energy of the proton after scattering. Using data of Tyre and Maris (37) on 618 MeV/c protons, which show the angular distribution to be flat at small angles and drop off rapidly at about 35^{o}, a geometric factor was computed for inelastic scattering. It is shown as the dashed curve in Figure 28. Little is known about the angular distribution at higher momenta. Azhgirei et al. (38), using 1300 MeV/c protons showed that the distribution is flat out to 30^{o}, but they did not show where it drops off. The distribution could be the same as at lower momenta, or it could be wider, which would make the geometric factor larger than the one shown. If there were any small angle pions produced, they would have made the geometric factor smaller. For lack of a better guess, the 618 MeV/c inelastic geometric factor was used at all momenta. The data on the relative amounts of elastic and inelastic scattering are not entirely consistent. The fitted values given by Batty (32) were taken as being a reasonable compromise. Using these values, the elastic and inelastic geometric factors were combined to give the factors shown in Figure 29. The resulting factors do not show much dependence on momentum. The 988 MeV/c curve was used in the analysis of all the data.

Figure 29

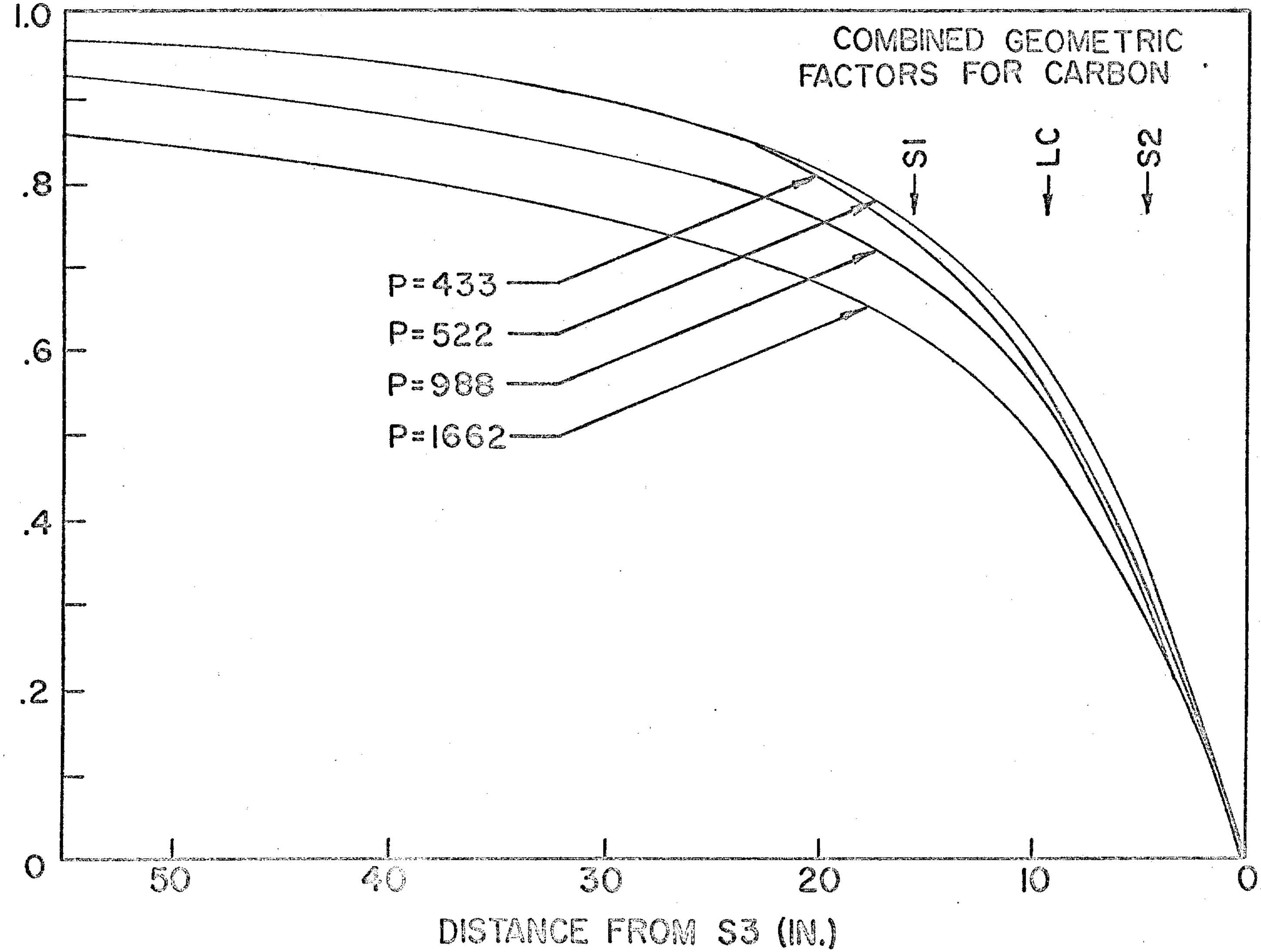
COMBINED GEOMETRIC
FACTORS FOR CARBON
S1
LC
S2
P=433
P=522
P=988
P=1662
1.0
.8
.6
.4
.2
0
50
40
30
20
10
0
DISTANCE FROM S3 (IN.)

As a check on the nuclear scattering calculations, runs were taken in which extra pieces of scattering material were inserted at various points in the spectrometer. Table 12 shows the predicted and measured changes in the counting rate caused by addition of 1 inch of polyethylene near A1 and 1 inch of polyethylene near A2. The addition of material changes the S3 loss rate due to Coulomb scattering also. Thus, this is a check on the sum of the two rates.

Table 12

Nuclear Absorption Measurements

Conf.	θ_p^{lab}	E_o (MeV)	P_o (MeV/c)	pred. change	meas. change
HEMA	49^o	870	588	14.5%	20 ± 2%
	16^o	870	985	6.7	5.9 ± 1.9
OUTR	16^o	870	985	7.5	10.7 ± 2
	16^o	1320	1308	8.6	13.2 ± 3

The agreement is not terribly good from a statistical point of view, but the measurements probably do not imply more than a 2% systematic error, except at the lowest momentum, which is fairly good, considering the number of questionable assumptions made.

A measurement with a special setup that allowed placing 2 inches of Lucite where LC normally is placed gave predicted and measured changes of 7.5% and 12.5 ± .9% at P_o = 588 MeV/c, which is not terribly good agreement. Internal inconsistencies in the rates for this measurement indicate that it is questionable. A similar measurement at P = 985 MeV/c gave 4.6% and 3.2 ± 1.1%, which is quite good.

APPENDIX VII. DATA REDUCTION

A. Cross section formulas

The counting rate for protons in the spectrometer can be written as a multiple integral over the center of mass cross section, a Jacobian to transform to the laboratory system, the beam spectrum, the hydrogen target density, and the magnet acceptance. The target density is discussed in Appendix I, and the magnet acceptance is discussed in Appendix II.

The spectrum of the photons in the beam is usually parameterized as follows:

$$n(k)dk = \frac{W}{E_o} B(E_o, k) \frac{dk}{k}$$

where

$n(k)$ = number of photons of energy k in dk

W = total energy in the beam

$B(E_o, k)$ is approximately 1 for $k < E_o$ and 0 for $k > E_o$. The actual values of $B(E_o, k)$, as determined by the radiator thickness and the beam collimation, were computed from a set of Fortran programs, BPAK I, written by the present author before he started this experiment (39).

If, in the multiple integral, the cross section is replaced by its average value, the integral becomes a constant, κ, such that the counting rate divided by κ gives the average cross section.

The evaluation of this integral is discussed by Thiessen (21). The program CRØS, written by Thiessen and Ecklund to evaluate the integral, became, almost without significant change, a subsection of the Phase 2 analysis program for the present experiment (cf. Appendix VII B). For this experiment it was convenient to separate out the nuclear absorption efficiency, ϵ_{NA}, and the S3 efficiency, ϵ_{S3}, from $\varkappa$. For this experiment we also had to include the gamma counter efficiency, ϵ_{γ}. Thus the cross section was given in terms of the counting rate R as

$$\sigma(k, \theta^{cm}_{\pi^o}) = \frac{R}{\varkappa \epsilon_{NA}\, \epsilon_{S3}\, \epsilon_{\gamma}} .$$

B. Computer processing

Calculation of cross sections from the raw data took place in two phases. Each phase was a separate program for the IBM 7094 computer.

Phase 1 (a) Stored and checked raw data.

(b) Computed monitor calibrations.

Phase 2 (a) Corrected for accidentals and subtracted backgrounds.

(b) Computed conversion, $\varkappa$, from rates to cross sections, ignoring efficiencies.

(c) Computed S3 and γ counter efficiencies by Monte Carlo.

(d) Combined results of (a), (b), (c) and the nuclear absorption and 2π corrections to get cross sections for various signatures.

The parameters, beam monitor readings and scaler counts for each run were recorded in the data book in a form that could be punched directly onto IBM cards. At the end of each day of running, a xerox copy of the runs was punched onto cards and the paper tape from the analyzer was converted to magnetic tape. These were then processed by Phase 1, which checked the card and tape data for internal consistency and stored both on magnetic disk. Magnetic disk was chosen over cards or magnetic tape because the large amount of data to be processed (over 1000 numbers per run) argued against cards, and the need for random accessing to obtain matching foreground and background runs argued against magnetic tape. The Phase 1 program also computed the total number of MeV in the beam for each run according to the monitor calibration method described in Appendix I and stored this on the disk. The printed output from Phase 1 contained error messages concerning any inconsistencies found and contained plots of the monitor calibrations. Phase 1 contained facilities for altering the data stored on the disk and correcting errors.

When both foreground and background data were available at a given point, the Phase 2 program collected the runs from the disk. Only the rates having a proton in the spectrometer were considered. These were the 256 rates stored in the first quadrant of the analyzer, and they corresponded to the possible logic combinations of the 4 momentum channels and the 4 gamma channels. Ideally, there would be no counts where more than one momentum channel would count, but such counts did exist. Presumably these were caused by a knock-on electron triggering one channel while the proton that produced it triggered another. Where these events occurred in adjacent channels, one half of the events were put in each channel. The number of times where there were counts in non-adjacent channels or in three or more channels was always small and such events were ignored. The resulting 64 rates (4 momentum channels × 16 gamma rates) were carried through the rest of the analysis. It proved to be extremely useful to postpone combining the rates to get various gamma signatures. The rates were corrected for accidentals. Then the foreground runs were averaged together, the background runs were averaged together, and the background rates were subtracted from the foreground rates. The resultant rates were punched onto IBM cards so that re-analysis at another time would not require repeating the subtraction.

Next, considering only the proton in the spectrometer, the conversion, κ, from counting rate to cross section was computed for each momentum channel assuming the spectrometer was 100% efficient. This calculation involved an integral containing the magnet resolution functions and the bremsstrahlung beam spectrum. The calculation had already been programmed for the IBM 7094 by Ecklund and Thiessen (21) for analyzing π^+ photoproduction. The relevant portion of their analysis program was, after changing the particle masses and eliminating the μ decay corrections, inserted directly into Phase 2. The values of κ were punched onto a second set of IBM cards.

It was then necessary to compute the probability that the proton would be accompanied by counts in various combinations of the gamma counters. This computation also yielded the geometric inefficiency of S3 including multiple coulomb scattering in the spectrometer. These results were punched on a third set of cards.

The final step of the calculation was to compute cross sections. For each momentum channel, the counting rates and gamma and S3 efficiencies for the 16 gamma combinations were combined according to the signature desired. Then the counting rates were divided by kappa, the gamma and S3 efficiency, and the nuclear absorption efficiency to get the cross section. In practice several signatures were computed at once. The cross sections were punched onto IBM cards.

Because dk/dp for the production reaction is a function of proton laboratory angle and because the two spectrometer configurations have different channel spacings, the cross sections for a given endpoint energy and momentum channel were not angular distributions at constant k. To obtain angular distributions, the same method was used as was used by Ecklund (14). A standard k value was chosen for each channel at each energy. Then, at each point, a quadratic fit was made to the four channels and the four cross sections were moved to the standard energies, moving parallel to the fit. The error bars were arbitrarily kept the same size. This method of interpolation has the advantage of not smoothing the data. The amount by which the points were moved was usually small, but was 80 MeV in the largest case. Repeated measurements at a given point were averaged together. The results of the interpolation and averaging are the final cross sections shown in Table 2 and Figures 7 and 12.

C. Errors

The cross section plots and tables indicate counting and Monte Carlo errors. In the case of the 4° and 8° data, the error on the empirical pi pair correction is included also.

There is an additional 2% rms random error in the beam monitoring.

Estimated systematic errors are listed in Table 13.

The photon energy resolution was not unfolded. The largest errors due to this occur at the peaks of the two resonances. For an estimation of the amount of error, the reader is referred to Reference 1. The rms resolution widths for the present experiment are in Appendix IX. Note that Reference 1 deals with the full width at half maximum of the resolution functions.

Table 13

Systematic Errors

Quantameter calibration	3%
Nuclear absorption	3%
Bremsstrahlung shape	2%
Conversion efficiency	2%
Liquid hydrogen target	1%
Electronic efficiency	1%
Magnet acceptance	1%
Total	5% rms
	13% maximum

APPENDIX VIII. EXCITATION CURVES

Runs were taken at the $\theta_p^{lab} = 16^o$, $k = 772$ MeV, point with several values of the endpoint energy, E_o, above and below the regular 870 MeV. This setting was chosen because of the large amount of pi pair contamination in the proton rate. It has the disadvantage that the cross section changes rapidly as a function of k in this region. This makes the results a little more difficult to interpret than if the cross section were constant.

The rates for these runs, given in Table 15 , together with the rates for the normal runs given in Table 14 (16^o point numbers 8 through 13), form four separate excitation curves, one for each momentum channel. Let us consider the bottom channel excitation curve only. The bottom channel is the most interesting because it has the largest values of $E_o - k_{chan}$, the quantity of interest in studying pi pair contamination.

More convenient for the present purposes than the raw rates are cross sections computed from the rates. The cross sections are given in Tables 19 and 18 .

The cross sections for the P signature are plotted in Figure 30. They are plotted versus the true, or corrected, endpoint energy, which is 1.025 times the nominal energy. Also indicated on the graph are the k value for the bottom channel, the approximate energy resolutions function, and the normal endpoint setting.

The cross section for π^o production should not depend on the endpoint energy used in the measurement. Therefore the points should, to first approximation, lie on a horizontal line at the proper cross section value for this point. This is strictly

Figure 30

P signature excitation curve. Points measured with the HEMA or OUTR configurations are denoted by squares and diamonds, respectively. Open and filled-in symbols denote measurements with the four-counter and veto configurations, respectively.

Figure 30

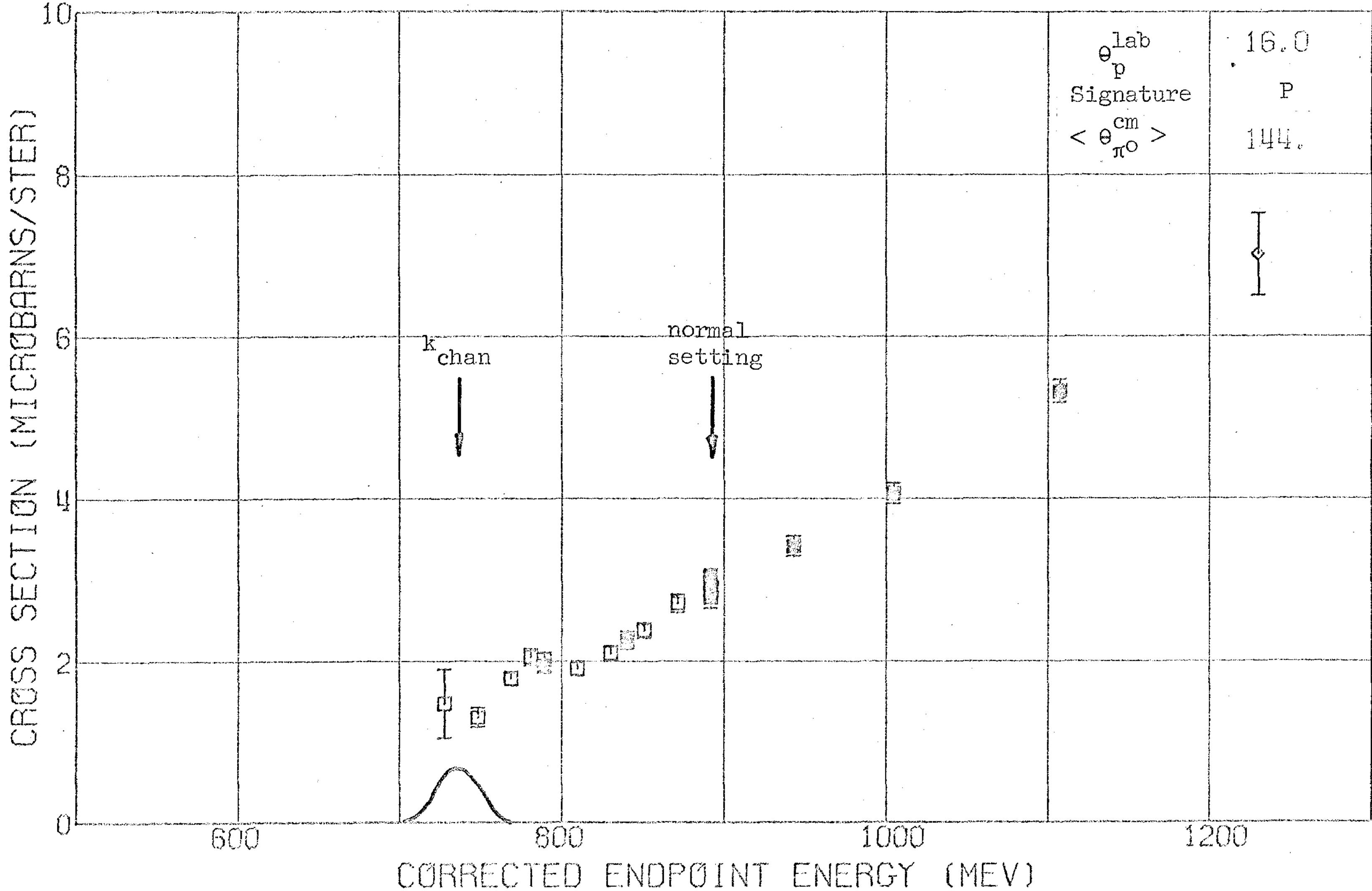

10
8
6
4
2
0
CRØSS SECTIØN (MICRØBARNS/STER)
600
800
1000
1200
CØRRECTED ENDPØINT ENERGY (MEV)
k_{chan}
normal setting
θ_p^{lab} 16.0
Signature P
$< \theta_{\pi^o}^{cm} >$ 144.

true only at energies above the energy where the resolution function goes to zero, i.e., ~ 775 MeV. Below this energy, the mean k value of the product of the resolution function and the bremsstrahlung spectrum decreases with decreasing endpoint so that the cross section corresponds to a different average k. It is in this respect that it is a disadvantage to have the cross section varying rapidly with k. One would like to see if the cross sections are correct with the endpoint very near to k_{chan}.

Turning to the region above 775 MeV, the measured points are consistent with a horizontal line only for about 50 MeV. Then the cross sections increase rapidly with increasing endpoint indicating pi pair contamination. Note that the normal setting is on the rising part of the curve and that the contamination at the normal setting is about 40% of the real π^o cross section (as read from the flat portion between 775 and 825 MeV).

The cross section for the $P \cdot \gamma$ signature for the same points is shown in Figure 31. This time the cross section is nearly independent of E_o above 775 MeV as it should be. The filled in points were measured with the veto cross configuration.

The very slight rise indicated by the high energy points only indicates an error of 5 % at the normal setting. It should be noted that since these are bottom channel cross sections in a region where the pi pair contamination is large, this example is a worst case.

Figure 31

$P \cdot \gamma$ signature excitation curve. Points measured with the HEMA or OUTR configurations are denoted by squares and diamonds, respectively. Open and filled-in symbols denote measurements with the four-counter and veto configurations, respectively.

Figure 31

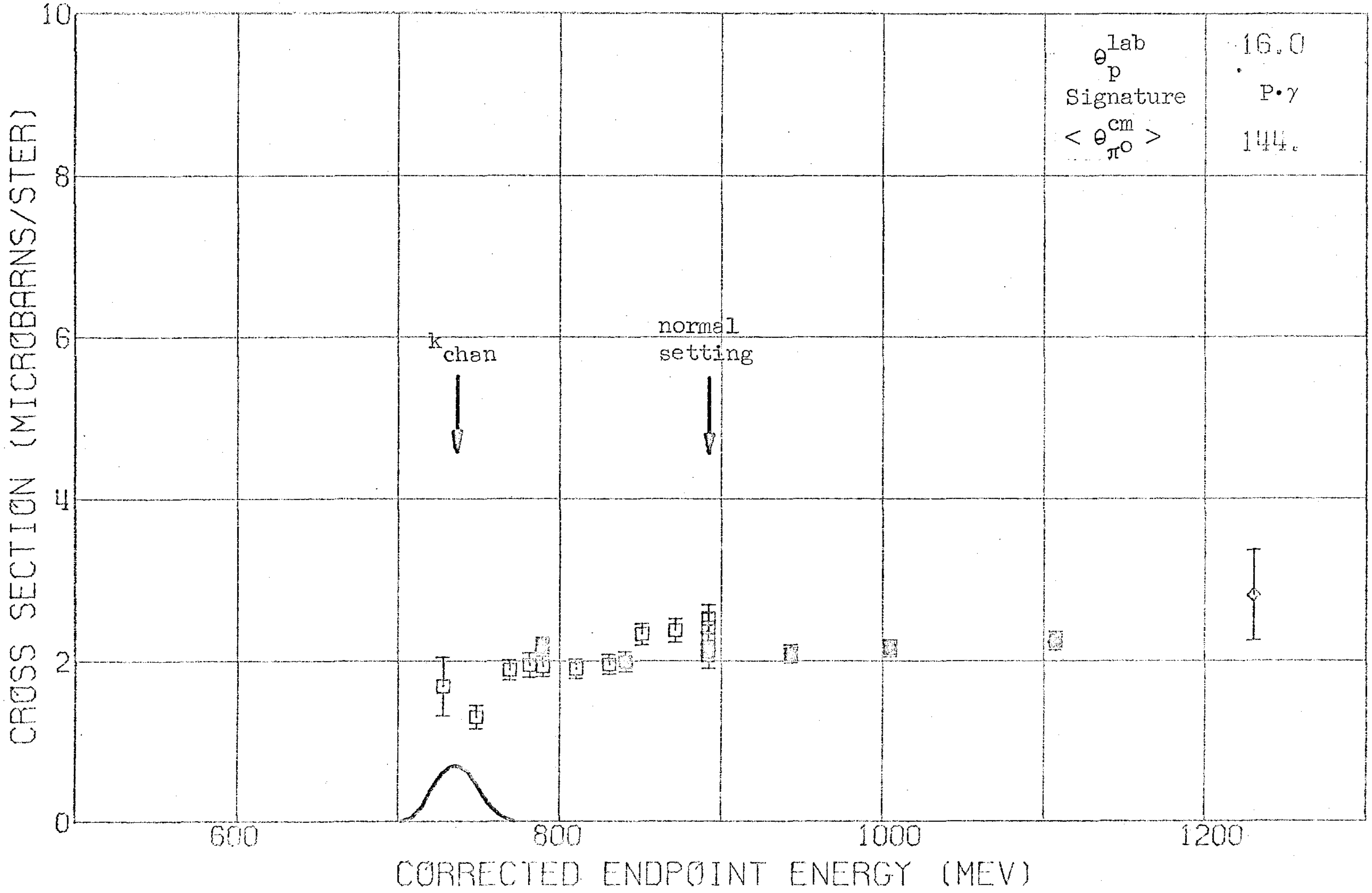

10
8
6
4
2
0
CROSS SECTION (MICROBARNS/STER)
600
800
1000
1200
CORRECTED ENDPOINT ENERGY (MEV)
k chan
normal setting
θ_p^{lab} 16.0
Signature P·γ
$< \theta_{\pi^o}^{cm} >$ 144.

APPENDIX IX. TABLES OF DATA POINTS

The following tables list counting rates, intermediate computed results and uninterpolated cross sections for all the cross section data and for the excitation curve data.

The cross section data are grouped by increasing laboratory proton angle θ_p. Within each angle the data are ordered by decreasing central laboratory photon energy k and labeled by a sequential point number. The four lines at each point correspond to the four momentum channels of the spectrometer. A blank line separates data at different central k.

The excitation curve data are placed in separate tables and are ordered by decreasing E_o.

A. Counting Rates

Tables 14 and 15 contain setup information and counting rates for the cross section data and the excitation data, respectively. The counting rates have been corrected for accidentals and have had empty target rates subtracted. The rates for each signature have been computed as described in Part VI B. In cases where a momentum channel was not working properly, the rates are left blank.

Columns in the tables list the following quantities:

P LAB ANGLE = proton laboratory angle, i.e., spectrometer angle.

PT NO = point number

Table 14

Counting rates for cross section data. See text for definitions.

P LAB ANGLE	PT NO	NOM E0	LAB K	CONF	MAGNET P	AP HT	GAM B ANGLE	GAM C ANGLE	MOM CH	COUNTING RATES AND ERRORS FOR 10**16 MEV PROTON		PROTON.GAM		PROTON.2GAM	
4.0	1	1320	1171	OLD4	1478.8	6	197.7	163.2	A	244.	14.	81.	9.	11.	2.
									B	209.	15.	61.	9.	5.	2.
									C	262.	15.	84.	9.	7.	2.
									D	265.	15.	60.	9.	6.	2.
4.0	2	1200	1062	OLD4	1360.8	6	197.7	163.2	A	244.	14.	81.	9.	11.	2.
									B	290.	32.	93.	15.	16.	7.
									C	342.	37.	99.	16.	18.	9.
									D	395.	36.	96.	15.	12.	8.
4.0	3	1200	1062	OLD4	1360.8	6	197.7	163.2	A	296.	21.	100.	11.	16.	4.
									B	327.	24.	110.	11.	14.	5.
									C	318.	25.	94.	11.	10.	4.
									D	300.	26.	90.	11.	13.	4.
4.0	4	1080	964	OLD4	1252.5	6	197.7	163.2	A	290.	51.	115.	23.	11.	5.
									B	462.	45.	105.	17.	11.	5.
									C	447.	49.	90.	20.	12.	5.
									D	516.	55.	83.	16.	7.	4.
4.0	5	1080	963	OLDV	1252.6	6	197.7	165.6	A	365.	34.	76.	10.	11.	5.
									B	423.	37.	92.	11.	11.	5.
									C	402.	49.	85.	17.	12.	5.
									D	472.	47.	89.	11.	7.	4.
4.0	6	980	873	HLD4	1152.2	6	197.8	163.2	A	572.	47.	162.	16.	26.	5.
									B	697.	52.	201.	15.	28.	5.
									C	711.	55.	201.	16.	28.	7.
									D	691.	60.	172.	17.	28.	5.
4.0	7	870	772	HLDV	1036.8	6	200.2	166.2	A	670.	64.	183.	21.	26.	5.
									B	796.	69.	190.	22.	28.	5.
									C	794.	72.	211.	21.	28.	7.
									D	835.	73.	148.	22.	28.	5.
4.0	8	770	683	HLD4	934.6	6	202.8	163.2	A	616.	70.	209.	23.	23.	8.
									B	536.	72.	111.	20.	9.	4.
									C	457.	76.	98.	16.	13.	5.
									D	558.	77.	83.	18.	9.	4.
4.0	9	770	683	HLD4	934.6	6	202.8	163.2	A	505.	122.	156.	26.	16.	8.
									B	630.	123.	161.	27.	25.	10.
									C	658.	131.	127.	24.	16.	8.
									D	311.	143.	86.	21.	17.	8.
4.0	10	680	604	HLDV	839.3	6	205.8	165.6	A	244.	59.	69.	15.	16.	8.
									B	266.	62.	72.	12.	25.	10.
									C	300.	65.	53.	13.	16.	8.
									D	252.	70.	76.	15.	17.	8.
8.0	1	1320	1171	OLD4	1458.4	9	197.7	151.3	A	342.	22.	179.	16.	9.	3.
									B	346.	23.	165.	17.	9.	3.
									C	379.	25.	192.	17.	11.	3.
									D	408.	27.	184.	18.	7.	3.
8.0	2	1200	1062	OLD4	1343.2	9	197.7	153.0	A	471.	32.	235.	21.	14.	5.
									B	510.	35.	264.	22.	14.	5.
									C	621.	35.	264.	23.	14.	7.
									D	617.	39.	275.	22.	19.	6.
8.0	3	1200	1062	OLD4	1343.2	9	197.7	153.0	A	446.	28.	243.	18.	13.	5.
									B	474.	29.	232.	19.	15.	5.
									C	596.	29.	261.	20.	8.	4.
									D	647.	31.	266.	20.	8.	7.
8.0	4	1080	963	OLD4	1237.0	9	197.7	154.5	A	583.	33.	345.	22.	24.	7.
									B	690.	30.	298.	19.	17.	4.
									C	700.	34.	262.	22.	21.	7.
									D	737.	35.	270.	22.	16.	5.
8.0	5	980	873	HLD4	1138.8	9	197.7	155.9	A	1001.	58.	509.	32.	23.	7.
									B	1070.	62.	521.	33.	36.	8.
									C	1260.	65.	515.	30.	17.	6.
									D	1441.	67.	486.	29.	11.	5.
8.0	6	870	772	HLD4	1026.2	9	197.7	157.5	A	1108.	114.	610.	53.	35.	14.
									B	1373.	119.	572.	52.	24.	11.
									C	1204.	124.	448.	56.	38.	14.
									D	1516.	118.	403.	42.	40.	14.
8.0	7	770	683	HLD4	924.6	9	197.7	158.8	A	821.	75.	377.	36.	10.	11.
									B	746.	75.	301.	35.	28.	12.
									C	952.	81.	280.	36.	23.	14.
									D	908.	80.	216.	31.	20.	10.
8.0	8	680	604	HLDV	830.6	9	201.4	165.6	A	587.	131.	106.	26.	10.	11.
									B	538.	140.	89.	33.	28.	12.
									C	422.	161.	44.	30.	23.	14.
									D	701.	160.	62.	38.	20.	10.

COUNTING RATES AND ERRORS FOR 10**16 MEV

P LAB ANGLE	PT NO	NCM EO	LAB K	CONF	MAGNET P	AP HT	GAM B ANGLE	GAM C ANGLE	MOM CH	PROTON		PROTON.GAM		PROTON.2GAM	
12.0	1	1320	1171	OLD4	1425.4	9	135.1	119.9	A	243.	33.	136.	27.	24.	9.
									B	311.	34.	147.	30.	26.	10.
									C	352.	36.	156.	31.	44.	13.
									D	351.	37.	241.	33.	39.	12.
12.0	2	1320	1171	OLU4	1427.0	12	128.8	113.6	A	409.	25.	235.	22.	59.	11.
									B	384.	26.	178.	23.	33.	8.
									C	380.	26.	169.	21.	27.	9.
									D	351.	37.	241.	33.	39.	12.
12.0	3	1200	1062	OLD4	1314.1	12	137.4	122.2	A	593.	42.	342.	36.	57.	12.
									B	810.	43.	400.	36.	65.	11.
									C	933.	47.	460.	39.	61.	12.
									D	1008.	47.	471.	39.	65.	12.
12.0	4	1200	1062	OLD4	1314.1	12	137.4	122.2	A	632.	30.	370.	27.	51.	9.
									B	790.	34.	444.	29.	72.	10.
									C	941.	36.	527.	32.	74.	9.
									D	914.	38.	497.	33.	65.	9.
12.0	5	1080	963	OLD4	1211.5	12	139.5	124.3	A	1004.	40.	590.	35.	95.	11.
									B	1084.	40.	611.	35.	78.	11.
									C	1069.	40.	530.	34.	97.	12.
									D	1066.	41.	391.	33.	61.	9.
12.0	6	1080	963	OLD4	1211.5	12	139.5	124.3	A	969.	40.	599.	35.	66.	10.
									B	1027.	42.	619.	37.	85.	10.
									C	1003.	39.	532.	34.	74.	11.
									D	988.	41.	448.	34.	72.	9.
12.0	7	980	873	HLD4	1116.4	12	141.4	126.2	A	1504.	66.	817.	53.	87.	15.
									B	1453.	70.	799.	54.	88.	13.
									C	1640.	74.	772.	55.	109.	14.
									D	1742.	76.	830.	54.	76.	12.
12.0	8	870	772	HLD4	1007.3	12	143.5	128.3	A	1574.	78.	922.	62.	112.	15.
									B	1654.	77.	804.	58.	94.	18.
									C	1852.	76.	729.	60.	61.	14.
									D	1681.	84.	512.	59.	61.	14.
-12.0	9	870	772	HLD4	1007.3	12	231.7	216.5	A	1543.	67.	889.	58.	107.	15.
									B	1677.	68.	872.	58.	87.	14.
									C	1678.	74.	641.	60.	80.	14.
									D	1690.	71.	685.	56.	79.	13.
-12.0	10	870	772	HLD4	1007.3	12	231.7	216.5	A	1287.	77.	775.	59.	105.	14.
									B	1586.	77.	832.	59.	105.	14.
									C	1531.	79.	760.	58.	69.	12.
									D	1533.	82.	756.	56.	93.	13.
-12.0	11	870	772	HLDV	1006.4	12	231.7	216.5	A	1424.	83.	616.	43.	105.	14.
									B	1382.	98.	594.	41.	105.	14.
									C	1339.	93.	536.	39.	69.	12.
									D	1467.	96.	503.	35.	93.	13.
12.0	12	770	683	HLD4	908.2	12	145.4	130.2	A	1071.	98.	601.	80.	55.	19.
									B	1193.	92.	525.	71.	39.	13.
									C	1007.	101.	368.	74.	10.	9.
									D	997.	103.	133.	75.	29.	12.
12.0	13	770	683	HLD4	908.2	9	145.4	130.2	A	775.	106.	396.	74.	50.	15.
									B	812.	92.	312.	64.	64.	17.
									C	951.	99.	403.	73.	18.	10.
									D	886.	109.	388.	79.	39.	13.
12.0	14	770	683	HLD4	908.4	12	145.4	130.2	A	1158.	77.	629.	57.	75.	13.
									B	1106.	72.	548.	54.	36.	9.
									C	981.	76.	406.	55.	44.	10.
									D	1025.	84.	351.	51.	42.	10.
-12.0	15	770	683	HLD4	908.4	12	229.8	214.6	A	1204.	68.	601.	56.	56.	12.
									B	1058.	66.	553.	52.	45.	12.
									C	933.	67.	359.	50.	31.	9.
									D	949.	68.	377.	50.	34.	9.
12.0	16	680	604	HLD4	818.1	12	147.0	131.8	A	725.	69.	305.	46.	33.	8.
									B	625.	79.	300.	49.	35.	8.
									C	721.	80.	358.	59.	27.	7.
									D	863.	82.	191.	56.	8.	4.

P LAB ANGLE	PT NO	NOM E0	LAB K	CONF	MAGNET P	AP HT	GAM B ANGLE	GAM C ANGLE	MOM CH	COUNTING RATES AND ERRORS FOR 10**16 MEV PROTON		PROTON.GAM		PROTON.2GAM	
16.0	1	1320	1171	OLU4	1380.7	12	120.4	105.2	A	356.	17.	201.	15.	54.	6.
									B	354.	18.	209.	16.	42.	6.
									C	436.	19.	217.	16.	46.	6.
									D	501.	21.	286.	18.	58.	6.
16.0	2	1200	1062	OLD4	1274.8	12	123.1	107.9	A	356.	17.	201.	15.	54.	6.
									B	792.	50.	510.	39.	80.	13.
									C	949.	50.	529.	45.	89.	14.
									D	1002.	53.	423.	46.	69.	12.
16.0	3	1200	1062	OLD4	1274.8	12	123.1	107.9	A	703.	32.	440.	30.	69.	10.
									B	795.	36.	470.	32.	116.	12.
									C	990.	39.	554.	34.	97.	11.
									D	1074.	38.	579.	34.	127.	13.
16.0	4	1200	1062	OLU4	1275.7	12	123.1	107.9	A	598.	26.	388.	23.	73.	10.
									B	748.	31.	443.	27.	89.	11.
									C	885.	34.	572.	29.	112.	11.
									D	940.	37.	525.	32.	90.	10.
16.0	5	1080	963	OLD4	1177.1	12	125.5	110.3	A	1068.	40.	668.	35.	121.	12.
									B	1050.	40.	623.	33.	101.	13.
									C	1079.	40.	588.	35.	92.	11.
									D	990.	40.	503.	33.	71.	9.
-16.0	6	1080	965	HLUV	1176.4	12	249.7	234.5	A	1508.	46.	826.	31.	22.	5.
									B	1532.	52.	721.	36.	8.	3.
									C	1536.	49.	705.	28.	9.	3.
									D	1745.	49.	718.	29.	12.	4.
-16.0	7	980	873	HLD4	1086.1	12	247.4	232.2	A	1398.	61.	857.	51.	134.	17.
									B	1586.	62.	980.	51.	144.	15.
									C	1583.	64.	848.	53.	120.	14.
									D	1673.	65.	827.	53.	121.	16.
16.0	8	870	772	HLD4	981.0	12	130.4	115.2	A	1672.	74.	999.	61.	150.	17.
									B	1735.	77.	959.	63.	103.	15.
									C	1626.	74.	853.	60.	100.	14.
									D	1694.	78.	805.	58.	78.	13.
16.0	9	870	772	HLD4	981.2	12	130.4	115.2	A	1555.	64.	973.	53.	114.	15.
									B	1807.	65.	1027.	54.	138.	16.
									C	1688.	69.	885.	52.	120.	16.
									D	1708.	69.	737.	50.	89.	15.
16.0	10	870	772	HLU4	981.0	12	128.8	113.6	A	1669.	73.	1060.	63.	129.	16.
									B	1753.	74.	954.	61.	119.	15.
									C	1715.	78.	724.	61.	96.	16.
									D	1621.	77.	755.	62.	68.	15.
-16.0	11	870	772	HLD4	981.0	12	244.8	229.6	A	1456.	61.	889.	53.	116.	15.
									B	1516.	64.	885.	55.	134.	16.
									C	1565.	66.	773.	56.	96.	14.
									D	1651.	64.	666.	53.	88.	13.
-16.0	12	870	772	HLD4	981.2	12	244.8	229.6	A	1617.	49.	943.	42.	122.	11.
									B	1590.	53.	978.	43.	111.	12.
									C	1698.	53.	886.	43.	113.	11.
									D	1673.	54.	688.	43.	85.	11.
-16.0	13	870	772	HLUV	979.3	12	244.8	229.6	A	1522.	52.	735.	29.	12.	4.
									B	1792.	56.	770.	30.	111.	12.
									C	1583.	59.	670.	28.	113.	11.
									D	1768.	57.	598.	27.	85.	11.
16.0	14	770	683	HLD4	885.8	12	132.6	117.4	A	1144.	77.	709.	58.	98.	14.
									B	1146.	69.	535.	52.	41.	12.
									C	1080.	69.	429.	51.	37.	9.
									D	1254.	71.	392.	50.	40.	9.
16.0	15	770	683	HLD4	885.9	12	132.6	117.4	A	1315.	71.	743.	53.	98.	18.
									B	1158.	71.	671.	52.	59.	14.
									C	1170.	75.	485.	52.	50.	10.
									D	1265.	76.	495.	52.	33.	8.
16.0	16	770	683	HLD4	885.9	12	132.6	117.4	A	1272.	77.	612.	63.	79.	17.
									B	1180.	67.	500.	53.	59.	11.
									C	1118.	74.	570.	51.	54.	10.
									D	1130.	80.	398.	57.	76.	12.
-16.0	17	770	683	HLD4	885.9	12	242.6	227.4	A	1340.	62.	690.	52.	79.	14.
									B	1064.	63.	581.	49.	68.	13.
									C	1017.	63.	525.	51.	71.	16.
									D	1152.	64.	431.	51.	42.	9.
16.0	18	680	604	HLD4	798.6	12	134.6	119.4	A	657.	99.	457.	53.	66.	11.
									B	916.	96.	457.	49.	43.	9.
									C	898.	103.	443.	71.	25.	7.
									D	1143.	103.	406.	75.	21.	7.

P LAB ANGLE	PT NO	NOM EO	LAB K	CONF	MAGNET P	AP HT	GAM B ANGLE	GAM C ANGLE	MOM CH	COUNTING RATES AND ERRORS FOR 10**16 MEV PROTON		PROTON.GAM		PROTON.2GAM	
20.5	1	1320	1171	OLU4	1319.0	12	106.0	90.8	A	274.	20.	179.	17.	47.	8.
									B	359.	22.	230.	21.	70.	15.
									C	359.	23.	230.	18.	59.	9.
									D	453.	25.	266.	21.	54.	10.
20.5	2	1200	1062	OLU4	1220.0	12	108.8	93.6	A	567.	27.	393.	24.	94.	10.
									B	719.	29.	455.	27.	127.	12.
									C	867.	33.	518.	30.	140.	12.
									D	938.	33.	507.	29.	110.	12.
-20.5	3	1080	963	HLDV	1127.9	12	263.7	248.5	A	1333.	60.	808.	43.	42.	9.
									B	1560.	62.	881.	42.	33.	8.
									C	1369.	61.	716.	37.	22.	6.
									D	1547.	59.	682.	35.	19.	6.
-20.5	4	980	873	HLD4	1042.3	12	261.2	246.0	A	1409.	60.	968.	56.	182.	20.
									B	1501.	64.	885.	57.	166.	20.
									C	1481.	65.	960.	61.	140.	19.
									D	1541.	64.	855.	58.	159.	20.
-20.5	5	870	772	HLDV	942.5	12	258.4	243.2	A	1647.	117.	957.	72.	29.	12.
									B	1780.	113.	857.	69.	14.	8.
									C	1734.	118.	753.	68.	9.	7.
									D	1627.	121.	701.	67.	159.	20.
-20.5	6	770	683	HLD4	852.6	12	255.8	240.6	A	1632.	65.	952.	55.	138.	17.
									B	1305.	66.	772.	51.	107.	15.
									C	1207.	68.	625.	54.	112.	15.
									D	1228.	70.	518.	52.	80.	13.
-20.5	7	770	683	HLDV	851.6	12	255.8	240.6	A	1372.	79.	684.	46.	14.	6.
									B	1277.	80.	585.	44.	107.	15.
									C	1056.	82.	479.	36.	112.	15.
									D	1276.	78.	381.	40.	80.	13.
-20.5	8	680	604	HLDV	768.3	12	253.6	238.4	A	1116.	74.	487.	36.	14.	6.
									B	1022.	84.	434.	41.	107.	15.
									C	1025.	96.	494.	42.	112.	15.
									D	1289.	96.	466.	35.	80.	13.
25.0	1	1320	1171	OLU4	1246.0	12	93.4	78.2	A	209.	19.	145.	15.	46.	9.
									B	305.	19.	205.	17.	72.	10.
									C	309.	23.	188.	20.	52.	10.
									D	379.	25.	254.	23.	72.	13.
25.0	2	1200	1062	OLU4	1155.2	12	96.3	81.1	A	438.	24.	285.	21.	75.	12.
									B	618.	29.	368.	24.	123.	12.
									C	769.	31.	443.	27.	117.	13.
									D	818.	31.	485.	27.	125.	12.
25.0	3	1080	963	OLU4	1070.4	12	99.0	83.8	A	821.	32.	565.	28.	161.	14.
									B	816.	32.	525.	29.	135.	13.
									C	850.	33.	548.	30.	159.	15.
									D	800.	34.	497.	30.	120.	13.
-25.0	4	980	873	HLD4	991.3	12	273.6	258.4	A	1193.	53.	883.	48.	201.	20.
									B	1308.	54.	933.	47.	222.	20.
									C	1352.	61.	834.	53.	167.	20.
									D	1489.	63.	966.	54.	191.	18.
-25.0	5	870	772	HLDV	898.4	12	270.6	255.4	A	1573.	103.	834.	71.	33.	13.
									B	1746.	119.	1032.	74.	-2.	22.
									C	1846.	117.	945.	71.	23.	11.
									D	1846.	110.	859.	65.	9.	7.
-25.0	6	770	683	HLDV	813.4	12	267.9	252.7	A	1571.	87.	914.	52.	16.	6.
									B	1695.	83.	839.	50.	11.	5.
									C	1475.	81.	645.	42.	27.	8.
									D	1466.	75.	602.	40.	7.	4.
-25.0	7	680	604	HLDV	734.8	12	265.6	250.4	A	1171.	83.	624.	42.	15.	6.
									B	1335.	86.	638.	44.	11.	5.
									C	1513.	92.	569.	48.	27.	8.
									D	1547.	94.	644.	43.	7.	4.

P LAB ANGLE	PT NO	NOM EO	LAB K	CONF	MAGNET P	AP HT	GAM B ANGLE	GAM C ANGLE	MOM CH	COUNTING RATES AND ERRORS FOR 10**16 MEV PROTON		PROTON.GAM		PROTON.2GAM	
29.5	1	1320	1171	OLD4	1163.4	12	82.6	67.4	A	182.	20.	112.	17.	49.	9.
									B	224.	22.	121.	20.	32.	10.
									C	255.	25.	179.	20.	53.	9.
									D	313.	29.	213.	26.	64.	14.
29.5	2	1320	1171	OLU4	1164.7	12	82.6	67.4	A	163.	16.	142.	15.	42.	8.
									B	208.	18.	177.	17.	58.	9.
									C	280.	22.	201.	19.	78.	10.
									D	380.	23.	257.	21.	90.	11.
29.5	3	1200	1062	OLD4	1082.1	12	85.4	70.2	A	365.	26.	324.	23.	116.	14.
									B	493.	28.	368.	25.	132.	15.
									C	551.	32.	409.	27.	129.	13.
									D	592.	31.	419.	28.	127.	14.
29.5	4	1200	1063	HLDV	1083.3	12	85.4	70.2	A	392.	38.	297.	26.	38.	9.
									B	725.	44.	427.	33.	38.	9.
									C	916.	51.	566.	37.	71.	12.
									D	1121.	54.	617.	38.	52.	12.
29.5	5	1080	963	OLD4	1005.8	12	88.1	72.9	A	628.	31.	472.	26.	136.	13.
									B	600.	32.	476.	27.	139.	13.
									C	609.	31.	457.	26.	143.	13.
									D	636.	33.	446.	30.	130.	12.
29.5	6	980	873	HLD4	933.7	12	90.6	75.4	A	1110.	67.	768.	61.	213.	28.
									B	1155.	67.	838.	59.	201.	26.
									C	1257.	72.	835.	65.	209.	27.
									D	1364.	77.	871.	68.	252.	29.
29.5	7	870	773	HLDV	848.1	12	93.6	78.4	A	1410.	97.	932.	68.	28.	12.
									B	1530.	102.	983.	73.	42.	14.
									C	1873.	110.	1146.	80.	42.	14.
									D	1926.	106.	1065.	73.	47.	15.
29.5	8	870	773	HLDV	848.1	12	93.6	78.4	A	1366.	103.	839.	66.	36.	13.
									B	1668.	106.	1024.	72.	22.	10.
									C	1756.	112.	960.	79.	17.	9.
									D	1609.	114.	902.	68.	36.	13.
29.5	9	770	683	HLD4	769.9	12	96.3	81.1	A	1637.	72.	1075.	59.	227.	22.
									B	1734.	75.	1139.	63.	219.	22.
									C	1417.	70.	939.	53.	168.	20.
									D	1472.	67.	896.	55.	142.	18.
29.5	10	680	605	HLDV	695.9	12	98.6	83.4	A	1065.	92.	642.	50.	20.	7.
									B	1483.	85.	789.	47.	15.	6.
									C	1174.	90.	693.	44.	12.	6.
									D	1370.	86.	677.	44.	25.	8.
34.0	1	1320	1172	OLD4	1076.3	12	73.2	58.0	A	140.	12.	111.	10.	46.	5.
									B	162.	15.	135.	11.	48.	6.
									C	231.	15.	168.	13.	64.	6.
									D	292.	15.	190.	13.	72.	8.
34.0	2	1200	1062	OLD4	1004.3	12	75.8	60.6	A	336.	23.	248.	19.	100.	12.
									B	363.	25.	285.	20.	93.	11.
									C	497.	26.	366.	22.	140.	13.
									D	528.	28.	406.	26.	141.	14.
34.0	3	1200	1063	HLD4	1004.6	12	75.8	60.6	A	376.	24.	311.	19.	106.	11.
									B	553.	27.	409.	23.	150.	13.
									C	839.	31.	565.	26.	208.	14.
									D	844.	32.	595.	27.	193.	13.
34.0	4	1080	963	OLD4	935.7	12	78.3	63.1	A	588.	32.	445.	28.	178.	18.
									B	470.	33.	411.	26.	131.	15.
									C	590.	33.	441.	28.	137.	15.
									D	641.	32.	454.	27.	153.	14.
34.0	5	1080	964	HNDV	935.9	12	78.3	63.1	A	803.	54.	560.	39.	85.	17.
									B	918.	58.	608.	40.	91.	15.
									C	1024.	57.	586.	38.	55.	11.
									D	1066.	63.	543.	41.	64.	12.
34.0	6	980	874	HLD4	870.5	12	80.8	65.6	A	870.	47.	678.	37.	218.	20.
									B	893.	55.	694.	45.	213.	20.
									C	1205.	57.	913.	44.	264.	21.
									D	1301.	60.	905.	52.	248.	26.
34.0	7	870	773	HLDV	792.7	12	83.6	68.4	A	1513.	75.	979.	53.	117.	17.
									B	1825.	79.	1125.	53.	114.	16.
									C	1800.	84.	1045.	56.	70.	13.
									D	1941.	84.	1118.	57.	76.	17.
34.0	8	770	683	HLD4	721.1	12	86.2	71.0	A	1971.	77.	1392.	64.	350.	25.
									B	1744.	75.	1204.	63.	272.	26.
									C	1579.	73.	1087.	54.	239.	22.
									D	1635.	70.	1029.	56.	239.	25.
34.0	9	680	605	HNU4	652.8	12	88.6	73.4	A	1558.	109.	1064.	65.	209.	23.
									B	1708.	115.	1040.	80.	213.	33.
									C	1849.	117.	1089.	82.	206.	22.
									D	1732.	131.	1186.	76.	242.	24.

P LAB ANGLE	PT NO	NOM E0	LAB K	CONF	MAGNET P	AP HT	GAM B ANGLE	GAM C ANGLE	MOM CH	COUNTING RATES AND ERRORS FOR 10**16 MEV PROTON		PROTON.GAM		PROTON.2GAM	
39.0	1	1320	1172	OLD4	975.6	12	64.0	48.8	A	145.	15.	87.	12.	44.	6.
									B	189.	19.	149.	17.	64.	9.
									C	215.	19.	157.	16.	55.	9.
									D	239.	23.	215.	18.	89.	9.
39.0	2	1200	1063	HLD4	913.2	12	66.4	51.2	A	336.	61.	334.	49.	113.	30.
									B	525.	63.	389.	47.	144.	27.
									C	528.	66.	401.	57.	187.	31.
									D	784.	78.	582.	63.	250.	40.
39.0	3	1200	1062	OLD4	912.8	12	66.4	51.2	A	270.	20.	206.	16.	79.	10.
									B	311.	23.	233.	19.	101.	11.
									C	422.	25.	335.	21.	122.	12.
									D	478.	24.	362.	20.	140.	11.
39.0	4	1200	1063	HLD4	913.2	12	66.4	51.2	A	359.	23.	303.	18.	118.	10.
									B	551.	26.	436.	22.	185.	13.
									C	616.	29.	452.	23.	157.	13.
									D	683.	32.	518.	27.	193.	16.
39.0	5	1080	964	OLD4	852.9	12	68.8	53.6	A	454.	39.	367.	32.	129.	19.
									B	423.	41.	303.	34.	134.	20.
									C	531.	43.	425.	36.	154.	18.
									D	563.	44.	392.	34.	169.	19.
39.0	6	980	874	HLD4	795.5	12	71.0	55.8	A	726.	53.	566.	40.	191.	22.
									B	844.	55.	676.	45.	206.	24.
									C	1051.	57.	793.	45.	249.	23.
									D	1297.	62.	1018.	48.	368.	26.
39.0	7	870	773	HLDV	726.3	12	73.7	58.5	A	1451.	75.	1043.	50.	120.	17.
									B	1775.	81.	1159.	53.	119.	17.
									C	1846.	88.	1207.	61.	144.	21.
									D	1970.	85.	1130.	53.	87.	14.
39.0	8	770	684	HNDV	661.6	12	76.1	60.9	A	1904.	99.	1359.	59.	122.	18.
									B	1937.	96.	1327.	59.	78.	14.
									C	1815.	91.	1159.	56.	76.	14.
									D	1470.	94.	924.	51.	90.	15.
39.0	9	680	605	HNU4	600.4	12	78.3	63.1	A	1424.	102.	1093.	78.	304.	30.
									B	1571.	105.	1179.	77.	255.	33.
									C	1400.	103.	1119.	74.	263.	31.
									D	1644.	99.	1182.	73.	196.	25.
41.9	1	980	873	HLU4	749.4	12	65.8	50.6	A	769.	64.	581.	52.	208.	30.
									B	783.	86.	577.	62.	208.	30.
									C	918.	87.	767.	69.	256.	33.
									D	1227.	105.	1006.	76.	373.	40.
41.9	2	980	873	HLDV	749.4	12	65.8	50.6	A	763.	63.	536.	39.	113.	16.
									B	816.	63.	572.	40.	120.	17.
									C	941.	71.	655.	44.	78.	20.
									D	1318.	70.	817.	47.	139.	18.
41.9	3	870	772	HNDV	685.3	12	68.4	53.2	A	1551.	76.	1011.	53.	114.	17.
									B	1702.	85.	1181.	56.	158.	19.
									C	1536.	93.	1123.	58.	148.	19.
									D	1782.	82.	1131.	54.	133.	18.
41.9	4	770	683	HNDV	625.0	12	70.6	55.4	A	1972.	99.	1361.	58.	151.	19.
									B	1611.	94.	1096.	54.	97.	16.
									C	1548.	93.	1050.	52.	110.	17.
									D	1200.	94.	778.	45.	36.	10.
41.9	5	680	604	HNU4	567.6	12	72.7	57.5	A	1330.	121.	1068.	88.	283.	42.
									B	1403.	108.	846.	83.	233.	37.
									C	1531.	124.	1117.	88.	255.	38.
									D	1341.	123.	992.	88.	153.	28.
41.9	6	680	604	HNDV	567.6	12	72.7	57.5	A	1547.	88.	901.	50.	62.	13.
									B	1371.	99.	877.	51.	49.	11.
									C	1310.	101.	880.	54.	10.	14.
									D	1459.	91.	875.	48.	35.	10.

P LAB ANGLE	PT NO	NOM E0	LAB K	CONF	MAGNET P	AP HT	GAM B ANGLE	GAM C ANGLE	MCM CH	COUNTING RATES AND ERRORS FOR 10**16 MEV PROTON		PROTON.GAM		PROTON.2GAM	
44.0	1	1200	1063	HLD4	818.9	12	58.1	42.9	A	404.	27.	344.	20.	127.	11.
									B	466.	29.	355.	23.	158.	13.
									C	544.	30.	457.	23.	166.	12.
									D	612.	30.	467.	23.	191.	14.
44.0	2	1200	1063	HLD4	818.9	12	58.1	42.9	A	347.	26.	257.	19.	131.	12.
									B	485.	27.	349.	21.	144.	13.
									C	591.	28.	441.	23.	181.	14.
									D	565.	29.	446.	23.	184.	13.
44.0	3	1080	964	HLDV	767.1	12	60.2	45.0	A	571.	34.	373.	23.	79.	12.
									B	640.	37.	441.	23.	119.	11.
									C	589.	40.	408.	23.	84.	10.
									D	608.	42.	426.	24.	66.	11.
44.0	4	980	874	HLD4	716.9	12	62.3	47.1	A	552.	54.	432.	39.	163.	22.
									B	713.	59.	574.	41.	239.	22.
									C	857.	60.	703.	44.	267.	23.
									D	1022.	65.	756.	51.	262.	29.
44.0	5	870	773	HNDV	656.0	12	64.7	49.5	A	1305.	80.	914.	51.	148.	19.
									B	1607.	86.	1134.	53.	152.	19.
									C	1716.	84.	1147.	54.	132.	18.
									D	1757.	84.	1070.	55.	158.	22.
44.0	6	770	684	HNDV	598.6	12	66.9	51.7	A	1780.	88.	1139.	57.	102.	16.
									B	1537.	90.	1047.	54.	125.	18.
									C	1465.	86.	964.	52.	94.	15.
									D	1267.	88.	750.	48.	64.	13.
44.0	7	680	604	HND4	544.4	9	68.8	53.6	A	980.	67.	755.	44.	207.	20.
									B	925.	64.	706.	41.	155.	17.
									C	846.	62.	599.	43.	134.	18.
									D	942.	65.	628.	47.	161.	18.
49.0	1	1320	1171	HLDV	768.7	12	50.7	35.5	A	168.	45.	143.	25.	41.	14.
									B	329.	40.	226.	23.	48.	10.
									C	345.	52.	326.	29.	92.	14.
									D	532.	45.	348.	28.	99.	15.
49.0	2	1200	1062	HLD4	722.6	12	50.8	35.6	A	458.	64.	345.	51.	169.	32.
									B	565.	64.	420.	53.	199.	32.
									C	504.	67.	393.	51.	154.	30.
									D	447.	64.	364.	47.	179.	30.
49.0	3	1080	963	HNDV	678.3	12	52.6	37.4	A	536.	54.	336.	35.	104.	18.
									B	486.	54.	370.	28.	90.	14.
									C	509.	53.	358.	30.	74.	13.
									D	557.	55.	334.	31.	63.	12.
49.0	4	980	873	HNDV	634.8	12	54.4	39.2	A	452.	61.	310.	31.	91.	14.
									B	598.	67.	433.	36.	119.	17.
									C	589.	74.	353.	43.	68.	20.
									D	884.	69.	554.	36.	115.	16.
49.0	5	870	773	HNDV	582.3	12	56.5	41.3	A	1109.	74.	727.	45.	145.	18.
									B	1399.	77.	913.	48.	172.	20.
									C	1474.	78.	931.	50.	205.	22.
									D	1254.	77.	844.	46.	165.	20.
54.0	1	1320	1171	HNDV	665.2	12	50.7	35.5	A	177.	47.	106.	21.	14.	6.
									B	241.	45.	157.	19.	23.	7.
									C	297.	51.	215.	24.	25.	7.
									D	457.	48.	280.	25.	30.	8.
54.0	2	1200	1062	HNDV	626.9	12	50.7	35.5	A	413.	53.	289.	27.	47.	10.
									B	488.	57.	349.	31.	30.	8.
									C	590.	55.	362.	33.	49.	10.
									D	409.	59.	256.	26.	44.	10.
54.0	3	1080	963	HNDV	589.1	12	50.7	35.5	A	439.	63.	310.	32.	61.	12.
									B	524.	64.	368.	29.	66.	12.
									C	477.	63.	304.	32.	64.	12.
									D	375.	63.	251.	26.	44.	10.
54.0	4	980	873	HNDV	552.1	12	50.7	35.5	A	331.	58.	202.	24.	26.	8.
									B	373.	62.	277.	29.	40.	9.
									C	473.	68.	311.	30.	55.	11.
									D	609.	64.	299.	35.	74.	13.

Table 15

Counting rates for excitation curve data. See text for definitions.

P LAB ANGLE	PT NO	NOM E0	LAB K	CONF	MAGNET P	AP HT	GAM B ANGLE	GAM C ANGLE	MOM CH	COUNTING RATES AND ERRORS FOR 10**16 MEV PROTON		PROTON.GAM		PROTON.2GAM	
16.0	1	1200	772	OLD4	981.2	12	130.4	115.2	A	1869.	153.	372.	108.	50.	20.
									B	1983.	137.	460.	90.	29.	15.
									C	1872.	162.	418.	95.	66.	22.
									D	1916.	140.	434.	87.	65.	22.
-16.0	2	1080	772	HLUV	980.3	12	244.8	229.6	A	2367.	67.	647.	29.	6.	2.
									B	2457.	68.	559.	28.	29.	15.
									C	2540.	68.	602.	27.	66.	22.
									D	2529.	66.	505.	25.	65.	22.
-16.0	3	980	772	HLUV	979.8	12	244.8	229.6	A	2039.	60.	728.	29.	4.	2.
									B	2166.	63.	672.	28.	29.	15.
									C	2196.	65.	640.	29.	12.	4.
									D	2110.	64.	542.	26.	65.	22.
-16.0	4	920	772	HLUV	979.5	12	244.8	229.6	A	1792.	63.	759.	35.	20.	5.
									B	1928.	65.	717.	32.	1.	5.
									C	1936.	65.	638.	31.	12.	4.
									D	1884.	68.	546.	29.	65.	22.
-16.0	5	850	772	HLD4	981.2	12	244.8	229.6	A	1562.	54.	896.	46.	118.	12.
									B	1486.	60.	942.	48.	132.	14.
									C	1593.	63.	873.	45.	122.	13.
									D	1608.	63.	776.	49.	91.	13.
-16.0	6	830	772	HLD4	981.2	12	244.8	229.6	A	1307.	51.	784.	42.	118.	12.
									B	1513.	53.	825.	46.	94.	12.
									C	1451.	57.	850.	45.	84.	12.
									D	1436.	55.	788.	45.	95.	11.
-16.0	7	820	772	HLUV	979.0	12	244.8	229.6	A	1247.	64.	630.	41.	118.	12.
									B	1471.	68.	776.	40.	94.	12.
									C	1488.	67.	734.	39.	19.	6.
									D	1379.	66.	585.	36.	95.	11.
-16.0	8	810	772	HLD4	981.2	12	244.8	229.6	A	839.	45.	513.	34.	72.	9.
									B	1360.	54.	857.	44.	111.	12.
									C	1475.	55.	830.	43.	125.	12.
									D	1289.	57.	672.	44.	71.	9.
-16.0	9	790	772	HLD4	981.2	12	244.8	229.6	A	262.	31.	166.	21.	24.	6.
									B	941.	48.	565.	38.	76.	10.
									C	1356.	55.	790.	46.	89.	11.
									D	1184.	55.	665.	43.	64.	12.
-16.0	10	770	772	HLD4	981.2	12	244.8	229.6	A	51.	26.	11.	7.	-0.	0.
									B	363.	39.	201.	28.	21.	5.
									C	1094.	54.	579.	45.	80.	11.
									D	1200.	54.	669.	45.	73.	10.
-16.0	11	770	772	HLUV	978.8	12	244.8	229.6	A	2.	26.	17.	6.	-0.	0.
									B	529.	37.	270.	19.	21.	5.
									C	1228.	49.	576.	28.	80.	11.
									D	1260.	53.	639.	29.	73.	10.
16.0	12	762	772	HLD4	981.2	12	130.4	115.2	A	39.	32.	17.	7.	-0.	0.
									B	242.	50.	136.	31.	15.	5.
									C	1114.	60.	560.	45.	91.	13.
									D	1266.	64.	658.	52.	89.	13.
-16.0	13	750	772	HLD4	981.2	12	244.8	229.6	A	39.	21.	13.	8.	-0.	0.
									B	46.	32.	47.	14.	11.	5.
									C	516.	37.	263.	27.	39.	8.
									D	1020.	48.	598.	40.	87.	11.
-16.0	14	730	772	HLD4	981.2	12	244.8	229.6	A	39.	21.	13.	8.	-0.	0.
									B	8.	26.	47.	14.	11.	5.
									C	95.	28.	68.	12.	7.	3.
									D	456.	41.	256.	29.	27.	8.
-16.0	15	710	772	HLD4	981.2	12	244.8	229.6	A	9.	23.	14.	11.	1.	1.
									B	60.	22.	-3.	5.	-0.	0.
									C	14.	27.	-9.	12.	1.	1.
									D	113.	33.	74.	16.	7.	3.
-16.0	16	690	772	HLD4	981.2	12	244.8	229.6	A	28.	19.	8.	4.	3.	3.
									B	11.	22.	16.	10.	5.	3.
									C	18.	24.	0.	9.	3.	3.
									D	15.	28.	6.	8.	5.	3.
-16.0	17	670	772	HLD4	981.2	12	244.8	229.6	A	61.	16.	17.	7.	10.	4.
									B	30.	19.	-1.	5.	3.	2.
									C	13.	24.	6.	5.	5.	3.
									D	34.	27.	2.	8.	2.	2.

NOM EO = $(E_o)_{meter}$

LAB K = nominal central laboratory photon energy.

CONF = four characters describing the configuration where

(1) = H if magnet is in HEMA configuration.
= O if magnet is in ØUTR configuration.

(2) = L if 1/4 inch of lead in front of S3.
= N if no lead in front of S3.

(3) = D if hydrogen target large horn is downstream.
= U if hydrogen target large horn is upstream.

(4) = 4 if gamma counters are in four counter configuration.
= V if gamma counters are in veto configuration.

MAGNET P = central momentum to which magnet was set.

AP HT = aperture counter height in inches (width was 2.75 inches).

GAM B ANGLE = angle of γB w.r.t. synchrotron beam measured in opposite direction from proton angle.

$$\theta_{\gamma A} = \begin{cases} \theta_{\gamma B} + 15^{\circ} & \text{in four counter configuration} \\ \theta_{\gamma B} & \text{in veto configuration} \end{cases}$$

GAM C ANGLE = angle of γC w. r. t. synchrotron beam is opposite direction from proton angle.

$$\theta_{\gamma D} = \begin{cases} \theta_{\gamma C} - 15^{o} & \text{in four counter configuration} \\ \theta_{\gamma C} & \text{in veto configuration} \end{cases}$$

MOM CH = momentum channel

COUNTING RATES = counting rates and statistical errors in counts per 10^{16} MeV total energy in the beam.

PROTON = P signature

PROTON· GAM = P· γ signature

PROTON· 2 GAM = P· 2γ signature

B. Computed Quantities

Tables 16 and 17 contain intermediate computed results for the cross section and excitation data, respectively. The computed results given here are for the data tabulated in the previous section. The proton angle and point number are useful in cross referencing to determine the parameters for any particular calculation.

Columns in the table list the following quantities:

P LAB ANGLE = proton laboratory angle, i. e., spectrometer angle.

PT NO = point number

LAB K CH = laboratory photon energy for each momentum channel.

PI CM ANGLE = pion c. m. angle.

Table 16

Computed quantities for cross section data. See text for definitions.

P LAB ANGLE	PT NO	LAB K CM	PI CM ANGLE	KAPPA	RMS DK	S3 PC LOSS AND ERROR		GAMMA PC EFF AND ERRORS P.G		P.2G		PC NA
4.0	1	1208	170.2	192.5	21.5	9.3	0.4	33.1	0.7	2.1	0.2	13.5
		1178	170.3	186.9	20.9	10.6	0.6	34.6	1.1	1.9	0.3	13.5
		1151	170.3	183.4	20.7	10.1	0.4	33.5	0.7	2.7	0.2	13.5
		1124	170.4	182.4	20.9	9.5	0.4	33.6	0.7	2.2	0.2	13.5
4.0	2	1208	170.4	192.5	20.1	9.3	0.4	33.1	0.7	2.1	0.2	13.0
		1069	170.5	199.2	19.6	12.1	1.0	32.2	1.6	1.8	0.4	13.0
		1044	170.5	195.6	19.5	8.8	0.9	33.1	1.6	2.5	0.5	13.0
		1020	170.5	194.6	19.7	11.4	0.8	32.2	1.4	2.7	0.5	13.0
4.0	3	1096	170.4	205.2	20.1	10.2	0.5	33.2	0.9	2.8	0.3	13.0
		1069	170.5	199.2	19.6	10.9	0.6	33.0	1.1	2.3	0.3	13.0
		1044	170.5	195.6	19.5	9.4	0.6	33.4	1.0	2.8	0.4	13.0
		1020	170.5	194.6	19.7	10.1	0.6	31.9	1.0	2.5	0.3	13.0
4.0	4	994	170.6	220.4	18.9	8.9	0.8	33.4	1.4	2.9	0.5	12.6
		970	170.6	214.4	18.5	10.7	0.7	30.6	1.1	2.3	0.3	12.6
		947	170.6	210.7	18.4	10.7	0.6	31.0	1.0	2.5	0.3	12.6
		925	170.7	209.7	18.6	9.9	0.6	30.8	1.0	2.9	0.3	12.6
4.0	5	994	170.6	220.4	18.9	10.5	0.7	30.2	1.1	3.0	0.5	12.6
		970	170.6	214.4	18.5	8.9	0.7	29.2	1.2	2.3	0.3	12.6
		947	170.6	210.7	18.4	10.0	0.9	29.5	1.5	2.5	0.3	12.6
		925	170.7	209.7	18.6	10.1	0.7	29.4	1.1	2.9	0.3	12.6
4.0	6	915	170.7	335.8	15.0	-0.0	0.0	31.5	0.6	3.1	0.2	11.5
		885	170.7	329.7	13.9	-0.0	0.0	30.6	0.5	3.1	0.2	11.5
		858	170.8	322.4	13.7	0.0	0.0	31.4	0.7	3.4	0.3	11.5
		832	170.8	316.0	14.1	0.0	0.0	29.0	0.5	3.1	0.2	11.5
4.0	7	808	170.8	366.0	13.6	-0.0	0.0	26.4	1.1	3.1	0.2	11.0
		782	170.9	359.1	12.7	0.0	0.0	26.0	1.0	3.1	0.2	11.0
		758	170.9	351.2	12.6	0.0	0.0	27.7	1.2	3.4	0.3	11.0
		736	170.9	344.3	12.9	-0.0	0.0	25.9	1.0	3.1	0.2	11.0
4.0	8	716	171.0	400.2	12.5	0.0	0.0	27.8	0.9	3.0	0.3	10.6
		693	171.0	393.1	11.8	0.0	0.0	25.2	0.8	2.6	0.3	10.6
		672	171.0	384.7	11.7	0.0	0.0	25.2	0.8	2.4	0.3	10.6
		652	171.0	377.3	12.0	0.1	0.0	24.4	0.7	2.1	0.2	10.6
4.0	9	716	171.0	400.2	12.5	0.0	0.0	24.1	1.2	2.8	0.5	10.6
		693	171.0	393.1	11.8	0.0	0.0	24.6	1.1	2.4	0.4	10.6
		672	171.0	384.7	11.7	0.1	0.1	25.3	1.0	3.2	0.4	10.6
		652	171.0	377.3	12.0	0.0	0.0	22.3	1.5	3.0	0.6	10.6
4.0	10	633	171.1	437.9	11.5	0.0	0.0	19.3	2.1	2.8	0.5	10.4
		612	171.1	430.6	11.0	0.0	0.0	22.3	1.7	2.4	0.4	10.4
		594	171.1	421.6	11.0	0.0	0.0	19.7	1.7	3.2	0.4	10.4
		576	171.1	413.8	11.3	0.2	0.1	21.6	1.3	3.0	0.6	10.4
8.0	1	1208	160.5	285.5	21.9	9.3	0.7	58.0	1.3	0.4	0.2	13.5
		1179	160.6	277.2	21.3	8.7	0.7	58.6	1.3	0.4	0.2	13.5
		1151	160.7	272.2	21.1	10.5	0.7	56.3	1.3	0.6	0.2	13.5
		1124	160.8	270.7	21.3	10.4	0.7	54.2	1.3	0.6	0.2	13.5
8.0	2	1096	160.9	304.6	20.5	9.8	0.7	56.1	1.3	0.8	0.2	13.0
		1069	160.9	295.8	20.0	9.9	0.7	54.0	1.3	0.7	0.2	13.0
		1044	161.0	290.4	19.9	10.5	0.6	56.2	1.2	0.7	0.2	13.0
		1020	161.1	288.9	20.0	9.7	0.6	55.3	1.1	0.5	0.1	13.0
8.0	3	1096	160.9	304.6	20.5	11.0	0.7	55.2	1.2	0.6	0.2	13.0
		1069	160.9	295.8	20.0	9.9	0.7	56.6	1.2	0.7	0.2	13.0
		1044	161.0	290.4	19.9	9.8	0.5	55.5	1.0	0.4	0.1	13.0
		1020	161.1	288.9	20.0	9.8	0.5	52.1	1.0	0.6	0.1	13.0
8.0	4	994	161.2	327.3	19.3	10.0	0.6	54.4	1.2	0.6	0.2	12.5
		970	161.2	318.4	18.8	9.7	0.4	53.0	0.8	0.8	0.1	12.5
		947	161.3	312.9	18.8	10.4	0.6	51.8	1.0	0.9	0.2	12.5
		925	161.4	311.5	19.0	10.4	0.5	51.6	0.9	0.6	0.1	12.5
8.0	5	915	161.4	498.6	15.2	-0.0	0.0	52.4	0.9	0.6	0.1	11.4
		886	161.5	489.8	14.1	0.0	0.0	49.1	0.9	0.7	0.1	11.4
		858	161.6	479.0	13.9	0.0	0.0	50.2	0.7	0.7	0.1	11.4
		832	161.6	469.5	14.3	-0.0	0.0	48.3	0.6	0.8	0.1	11.4
8.0	6	810	161.7	543.9	13.8	0.0	0.0	47.3	1.4	0.6	0.2	11.0
		783	161.8	534.0	13.0	0.0	0.0	43.8	1.2	0.7	0.2	11.0
		759	161.8	522.3	12.8	0.0	0.0	45.1	1.4	0.8	0.3	11.0
		736	161.9	512.1	13.1	0.0	0.0	45.6	1.0	0.8	0.2	11.0
8.0	7	717	162.0	594.7	12.7	-0.0	0.0	45.8	1.4	1.0	0.3	10.6
		694	162.0	584.4	12.0	0.0	0.0	43.1	1.4	0.6	0.2	10.6
		672	162.1	571.9	11.9	0.1	0.1	39.3	1.2	0.6	0.2	10.6
		652	162.1	561.0	12.2	-0.0	0.0	41.8	1.1	0.4	0.2	10.6
8.0	8	633	162.2	650.8	11.7	0.0	0.0	15.0	2.5	1.0	0.3	10.4
		613	162.2	640.0	11.2	0.0	0.0	15.0	3.2	0.6	0.2	10.4
		594	162.3	626.7	11.1	0.0	0.0	19.7	2.8	0.6	0.2	10.4
		577	162.3	615.1	11.5	0.0	0.0	27.2	3.8	0.4	0.2	10.4

P LAB ANGLE	PT NO	LAB K CH	PI CM ANGLE	KAPPA	RMS DK	S3 PC LOSS AND ERROR		GAMMA PC EFF AND ERRORS P.G		P.2G		PC NA
12.0	1	1210	150.9	280.3	22.7	10.3	1.1	68.1	2.0	10.1	1.2	13.3
		1179	151.0	272.3	22.0	10.4	1.1	65.7	1.9	10.3	1.1	13.3
		1151	151.1	267.4	21.8	12.7	1.1	67.8	1.8	9.9	1.0	13.3
		1124	151.3	266.0	22.0	10.3	1.0	65.7	1.7	8.9	1.0	13.3
12.0	2	1212	150.9	373.6	22.7	9.9	0.7	65.4	1.3	9.2	0.7	13.9
		1182	151.0	363.1	22.0	10.2	0.7	61.8	1.2	9.2	0.7	13.9
		1154	151.1	356.6	21.8	10.1	0.8	61.6	1.4	8.1	0.8	13.9
		1124	151.3	266.0	22.0	10.3	1.0	65.7	1.7	8.9	1.0	13.9
12.0	3	1097	151.4	399.1	21.1	9.6	0.6	62.9	1.1	7.3	0.5	12.9
		1070	151.5	387.6	20.6	10.5	0.4	63.6	0.8	7.6	0.4	12.9
		1044	151.6	380.7	20.5	11.0	0.5	63.3	0.9	7.3	0.4	12.9
		1019	151.7	378.7	20.6	10.6	0.5	61.7	0.8	7.3	0.4	12.9
12.0	4	1097	151.4	399.1	21.1	9.7	0.4	63.2	0.8	7.4	0.4	12.9
		1070	151.5	387.6	20.6	10.4	0.4	62.6	0.7	7.8	0.4	12.9
		1044	151.6	380.7	20.5	9.9	0.3	63.2	0.6	6.9	0.3	12.9
		1019	151.7	378.7	20.6	10.1	0.3	62.2	0.6	7.0	0.3	12.9
12.0	5	995	151.8	429.0	19.8	9.6	0.3	62.4	0.6	6.6	0.3	12.4
		970	151.9	417.5	19.4	10.8	0.4	59.8	0.6	6.2	0.3	12.4
		947	152.0	410.5	19.3	10.1	0.3	60.4	0.6	6.6	0.3	12.4
		925	152.1	408.7	19.5	10.4	0.3	59.9	0.6	5.9	0.3	12.4
12.0	6	995	151.8	429.0	19.8	10.4	0.4	61.6	0.7	6.6	0.3	12.4
		970	151.9	417.5	19.4	10.9	0.3	60.0	0.6	6.4	0.3	12.4
		947	152.0	410.5	19.3	10.7	0.4	60.6	0.7	6.3	0.3	12.4
		925	152.1	408.7	19.5	10.0	0.3	59.6	0.6	5.6	0.3	12.4
12.0	7	916	152.2	653.5	15.6	-0.0	0.0	58.7	0.6	5.9	0.3	11.4
		886	152.3	642.4	14.5	0.0	0.0	57.0	0.5	5.2	0.2	11.4
		858	152.4	628.4	14.3	0.0	0.0	56.6	0.5	5.2	0.2	11.4
		832	152.5	616.0	14.7	0.0	0.0	55.7	0.5	5.1	0.2	11.4
12.0	8	810	152.6	713.0	14.2	0.0	0.0	53.5	0.6	4.7	0.2	10.9
		784	152.7	700.4	13.3	0.0	0.0	54.0	0.7	4.3	0.3	10.9
		759	152.8	685.2	13.1	0.0	0.0	52.8	0.6	3.9	0.2	10.9
		737	152.9	671.9	13.5	0.0	0.0	52.6	0.6	4.1	0.3	10.9
-12.0	9	812	152.6	710.8	14.2	-0.0	0.0	53.1	0.6	4.4	0.2	11.4
		785	152.7	698.6	13.3	0.0	0.0	53.7	0.6	4.5	0.2	11.4
		761	152.8	683.6	13.1	0.0	0.0	51.7	0.6	4.2	0.2	11.4
		738	152.9	670.4	13.5	0.0	0.0	51.7	0.5	4.1	0.2	11.4
-12.0	10	812	152.6	710.8	14.2	-0.0	0.0	53.5	0.6	4.8	0.3	11.4
		785	152.7	698.6	13.3	0.0	0.0	53.6	0.5	4.1	0.2	11.4
		761	152.8	683.6	13.1	0.0	0.0	52.9	0.6	4.5	0.2	11.4
		738	152.9	670.4	13.5	0.0	0.0	51.2	0.5	4.0	0.2	11.4
-12.0	11	811	152.6	711.1	14.2	0.0	0.0	46.8	0.7	4.8	0.3	11.4
		784	152.7	698.7	13.3	0.0	0.0	45.4	0.7	4.1	0.2	11.4
		760	152.8	683.6	13.1	0.0	0.0	45.2	0.7	4.5	0.2	11.4
		737	152.9	670.3	13.5	0.0	0.0	43.6	0.7	4.0	0.2	11.4
12.0	12	717	153.0	780.3	13.0	0.0	0.0	50.1	1.2	3.7	0.5	10.5
		694	153.1	767.1	12.3	0.0	0.0	48.4	0.9	3.0	0.3	10.5
		672	153.2	750.8	12.2	0.1	0.1	47.7	1.3	2.9	0.4	10.5
		652	153.2	736.5	12.5	0.0	0.0	46.4	1.0	3.5	0.4	10.5
12.0	13	717	153.0	585.3	13.0	-0.0	0.0	51.1	1.2	4.1	0.5	10.5
		694	153.1	575.3	12.3	0.0	0.0	49.4	1.1	4.3	0.5	10.5
		672	153.2	563.1	12.2	0.0	0.0	47.8	1.2	3.2	0.4	10.5
		652	153.2	552.4	12.5	0.1	0.0	48.5	1.1	3.3	0.4	10.5
12.0	14	717	153.0	780.3	13.0	0.0	0.0	49.6	0.7	3.2	0.2	10.5
		694	153.1	767.1	12.3	0.1	0.0	48.3	0.7	3.0	0.2	10.5
		672	153.2	750.8	12.2	0.0	0.0	45.6	0.7	3.0	0.2	10.5
		652	153.2	736.6	12.5	0.1	0.0	46.2	0.7	2.7	0.2	10.5
-12.0	15	719	153.0	776.6	13.0	0.0	0.0	49.9	0.7	3.5	0.3	11.0
		695	153.1	764.0	12.3	0.0	0.0	48.1	0.8	3.0	0.3	11.0
		674	153.1	748.1	12.2	0.0	0.0	47.9	0.8	2.7	0.2	11.0
		654	153.2	733.9	12.5	0.1	0.0	45.7	0.7	2.2	0.2	11.0
12.0	16	635	153.3	853.1	12.0	0.1	0.0	45.5	0.8	2.4	0.2	10.4
		614	153.3	840.2	11.4	0.1	0.0	44.3	0.8	2.0	0.2	10.4
		596	153.4	823.2	11.4	0.1	0.1	42.5	0.8	1.7	0.2	10.4
		578	153.5	808.1	11.7	0.2	0.1	41.1	0.8	1.2	0.2	10.4

P LAB ANGLE	PT NO	LAB K CH	PI CM ANGLE	KAPPA	RMS DK	S3 PC LOSS AND ERROR		GAMMA PC EFF AND ERRORS P.G		P.2G		PC NA
16.0	1	1212	141.4	364.2	23.7	9.2	0.4	69.8	0.8	12.3	0.5	13.7
		1181	141.5	354.1	23.0	9.9	0.5	71.1	0.8	11.9	0.5	13.7
		1152	141.7	347.9	22.8	10.7	0.4	70.0	0.8	12.0	0.5	13.7
		1124	141.9	346.1	23.0	10.8	0.4	68.6	0.7	11.0	0.4	13.7
16.0	2	1212	142.0	364.2	22.1	9.2	0.4	69.8	0.8	12.3	0.5	12.7
		1070	142.2	378.5	21.5	9.8	0.5	69.1	0.9	10.3	0.5	12.7
		1044	142.3	371.8	21.4	9.5	0.4	67.0	0.8	9.3	0.5	12.7
		1019	142.5	369.9	21.5	11.0	0.5	67.4	0.8	10.3	0.5	12.7
16.0	3	1098	142.0	389.4	22.1	10.4	0.4	68.0	0.8	9.9	0.5	12.7
		1070	142.2	378.5	21.5	10.5	0.4	68.4	0.7	10.3	0.4	12.7
		1044	142.3	371.8	21.4	10.0	0.3	67.0	0.6	9.8	0.4	12.7
		1019	142.5	369.9	21.5	9.6	0.3	66.1	0.6	8.5	0.3	12.7
16.0	4	1100	142.0	389.4	22.1	10.2	0.5	67.9	0.9	10.2	0.5	13.2
		1072	142.1	378.6	21.5	10.0	0.4	68.1	0.7	10.1	0.4	13.2
		1046	142.3	372.0	21.4	10.1	0.4	67.3	0.6	9.6	0.4	13.2
		1021	142.4	370.2	21.5	10.3	0.3	67.5	0.6	9.6	0.4	13.2
16.0	5	996	142.6	418.9	20.7	10.6	0.3	65.8	0.6	9.1	0.3	12.2
		971	142.7	408.0	20.2	10.1	0.4	65.8	0.7	8.4	0.4	12.2
		947	142.9	401.2	20.2	10.6	0.3	64.9	0.6	8.2	0.3	12.2
		925	143.0	399.5	20.3	10.5	0.3	64.3	0.6	7.9	0.3	12.2
-16.0	6	1012	142.5	593.9	17.5	0.0	0.0	59.0	0.5	0.5	0.1	12.1
		978	142.7	584.4	16.3	0.0	0.0	56.6	0.5	0.2	0.0	12.1
		947	142.9	571.8	16.0	0.0	0.0	57.6	0.5	0.2	0.0	12.1
		917	143.0	560.5	16.4	0.0	0.0	55.7	0.5	0.0	0.0	12.1
-16.0	7	918	143.0	637.0	16.1	0.0	0.0	63.0	0.6	7.6	0.3	11.7
		888	143.2	627.0	15.1	0.0	0.0	62.8	0.5	7.2	0.3	11.7
		860	143.3	613.6	14.8	0.0	0.0	60.8	0.5	6.3	0.2	11.7
		833	143.5	601.7	15.2	-0.0	0.0	59.8	0.5	6.7	0.3	11.7
16.0	8	811	143.6	695.6	14.6	0.0	0.0	58.5	0.5	5.8	0.3	10.8
		784	143.7	683.8	13.8	0.0	0.0	57.5	0.5	6.3	0.3	10.8
		759	143.9	669.1	13.6	0.0	0.0	56.5	0.5	5.0	0.2	10.8
		736	144.0	656.1	13.9	0.1	0.0	54.8	0.5	4.8	0.2	10.8
16.0	9	811	143.6	695.6	14.6	-0.0	0.0	59.9	0.5	6.0	0.3	10.8
		784	143.7	683.8	13.8	0.0	0.0	58.3	0.5	5.9	0.2	10.8
		760	143.9	669.1	13.6	0.0	0.0	56.2	0.6	5.4	0.3	10.8
		736	144.0	656.1	13.9	0.1	0.0	55.2	0.6	4.7	0.2	10.8
16.0	10	812	143.6	695.0	14.6	0.0	0.0	59.6	0.5	6.5	0.3	11.3
		786	143.7	683.5	13.8	0.0	0.0	58.1	0.5	5.6	0.2	11.3
		761	143.9	669.0	13.6	0.0	0.0	56.2	0.6	4.9	0.3	11.3
		738	144.0	656.1	13.9	0.0	0.0	53.9	0.7	5.1	0.3	11.3
-16.0	11	812	143.6	695.0	14.6	0.0	0.0	59.0	0.6	5.9	0.3	11.3
		786	143.7	683.5	13.8	0.0	0.0	57.9	0.5	5.3	0.2	11.3
		761	143.9	669.0	13.6	0.0	0.0	56.9	0.6	5.1	0.3	11.3
		738	144.0	656.1	13.9	0.0	0.0	55.3	0.5	5.0	0.2	11.3
-16.0	12	813	143.6	694.9	14.6	0.0	0.0	59.3	0.5	6.2	0.2	11.3
		786	143.7	683.5	13.8	0.0	0.0	57.9	0.5	5.8	0.2	11.3
		761	143.8	669.0	13.6	0.0	0.0	57.0	0.5	5.4	0.2	11.3
		738	144.0	656.1	13.9	0.0	0.0	55.9	0.5	5.1	0.2	11.3
-16.0	13	811	143.6	695.7	14.6	0.0	0.0	51.0	0.5	0.0	0.0	11.3
		784	143.7	683.6	13.8	0.0	0.0	50.1	0.5	5.8	0.2	11.3
		759	143.9	668.9	13.6	0.0	0.0	47.9	0.6	5.4	0.2	11.3
		736	144.0	655.9	13.9	0.0	0.0	48.2	0.5	5.1	0.2	11.3
16.0	14	718	144.1	762.1	13.4	0.0	0.0	54.6	0.6	4.8	0.3	10.5
		694	144.2	749.6	12.7	0.1	0.0	52.4	0.9	4.6	0.4	10.5
		673	144.3	733.9	12.6	0.1	0.0	51.3	0.7	3.6	0.2	10.5
		652	144.4	719.9	12.9	0.0	0.0	49.6	0.6	3.9	0.2	10.5
16.0	15	718	144.1	762.0	13.4	0.0	0.0	54.2	0.8	4.9	0.3	10.5
		695	144.2	749.6	12.7	0.1	0.0	53.0	0.8	4.5	0.3	10.5
		673	144.3	733.9	12.6	0.0	0.0	51.3	0.6	4.0	0.2	10.5
		652	144.4	720.0	12.9	0.0	0.0	49.1	0.6	3.6	0.2	10.5
16.0	16	718	144.1	762.0	13.4	0.0	0.0	53.0	0.8	4.3	0.3	10.5
		695	144.2	749.6	12.7	0.1	0.0	52.8	0.6	4.5	0.3	10.5
		673	144.3	733.9	12.6	0.1	0.0	51.6	0.6	4.1	0.3	10.5
		652	144.4	720.0	12.9	0.0	0.0	49.9	0.6	3.2	0.2	10.5
-16.0	17	720	144.1	759.4	13.4	0.1	0.0	54.9	0.7	5.0	0.3	10.9
		696	144.2	747.7	12.7	0.0	0.0	53.8	0.7	4.4	0.3	10.9
		674	144.3	732.2	12.6	0.0	0.0	51.8	0.9	3.9	0.4	10.9
		654	144.4	718.4	13.0	0.1	0.0	49.7	0.6	4.2	0.3	10.9
16.0	18	635	144.4	834.2	12.4	0.0	0.0	48.8	0.9	3.5	0.3	10.4
		615	144.5	822.1	11.9	0.1	0.1	47.7	0.7	2.6	0.2	10.4
		596	144.6	805.6	11.8	0.1	0.1	45.7	0.8	3.2	0.3	10.4
		578	144.7	790.7	12.2	0.1	0.0	45.6	0.7	2.3	0.2	10.4

P LAB ANGLE	PT NO	LAB K CH	PI CM ANGLE	KAPPA	RMS DK	S3 PC LOSS	AND ERROR	GAMMA PC EFF P.G		AND ERRORS P.2G		PC NA
20.5	1	1215	130.8	350.8	25.3	9.7	0.7	73.9	1.2	18.3	1.0	13.4
		1183	131.0	341.5	24.6	10.0	0.9	74.7	1.6	17.9	1.3	13.4
		1153	131.2	335.7	24.4	9.6	0.6	73.0	1.1	17.1	0.9	13.4
		1125	131.4	334.1	24.5	10.0	0.6	73.3	1.1	16.0	0.8	13.4
20.5	2	1101	131.6	375.5	23.5	10.7	0.4	72.3	0.8	16.3	0.6	12.9
		1073	131.8	365.3	22.9	10.7	0.4	73.5	0.7	13.9	0.5	12.9
		1046	132.0	359.0	22.8	10.8	0.4	71.6	0.6	13.6	0.4	12.9
		1020	132.2	357.3	22.9	10.9	0.4	70.5	0.6	13.6	0.4	12.9
-20.5	3	1014	132.2	572.9	18.5	0.0	0.0	63.2	0.5	1.5	0.1	11.9
		979	132.4	564.6	17.2	0.0	0.0	64.0	0.5	1.3	0.1	11.9
		947	132.6	552.7	16.9	0.0	0.0	61.6	0.5	1.0	0.1	11.9
		917	132.8	541.9	17.3	0.0	0.0	61.4	0.5	0.9	0.1	11.9
-20.5	4	919	132.8	615.0	17.0	0.0	0.0	67.3	0.6	9.9	0.4	11.6
		888	133.0	606.0	15.9	0.0	0.0	67.6	0.6	10.0	0.4	11.6
		859	133.2	593.3	15.7	0.0	0.0	66.5	0.6	9.1	0.4	11.6
		832	133.4	581.8	16.0	0.0	0.0	65.3	0.6	8.3	0.4	11.6
-20.5	5	812	133.5	671.8	15.4	0.1	0.0	56.0	0.8	0.2	0.1	11.1
		785	133.7	661.0	14.5	0.0	0.0	54.5	0.8	0.1	0.1	11.1
		760	133.9	647.0	14.3	0.0	0.0	53.3	0.8	0.0	0.0	11.1
		736	134.0	634.5	14.7	0.0	0.0	52.7	0.9	8.4	0.4	11.1
-20.5	6	719	134.1	734.9	14.0	0.1	0.0	59.5	0.5	6.1	0.3	10.9
		696	134.2	723.8	13.4	0.1	0.0	59.7	0.6	5.9	0.3	10.9
		673	134.4	708.8	13.3	0.1	0.0	57.6	0.6	5.7	0.3	10.9
		653	134.5	695.4	13.6	0.1	0.0	56.6	0.6	5.3	0.3	10.9
-20.5	7	718	134.1	735.4	14.0	0.0	0.0	51.9	0.7	0.0	0.0	10.9
		695	134.2	723.8	13.4	0.1	0.0	50.2	0.7	5.9	0.3	10.9
		673	134.4	708.7	13.3	0.1	0.0	50.0	0.8	5.7	0.3	10.9
		652	134.5	695.2	13.6	0.1	0.0	48.1	0.7	5.3	0.3	10.9
-20.5	8	636	134.6	803.5	13.0	0.2	0.1	48.6	1.1	0.0	0.0	10.9
		615	134.7	792.3	12.5	0.1	0.1	44.9	0.9	5.9	0.3	10.9
		596	134.8	776.4	12.5	0.3	0.1	45.6	0.9	5.7	0.3	10.9
		578	134.8	762.0	12.8	0.2	0.1	43.1	0.7	5.3	0.3	10.9
25.0	1	1218	120.5	334.8	27.4	11.5	0.9	79.4	1.5	21.9	1.3	13.1
		1185	120.8	326.3	26.7	10.8	0.7	77.9	1.2	22.1	1.0	13.1
		1154	121.0	320.9	26.4	9.5	0.8	76.8	1.4	20.8	1.2	13.1
		1124	121.2	319.5	26.5	10.3	0.8	77.1	1.3	21.9	1.1	13.1
25.0	2	1103	121.4	358.5	25.3	10.4	0.7	75.6	1.2	18.5	0.9	12.6
		1074	121.6	349.1	24.8	10.8	0.5	75.3	0.8	20.2	0.6	12.6
		1046	121.8	343.2	24.6	10.8	0.4	74.4	0.7	19.2	0.6	12.6
		1019	122.1	341.7	24.7	10.7	0.4	74.9	0.6	18.3	0.5	12.6
25.0	3	1000	122.2	386.5	23.6	11.3	0.4	74.0	0.7	17.1	0.5	12.2
		973	122.4	377.1	23.2	10.7	0.4	74.0	0.7	16.0	0.5	12.2
		948	122.6	371.2	23.1	11.2	0.4	72.2	0.7	15.9	0.5	12.2
		924	122.8	369.8	23.3	11.0	0.4	71.7	0.7	15.6	0.5	12.2
-25.0	4	922	122.8	588.1	18.1	0.1	0.0	70.7	0.6	14.5	0.5	11.3
		889	123.0	580.6	17.0	0.1	0.0	71.7	0.6	13.2	0.4	11.3
		860	123.3	568.8	16.8	0.0	0.0	69.0	0.6	12.1	0.4	11.3
		832	123.5	557.9	17.1	0.0	0.0	69.3	0.5	11.6	0.3	11.3
-25.0	5	814	123.6	643.2	16.4	0.1	0.0	61.9	0.8	0.9	0.2	11.0
		786	123.8	633.9	15.5	0.1	0.1	60.5	1.6	0.7	0.3	11.0
		760	124.0	620.7	15.4	0.1	0.0	60.1	0.8	0.4	0.1	11.0
		736	124.1	608.8	15.7	0.1	0.1	59.1	0.8	0.3	0.1	11.0
-25.0	6	720	124.2	703.1	14.9	0.0	0.0	57.2	0.6	0.2	0.0	10.9
		696	124.4	693.2	14.3	0.1	0.0	55.1	0.6	0.0	0.0	10.9
		673	124.5	679.0	14.2	0.2	0.1	54.9	0.6	0.0	0.0	10.9
		653	124.7	666.1	14.6	0.2	0.1	53.2	0.6	0.0	0.0	10.9
-25.0	7	637	124.8	768.8	13.8	0.3	0.1	51.1	0.7	0.0	0.0	11.0
		616	124.9	759.3	13.4	0.2	0.1	49.4	0.7	0.0	0.0	11.0
		597	125.0	744.4	13.4	0.2	0.1	48.3	0.7	0.0	0.0	11.0
		578	125.1	730.7	13.7	0.4	0.1	48.3	0.7	0.0	0.0	11.0

P LAB ANGLE	PT NO	LAB K CH	PI CM ANGLE	KAPPA	RMS DK	S3 PC LOSS	AND ERROR	GAMMA PC EFF AND ERRORS P.G		P.2G		PC NA
29.5	1	1219	110.5	316.1	30.0	11.6	1.0	81.7	1.7	24.8	1.5	12.7
		1185	110.8	308.5	29.3	10.8	1.2	79.7	1.9	27.5	1.8	12.7
		1153	111.0	303.6	29.0	10.7	0.8	79.0	1.4	24.9	1.2	12.7
		1122	111.3	302.4	29.1	10.9	1.0	80.9	1.7	24.8	1.6	12.7
29.5	2	1221	110.4	315.9	30.1	12.3	1.1	80.8	1.7	25.9	1.5	12.7
		1187	110.7	306.5	29.3	10.1	0.9	79.8	1.5	27.8	1.4	12.7
		1154	111.0	303.6	29.1	11.1	0.8	78.2	1.3	23.5	1.1	12.7
		1123	111.3	302.4	29.1	10.4	0.7	79.0	1.1	25.1	1.0	12.7
29.5	3	1105	111.4	339.8	27.8	11.0	0.8	76.7	1.3	23.9	1.1	12.3
		1074	111.7	331.3	27.2	11.2	0.7	78.7	1.1	23.3	0.9	12.3
		1046	111.9	325.9	27.0	11.0	0.5	77.6	0.9	22.5	0.8	12.3
		1018	112.2	324.6	27.1	11.4	0.5	77.5	0.9	21.1	0.8	12.3
29.5	4	1126	111.2	481.5	23.6	-0.0	0.0	73.2	1.0	9.9	0.7	11.7
		1084	111.6	475.3	22.1	0.0	0.0	73.8	0.7	8.6	0.5	11.7
		1046	111.9	465.4	21.6	0.1	0.0	73.1	0.7	9.2	0.4	11.7
		1011	112.2	456.2	21.9	0.0	0.0	72.4	0.7	8.0	0.4	11.7
29.5	5	1002	112.3	365.7	25.8	12.1	0.5	77.6	0.8	21.5	0.7	12.0
		975	112.5	357.5	25.4	11.3	0.5	76.5	0.8	20.8	0.7	12.0
		949	112.7	352.1	25.4	11.4	0.5	76.5	0.8	21.4	0.7	12.0
		924	112.9	350.9	25.5	12.0	0.5	74.9	0.8	19.8	0.6	12.0
29.5	6	924	112.9	556.4	19.6	-0.0	0.0	75.3	0.8	17.9	0.7	11.1
		891	113.2	551.0	18.5	0.0	0.0	75.3	0.8	18.0	0.7	11.1
		861	113.4	540.1	18.3	-0.0	0.0	74.4	0.8	16.4	0.6	11.1
		832	113.7	529.9	18.6	0.0	0.0	72.3	0.7	15.3	0.6	11.1
29.5	7	817	113.8	609.8	17.6	0.1	0.1	66.2	0.8	2.4	0.3	10.9
		788	114.0	602.3	16.9	0.0	0.0	66.0	0.8	2.4	0.3	10.9
		761	114.2	590.1	16.7	0.1	0.1	63.4	0.8	1.5	0.2	10.9
		737	114.4	578.9	17.0	0.3	0.1	63.3	0.7	1.2	0.2	10.9
29.5	8	817	113.8	609.8	17.6	0.1	0.1	65.8	0.8	2.9	0.3	10.9
		788	114.0	602.3	16.9	0.1	0.0	65.7	0.8	2.3	0.2	10.9
		761	114.2	590.1	16.7	0.1	0.1	65.0	0.8	2.1	0.2	10.9
		737	114.4	578.9	17.0	0.2	0.1	63.1	0.8	1.6	0.2	10.9
29.5	9	723	114.5	665.9	16.1	0.2	0.1	69.4	0.6	11.1	0.4	10.9
		698	114.7	658.3	15.6	0.1	0.0	68.7	0.5	10.2	0.3	10.9
		675	114.8	645.3	15.5	0.3	0.1	66.6	0.6	9.4	0.4	10.9
		654	115.0	633.2	15.9	0.2	0.1	65.6	0.6	9.1	0.4	10.9
29.5	10	639	115.1	727.2	14.9	0.2	0.1	57.1	0.8	0.1	0.1	11.2
		618	115.2	720.1	14.6	0.4	0.1	54.9	0.7	0.1	0.0	11.2
		598	115.3	706.3	14.6	0.4	0.1	53.2	0.7	0.0	0.0	11.2
		579	115.4	693.3	15.0	0.4	0.1	52.8	0.7	0.0	0.0	11.2
34.0	1	1223	100.7	296.1	33.5	11.1	0.7	79.4	1.2	29.8	1.1	12.3
		1187	101.0	289.6	32.8	11.9	0.8	80.1	1.2	27.5	1.2	12.3
		1153	101.3	285.2	32.5	11.5	0.5	81.1	0.8	28.5	0.8	12.3
		1121	101.6	284.2	32.5	13.1	0.6	79.8	1.0	26.6	0.9	12.3
34.0	2	1109	101.7	318.0	30.9	11.8	0.7	80.1	1.2	26.8	1.1	12.0
		1077	102.0	310.7	30.4	12.9	0.7	80.0	1.1	26.5	1.0	12.0
		1047	102.2	306.0	30.2	12.1	0.6	78.5	0.9	26.7	0.8	12.0
		1018	102.5	304.8	30.3	11.5	0.6	78.6	0.9	25.9	0.8	12.0
34.0	3	1129	101.5	450.2	25.9	0.1	0.0	79.4	0.8	27.4	0.8	11.4
		1086	101.9	445.8	24.4	0.0	0.0	79.9	0.6	26.7	0.7	11.4
		1046	102.2	436.9	23.9	0.1	0.0	78.9	0.5	25.8	0.5	11.4
		1009	102.5	428.4	24.1	0.0	0.0	79.1	0.4	25.2	0.5	11.4
34.0	4	1006	102.6	342.5	28.6	12.8	0.7	77.9	1.1	26.0	1.0	11.6
		977	102.8	335.7	28.4	11.7	0.7	77.2	1.1	22.7	1.0	11.6
		950	103.1	331.0	28.3	12.1	0.6	77.5	1.0	23.9	0.9	11.6
		925	103.3	329.9	28.5	11.0	0.5	78.4	0.8	22.7	0.7	11.6
34.0	5	1024	102.4	483.8	23.4	0.0	0.0	72.6	0.9	11.4	0.7	9.9
		985	102.8	481.6	22.3	0.1	0.0	73.4	0.7	10.8	0.5	9.9
		950	103.1	472.7	21.9	0.1	0.0	73.5	0.7	10.0	0.4	9.9
		917	103.3	463.8	22.1	0.0	0.0	73.2	0.6	8.4	0.4	9.9
34.0	6	928	103.2	521.2	21.4	0.1	0.0	77.4	0.7	20.9	0.7	10.9
		893	103.5	518.4	20.5	0.1	0.1	77.0	0.7	21.3	0.6	10.9
		862	103.8	508.6	20.2	0.1	0.0	75.4	0.5	20.2	0.5	10.9
		833	104.0	499.1	20.5	0.1	0.0	76.2	0.6	19.8	0.6	10.9
34.0	7	819	104.1	570.4	19.3	0.1	0.0	69.8	0.6	5.0	0.3	10.9
		790	104.4	565.4	18.7	0.2	0.0	68.8	0.5	4.4	0.2	10.9
		763	104.6	554.4	18.5	0.2	0.1	67.5	0.5	3.7	0.2	10.9
		737	104.8	543.8	18.8	0.1	0.0	67.0	0.6	3.6	0.3	10.9
34.0	8	726	104.9	622.7	17.7	0.3	0.1	71.5	0.5	14.3	0.4	11.1
		700	105.0	618.1	17.3	0.2	0.1	70.7	0.6	14.0	0.4	11.1
		677	105.2	606.4	17.3	0.5	0.1	69.5	0.5	12.3	0.4	11.1
		655	105.3	595.1	17.6	0.3	0.1	69.2	0.6	11.8	0.4	11.1
34.0	9	642	105.4	678.3	16.3	0.3	0.1	68.5	0.6	11.1	0.4	10.1
		620	105.6	674.9	16.2	0.6	0.1	66.9	0.8	9.6	0.5	10.1
		599	105.7	662.6	16.3	0.7	0.1	65.7	0.6	8.6	0.3	10.1
		581	105.8	650.4	16.7	0.8	0.1	64.3	0.6	8.3	0.3	10.1

P LAB ANGLE	PT NO	LAB K CH	PI CM ANGLE	KAPPA	RMS DK	S3 PC LOSS AND ERROR		GAMMA PC EFF AND ERRORS P.G		P.2G		PC NA
39.0	1	1229	90.1	270.7	38.3	11.8	0.9	81.8	1.5	31.5	1.5	11.8
		1191	90.4	266.2	37.9	13.2	1.0	83.6	1.5	32.2	1.5	11.8
		1155	90.7	262.5	37.6	12.4	0.9	82.1	1.5	31.1	1.4	11.8
		1122	91.0	261.7	37.5	12.3	0.8	82.0	1.2	32.5	1.3	11.8
39.0	2	1135	90.9	411.1	29.1	0.3	0.3	84.8	2.1	34.8	2.7	11.0
		1090	91.3	410.2	27.9	-0.0	0.0	82.1	1.3	30.2	1.6	11.0
		1048	91.7	402.6	27.3	0.1	0.1	81.5	1.4	29.7	1.7	11.0
		1010	92.0	394.9	27.5	0.1	0.1	81.4	1.3	28.2	1.5	11.0
39.0	3	1114	91.1	291.4	35.4	11.7	0.8	80.7	1.3	30.1	1.2	11.6
		1080	91.4	285.9	35.1	12.2	0.7	81.9	1.2	29.3	1.1	11.6
		1049	91.7	281.8	34.9	13.1	0.6	79.2	1.0	29.2	1.0	11.6
		1019	91.9	280.9	35.0	12.5	0.5	79.1	0.8	28.4	0.8	11.6
39.0	4	1135	90.9	411.1	29.1	0.1	0.0	81.5	0.7	29.4	0.8	11.0
		1090	91.3	410.2	27.9	0.1	0.0	81.4	0.6	28.8	0.7	11.0
		1048	91.7	402.6	27.3	0.2	0.1	80.3	0.6	29.6	0.7	11.0
		1010	92.0	394.9	27.5	0.2	0.1	80.0	0.6	28.5	0.7	11.0
39.0	5	1010	92.0	313.3	32.6	13.0	1.0	78.6	1.5	27.0	1.4	11.4
		980	92.3	309.2	32.7	12.6	1.0	80.2	1.6	26.4	1.4	11.4
		952	92.5	305.3	32.8	12.2	0.8	79.9	1.2	28.2	1.1	11.4
		926	92.8	304.5	33.0	12.9	0.8	81.1	1.2	26.5	1.1	11.4
39.0	6	933	92.7	474.1	23.9	0.3	0.1	79.2	0.8	25.7	0.9	10.9
		897	93.0	476.2	23.4	0.2	0.1	77.5	0.8	25.7	0.9	10.9
		864	93.3	468.0	23.2	0.3	0.1	77.3	0.7	22.5	0.7	10.9
		834	93.5	459.4	23.5	0.2	0.1	77.5	0.6	22.7	0.6	10.9
39.0	7	824	93.6	520.7	21.7	0.2	0.1	73.1	0.6	7.6	0.3	11.0
		793	93.8	520.2	21.4	0.4	0.1	71.5	0.5	6.9	0.3	11.0
		765	94.1	510.8	21.3	0.4	0.1	71.1	0.6	6.4	0.3	11.0
		739	94.2	501.2	21.6	0.4	0.1	70.5	0.5	5.8	0.2	11.0
39.0	8	729	94.3	567.0	19.9	0.4	0.1	69.4	0.5	4.8	0.2	10.1
		703	94.5	567.4	19.8	0.6	0.1	68.0	0.5	4.5	0.2	10.1
		679	94.7	557.3	19.9	0.6	0.1	68.4	0.5	4.1	0.2	10.1
		656	94.8	546.9	20.3	0.7	0.1	66.3	0.6	3.1	0.2	10.1
39.0	9	646	94.9	612.8	18.4	1.0	0.2	69.9	0.7	13.5	0.5	10.9
		623	95.0	617.5	18.7	0.8	0.2	70.8	0.8	12.8	0.6	10.9
		602	95.1	607.5	18.9	1.0	0.2	70.6	0.8	12.1	0.6	10.9
		583	95.2	596.6	19.4	1.3	0.2	69.2	0.7	10.9	0.4	10.9
41.9	1	934	86.7	445.1	25.7	0.4	0.2	81.2	1.0	29.0	1.2	11.0
		898	87.0	450.7	25.6	0.4	0.2	79.6	1.1	25.7	1.1	11.0
		865	87.3	443.3	25.4	0.3	0.1	78.1	1.0	24.3	1.0	11.0
		834	87.5	435.2	25.7	0.4	0.1	78.9	0.9	24.5	0.9	11.0
41.9	2	934	86.7	445.1	25.7	0.2	0.1	75.9	0.8	14.4	0.6	11.0
		898	87.0	450.7	25.6	0.3	0.1	75.5	0.8	13.5	0.6	11.0
		865	87.3	443.3	25.4	0.6	0.2	74.9	1.0	11.7	0.8	11.0
		834	87.5	435.2	25.7	0.5	0.1	75.1	0.6	12.1	0.4	11.0
41.9	3	826	87.6	488.2	23.4	0.4	0.1	73.6	0.6	9.6	0.4	9.9
		795	87.8	491.4	23.4	0.6	0.1	73.4	0.5	9.1	0.3	9.9
		766	88.0	482.9	23.4	0.5	0.1	73.1	0.6	8.5	0.3	9.9
		740	88.2	473.9	23.8	0.6	0.1	71.8	0.5	7.1	0.3	9.9
41.9	4	731	88.3	529.9	21.4	0.9	0.1	71.0	0.5	6.3	0.3	10.5
		705	88.4	535.1	21.8	0.7	0.1	70.4	0.6	5.8	0.3	10.5
		680	88.6	526.3	22.0	0.9	0.1	68.5	0.6	5.2	0.3	10.5
		658	88.7	516.6	22.4	1.0	0.1	68.2	0.7	3.7	0.3	10.5
41.9	5	648	88.8	567.2	19.7	1.2	0.2	71.2	1.1	15.8	0.8	11.9
		625	88.9	578.9	20.6	1.2	0.2	72.9	0.9	14.0	0.7	11.9
		604	89.0	570.8	21.0	0.9	0.2	71.9	0.9	12.8	0.7	11.9
		585	89.0	560.7	21.5	2.0	0.3	69.9	0.9	12.2	0.7	11.9
41.9	6	648	88.8	567.2	19.7	1.0	0.1	67.9	0.6	3.4	0.2	11.9
		625	88.9	578.9	20.6	1.2	0.1	64.4	0.7	2.6	0.2	11.9
		604	89.0	570.8	21.0	1.5	0.4	63.7	1.7	2.1	0.5	11.9
		585	89.0	560.7	21.5	1.9	0.2	63.5	0.7	1.8	0.2	11.9

P LAB ANGLE	PT NO	LAB K CH	PI CM ANGLE	KAPPA	RMS DK	S3 PC LOSS AND ERROR		GAMMA PC EFF AND ERRORS P.G		P.2G		PC NA
44.0	1	1143	80.6	365.7	32.9	0.1	0.1	83.5	0.7	31.5	0.8	10.9
		1095	81.1	371.3	32.7	0.1	0.1	82.5	0.7	30.9	0.8	10.9
		1051	81.4	365.2	32.1	0.2	0.1	80.5	0.6	31.2	0.7	10.9
		1011	81.8	358.3	32.2	0.2	0.1	81.1	0.6	29.3	0.7	10.9
44.0	2	1143	80.6	365.7	32.9	0.1	0.1	81.3	0.8	31.0	1.0	10.9
		1095	81.1	371.3	32.7	0.1	0.1	82.0	0.7	32.8	0.8	10.9
		1051	81.4	365.2	32.1	0.1	0.0	80.8	0.6	31.5	0.7	10.9
		1011	81.8	358.3	32.2	0.4	0.1	81.2	0.6	30.1	0.7	10.9
44.0	3	1036	81.6	388.5	29.4	0.3	0.1	75.5	0.8	19.0	0.7	10.9
		994	81.9	400.8	29.8	0.3	0.1	76.8	0.6	17.8	0.5	10.9
		955	82.2	395.2	29.5	0.3	0.1	76.8	0.6	18.2	0.5	10.9
		920	82.5	388.1	29.7	0.3	0.1	76.8	0.8	16.3	0.7	10.9
44.0	4	939	82.4	418.4	27.0	0.3	0.1	81.6	1.0	27.3	1.2	11.1
		902	82.7	430.4	27.5	0.1	0.1	80.4	0.8	28.8	0.9	11.1
		868	82.9	424.2	27.4	0.4	0.1	78.4	0.7	26.9	0.8	11.1
		836	83.2	416.6	27.7	0.4	0.1	77.2	0.8	24.1	0.8	11.1
44.0	5	829	83.2	460.2	24.6	0.6	0.1	73.4	0.6	11.3	0.4	10.1
		798	83.5	469.0	25.2	0.6	0.1	73.9	0.5	10.8	0.4	10.1
		769	83.7	461.8	25.3	0.6	0.1	73.0	0.5	10.0	0.3	10.1
		742	83.9	453.3	25.7	0.7	0.1	72.9	0.6	8.5	0.4	10.1
44.0	6	735	83.9	497.5	22.6	0.8	0.1	71.4	0.5	7.7	0.3	11.0
		707	84.1	509.6	23.5	1.0	0.1	71.2	0.6	6.8	0.3	11.0
		683	84.2	502.4	23.8	1.0	0.1	70.4	0.6	5.6	0.3	11.0
		660	84.3	493.3	24.3	1.5	0.2	68.6	0.7	4.6	0.3	11.0
44.0	7	652	84.4	392.9	20.8	1.4	0.2	74.0	0.7	17.5	0.6	12.8
		629	84.5	410.8	22.1	1.5	0.2	72.4	0.7	16.1	0.6	12.8
		608	84.6	407.2	22.8	1.6	0.2	71.9	0.8	15.6	0.6	12.8
		588	84.6	400.4	23.3	2.8	0.2	71.3	0.7	14.3	0.5	12.8
49.0	1	1274	69.7	282.4	41.2	-0.0	0.1	78.8	2.4	17.2	2.2	10.9
		1216	70.1	305.2	43.2	0.1	0.1	78.7	1.1	22.3	1.1	10.9
		1164	70.6	302.5	42.8	0.2	0.1	77.5	1.2	22.2	1.2	10.9
		1116	70.9	297.3	42.6	0.5	0.2	78.4	0.9	25.1	0.9	10.9
49.0	2	1152	70.6	310.9	37.7	0.0	0.1	82.1	1.7	36.6	2.1	11.1
		1101	71.0	328.7	39.3	0.3	0.2	83.3	1.4	35.3	1.7	11.1
		1056	71.4	324.9	39.1	0.3	0.2	84.2	1.4	34.3	1.8	11.1
		1014	71.7	319.0	39.1	0.2	0.2	82.1	1.6	31.5	1.9	11.1
49.0	3	1044	71.5	325.6	33.7	0.9	0.2	78.3	1.1	21.9	1.1	9.9
		1000	71.8	353.0	35.8	0.6	0.2	78.2	0.9	19.9	0.9	9.9
		959	72.2	350.7	36.1	0.8	0.2	76.5	0.9	21.8	0.9	9.9
		923	72.4	344.8	36.3	0.6	0.2	77.2	0.8	19.3	0.8	9.9
49.0	4	946	72.3	350.8	31.1	0.7	0.2	78.0	1.0	20.6	1.0	10.3
		907	72.5	378.1	33.1	1.0	0.2	75.7	0.9	17.4	0.8	10.3
		872	72.8	375.7	33.7	0.9	0.3	75.8	1.4	18.5	1.2	10.3
		839	73.0	369.3	34.0	1.0	0.2	75.9	0.7	16.5	0.6	10.3
49.0	5	837	73.0	383.4	28.4	1.1	0.2	75.1	0.6	15.2	0.5	11.4
		804	73.3	409.4	30.5	1.2	0.1	75.4	0.6	13.5	0.5	11.4
		774	73.4	406.9	31.3	1.6	0.2	75.6	0.6	13.2	0.4	11.4
		747	73.6	400.1	31.9	1.5	0.2	74.3	0.6	11.4	0.4	11.4
54.0	1	1290	60.0	216.1	49.7	0.4	0.2	78.0	1.5	4.8	0.8	10.0
		1229	60.4	257.7	52.2	0.2	0.1	78.6	1.3	5.2	0.7	10.0
		1173	60.8	261.7	54.0	0.7	0.2	77.9	1.1	7.7	0.7	10.0
		1123	61.2	258.2	54.3	0.9	0.2	78.4	0.9	9.1	0.6	10.0
54.0	2	1168	60.9	239.2	45.3	1.2	0.3	79.9	1.0	6.6	0.6	10.4
		1114	61.2	277.2	48.1	0.8	0.2	79.3	0.9	9.0	0.6	10.4
		1066	61.6	280.4	49.7	1.0	0.2	78.5	0.8	10.9	0.6	10.4
		1023	61.9	276.5	50.2	0.7	0.2	79.0	1.0	11.3	0.7	10.4
54.0	3	1058	61.6	245.4	41.6	0.8	0.2	79.9	0.9	10.7	0.7	11.2
		1011	62.0	293.3	43.3	1.1	0.2	77.2	0.9	12.1	0.7	11.2
		969	62.2	300.6	45.9	1.2	0.2	77.4	1.0	12.4	0.7	11.2
		931	62.5	297.4	46.8	2.0	0.4	75.6	1.1	13.2	0.9	11.2
54.0	4	959	62.3	261.0	38.7	1.3	0.3	77.6	1.1	14.3	0.9	12.5
		919	62.6	310.1	40.3	2.0	0.3	78.1	1.1	12.6	0.8	12.5
		882	62.8	319.1	42.8	1.6	0.3	78.5	0.9	14.9	0.8	12.5
		849	63.0	316.4	44.2	2.1	0.3	75.9	0.9	14.9	0.7	12.5

Table 17

Computed quantities for excitation curve data. See text for definitions.

P LAB ANGLE	PT NO	LAB K CH	PI CM ANGLE	KAPPA	RMS DK	S3 PC LOSS AND ERROR		GAMMA PC EFF AND ERRORS P.G		P.2G		PC NA
16.0	1	799	143.7	368.8	18.3	10.4	0.6	59.7	1.1	6.4	0.5	11.4
		779	143.8	356.5	18.1	11.0	0.6	60.2	1.1	5.9	0.5	11.4
		760	143.9	349.7	18.1	10.7	0.6	59.3	1.1	6.1	0.5	11.4
		742	143.9	348.1	18.4	11.4	0.6	56.6	1.1	4.9	0.4	11.4
-16.0	2	812	143.6	580.5	14.7	0.0	0.0	50.0	0.5	0.0	0.0	11.3
		785	143.7	562.5	13.8	0.0	0.0	50.0	0.5	5.3	0.4	11.3
		760	143.9	547.6	13.6	0.0	0.0	49.0	0.5	5.5	0.4	11.3
		737	144.0	536.3	13.9	0.0	0.0	47.4	0.5	4.3	0.4	11.3
-16.0	3	811	143.6	636.5	14.7	0.0	0.0	51.0	0.5	0.0	0.0	11.3
		784	143.7	616.1	13.8	0.0	0.0	50.1	0.5	5.3	0.4	11.3
		760	143.9	599.1	13.6	0.0	0.0	48.7	0.5	0.0	0.0	11.3
		736	144.0	586.0	13.9	0.0	0.0	48.6	0.5	4.4	0.4	11.3
-16.0	4	811	143.6	672.7	14.7	0.0	0.0	51.3	0.5	0.0	0.0	11.3
		784	143.7	653.7	13.8	0.0	0.0	51.2	0.6	0.0	0.0	11.3
		759	143.9	636.4	13.6	0.0	0.0	48.5	0.5	0.0	0.0	11.3
		736	144.0	622.2	13.9	0.0	0.0	47.5	0.5	4.4	0.4	11.3
-16.0	5	813	143.6	693.2	14.5	0.0	0.0	59.8	0.5	6.2	0.2	11.3
		786	143.7	692.3	13.8	0.0	0.0	58.0	0.5	5.8	0.2	11.3
		761	143.8	681.2	13.6	0.0	0.0	57.8	0.5	5.1	0.2	11.3
		738	144.0	669.5	13.9	0.0	0.0	55.1	0.5	4.8	0.2	11.3
-16.0	6	813	143.6	661.5	13.9	0.0	0.0	59.3	0.5	5.8	0.2	11.3
		786	143.7	695.3	13.7	0.0	0.0	58.6	0.5	5.8	0.2	11.3
		761	143.8	691.5	13.6	0.0	0.0	57.1	0.5	5.5	0.2	11.3
		738	144.0	682.4	13.9	0.0	0.0	56.0	0.5	4.9	0.2	11.3
-16.0	7	810	143.6	623.9	13.3	-0.0	0.0	50.1	0.7	5.8	0.2	11.3
		784	143.7	694.6	13.7	0.0	0.0	50.7	0.6	5.8	0.2	11.3
		759	143.9	695.9	13.6	0.0	0.0	48.9	0.6	0.0	0.0	11.3
		736	144.0	688.5	13.9	0.0	0.0	48.3	0.6	4.9	0.2	11.3
-16.0	8	813	143.6	502.6	12.8	0.0	0.0	59.0	0.6	5.5	0.3	11.3
		786	143.7	681.5	13.5	0.0	0.0	57.9	0.5	5.9	0.2	11.3
		761	143.8	697.1	13.6	0.0	0.0	57.1	0.5	5.8	0.2	11.3
		738	144.0	693.8	13.9	0.0	0.0	56.0	0.5	4.7	0.2	11.3
-16.0	9	813	143.6	182.9	19.0	-0.0	0.0	56.7	1.2	4.8	0.5	11.3
		786	143.7	582.1	12.3	0.0	0.0	58.8	0.6	6.2	0.3	11.3
		761	143.8	690.4	13.5	0.0	0.0	57.6	0.5	5.3	0.2	11.3
		738	144.0	701.2	13.9	0.0	0.0	56.4	0.7	5.6	0.3	11.3
-16.0	10	813	143.6	13.6	32.1	0.0	0.0	60.2	2.7	6.0	1.3	11.3
		786	143.7	273.1	15.1	0.0	0.0	58.7	0.9	5.2	0.4	11.3
		761	143.8	624.2	12.6	0.0	0.0	57.8	0.6	5.1	0.3	11.3
		738	144.0	697.7	13.8	0.0	0.0	56.2	0.5	4.9	0.2	11.3
-16.0	11	810	143.6	20.5	30.5	-0.0	0.2	50.0	10.7	6.0	1.3	11.3
		783	143.7	314.4	14.2	0.0	0.0	51.6	0.7	5.2	0.4	11.3
		759	143.9	640.6	12.7	0.0	0.0	48.8	0.5	5.1	0.3	11.3
		736	144.0	700.6	13.8	0.0	0.0	47.0	0.5	4.9	0.2	11.3
16.0	12	811	143.6	3.1	37.3	0.0	0.0	62.0	4.8	3.0	1.7	10.8
		784	143.7	162.9	18.5	0.1	0.1	59.2	1.3	5.0	0.6	10.8
		760	143.9	559.7	12.1	0.0	0.0	57.5	0.6	5.8	0.3	10.8
		736	144.0	691.5	13.7	-0.0	0.0	55.0	0.6	5.0	0.3	10.8
-16.0	13	813	143.6	0.	50.3	0.0	0.0	59.0	4.9	7.0	2.6	11.3
		786	143.7	32.7	27.5	0.0	0.1	58.7	3.5	7.7	1.9	11.3
		761	143.8	347.5	13.6	0.0	0.0	57.7	0.8	5.1	0.4	11.3
		738	144.0	645.6	13.0	0.0	0.0	55.6	0.6	5.2	0.3	11.3
-16.0	14	813	143.6	0.	0.	0.0	0.0	59.0	4.9	7.0	2.6	11.3
		786	143.7	0.3	46.3	0.	0.	58.7	3.5	7.6	1.9	11.3
		761	143.8	59.5	25.3	-0.0	0.0	57.1	1.8	4.8	0.8	11.3
		738	144.0	395.3	13.3	0.1	0.1	56.5	1.1	5.4	0.5	11.3
-16.0	15	813	143.6	0.	0.	-0.0	0.1	53.1	6.2	9.4	3.6	11.3
		786	143.7	0.	61.2	-0.0	0.0	59.7	2.4	4.4	1.0	11.3
		761	143.8	1.5	40.8	0.0	0.0	56.6	4.8	3.8	1.9	11.3
		738	144.0	86.7	23.4	-0.0	0.0	57.6	1.7	5.4	0.8	11.3
-16.0	16	813	143.6	0.	0.	0.0	0.1	61.1	4.3	5.3	2.0	11.3
		786	143.7	0.	0.	0.0	0.0	54.8	8.9	3.2	3.2	11.3
		761	143.8	0.	58.6	0.0	0.2	56.4	5.6	9.0	3.2	11.3
		738	144.0	3.8	39.2	0.0	0.1	49.0	7.0	-0.0	0.0	11.3
-16.0	17	813	143.6	0.	0.	-0.0	0.1	57.3	2.8	6.2	1.4	11.3
		786	143.7	0.	0.	0.0	0.1	55.6	3.9	3.1	1.4	11.3
		761	143.8	0.	0.	-0.0	0.2	34.1	7.1	4.5	3.1	11.3
		738	144.0	0.	59.1	0.0	0.0	58.4	3.5	7.1	1.8	11.3

KAPPA	= κ, conversion from proton counting rate to cross section, ignoring inefficiencies and absorptions, in units of (counts/10^{16} MeV)/(μb./sr.).
RMS DK	= root mean square width of the photon energy resolution in MeV.
S3 PC LOSS...	= S3 per cent loss due to horizontal multiple scattering and Monte Carlo error.
GAMMA PC EFF...	= gamma counter per cent efficiency and Monte Carlo error.
P · G	= P · γ signature.
P · 2G	= P · 2γ signature.
PC NA	= per cent proton nuclear absorption.

C. Cross sections

Table 18 contains cross sections before interpreting and averaging for the data listed in Table 14. The proton angle and point number are provided to facilitate cross referencing to determine details of the setup for each point. The cross sections from the P · γ signature are plotted in Figure 6 of Part III A. Some of the P signature cross sections are plotted in Figures 8 and 9 of Part III B.

Table 19 contains cross sections for the excitation curve data in Table 15 . These cross sections are discussed in Appendix VIII.

Table 18

Cross sections before interpolating and averaging for cross section data. See text for definitions.

P LAB ANGLE	PT NO	LAB K CH	PION CROSS SECTIONS AND ERRORS PROTON		PROTON.G		PROTON.2G	
4.0	1	1208	1.62	0.09	1.63	0.19	3.55	0.79
		1178	1.44	0.11	1.22	0.19	1.72	0.83
		1151	1.84	0.11	1.76	0.19	1.78	0.54
		1124	1.86	0.11	1.25	0.18	1.84	0.60
4.0	2	1208	1.62	0.09	1.63	0.19	3.55	0.79
		1069	1.90	0.21	1.89	0.32	6.00	3.06
		1044	2.21	0.24	1.93	0.32	4.68	2.39
		1020	2.63	0.24	1.99	0.32	3.00	2.05
4.0	3	1096	1.85	0.13	1.88	0.22	3.49	0.95
		1069	2.12	0.16	2.16	0.23	3.98	1.41
		1044	2.06	0.16	1.82	0.22	2.26	0.96
		1020	1.97	0.17	1.85	0.24	3.29	1.10
4.0	4	994	1.65	0.29	1.96	0.40	2.22	1.07
		970	2.76	0.27	2.04	0.33	2.91	1.41
		947	2.72	0.30	1.76	0.41	3.00	1.30
		925	3.13	0.33	1.63	0.32	1.54	0.86
4.0	5	994	2.12	0.20	1.45	0.19	2.22	1.07
		970	2.48	0.22	1.85	0.23	2.91	1.41
		947	2.42	0.29	1.73	0.36	3.00	1.30
		925	2.86	0.28	1.85	0.24	1.54	0.86
4.0	6	915	1.92	0.16	1.73	0.17	2.81	0.60
		885	2.39	0.18	2.26	0.17	3.09	0.63
		858	2.49	0.19	2.24	0.19	2.87	0.73
		832	2.47	0.21	2.12	0.21	3.29	0.67
4.0	7	808	2.06	0.20	2.13	0.26	2.81	0.60
		782	2.49	0.22	2.29	0.27	3.09	0.63
		758	2.54	0.23	2.44	0.27	2.87	0.73
		736	2.73	0.24	1.86	0.28	3.29	0.67
4.0	8	716	1.72	0.20	2.10	0.24	2.13	0.78
		693	1.53	0.21	1.26	0.23	1.01	0.50
		672	1.33	0.22	1.13	0.19	1.53	0.61
		652	1.66	0.23	1.01	0.22	1.33	0.61
4.0	9	716	1.41	0.34	1.81	0.32	1.62	0.85
		693	1.79	0.35	1.87	0.32	2.96	1.26
		672	1.91	0.38	1.46	0.29	1.46	0.76
		652	0.92	0.42	1.15	0.29	1.65	0.88
4.0	10	633	0.62	0.15	0.91	0.22	1.62	0.85
		612	0.69	0.16	0.84	0.15	2.96	1.26
		594	0.79	0.17	0.71	0.19	1.46	0.76
		576	0.68	0.19	0.95	0.20	1.65	0.88
8.0	1	1208	1.53	0.10	1.38	0.13	9.21	4.66
		1179	1.58	0.10	1.29	0.13	11.00	5.74
		1151	1.80	0.12	1.62	0.15	8.41	3.72
		1124	1.94	0.13	1.62	0.16	6.16	3.07
8.0	2	1096	1.97	0.13	1.76	0.16	7.33	3.48
		1069	2.20	0.15	2.11	0.18	8.74	3.87
		1044	2.75	0.16	2.08	0.19	8.53	5.07
		1020	2.72	0.17	2.19	0.18	16.81	7.16
8.0	3	1096	1.89	0.12	1.87	0.14	9.21	4.41
		1069	2.05	0.13	1.76	0.15	9.55	4.15
		1044	2.62	0.13	2.06	0.16	7.52	4.82
		1020	2.85	0.14	2.25	0.17	6.04	4.99
8.0	4	994	2.26	0.13	2.46	0.17	15.68	6.59
		970	2.74	0.12	2.24	0.15	8.89	2.82
		947	2.85	0.14	2.06	0.17	9.62	3.71
		925	3.02	0.15	2.15	0.18	10.36	3.68
8.0	5	915	2.27	0.13	2.20	0.15	8.98	3.49
		886	2.47	0.14	2.45	0.16	11.82	3.59
		858	2.97	0.15	2.42	0.15	5.58	2.29
		832	3.46	0.16	2.42	0.15	3.14	1.59
8.0	6	810	2.29	0.24	2.67	0.25	12.43	6.75
		783	2.89	0.25	2.75	0.26	7.36	4.02
		759	2.59	0.27	2.13	0.28	9.80	4.74
		736	3.33	0.26	1.94	0.21	10.73	4.47
8.0	7	717	1.54	0.14	1.55	0.16	1.79	2.03
		694	1.43	0.14	1.34	0.16	8.96	5.09
		672	1.86	0.16	1.39	0.18	7.89	5.41
		652	1.81	0.16	1.03	0.15	9.23	5.62
8.0	8	633	1.01	0.22	1.21	0.36	1.79	2.03
		613	0.94	0.24	1.04	0.44	8.96	5.09
		594	0.75	0.29	0.40	0.27	7.89	5.41
		577	1.27	0.29	0.41	0.26	9.23	5.62
12.0	1	1210	1.11	0.15	0.92	0.19	1.09	0.42
		1179	1.47	0.16	1.06	0.22	1.17	0.48
		1151	1.74	0.18	1.13	0.23	2.18	0.67
		1124	1.70	0.18	1.77	0.25	2.14	0.68
12.0	2	1212	1.41	0.09	1.24	0.12	2.22	0.45
		1182	1.37	0.09	1.02	0.13	1.27	0.31
		1154	1.37	0.09	0.99	0.13	1.22	0.40
		1124	1.70	0.18	1.77	0.25	2.14	0.68
12.0	3	1097	1.89	0.13	1.73	0.18	2.47	0.54
		1070	2.68	0.14	2.08	0.19	2.84	0.48
		1044	3.16	0.16	2.46	0.21	2.81	0.58
		1019	3.42	0.16	2.59	0.22	3.01	0.59
12.0	4	1097	2.01	0.10	1.86	0.14	2.20	0.39
		1070	2.61	0.11	2.34	0.16	3.06	0.44
		1044	3.15	0.12	2.79	0.17	3.59	0.47
		1019	3.08	0.13	2.69	0.18	3.14	0.44
12.0	5	995	2.96	0.12	2.78	0.17	4.27	0.53
		970	3.32	0.12	3.13	0.18	3.88	0.56
		947	3.31	0.12	2.72	0.18	4.56	0.58
		925	3.32	0.13	2.04	0.17	3.23	0.49
12.0	6	995	2.87	0.12	2.89	0.17	2.98	0.48
		970	3.15	0.13	3.16	0.19	4.08	0.52
		947	3.12	0.12	2.73	0.18	3.67	0.55
		925	3.07	0.13	2.33	0.18	3.95	0.55
12.0	7	916	2.60	0.11	2.40	0.16	2.57	0.45
		886	2.55	0.12	2.46	0.17	2.99	0.45
		858	2.95	0.13	2.45	0.18	3.76	0.51
		832	3.19	0.14	2.73	0.18	2.74	0.44
12.0	8	810	2.48	0.12	2.71	0.18	3.75	0.53
		784	2.65	0.12	2.39	0.17	3.54	0.71
		759	3.03	0.12	2.26	0.19	2.56	0.61
		737	2.81	0.14	1.63	0.19	2.50	0.58
-12.0	9	812	2.45	0.11	2.66	0.18	3.87	0.60
		785	2.71	0.11	2.63	0.18	3.09	0.53
		761	2.77	0.12	2.05	0.19	3.13	0.56
		738	2.85	0.12	2.23	0.18	3.23	0.55
-12.0	10	812	2.04	0.12	2.30	0.18	3.49	0.50
		785	2.56	0.12	2.51	0.18	4.17	0.60
		761	2.53	0.13	2.37	0.18	2.51	0.45
		738	2.58	0.14	2.48	0.18	3.92	0.60
-12.0	11	811	2.26	0.13	2.09	0.15	3.49	0.50
		784	2.23	0.16	2.11	0.15	4.17	0.60
		760	2.21	0.15	1.96	0.15	2.51	0.45
		737	2.47	0.16	1.94	0.14	3.92	0.60
12.0	12	717	1.53	0.14	1.72	0.23	2.11	0.76
		694	1.74	0.13	1.58	0.22	1.92	0.68
		672	1.50	0.15	1.15	0.23	0.50	0.46
		652	1.51	0.16	0.44	0.25	1.25	0.52
12.0	13	717	1.48	0.20	1.48	0.28	2.30	0.74
		694	1.58	0.18	1.23	0.26	2.87	0.81
		672	1.89	0.20	1.67	0.31	1.11	0.64
		652	1.79	0.22	1.62	0.33	2.40	0.83
12.0	14	717	1.66	0.11	1.82	0.17	3.41	0.62
		694	1.61	0.11	1.65	0.16	1.78	0.47
		672	1.46	0.11	1.33	0.18	2.17	0.51
		652	1.56	0.13	1.15	0.17	2.39	0.59
-12.0	15	719	1.74	0.10	1.75	0.16	2.34	0.54
		695	1.56	0.10	1.69	0.16	2.16	0.62
		674	1.40	0.10	1.13	0.16	1.76	0.51
		654	1.45	0.10	1.26	0.17	2.42	0.67
12.0	16	635	0.95	0.09	0.88	0.13	1.78	0.45
		614	0.83	0.11	0.90	0.15	2.38	0.60
		596	0.98	0.11	1.14	0.19	2.17	0.63
		578	1.19	0.11	0.64	0.19	0.96	0.55

P LAB ANGLE	PT NO	LAB K CH	PION CROSS SECTIONS AND ERRORS PROTON		PROTON.G		PROTON.2G	
16.0	1	1212	1.25	0.06	1.01	0.08	1.52	0.19
		1181	1.28	0.07	1.07	0.08	1.28	0.19
		1152	1.63	0.07	1.16	0.09	1.42	0.21
		1124	1.88	0.08	1.56	0.10	1.97	0.23
16.0	2	1212	1.25	0.06	1.01	0.08	1.52	0.19
		1070	2.66	0.17	2.47	0.19	2.59	0.45
		1044	3.23	0.17	2.69	0.23	3.24	0.53
		1019	3.49	0.19	2.18	0.24	2.35	0.43
16.0	3	1098	2.31	0.11	2.12	0.15	2.29	0.35
		1070	2.69	0.12	2.32	0.16	3.83	0.41
		1044	3.39	0.14	2.83	0.18	3.39	0.42
		1019	3.68	0.13	3.00	0.18	5.08	0.56
16.0	4	1100	1.97	0.09	1.89	0.12	2.36	0.36
		1072	2.53	0.11	2.20	0.14	2.98	0.38
		1046	3.05	0.12	2.93	0.15	4.00	0.44
		1021	3.26	0.13	2.70	0.16	3.27	0.39
16.0	5	996	3.25	0.12	3.08	0.16	4.02	0.44
		971	3.26	0.12	2.94	0.16	3.75	0.50
		947	3.43	0.13	2.88	0.17	3.53	0.44
		925	3.16	0.13	2.49	0.16	2.87	0.39
-16.0	6	1012	2.89	0.09	2.68	0.10	9.01	2.39
		978	2.98	0.10	2.48	0.12	7.69	3.39
		947	3.06	0.10	2.43	0.10	8.41	3.41
		917	3.54	0.10	2.62	0.11		
-16.0	7	918	2.49	0.11	2.42	0.15	3.12	0.41
		888	2.87	0.11	2.82	0.15	3.62	0.41
		860	2.92	0.12	2.57	0.16	3.50	0.44
		833	3.15	0.12	2.60	0.17	3.42	0.47
16.0	8	811	2.69	0.12	2.75	0.17	4.15	0.52
		784	2.84	0.13	2.73	0.18	2.71	0.40
		759	2.72	0.12	2.53	0.18	3.36	0.51
		736	2.90	0.13	2.51	0.18	2.77	0.47
16.0	9	811	2.51	0.10	2.62	0.14	3.07	0.41
		784	2.96	0.11	2.89	0.15	3.86	0.47
		760	2.83	0.12	2.64	0.16	3.73	0.53
		736	2.92	0.12	2.28	0.16	3.24	0.56
16.0	10	812	2.71	0.12	2.88	0.17	3.21	0.41
		786	2.89	0.12	2.71	0.17	3.52	0.48
		761	2.89	0.13	2.17	0.18	3.33	0.59
		738	2.78	0.13	2.41	0.20	2.29	0.51
-16.0	11	812	2.36	0.10	2.44	0.15	3.21	0.44
		786	2.50	0.11	2.52	0.16	4.20	0.53
		761	2.64	0.11	2.29	0.17	3.19	0.50
		738	2.84	0.11	2.07	0.17	3.06	0.48
-16.0	12	813	2.62	0.08	2.58	0.12	3.18	0.32
		786	2.62	0.09	2.78	0.12	3.15	0.35
		761	2.66	0.09	2.62	0.13	3.54	0.36
		738	2.87	0.09	2.12	0.13	2.84	0.40
-16.0	13	811	2.47	0.08	2.34	0.10		
		784	2.96	0.09	2.54	0.10	3.15	0.35
		759	2.67	0.10	2.36	0.10	3.54	0.36
		736	3.04	0.10	2.13	0.10	2.84	0.40
16.0	14	718	1.68	0.11	1.90	0.16	2.99	0.45
		694	1.71	0.10	1.52	0.15	1.33	0.42
		673	1.65	0.11	1.27	0.15	1.58	0.38
		652	1.95	0.11	1.23	0.16	1.62	0.37
16.0	15	718	1.93	0.10	2.01	0.15	2.93	0.58
		695	1.73	0.11	1.89	0.15	1.98	0.48
		673	1.78	0.11	1.44	0.16	1.92	0.40
		652	1.96	0.12	1.57	0.16	1.40	0.36
16.0	16	718	1.87	0.11	1.69	0.18	2.70	0.62
		695	1.76	0.10	1.41	0.15	1.95	0.37
		673	1.70	0.11	1.68	0.15	2.03	0.40
		652	1.75	0.12	1.24	0.18	3.75	0.65
-16.0	17	720	1.98	0.09	1.86	0.14	2.33	0.45
		696	1.60	0.09	1.62	0.14	2.33	0.47
		674	1.56	0.10	1.56	0.15	2.83	0.69
		654	1.80	0.10	1.36	0.16	1.59	0.35
16.0	18	635	0.88	0.13	1.25	0.15	2.52	0.49
		615	1.25	0.13	1.30	0.14	2.23	0.52
		596	1.25	0.14	1.34	0.22	1.06	0.33
		578	1.62	0.15	1.26	0.23	1.27	0.43

P LAB ANGLE	PT NO	LAB K CH	PION CROSS SECTIONS AND ERRORS PROTON		PROTON.G		PROTON.2G	
20.5	1	1215	1.00	0.07	0.89	0.08	0.94	0.17
		1183	1.35	0.08	1.16	0.11	1.48	0.33
		1153	1.37	0.09	1.20	0.10	1.31	0.22
		1125	1.74	0.10	1.39	0.11	1.30	0.26
20.5	2	1101	1.94	0.09	1.86	0.11	1.98	0.22
		1073	2.53	0.10	2.18	0.13	3.24	0.32
		1046	3.11	0.12	2.59	0.15	3.68	0.35
		1020	3.38	0.12	2.60	0.15	2.92	0.32
-20.5	3	1014	2.64	0.12	2.53	0.14	5.65	1.28
		979	3.14	0.13	2.77	0.13	4.98	1.24
		947	2.81	0.13	2.39	0.13	4.40	1.33
		917	3.24	0.12	2.33	0.12	4.42	1.45
-20.5	4	919	2.59	0.11	2.64	0.15	3.38	0.40
		888	2.80	0.12	2.44	0.16	3.09	0.39
		859	2.82	0.12	2.75	0.18	2.94	0.43
		832	2.99	0.13	2.54	0.17	3.71	0.49
-20.5	5	812	2.76	0.20	2.86	0.22		
		785	3.03	0.19	2.68	0.22		
		760	3.02	0.21	2.46	0.23		
		736	2.89	0.21	2.36	0.23	3.71	0.49
-20.5	6	719	2.49	0.10	2.44	0.14	3.44	0.44
		696	2.03	0.10	2.01	0.13	2.84	0.41
		673	1.91	0.11	1.72	0.15	3.11	0.44
		653	1.98	0.11	1.48	0.15	2.41	0.40
-20.5	7	718	2.09	0.12	2.01	0.14		
		695	1.98	0.12	1.81	0.14	2.84	0.41
		673	1.67	0.13	1.52	0.12	3.11	0.44
		652	2.06	0.13	1.28	0.14	2.41	0.40
-20.5	8	636	1.56	0.10	1.40	0.11		
		615	1.45	0.12	1.37	0.13	2.84	0.41
		596	1.49	0.14	1.57	0.14	3.11	0.44
		578	1.90	0.14	1.59	0.12	2.41	0.40
25.0	1	1218	0.81	0.07	0.71	0.07	0.82	0.16
		1185	1.21	0.08	1.04	0.09	1.29	0.19
		1154	1.23	0.09	0.97	0.10	1.00	0.20
		1124	1.52	0.10	1.32	0.12	1.32	0.25
25.0	2	1103	1.56	0.09	1.34	0.10	1.45	0.25
		1074	2.27	0.11	1.80	0.12	2.24	0.24
		1046	2.87	0.12	2.23	0.14	2.27	0.26
		1019	3.07	0.12	2.43	0.14	2.58	0.25
25.0	3	1000	2.73	0.11	2.54	0.13	3.13	0.29
		973	2.76	0.11	2.40	0.13	2.87	0.28
		948	2.94	0.12	2.62	0.14	3.46	0.35
		924	2.77	0.12	2.40	0.15	2.66	0.30
-25.0	4	922	2.29	0.10	2.40	0.13	2.65	0.27
		889	2.54	0.10	2.53	0.13	3.26	0.32
		860	2.68	0.12	2.40	0.15	2.74	0.34
		832	3.01	0.13	2.82	0.16	3.33	0.32
-25.0	5	814	2.75	0.18	2.35	0.20	6.48	2.76
		786	3.10	0.21	3.03	0.23		
		760	3.34	0.21	2.85	0.22	10.63	5.60
		736	3.41	0.20	2.69	0.21	5.60	4.71
-25.0	6	720	2.51	0.14	2.55	0.15	17.34	8.84
		696	2.75	0.13	2.47	0.15		
		673	2.44	0.13	1.95	0.13		
		653	2.47	0.13	1.91	0.13		
-25.0	7	637	1.72	0.12	1.79	0.12		
		616	1.98	0.13	1.91	0.14		
		597	2.29	0.14	1.78	0.15		
		578	2.39	0.15	2.06	0.14		

P LAB ANGLE	PT NO	LAB K CH	PION CROSS SECTIONS AND ERRORS PROTON		PROTON.G		PROTON.2G	
29.5	1	1219	0.74	0.08	0.56	0.09	0.80	0.15
		1185	0.93	0.09	0.63	0.11	0.49	0.16
		1153	1.08	0.11	0.96	0.11	0.90	0.16
		1122	1.33	0.12	1.12	0.14	1.10	0.25
29.5	2	1221	0.67	0.07	0.73	0.08	0.68	0.13
		1187	0.86	0.07	0.92	0.09	0.87	0.14
		1154	1.19	0.09	1.09	0.10	1.40	0.20
		1123	1.61	0.10	1.38	0.11	1.52	0.20
29.5	3	1105	1.38	0.10	1.59	0.11	1.82	0.23
		1074	1.91	0.11	1.81	0.12	2.20	0.27
		1046	2.16	0.13	2.07	0.14	2.26	0.24
		1018	2.35	0.12	2.14	0.14	2.38	0.28
29.5	4	1126	0.92	0.09	0.96	0.08	0.89	0.22
		1084	1.73	0.11	1.38	0.11	1.05	0.26
		1046	2.23	0.12	1.89	0.13	1.87	0.34
		1011	2.78	0.13	2.12	0.13	1.60	0.40
29.5	5	1002	2.22	0.11	2.15	0.12	2.24	0.22
		975	2.15	0.11	2.23	0.13	2.40	0.24
		949	2.22	0.11	2.18	0.13	2.43	0.23
		924	2.34	0.12	2.19	0.15	2.41	0.24
29.5	6	924	2.24	0.14	2.06	0.17	2.41	0.33
		891	2.36	0.14	2.27	0.16	2.28	0.30
		861	2.62	0.15	2.33	0.18	2.65	0.36
		832	2.90	0.16	2.55	0.20	3.49	0.42
29.5	7	817	2.60	0.18	2.59	0.19	2.17	0.95
		788	2.65	0.19	2.77	0.21	3.21	1.15
		761	3.57	0.21	3.44	0.24	5.26	1.93
		737	3.74	0.21	3.27	0.23	7.32	2.56
29.5	8	817	2.52	0.19	2.35	0.19	2.27	0.85
		788	3.11	0.20	2.90	0.21	1.81	0.87
		761	3.34	0.21	2.81	0.23	1.54	0.84
		737	3.12	0.22	2.78	0.21	4.43	1.69
29.5	9	723	2.77	0.12	2.62	0.14	3.45	0.36
		698	2.96	0.13	2.83	0.16	3.66	0.39
		675	2.47	0.12	2.46	0.14	3.13	0.39
		654	2.61	0.12	2.42	0.15	2.78	0.38
29.5	10	639	1.65	0.14	1.74	0.14		
		618	2.33	0.13	2.25	0.14		
		598	1.88	0.14	2.08	0.14		
		579	2.23	0.14	2.09	0.14		
34.0	1	1223	0.61	0.05	0.60	0.05	0.67	0.08
		1187	0.72	0.07	0.75	0.06	0.78	0.10
		1153	1.04	0.07	0.94	0.07	1.02	0.10
		1121	1.35	0.07	1.10	0.08	1.25	0.14
34.0	2	1109	1.36	0.09	1.25	0.10	1.51	0.19
		1077	1.52	0.10	1.49	0.11	1.47	0.18
		1047	2.10	0.11	1.97	0.12	2.22	0.21
		1018	2.22	0.12	2.18	0.14	2.30	0.24
34.0	3	1129	0.94	0.06	0.98	0.06	0.97	0.10
		1086	1.40	0.07	1.30	0.07	1.42	0.13
		1046	2.17	0.08	1.85	0.09	2.08	0.15
		1009	2.23	0.08	1.98	0.09	2.02	0.14
34.0	4	1006	2.23	0.12	2.17	0.14	2.60	0.28
		977	1.79	0.13	2.03	0.13	2.21	0.27
		950	2.30	0.13	2.21	0.14	2.22	0.26
		925	2.47	0.13	2.23	0.13	2.59	0.25
34.0	5	1024	1.84	0.12	1.77	0.12	1.72	0.36
		985	2.12	0.13	1.91	0.13	1.96	0.33
		950	2.41	0.13	1.87	0.12	1.28	0.27
		917	2.55	0.15	1.77	0.13	1.84	0.36
34.0	6	928	1.88	0.10	1.89	0.11	2.25	0.22
		893	1.94	0.12	1.95	0.13	2.17	0.22
		862	2.66	0.13	2.67	0.13	2.89	0.24
		833	2.93	0.14	2.67	0.15	2.82	0.31
34.0	7	819	2.98	0.15	2.76	0.15	4.64	0.71
		790	3.63	0.16	3.25	0.15	5.12	0.79
		763	3.65	0.17	3.14	0.17	3.82	0.74
		737	4.01	0.17	3.45	0.18	4.36	1.03
34.0	8	726	3.57	0.14	3.52	0.16	4.43	0.35
		700	3.18	0.14	3.10	0.17	3.55	0.35
		677	2.94	0.14	2.91	0.15	3.63	0.35
		655	3.10	0.13	2.82	0.16	3.84	0.42
34.0	9	642	2.56	0.18	2.56	0.16	3.10	0.35
		620	2.83	0.19	2.58	0.20	3.68	0.60
		599	3.13	0.20	2.80	0.21	4.06	0.47
		581	2.99	0.23	3.18	0.21	5.05	0.55
39.0	1	1229	0.69	0.07	0.51	0.07	0.66	0.10
		1191	0.93	0.10	0.88	0.10	0.98	0.14
		1155	1.06	0.09	0.94	0.10	0.87	0.15
		1122	1.18	0.11	1.29	0.11	1.36	0.15
39.0	2	1135	0.92	0.17	1.08	0.16	0.89	0.25
		1090	1.44	0.17	1.30	0.16	1.30	0.25
		1048	1.48	0.18	1.37	0.20	1.76	0.31
		1010	2.23	0.22	2.04	0.22	2.53	0.43
39.0	3	1114	1.19	0.09	1.12	0.09	1.15	0.16
		1080	1.40	0.10	1.28	0.10	1.56	0.18
		1049	1.95	0.12	1.95	0.13	1.93	0.20
		1019	2.20	0.11	2.11	0.12	2.27	0.20
39.0	4	1135	0.98	0.06	1.02	0.06	1.10	0.10
		1090	1.51	0.07	1.47	0.07	1.76	0.13
		1048	1.72	0.08	1.57	0.08	1.48	0.13
		1010	1.95	0.09	1.84	0.10	1.93	0.16
39.0	5	1010	1.88	0.16	1.93	0.17	1.98	0.31
		980	1.77	0.17	1.58	0.18	2.13	0.33
		952	2.24	0.18	2.24	0.19	2.31	0.29
		926	2.40	0.19	2.06	0.18	2.71	0.33
39.0	6	933	1.72	0.12	1.70	0.12	1.76	0.21
		897	1.99	0.13	2.06	0.14	1.89	0.23
		864	2.53	0.14	2.47	0.14	2.66	0.26
		834	3.17	0.15	3.21	0.15	3.96	0.30
39.0	7	824	3.14	0.16	3.08	0.15	3.42	0.51
		793	3.85	0.18	3.52	0.16	3.75	0.55
		765	4.08	0.19	3.75	0.19	4.96	0.78
		739	4.44	0.19	3.61	0.17	3.42	0.59
39.0	8	729	3.75	0.20	3.86	0.17	4.99	0.76
		703	3.82	0.19	3.85	0.17	3.43	0.65
		679	3.64	0.18	3.40	0.17	3.77	0.72
		656	3.01	0.19	2.85	0.16	5.92	1.08
39.0	9	646	2.63	0.19	2.89	0.21	4.17	0.45
		623	2.88	0.19	3.05	0.20	3.65	0.50
		602	2.61	0.19	2.96	0.20	4.04	0.51
		583	3.13	0.19	3.26	0.20	3.44	0.46
41.9	1	934	1.95	0.16	1.82	0.16	1.82	0.27
		898	1.96	0.22	1.81	0.20	2.03	0.30
		865	2.33	0.22	2.49	0.23	2.67	0.37
		834	3.18	0.27	3.30	0.25	3.95	0.45
41.9	2	934	1.93	0.16	1.78	0.13	1.99	0.30
		898	2.04	0.16	1.89	0.13	2.24	0.33
		865	2.40	0.18	2.23	0.15	1.69	0.46
		834	3.42	0.18	2.82	0.16	2.97	0.40
41.9	3	826	3.54	0.17	3.14	0.17	2.70	0.41
		795	3.87	0.19	3.65	0.18	3.96	0.51
		766	3.55	0.22	3.55	0.19	4.04	0.54
		740	4.20	0.19	3.71	0.18	4.43	0.63
41.9	4	731	4.19	0.21	4.08	0.18	5.05	0.69
		705	3.39	0.20	3.27	0.16	3.51	0.60
		680	3.32	0.20	3.28	0.17	4.57	0.74
		658	2.62	0.20	2.49	0.15	2.10	0.59
41.9	5	648	2.69	0.25	3.04	0.26	3.63	0.57
		625	2.78	0.21	2.30	0.23	3.31	0.55
		604	3.07	0.25	3.12	0.25	4.00	0.63
		585	2.77	0.26	2.93	0.26	2.60	0.50
41.9	6	648	3.13	0.18	2.68	0.15	3.67	0.80
		625	2.72	0.20	2.70	0.16	3.66	0.92
		604	2.64	0.20	2.79	0.19	0.96	1.33
		585	3.01	0.19	2.84	0.16	3.90	1.17

P LAB ANGLE	PT NO	LAB K CH	PION CROSS SECTIONS AND ERRORS PROTON		PROTON.G		PROTON.2G	
44.0	1	1143	1.24	0.08	1.27	0.07	1.24	0.11
		1095	1.41	0.09	1.30	0.08	1.55	0.13
		1051	1.67	0.09	1.75	0.09	1.63	0.12
		1011	1.92	0.10	1.81	0.09	2.05	0.16
44.0	2	1143	1.07	0.08	0.97	0.07	1.30	0.12
		1095	1.47	0.08	1.29	0.08	1.33	0.12
		1051	1.82	0.09	1.68	0.09	1.77	0.14
		1011	1.77	0.09	1.73	0.09	1.92	0.15
44.0	3	1036	1.66	0.10	1.43	0.09	1.21	0.19
		994	1.80	0.10	1.61	0.09	1.88	0.19
		955	1.68	0.11	1.51	0.09	1.31	0.15
		920	1.76	0.12	1.61	0.09	1.17	0.20
44.0	4	939	1.49	0.15	1.43	0.13	1.61	0.23
		902	1.86	0.15	1.87	0.13	2.17	0.21
		868	2.28	0.16	2.39	0.15	2.63	0.24
		836	2.77	0.18	2.65	0.18	2.94	0.34
44.0	5	829	3.17	0.20	3.03	0.17	3.20	0.42
		798	3.83	0.20	3.66	0.17	3.38	0.44
		769	4.16	0.20	3.81	0.18	3.19	0.44
		742	4.34	0.21	3.63	0.19	4.59	0.67
44.0	6	735	4.05	0.20	3.63	0.18	3.01	0.49
		707	3.42	0.20	3.28	0.17	4.09	0.61
		683	3.31	0.19	3.10	0.17	3.79	0.65
		660	2.93	0.20	2.53	0.16	3.24	0.68
44.0	7	652	2.90	0.20	3.02	0.18	3.49	0.36
		629	2.62	0.18	2.77	0.16	2.73	0.32
		608	2.42	0.18	2.39	0.17	2.47	0.35
		588	2.78	0.19	2.60	0.19	3.32	0.39
49.0	1	1274	0.67	0.18	0.72	0.13	0.96	0.35
		1216	1.21	0.15	1.06	0.11	0.80	0.18
		1164	1.28	0.19	1.56	0.14	1.55	0.25
		1116	2.02	0.17	1.69	0.14	1.50	0.23
49.0	2	1152	1.66	0.23	1.52	0.23	1.67	0.33
		1101	1.94	0.22	1.73	0.22	1.94	0.33
		1056	1.75	0.23	1.62	0.21	1.55	0.31
		1014	1.58	0.23	1.57	0.21	2.00	0.36
49.0	3	1044	1.84	0.19	1.48	0.16	1.63	0.29
		1000	1.54	0.17	1.50	0.12	1.44	0.23
		959	1.63	0.17	1.49	0.13	1.09	0.19
		923	1.80	0.18	1.40	0.13	1.05	0.20
49.0	4	946	1.45	0.19	1.27	0.13	1.42	0.24
		907	1.78	0.20	1.70	0.14	2.03	0.30
		872	1.76	0.22	1.39	0.17	1.11	0.33
		839	2.70	0.21	2.23	0.15	2.13	0.31
49.0	5	837	3.30	0.22	2.88	0.18	2.84	0.37
		804	3.90	0.21	3.38	0.18	3.55	0.43
		774	4.16	0.22	3.47	0.19	4.37	0.49
		747	3.59	0.22	3.26	0.18	4.16	0.52
54.0	1	1290	0.91	0.24	0.70	0.14	1.49	0.65
		1229	1.04	0.20	0.86	0.10	1.93	0.65
		1173	1.27	0.22	1.18	0.13	1.41	0.44
		1123	1.58	0.21	1.55	0.14	1.43	0.41
54.0	2	1168	1.95	0.25	1.71	0.16	3.33	0.78
		1114	1.98	0.23	1.79	0.16	1.33	0.38
		1066	2.37	0.22	1.86	0.17	1.80	0.39
		1023	1.66	0.24	1.32	0.13	1.60	0.37
54.0	3	1058	2.03	0.29	1.80	0.19	2.67	0.94
		1011	2.04	0.25	1.85	0.15	2.13	0.41
		969	1.81	0.24	1.49	0.16	1.95	0.39
		931	1.45	0.24	1.28	0.14	1.30	0.31
54.0	4	959	1.47	0.26	1.15	0.14	0.80	0.24
		919	1.40	0.23	1.33	0.14	1.20	0.29
		882	1.72	0.25	1.44	0.14	1.33	0.28
		849	2.24	0.24	1.45	0.17	1.83	0.33

Table 19

Cross sections for excitation curve data. See text for definitions.

P LAB ANGLE	PT NO	LAB K CM	PION CROSS SECTIONS AND ERRORS PROTON		PROTON.G		PROTON.2G	
16.0	1	799	6.38	0.52	2.13	0.62	2.65	1.06
		779	7.05	0.49	2.72	0.53	1.72	0.89
		760	6.77	0.59	2.55	0.58	3.67	1.34
		742	7.01	0.51	2.80	0.56	4.87	1.70
-16.0*	2	812	4.60	0.13	2.51	0.11		
		785	4.93	0.14	2.24	0.12	1.72	0.89
		760	5.23	0.14	2.53	0.12	3.87	1.34
		737	5.31	0.14	2.24	0.11	4.87	1.70
-16.0	3	811	3.61	0.11	2.53	0.10		
		784	3.96	0.12	2.46	0.11	1.72	0.89
		760	4.13	0.12	2.48	0.11		
		736	4.06	0.12	2.15	0.11	4.87	1.70
-16.0	4	811	3.00	0.11	2.48	0.12		
		784	3.32	0.11	2.41	0.11		
		759	3.43	0.11	2.33	0.12		
		736	3.41	0.12	2.08	0.11	4.87	1.70
-16.0	5	813	2.54	0.09	2.44	0.13	3.10	0.34
		786	2.42	0.10	2.64	0.14	3.73	0.41
		761	2.64	0.10	2.50	0.13	3.99	0.45
		738	2.71	0.11	2.37	0.15	3.20	0.48
-16.0	6	813	2.23	0.09	2.25	0.12	3.45	0.38
		786	2.45	0.09	2.28	0.13	2.63	0.35
		761	2.37	0.09	2.43	0.13	2.50	0.36
		738	2.37	0.09	2.33	0.13	3.23	0.40
-16.0	7	810	2.25	0.11	2.27	0.15	3.45	0.38
		784	2.39	0.11	2.48	0.13	2.63	0.35
		759	2.41	0.11	2.43	0.13		
		736	2.26	0.11	1.98	0.13	3.23	0.40
-16.0	8	813	1.88	0.10	1.95	0.13	2.92	0.41
		786	2.25	0.09	2.45	0.13	3.10	0.35
		761	2.39	0.09	2.35	0.12	3.53	0.38
		738	2.10	0.09	1.95	0.13	2.47	0.35
-16.0	9	813	1.61	0.19	1.81	0.24	3.08	0.82
		786	1.82	0.09	1.86	0.13	2.37	0.33
		761	2.21	0.09	2.24	0.13	2.74	0.35
		738	1.90	0.09	1.89	0.13	1.86	0.36
-16.0	10	813	4.26	2.15	1.52	0.96	-0.00	-0.01
		786	1.50	0.16	1.41	0.20	1.62	0.42
		761	1.98	0.10	1.81	0.14	2.84	0.42
		738	1.94	0.09	1.93	0.13	2.41	0.34
-16.0	11	810	0.14	1.41	1.91	0.78	-0.00	-0.01
		783	1.90	0.13	1.88	0.14	1.62	0.42
		759	2.16	0.09	2.08	0.10	2.84	0.42
		736	2.03	0.08	2.19	0.10	2.41	0.34
16.0	12	811	14.07	11.48	9.79	4.29	-0.00	-0.06
		784	1.67	0.35	1.59	0.36	2.01	0.76
		760	2.23	0.12	1.95	0.16	3.18	0.49
		736	2.05	0.10	1.94	0.15	2.88	0.44
-16.0	13	813	0.	0.	0.	0.	-0.	-0.
		786	1.59	1.09	2.74	0.85	4.96	2.44
		761	1.67	0.12	1.48	0.15	2.51	0.53
		738	1.78	0.08	1.88	0.13	2.94	0.39
-16.0	14	813	0.	0.	0.	0.	-0.	-0.
		786	28.56	98.80	2.74	0.85	4.96	2.44
		761	1.80	0.54	2.25	0.41	2.94	1.32
		738	1.30	0.12	1.29	0.15	1.42	0.45
-16.0	15	813	0.	0.	0.	0.	0.	0.
		786	0.	0.	-0.	-0.	-0.	-0.
		761	10.37	20.31	-12.61	15.86	25.91	28.87
		738	1.47	0.43	1.68	0.37	1.79	0.79
-16.0	16	813	0.	0.	0.	0.	0.	0.
		786	0.	0.	0.	0.	0.	0.
		761	0.	0.	0.	0.	0.	0.
		738	4.42	8.22	3.57	4.84	132.00	52.00
-16.0	17	813	0.	0.	0.	0.	0.	0.
		786	0.	0.	-0.	-0.	0.	0.
		761	0.	0.	0.	0.	0.	0.
		738	0.	0.	0.	0.	0.	0.

REFERENCES

1. R. Diebold, Ph.D. Thesis, California Institute of Technology (1963). Also, R. Diebold, Phys. Rev. 130, 2089 (1963). Contains references to earlier experiments except Jackson et al.

2. H. E. Jackson, J. W. DeWire, and R. M. Littauer, Phys. Rev. 119, 1381 (1960).

3. R. Alvarez, Z. Bar-Yam, W. Kern, D. Luckey, L. S. Osborne, S. Tazzari, and R. Fessel, Phys. Rev. Lett. 12, 707 (1964).

4. H. DeStaebler, Jr., E. F. Erickson, A. C. Hearn, and C. Schaerf, Phys. Rev. 140, 336 (1965).

5. C. Ward, B. Kenton, and C. York, Phys. Rev. 159, 1176 (1967). Also C. B. Ward, Ph.D. Thesis, University of California at Los Angeles (1966).

6. G. Belletini, C. Bemporad, P. J. Biggs, and P. L. Braccini, Nuovo Cimento 44, 239 (1966).

7. G. L. Hatch, Ph.D. Thesis, California Institute of Technology (1967).

8. C. Bacci, G. Penso, G. Salvini, C. Mencuccini, A. Reale, V. Silvertrini, M. Spinetti and B. Stella, Phys. Rev. 159, 1124 (1967).

9. B. Kenton, Ph.D. Thesis, University of California at Los Angeles (1967).

10. D. E. Lundquist, Ph.D. Thesis, Stanford University (1967).

11. E. D. Bloom, Ph.D. Thesis, California Institute of Technology (1967).

12. G. Buschhorn, P. Heide, V. Kotz, R. A. Lewis, P. Schmuser, H. Skronn, Phys. Rev. Lett. 230 (1968).

13. E. Loh, A. Ito, G. Cassiday, and J. Rutherford, APS Meeting in Chicago (1968) and private communication.

14. S. D. Ecklund, Ph.D. Thesis, California Institute of Technology (1967).

15. F. Wolverton, "Calibration of the 1200 MeV/c and 1670 MeV/c Magnet Configurations", CTSL Internal Report No. 36, unpublished (1968).

16. H. A. Thiessen, "A Scaling Adapter for the Nuclear Data 1024 Channel Pulse Height Analyzer", CTSL Internal Report No. 16, unpublished (1966).

17. V. L. Highland and J. W. DeWire, Phys. Rev. 132, 1293 (1963).

18. S. D. Ecklund and R. L. Walker, Phys. Rev. 159, 1195 (1967).

19. J. T. Beale, S. D. Ecklund, and R. L. Walker, "Pion Photoproduction Data Below 1.5 GeV", CTSL-42, unpublished (1966).

20. Reference 9. and private communication.

21. H. A. Thiessen, Ph.D. Thesis, California Institute of Technology (1967).

22. H. A. Thiessen and J. Pine, "Calibration of the South Quantameter", CTSL Internal Report No. 22, unpublished (1966).

23. D. E. Groom, "A General Range-Energy-Light Output Program for High Energy Physics", CTSL Internal Report No. 20, unpublished (1965).

24. C. Y. Prescott, "A Magnetic System for the Selection of Beams of Monoenergetic Electrons and Photons", CTSL Internal Report No. 1, unpublished (1963).

25. F. B. Wolverton, "Tagged Photon Beam Spectrum", CTSL Internal Report No. 33, unpublished (1967).

26. C. A. Heusch and C. Y. Prescott, "Selective Detectors for High Energy Photons and Electrons", CTSL-41, unpublished (1964).

27. B. Rossi and K. Greisen, Revs. Mod. Phys. 13, 240 (1941).

28. M. G. Hauser, Ph.D. Thesis, California Institute of Technology (1967).

29. A. V. Tollestrup, "Description and Operation of the 'Non-Professional' Synchrotron Laboratory Electronics, Revised and Addended", CTSL Internal Report No. 31, unpublished (1967).

30. C. W. Peck, Ph.D. Thesis, California Institute of Technology (1964).

31. H. G. de Carvalho, Phys. Rev. 96, 398 (1954).

32. C. J. Batty, Nucl. Phys. 23, 562 (1961).

33. J. M. Dickson and D. C. Salter, Nu. Cim. 6, 235 (1957).

34. E. Heiberg, Phys. Rev. 106, 1271 (1957).

35. C. J. Batty, W. O. Lock, and P. V. March, Proc. Phys. Soc. 73, 100 (1959).

36. C. Caverzasio et A. Michalowicz, Le Journal de Physique et le Radium 21, 314 (1960).

37. H. Tyre and Th. A. J. Maris, Nucl. Phys. 3, 52 (1957).

38. L. S. Azhgirei, I. K. Vzorov, V. P. Zrelov, M. G. Meshcheryakov, B. S. Neganov, R. M. Ryndin, and A. F. Shabudin, Sov. Phys. JETP 36, 1163 (1959).

39. F. Wolverton, "Manual for BPAK I, Thick Radiator Bremsstrahlung Computer Program", unpublished (1965). On file in the Synchrotron Library as Program No. 34 of the Synchrotron Programming Library.